2016

Flood Disaster Resilient Bridge Structures For Sustainable Bridge Management Systems

Alper Durmus
University of Mississippi

FLOOD DISASTER RESILIENT BRIDGE STRUCTURES FOR SUSTAINABLE BRIDGE MANAGEMENT SYSTEMS

A Dissertation
Presented for the Degree of
Doctor of Philosophy
Department of Civil Engineering
The University of Mississippi

ALPER DURMUS

August 2016

ABSTRACT

Extreme weather events are occurring at an increasing ferocity and frequency. Floods are the most common and damaging natural disaster. More than 4,400 occurrences of flood disasters have been reported globally between 1900 and 2016. As a result, around seven million people were killed and millions more were displaced. Climate impacts are expected to intensify weather related flooding events, and sea level rise expected worldwide will increase the risk of coastal disasters. Transportation infrastructure, vital to the economy and society of every country, is especially prone to the inland and coastal floods. Bridge structures are under the constant threat of these natural disasters. Superstructures can be washed away due to lateral forces generated by floodwater. Floodwater can also accelerate scouring around bridge piers, which often contributes to bridge failures. This research used the results of an extreme flood simulation conducted by the Center for Advanced Infrastructure Technology at the University of Mississippi. A flood inundation model was implemented for an extreme flood scenario at a floodplain site of Little Tallahatchie River in Northern Mississippi that featured surface transportation corridor sites and other infrastructure assets. Geospatial analysis of flood inundation mapping and simulation results showed that total flood inundation covered an area of 22.46 mi^2 (58.16 km^2) in the floodplain, where maximum floodwater depth reached up to 34.19 ft (10.42 m) within the inundation area. The results of the extreme flood simulation were used for assessing structural integrity of a bridge structure subject to lateral floodwater forces, with primary focus on the superstructure. A Three Dimensional-Finite Element model of US-51 Highway bridge, located in the floodplain site, was developed for flood impact analysis considering bridge girder-deck

superstructure, bearings, pile caps and piers. The numerical results of finite element simulation showed that the bridge superstructure displaced 2.42 m under the lateral hydrodynamic force of floodwater. The dowel bars inserted at the bottom of each girder end through bearing to the top end of pile cap, failed in shear against lateral floodwater forces. This would lead to the failure of US-51 Highway bridge superstructure if an extreme flood event occurs in real life. A framework for structural integrity assessment of bridge structures is presented with Flood Resiliency Index. Recommendations for design enhancements and hardening of bridges are discussed for flood disaster resilience. An enhanced geospatial decision support system is recommended considering "vertical underclearance" criteria for bridge superstructure height above the channel and "flood probability" related to flood occurrence in 10, 50, 100, 500 and 1,000 years. These flood resilience parameters are missing from the traditional bridge management system (BMS) framework. Enhancing the current practice of BMS is proposed using optimization based prioritization of flood disaster vulnerable bridges, which considers vertical underclearance criteria, flood disaster risk probability and life cycle cost analysis. For this purpose, a Flood Vulnerability Rating (FVR) is proposed on a scale of 1 (catastrophic risk) to 6 (very low risk). The FVR scale was used for a case study of 270 bridges on major rivers in the state of Mississippi, which were analyzed using an optimization objective function to maximize benefits considering reconstruction/hardening costs and indirect benefits (cost avoidance from traffic disruption and economic loss related to bridge failure). Based on the present-worth life cycle analysis, total life cycle costs for the agency's pre-planned bridge hardening for flood resilience was 59.3% less than the case of no hardening of the same bridge. This dissertation advances flood risk assessment and resilience management methodologies for transportation infrastructure in the United States and across the globe.

DEDICATION

Dedicated to Waheed Uddin.

LIST OF ACRONYMS

1D	One-dimensional
2D	Two-dimensional
3D	Three-dimensional
3D-FE	Three Dimensional-Finite Element
AASHO	American Association of State Highway Officials
AASHTO	American Association of State Highway and Transportation Officials
ACI	American Concrete Institute
AIT	Asian Institute of Technology
ANN	Artificial Neural Network
ARIMA	Autoregressive Integrated Moving Average
BMS	Bridge Management System
CAIT	Center for Advanced Infrastructure Technology
CCS	Computational cell size
CFD	Computational fluid dynamics
CL	Centerline
DEM	Digital Elevation Model
DHS	Department of Homeland Security
DOF	Degree of freedom

DSS	Decision support system
DSS-WISE	Decision Support System for Water Infrastructural Security
EM-DAT	Emergency Events Database
ERDC	Engineer Research and Development Center
FBFM	Flood Boundary and Floodway Map
FEMA	Federal Emergency Management Agency
FHWA	Federal Highway Administration
FIAB	Fully integrated abutment bridges
FIRM	Flood Insurance Rate Map
FRI	Flood Resilience Index
FRP	Fiber-reinforced plastic
FS	Factor of safety
FVM	Finite Volume Method
FVR	Flood Vulnerability Rating
GIS	Geographic Information System
HEC-RAS	Hydrologic Engineering Center-River Analysis System
HLLC	Harten-Lax-van Leer-Contact
LCA	Life cycle analysis
LCC	Life cycle cost
LP	Linear programming
M,R&R	Maintenance, repair and rehabilitation
MARIS	Mississippi Automated Resource Information System
MDEQ	Mississippi Department of Environmental Quality

MDOT	Mississippi Department of Transportation
MEMA	Mississippi Emergency Management Agency
MMC	Modeling, Mapping & Consequences Production Center
NBI	National Bridge Inventory
NBIS	National Bridge Inspection Standards
NCCHE	National Center for Computational Hydroscience and Engineering
NCHRP	National Cooperative Highway Research Program
NCITEC	National Center for Intermodal Transportation for Economic Competitiveness
NFIP	National Flood Insurance Program
SFHA	Special Flood Hazard Area
SIAB	Semi-integrated abutment bridges
SLR	Sea level rise
USACE	United States Army Corps of Engineers
USDA	United States Department of Agriculture
USGS	United States Geological Survey
VE	Value engineering

ACKNOWLEDGMENTS

It was snowing in Chicago when Dr. Waheed Uddin discussed with me a detailed PhD plan. I knew I was going to the city of Oxford next. I thank Dr. Al-Ostaz, Dr. Najjar and Dr. McCarty for helping me at times as needed and serving in my PhD committee.

It happened to be my luck that I joined the NCITEC-CAIT flood simulation project, which was in collaboration with Dr. Mustafa Altinakar, director of the NCCHE. Planimetrics results of the flood simulation site were possible with the efforts of my colleague PhD student Quang Nguyen for geospatial analysis and mapping of the floodplain site. I am thankful to my fellow graduate students Seth Cobb, Fahmi Jaafar, Tucker Stafford and Gergo Arany.

I wouldn't be able to enter and exit the United States without the timely assistance of the Office of International Programs. I gratefully acknowledge the financial support from the NCITEC-CAIT project, Department of Civil Engineering and Graduate School as well as the Office of the Bursar. This dissertation wouldn't be possible without the School of Engineering's information technology staff Jeff, Gary and William, and Department of Civil Engineering technicians Tim and Jeff.

Nick and David: I'm over yonder.

NOTE: Trade/manufacturer names appear herein solely because they are considered essential to the objective of this dissertation.

TABLE OF CONTENTS

LIST OF TABLES

LIST OF FIGURES

I. INTRODUCTION

1.1 Background

Floods are the most common and damaging among all natural disasters. More than 4,400 occurrences of flood disasters have been reported globally between 1900 and 2016 [1]. As a result, around seven million people were killed, millions more were displaced and more than 3.4 billion people were affected [1]. Some of the most recent and devastating natural disasters worldwide are listed as follows [2, 3, 4, 5]:

- January 2010: Haiti and Chile (earthquakes)
- August 2010: Pakistan (flood)
- January 2011: Brazil (flood and landslide)
- March 2011: Japan (tsunami and Fukushima nuclear disaster)
- August 2011: Caribbean and U.S. Northeast Coast (Hurricane Irene)
- October 2011: Thailand (flood)
- October 2012: U.S. Northeast Coast, Caribbean and Canada (Hurricane Sandy)
- November 2013: Philippines (Typhoon Haiyan)
- May 2014: Southeast Europe (floods and landslides)
- April 2015: Nepal (earthquake)
- December 2015: United States (flood in Missouri)
- June 2016: United States (1000-year flood in West Virginia)

Apart from the countries listed above, Australia, Bangladesh, China, Dominican Republic, Ethiopia, France, Georgia, Hungary, India, Indonesia, Kenya, Lesotho, Mozambique, New Zealand, Oman, Peru, Russia, Saudi Arabia, Turkey, United Kingdom, Vietnam, Yemen and Zimbabwe were some of the other countries that were affected by floods during 2010 to 2015 [1, 2, 3]. Emergency Events Database (EM-DAT) lists 4,480 flood events globally between 1900 and 2015 as shown in Figure 1 [1]. Asia tops the list with 41% of all flood occurrences, followed by Americas (23%) and Africa (20%). Oceania witnessed the least percentage of floods; however, this still corresponds to 136 occurrences.

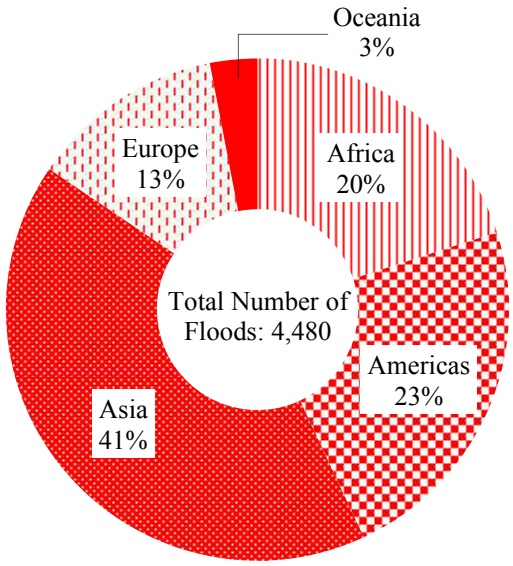

Figure 1. Occurrence of floods by continent, 1900-2015

Figure 2 shows top 20 countries with number of flood occurrence between 1900 and 2015 [1]. India tops the list with 264 occurrences followed by People's Republic of China (257) and United States (170). Islamic Republic of Iran and Vietnam have experienced 75 floods each, and

Ethiopia and Haiti had 51 floods occurred in each country. These 20 countries represent all five continents mentioned in Figure 1, and that they make up of almost 46% of all flood occurrences worldwide since 1900.

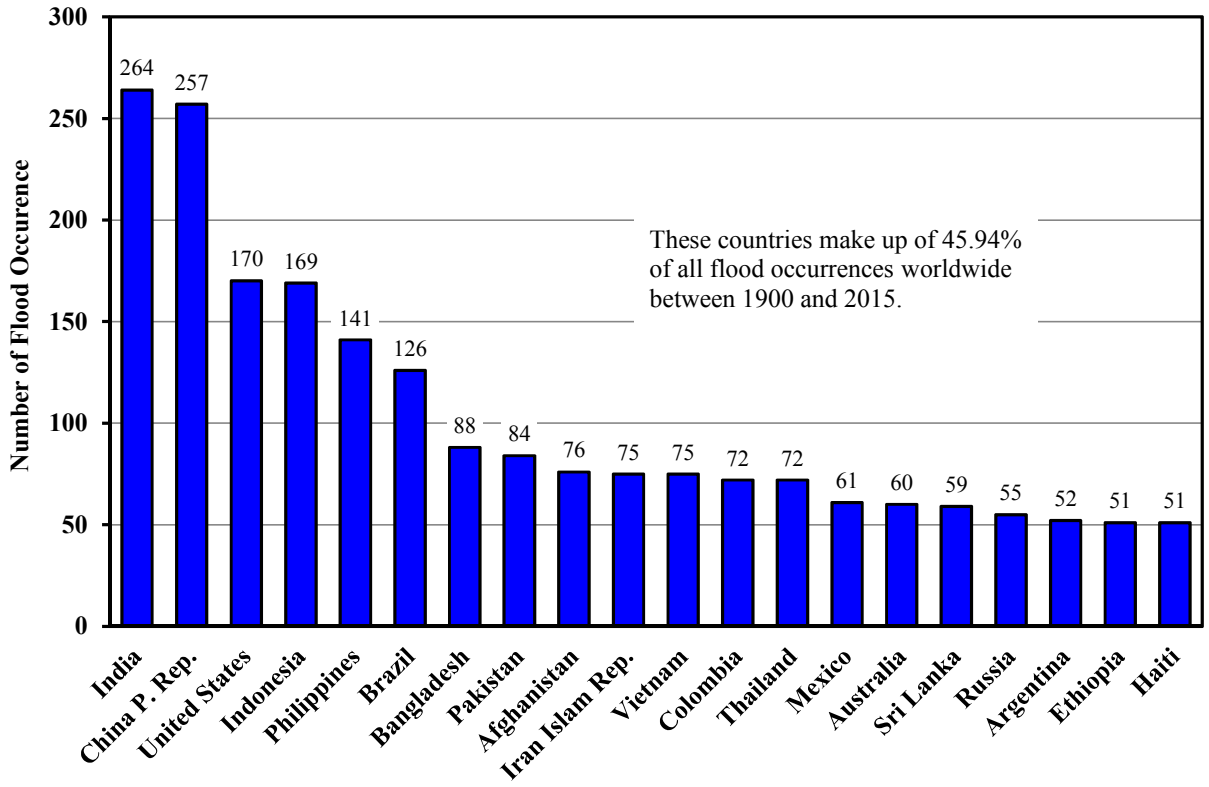

Figure 2. Top 20 countries with flood occurrence, 1900-2015

In 2010, almost 180 million people were affected by flood disasters [2]. Between 2008 and 2013, majority of people displacements were due to floods, and China, India, Philippines, Pakistan and Bangladesh suffered the most people displacements [3]. During 2013, 22 million people were displaced due to floods worldwide [3]. In the United States, the impacts are not much different.

According to the 2013 submissions of Threat and Hazard Identification and Risk Assessment to the United States Department of Homeland Security (DHS) [6], floods were identified to be the second worst threat for states and territories (70%), fourth worst threat for urban areas (63%) and the worst threat for tribal nations (48%) together with utility interruption. United States Geological Survey (USGS) [7] reported that more than 75 percent of declared federal disasters in the U.S. were related to floods.

Floods are reported to kill on average 140 people and cause $6 billion in property damage each year in the United States [8]. More than 100 significant flood events in the U.S. have been reported by Federal Emergency Management Agency (FEMA) as of February 2016 [9], where a significant event describes an event with 1,500 or more paid losses. About 60% of all disasters costing one billion dollars or more in the United States were related to weather and most occurred in the Southeastern states [10]. The Center for American Progress [11] reported that extreme weather events caused $208 billion of economic costs in the United States with more than 1,200 casualties between 2011 and 2013. Hurricane Katrina of 2005 on the Gulf Coast remains as the costliest natural disaster in U.S. history with more than $200 billion [8], followed by 2012 Hurricane Sandy on the East Coast, 2008 Hurricane Ike across many states and 2011 Hurricane Irene on the East Coast [9].

Between 1955 and 2000, total flood damage cost in the United States was nearly $87 billion [12]. A spatial map of billion-dollar flood damage cost in the Unites States between 1955 and 2000 is presented in Figure 3 [12]. According to Figure 3, states of Iowa, California and Louisiana suffered the most flood damage costs with $7.66 billion, $6.97 billion and $6.63 billion, respectively. These states are followed by Texas ($6.03 billion), Missouri ($4.67 billion), North Dakota ($4.51 billion) and Pennsylvania ($4.38 billion).

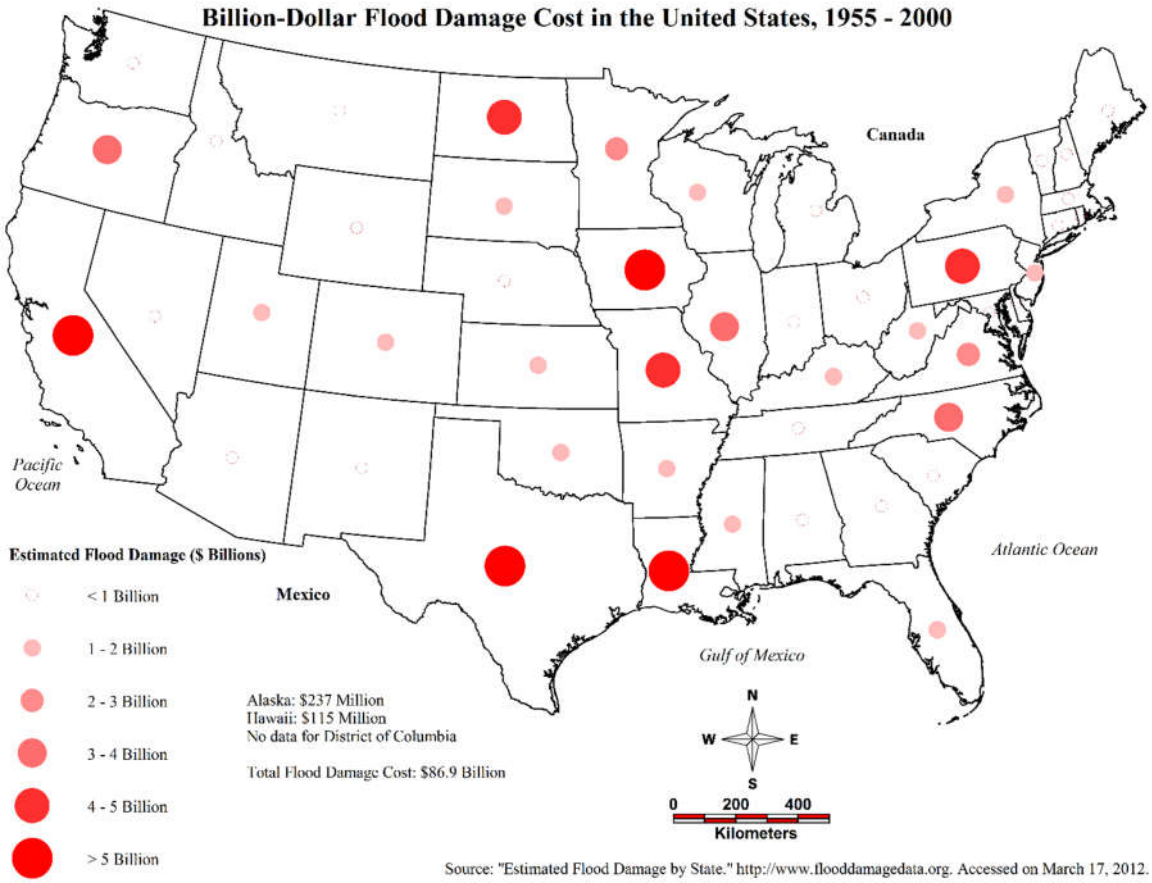

Figure 3. Billion-dollar flood damage costs in the United States, 1955-2000

The U.S. Global Change Research Program [13] reported that weather events, linked to climate impacts, are occurring at an increasing frequency. One of the key messages that the report points out is that disruption of transportation networks are happening nationwide due to extreme weather events; and that "such disruptions will increase" due to climate impacts. This agrees with the observation in U.S. National Climate Assessment report [14] that "very heavy rainstorms and snowstorms are getting more intense in most parts of the country." During the two-day heavy precipitation in August 2014, Baltimore-Washington International Airport witnessed "between a 500 year and 1,000 year rainfall" [15]. In 2015, flash floods caused further destruction in South Carolina [16] and Texas [17]. As reported by USGS [8], increasing

"urbanization and coastal development" mean increasing vulnerability. Climate impacts of SLR and ocean storm surges present other threats to the coastal infrastructure [13].

In view of climate impacts, the White House [18, 19] launched its Climate Action Plan in 2014 to prepare residents and communities in the United States for climate impact adaptation. Flood resilient design and the safeguard of infrastructure are important issues under current and future climate scenarios. The critical infrastructure assets include roads, bridges, rail lines, ports, airports, underground utilities, pipelines, levees/dikes and dams. Therefore, nationwide preparedness, mitigation and hardening for enhancing resilience against natural disasters remain a primary objective of the DHS to protect critical infrastructure [20].

Transportation infrastructure assets are vital in sustaining a strong economy [21]. Bridges are the most important critical infrastructure which serve for mobility and freight traffic. Disruption in mobility and freight services leads to huge economic losses as experienced in the U.S. and worldwide. Billions of dollars in repair and replacement costs of transportation assets were needed after the 2005 Hurricane Katrina, 2011 Hurricane Irene and 2012 Hurricane Sandy in the United States.

The Federal Highway Administration (FHWA) reported 605,411 bridges in the United States as of December 31, 2013 as shown in Figure 4 [22]. According to the spatial map in Figure 4, 10 states have 20,000 or more bridges. Texas ranks first with 52,561 bridges, which make up almost nine percent of the total National Bridge Inventory (NBI) of the United States [23]. "Deficient" defines those bridges which are structurally deficient or functionally obsolete. Thirteen states have less than 5,000 bridges and the District of Columbia has the lowest bridge count with 252 (0.04% of the total). Additionally, more than 24% of the total bridges in the U.S. are deficient (146,583). Furthermore, Texas and Pennsylvania have the highest percentage of

total deficient bridges (6.82% and 6.52%, respectively), followed by California (4.74%), New York (4.62%), Ohio (4.53%), Missouri (4.53%) and Iowa (4.28%). In 2013, the average age of the bridges in the United States was reported as 42 years [24].

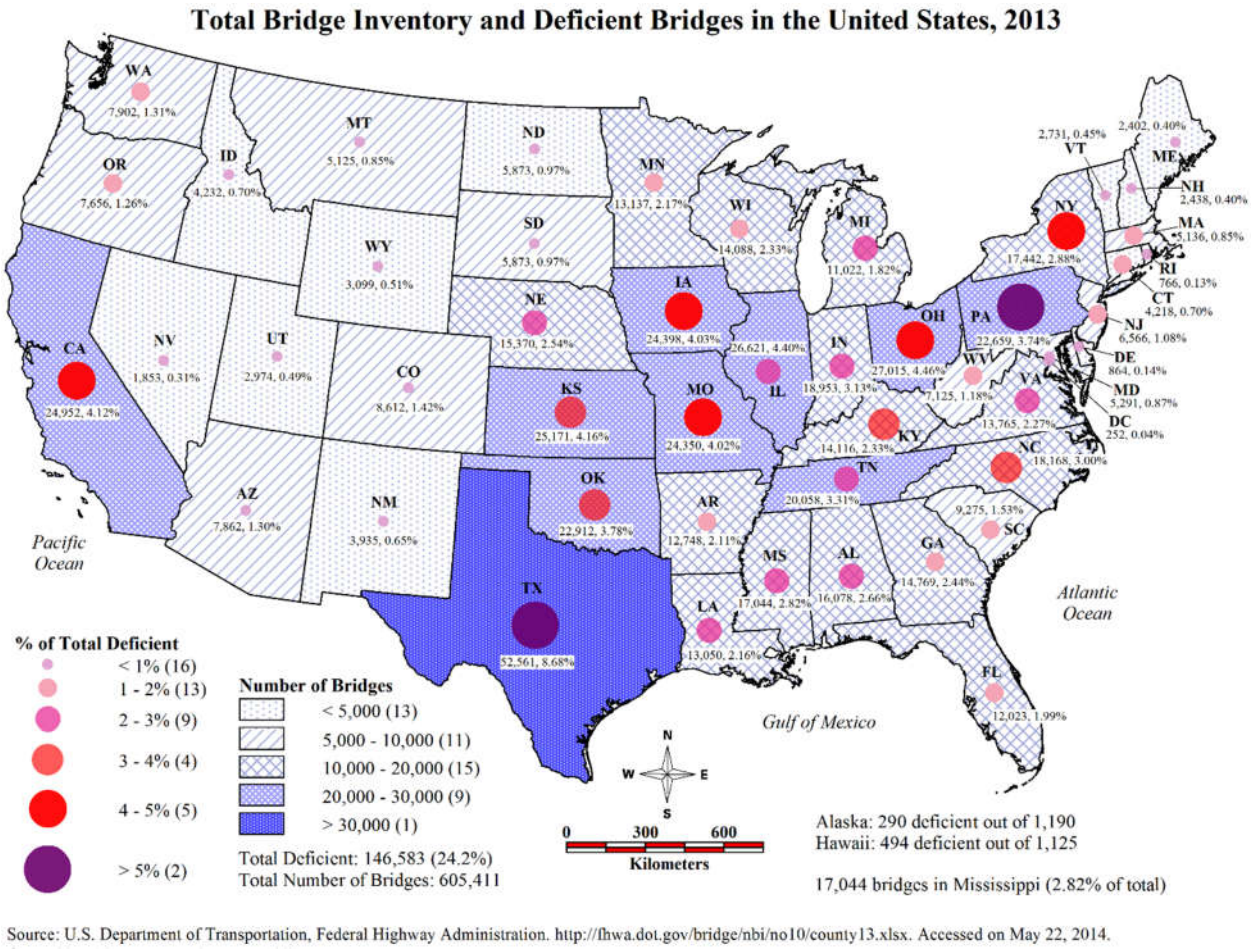

Source: U.S. Department of Transportation, Federal Highway Administration. http://fhwa.dot.gov/bridge/nbi/no10/county13.xlsx. Accessed on May 22, 2014.

Figure 4. Total bridge inventory and deficient bridges in the United States, 2013

1.2 Needs for Research Issues

1.2.1 Computational Flood Modeling

The general practice of flood simulation is based on one-dimensional (1D) modeling used in the Hydrologic Engineering Center-River Analysis System (HEC-RAS) software of the U.S.

Army Engineer Research and Development Center [25]. Most 1D models used in practice are inadequate for flood propagation due to discontinuous floodplains [26].

1.2.2 Flood Impact Assessment of Bridge Structures

Research has been done in recent years on the effects of storm surges, tsunamis, hurricanes and wave impacts on bridge structures [27, 28, 29, 30, 31, 32]. These studies introduced new formulas to calculate horizontal and vertical loads as well as improving drag, uplift and moment coefficients.

In 2014, after studying tsunami wave-loading impacts on five bridges, Azadbakht and Yim [33] introduced formulas for maximum horizontal force, downward maximum force and maximum uplift force. Lwin et al. [34] demonstrated how the performance of observed bridges was affected due to storm surge, wind, and debris and barges. They came up with estimated wave-induced vertical and horizontal load components. However, structural integrity assessment of the bridge structures was not investigated in these studies.

In 2010, Guo et al. [35] investigated hydraulic forces on bridge decks in a study. Their study was concerned with computational fluid dynamics (CFD) and reduced scale experiments. Minimum drag coefficient (found to be 0.5-0.8) was found to occur “perhaps” as the water reached the top of girders which was a transition to overtopping of the bridge deck. However, structural integrity assessment of the bridges was not a part of the study.

1.2.3 Finite Element Methodologies for Flood Impacts on Bridge Structures

In 2014, Yim et al. [36] developed a finite element model of a reinforced concrete arch bridge – Spencer Creek Bridge, Oregon subjected to lateral and uplift wave forces acquired with

by tsunami model. The ends of the superstructure were anticipated to move 132 mm (5.20 in) at the abutments. However, it was concluded that the bridge, which was constructed based on seismic design specifications, was able to resist the lateral and vertical forces generated by the tsunami model. Azadbakht and Yim [33] used finite element models to analyze strip sections of five bridges representative of California coast. The study employed CFD to compute horizontal and vertical forces as well as overturning moments on selected bridge superstructures, subjected to tsunami wave forces on bridge decks. However, bearings were not part of these finite element models.

1.2.4 Bridge Management System (BMS) Practice

Pioneering research on BMS framework, the Report 300 of the National Cooperative Highway Research Program (NCHRP) was released in 1987 [37]. FHWA supported the development of "Pontis" BMS optimization in 1993, as discussed in Chapter V.

The state of practice of BMS relies on the accumulation of inventory and condition data based on visual inspection and/or nondestructive testing [21]. However, one of the problems bridge management agencies constantly face is some missing data and inspection records. In 2007, Lee [38] came up with a method for a reliable bridge condition rating model which was based on the Artificial Neural Network (ANN) technique. Lee showed that missing condition/inspection records could be populated using ANN analysis based on the known condition ratings, which would help achieve a reliable bridge condition and inspection database.

An approach was presented by the NCHRP [39] that considered scour, fatigue, earthquakes and "other extreme events" as parts of network-level optimization. However, despite

the continuing improvements in BMS methodologies, Pontis BMS does not include an indicator of flood disaster impacts as a part of optimization formulation [40].

1.2.5 Motivation of the Dissertation and Summary of Research Needs

Further to the review presented in Section 1.1, year of 2011 witnessed one of the world's deadliest disasters which initiated with a 9.0-magnitude earthquake in the Pacific Ocean, off the coast of Japan. The earthquake triggered a tsunami which devastated northern part of Japan, which included Fukushima, Miyagi and Iwate. Due to nuclear reactor meltdown, Fukushima remains as the worst nuclear disaster since 1986 Chernobyl disaster [41].

During October-November 2011, Thailand suffered a flood disaster due to torrential rains, which ended up devastating Bangkok region. The green campus of Asian Institute of Technology (AIT) located north of Bangkok, a prominent higher education institution in Asia, was inundated with floodwater for several weeks in late October and most of November 2011 [12].

December 2015 floods in the United States caused severe devastation in Missouri and Illinois. Crest heights in Meramec River and parts of the Mississippi River were reported as record-high since the Great Flood of 1993. The flood caused the closure of I-70 in two locations, I-44 in three locations and a section of I-55 [4]. Photos from the affected areas are shown in Figures 5, 6 and 7.

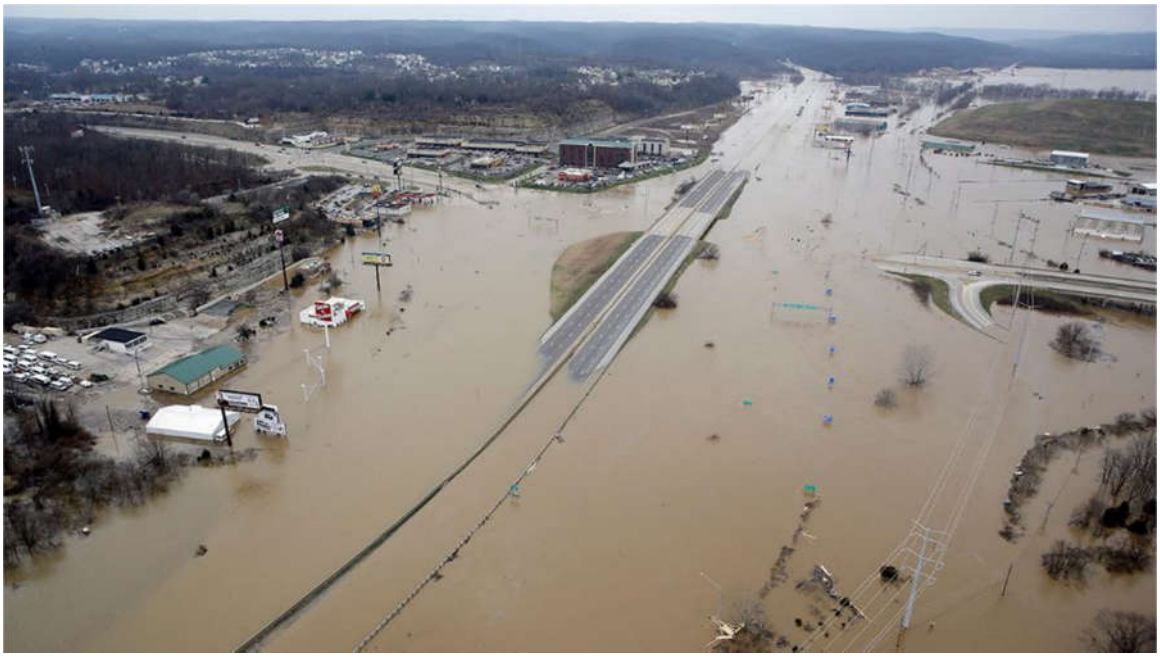

Figure 5. A view of I-44, Valley Park, MO, 2015
(Photo Credit: Weather.com)

Figure 6. Inundated homes in Pacific, MO, 2015
(Photo Credit: Weather.com)

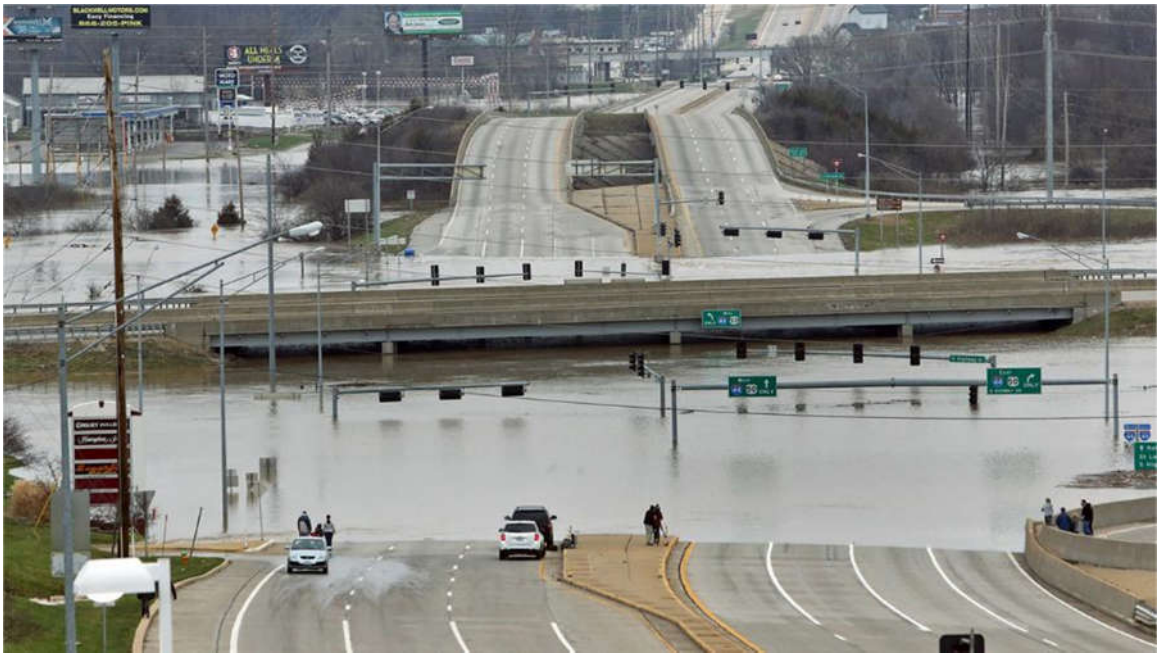

Figure 7. Inundated deck of I-44 Bridge and Highway 141, St. Louis, MO, 2015
(Photo Credit: Weather.com)

The extensive review in this research shows that there is no comprehensive approach for structural integrity assessment of bridge structures subjected to lateral floodwater forces. Furthermore, no results were reported for assessing the impacts of floodwater forces on bridge structures (i.e. floodwater velocity, floodwater depth, maximum discharge etc.). The literature review shows that there was no modeling of an extreme flood inundation, and no approach for expected floodwater velocities, which is one of the most difficult steps in quantifying moving water loads [29].

"Vertical underclearance" information on river-crossing bridges is not indicated in the NBI [23]. Even though the NBI takes "overtopping" into account ("Item 71 - Waterway Adequacy"), current state-of-practice of BMS do not include vertical underclearance data to indicate flood vulnerability, as part of their optimization criteria. There is a clear research need to

address the flood impacts on bridges which is currently not considered in existing design and BMS practice.

In order to address these research needs, Center for Advanced Infrastructure Technology (CAIT) at the University of Mississippi conducted Project 2012 – 25: "Disaster Protection of Transport Infrastructure and Mobility Using Flood Risk Modeling and Geospatial Visualization" in 2012 [42, 43]. The project addressed the National Center for Intermodal Transportation for Economic Competitiveness (NCITEC) theme of sustainable, efficient, safe and secure national intermodal transportation network that can be made resilient to disasters. Specific focus of the flood simulation project was on developing technologies to enhance decision support system (DSS) for flood resilient transportation infrastructure [43].

1.3 Research Objectives, Scope and Methodology

1.3.1 Research Objectives and Scope

The research objectives are to:

1. Implement flood inundation model for selected multimodal surface transportation corridor site.
2. Use a Three Dimensional-Finite Element (3D-FE) model of a reinforced concrete highway bridge over a river for analyzing flood impacts.
3. Assess structural integrity of the highway bridge structure subjected to lateral floodwater forces.
4. Recommend a geospatial DSS framework for sustainable bridge maintenance management considering flood risk vulnerability.

This research scope is limited to:

- Sardis, Panola County, Mississippi: Multimodal surface transportation corridors in this floodplain site for the extreme flood modeling and simulation.
- US-51 Highway bridge on downstream Little Tallahatchie River in the floodplain site: Reinforced concrete girder bridge for 3D-FE simulation and structural integrity assessment. The bridge is located in Sardis, Panola County, Mississippi.

1.3.2 Research Methodology

The research methodology is presented in a flowchart as shown in Figure 8. Roman numerals indicate chapters.

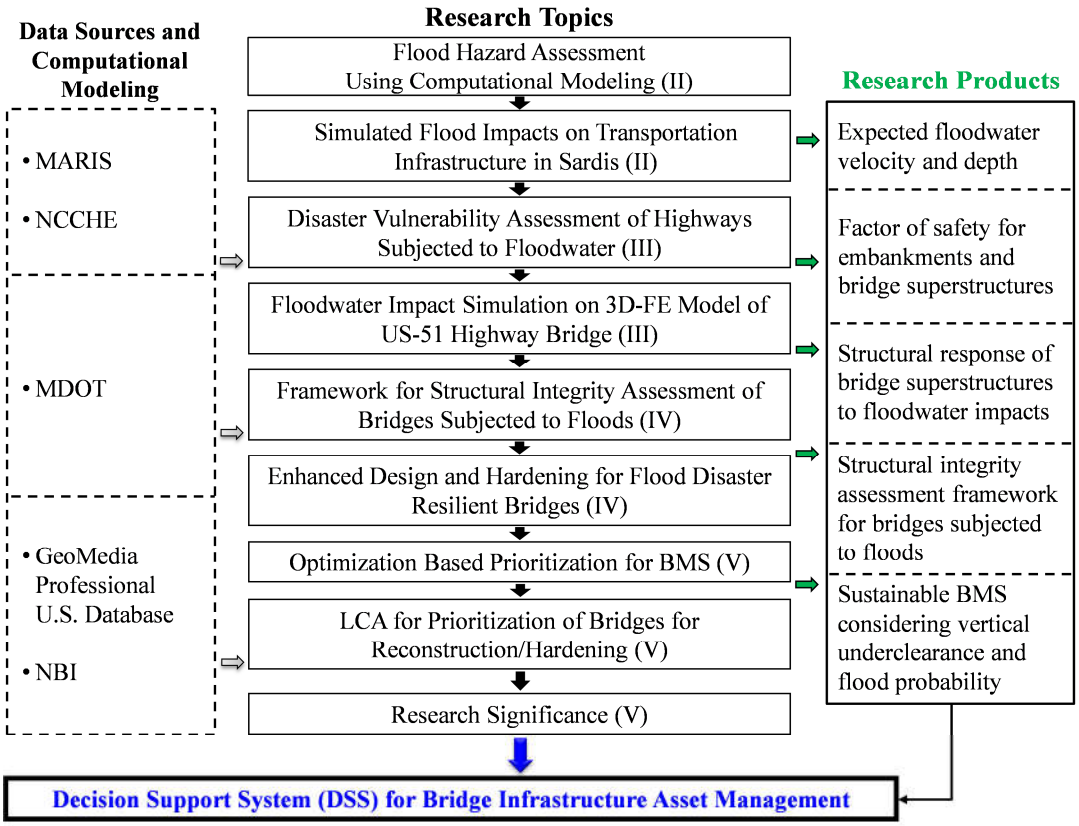

Figure 8. Research methodology flow chart

1.4 Overview of Dissertation

Chapter I describes out the background, needs for research issues, research objectives, research scope and methodology, and overview of the dissertation.

Chapter II presents a review of computational flood modeling methodologies, followed by the NCITEC flood disaster resilient transportation infrastructure project. Impacts of the simulated flood inundation on the transportation infrastructure are shown. Chapter II concludes with field evidence of bridge failures due to floodwater forces.

Chapter III, after a literature review of flood disaster impacts on bridge structures, discusses disaster vulnerability assessment of highways subjected to floodwater. Highway embankment stability, scouring at bridge foundations and structural integrity of bridge superstructures are presented. A floodwater impact simulation is performed on a 3D-FE model of the US-51 Highway bridge. Chapter III concludes with the lessons learned from the results of the 3D-FE simulation.

Chapter IV describes a framework for structural integrity assessment of bridge structures subjected to floods. Enhanced design and hardening considerations are presented for flood disaster resilient bridges. Resilience management considering hydrodynamic forces of ocean wave surges due to sea level rise (SLR) and tsunamis are discussed.

Chapter V reviews BMS practice in the United States and other countries. Optimization based prioritization for BMS considering vertical underclearance and flood probability is described. This is followed by an example of a life cycle analysis (LCA) for reconstruction and/or hardening for a highway bridge. Significance of this research concludes Chapter V.

Chapter VI presents the summary of research, conclusions of the dissertation, and recommendations for future research. This is followed by a list of the references that have been

used in the dissertation. Appendix and vita conclude the dissertation. Overview of the dissertation is presented in Figure 9. Necessary unit conversions are done as per Glover [44].

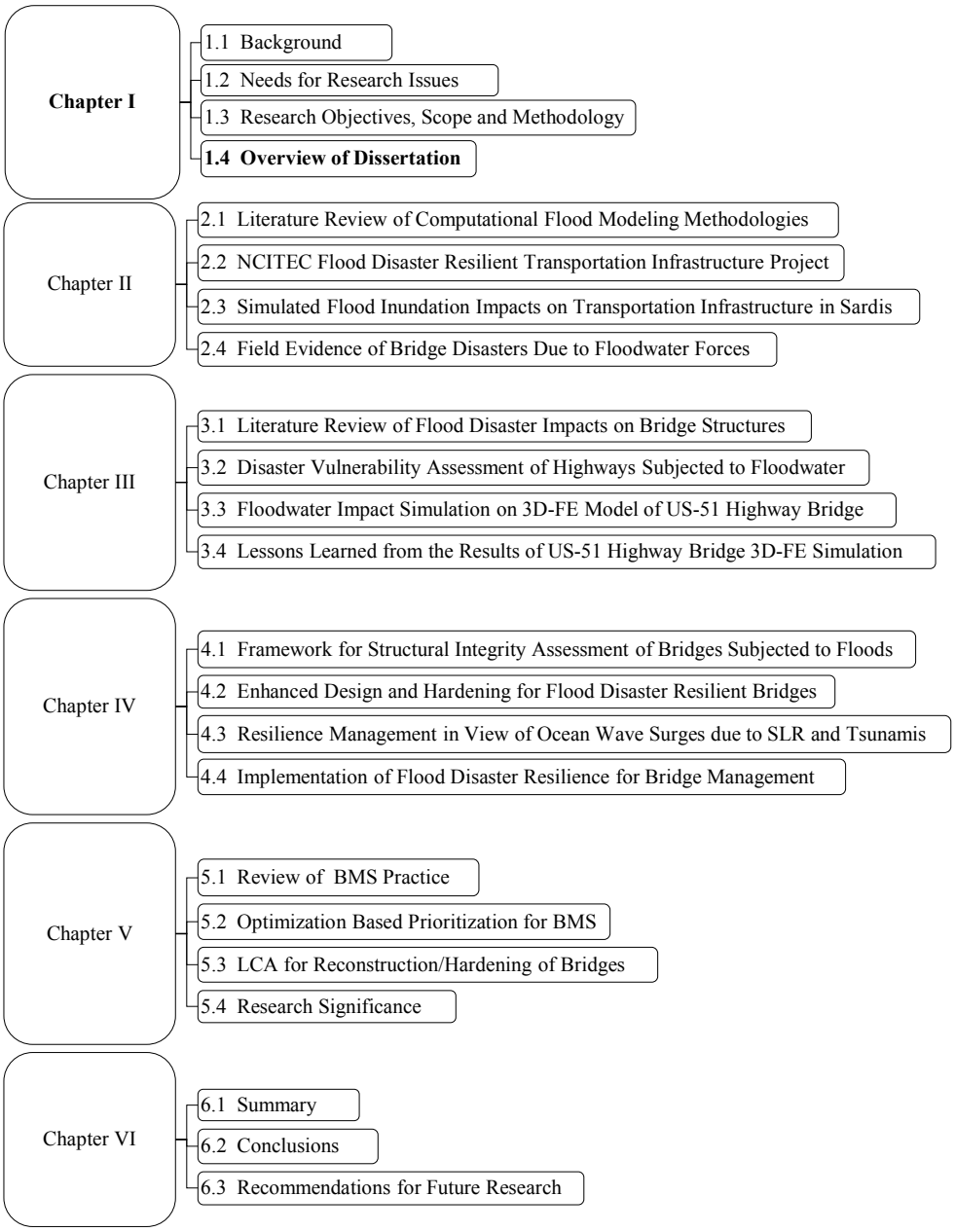

Figure 9. Dissertation overview

II. FLOOD HAZARD ASSESSMENT USING COMPUTATIONAL FLOOD MODELING

2.1 Literature Review of Computational Flood Modeling Methodologies

2.1.1 National Flood Insurance Program (NFIP)

As an outcome of the hurricanes in the Gulf Coast and Mississippi River floods in the 50s and 60s, Congress passed the National Flood Insurance Act in 1968. This enabled the subsequent National Flood Insurance Program (NFIP) to "guide future development away from flood hazard areas" [45]. Later in 1979, NFIP was transferred to FEMA [45].

Flood hazard information in the United States is presented on a Flood Insurance Rate Map (FIRM) and on a Flood Boundary and Floodway Map (FBFM). Floodplains on these maps are divided into (i) Riverine Floodplains and (ii) Coastal Floodplains. Some of the information FIRM and FBFM maps include [45]:

- Flood elevations of varying intensity,
- Area inundated by various magnitudes of flooding,
- Floodway boundaries.

By the year 2000, FEMA had paper maps for the entire United States. This was followed by the online and publicly available versions of those maps [46]. The FIRM maps are "developed based on statistical analyses of records of river flow, storm tides, and rainfall,

hydrologic and hydraulic analyses, topographic surveys, and information obtained through consultation with the community" [47]. The riverine and coastal floodplains in FIRM are divided into zones as described below [48]:

- Special Flood Hazard Area (SFHA): Flood hazard areas shown on a FIRM are identified as SFHA. FEMA defines SFHA as "the area that will be inundated by the flood event having a 1-percent chance of being equaled or exceeded in any given year" [48]. The annual 1-percent-annual-chance flood event is also referred to as the base flood or 100-year flood. Zones of SFHA are:
  - Zones A, AO, AH, A1-A30, AE, A99, AR, AR/AE, AR/AO, AR/A1-A30, AR/A,
  - Zones V, Zone VE and Zones V1-V30.
- Moderate flood hazard area: These areas are "the areas between the limits of the base flood and the 0.2-percent-annual-chance (or 500-year) flood:"
  - Zone B,
  - Zone X (shaded).
- Minimal flood hazard area: These are the areas outside the SFHA and are higher than the elevation of the 0.2-percent-annual-chance flood:
  - Zone C,
  - Zone X (unshaded).

The FIRM methodology can be applied to any location in the world. These flood hazard maps were made possible with the computational flood modeling software 1D HEC-RAS of the United States Army Corps of Engineers (USACE), which will be described in the next section.

2.1.2 HEC-RAS 4.1

HEC-RAS 4.1 [25] is 1D flood simulation software developed by USACE that is capable of simulating steady and unsteady flow routing. The steady flow component of HEC-RAS simulation engine is capable of modeling subcritical, supercritical and mixed flow regime water surface profiles. Outputs include floodwater inundation area, discharge, velocity, depth and arrival time [49].

For the case of water surface profiles (i.e. floodwater depth) in steady flow routing, HEC-RAS simulation engine solves the 1D energy equation (Equation 2.1) [49]. More theory can be found in hydraulic reference manual [49].

$$Z_2 + Y_2 + \frac{a_2 V_2^2}{2g} = Z_1 + Y_1 + \frac{a_1 V_1^2}{2g} + h_e \tag{2.1}$$

where,

Z_1, Z_2 = Elevation of the main channel inverts
Y_1, Y_2 = Depth of water at cross-sections
V_1, V_2 = Average velocities (total discharge ÷ total flow area)
a_1, a_2 = Velocity weighting coefficients
g = Gravitational acceleration
h_e = Energy head loss

In unsteady flow routing, the HEC-RAS' simulation engine evaluates the terms of continuity (Equation 2.2) and momentum (Equation 2.3) equations [49].

$$\frac{\partial A}{\partial t} + \frac{\partial S}{\partial t} + \frac{\partial Q}{\partial x} - q_1 = 0 \tag{2.2}$$

where,

A = Cross-sectional area

t = Time
S = Storage from non-conveying portions of cross-section
Q = Flow
x = Distance along the channel
q_l = Lateral inflow per unit distance

$$\frac{\partial Q}{\partial t}+\frac{\partial (VQ)}{\partial x}+gA\left(\frac{\partial z}{\partial x}+S_f\right)=0 \tag{2.3}$$

where,

Q = Flow
t = Time
V = Velocity
x = Distance along the channel
g = Gravitational acceleration
A = Cross-sectional area
z = Water surface elevation
S_f = Friction slope

Simulation results/output are calculated by implicit finite difference approximation of the above equations [49]. More theory can be found in hydraulic reference manual [49].

Some of the inherent limitations of 1D flood modeling include modeling non-channelized flows, information on flood arrival time, simulating shockwaves and flow direction when presented on 2D maps.

2.2 NCITEC Flood Disaster Resilient Transportation Infrastructure Project

2.2.1 CCHE2D-FLOOD

Two-dimensional (2D) flood modeling software CCHE2D-FLOOD [50] was implemented by the National Center for Computational Hydroscience and Engineering

(NCCHE) as part of the NCITEC project [43]. The NCCHE program analyzes mixed flow regimes differently than many other flood simulation programs [51]. This flood modeling software is a component of the Decision Support System for Water Infrastructural Security (DSS-WISE) software package [52], developed at the University of Mississippi. The DSS-WISE software is being used by the DHS, FEMA and USACE for river flooding simulations [52, 53]. During the record-breaking floods of the Mississippi River in 2011, on request from the Mississippi Emergency Management Agency (MEMA) and the United States Department of Agriculture (USDA), CCHE2D-FLOOD software was used for several simulations to support emergency planning activities and to help with the preparation of evacuation plans. CCHE2D-FLOOD has been used by engineers, Geographic Information System (GIS) technicians and emergency management agencies [52, 53].

The simulation engine of the CCHE2D-FLOOD flood modeling software offers unique capabilities that are not generally offered on commercially available flood simulation software packages [54]. It solves conservative forms of full dynamic 2D shallow water equations, which describe the unsteady non-uniform overland flow on flat to complex natural topography. The CCHE2D-FLOOD simulation engine discretizes shallow water equations over a regular Cartesian grid using the Finite Volume Method (FVM). The resulting model captures shocks, handles mixed flow regimes and discontinuous flow domains as well as wetting and drying. Details of the 2D scheme can be found in [54]. Some of the features of CCHE2D-FLOOD can be listed as follows [55]:

- Provides realistic scenario modeling for complex real-life engineering applications.
- Uses FVM and shock capturing scheme to solve conservative forms of full dynamic 2D shallow water equations.

- Calculates fluxes using the shock capturing Harten-Lax-van Leer-Contact (HLLC) scheme.
- Handles mixed flow regimes and disconnected flow domains.
- Analyzes wetting and drying areas of the simulation domain.
- Uses the Digital Elevation Model (DEM) as computational grid.
- Multi-core and multi-threaded parallel programming to increase computation speed.

The following outputs are provided after the flood simulations [55]:

- Georeferenced raster and vector (.shp) files for general risk mapping:
    - Extent of the flood,
    - Map of maximum flood depths (maximum depth achieved during the simulation),
    - Map of flood depths at final time step,
    - Map of flood arrival time (dry areas becoming wet regardless of the flow depth),
    - Map of maximum specific discharge (velocity × depth), which also gives an idea about the floodwater momentum,
    - Map of flow velocity vector (x and y components).

- Time series data (.csv files) for specified locations, particularly for evaluation of potential impacts to transportation and other infrastructure:
    - Time history of flow depths and flow velocity vectors (x and y components) along specified longitudinal observation profiles,
    - Discharge hydrographs at specified cross-sections,

- Time history of flow depth, floodwater surface elevation, flow velocity vector and flow direction at specified observation points.

➢ Products for easy communication of information:

- A .kmz file of the results for visualization on Google Earth (does not necessitate any special software).

Current users of DSS-WISE and CCHE2D-FLOOD include [54]:

- DHS Dams Sector
- USACE
- Engineer Research and Development Center (ERDC) of USACE
- Modeling, Mapping & Consequences Production Center (MMC) of USACE
- Mississippi Department of Environmental Quality (MDEQ)

2.2.2 Flood Simulation Approach

Ten major steps are involved in the flood simulation and impact assessment approach. This approach can be implemented with flood simulation software such as CCHE2D-FLOOD and any off-the-shelf geospatial software:

1. Select study sites (in Mississippi).
2. Acquire high-resolution 2 ft (61 cm) imagery for 2D feature extraction in GeoMedia Professional/ArcGIS geospatial software.
3. Create planimetrics and coordinates of river centerline (CL), cross-sections, highways, rail lines and other built infrastructure assets.

4. Setup a geospatial domain for flood simulation software CCHE2D-FLOOD – resample the DEM based on a specified computational cell size (CCS).
5. Run extreme flood simulations for high-resolution bare ground DEM.
6. Analyze flood simulation outputs for floodwater vectors and lateral hydrodynamic forces at river CL and cross-sections.
7. Run extreme flood simulations for DEM modified with built infrastructure elevations.
8. Analyze flood simulation outputs for floodwater vectors and lateral hydrodynamic forces at river CL and cross-sections.
9. Compare the flood depths and inundations in Steps 6 and 8.
10. Use floodwater simulation results for structural integrity assessment of transportation infrastructure.

The DEM (Figure 10) of the study area was acquired through the cooperation of Mississippi Department of Transportation (MDOT) and Mississippi Automated Resource Information System (MARIS). The DEM used in flood simulation has an absolute accuracy of elevation 1.55 m, whereas the relative accuracy of elevation is 0.81 m [56], which is sufficient to represent almost all important terrain and built infrastructure features that may influence the flood propagation, such as buildings, roads, embankments, etc. The DEM was based on the topographic data collected by an airborne laser survey (i.e. LIDAR) for the region and was used by USGS [56].

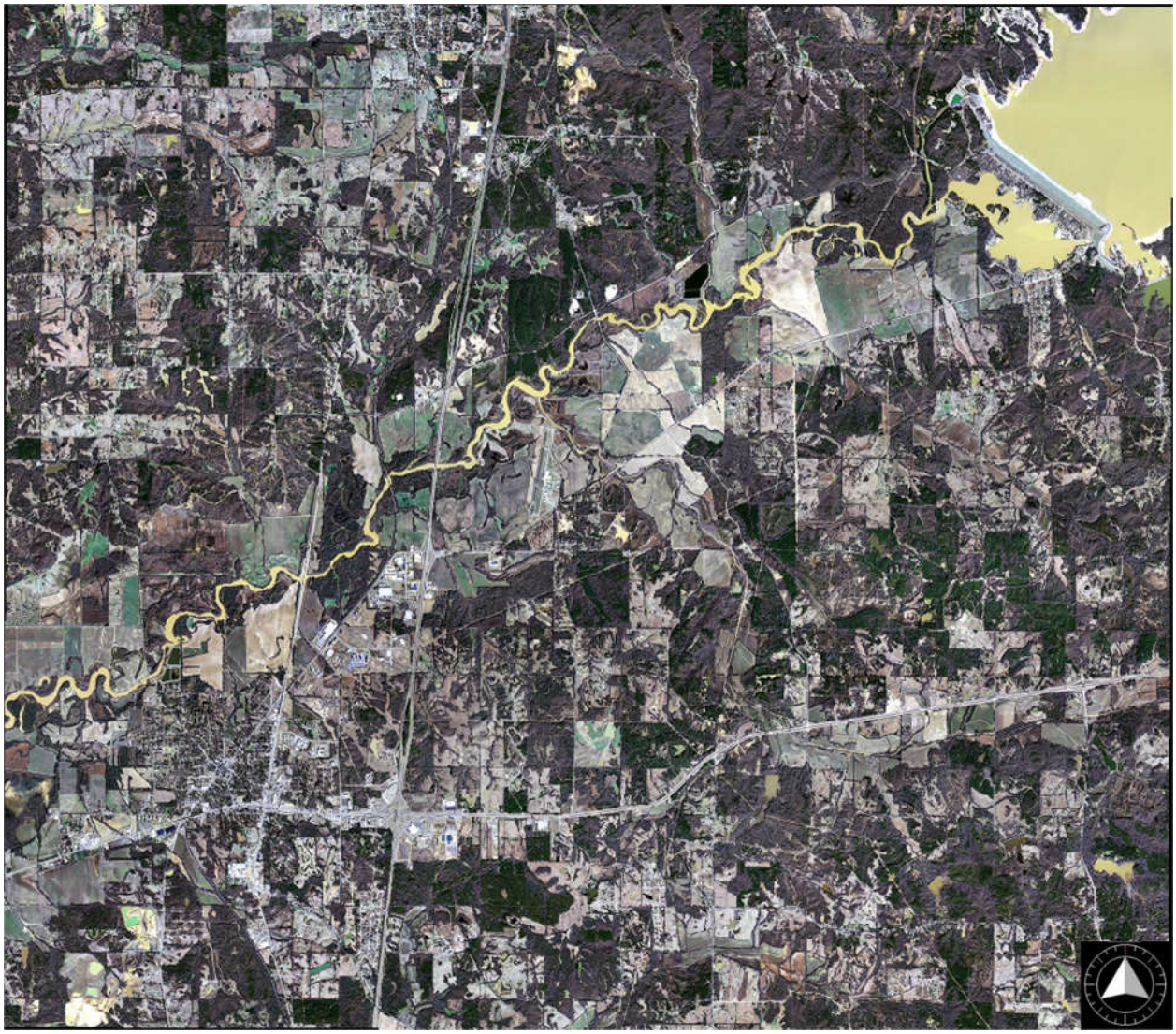

Figure 10. MARIS 2-ft DEM of Sardis (1:75,000 map scale)

The domain size of the simulation is 20,580 meters west-east by 17,260 meters north-south, corresponding to 2,058 columns and 1,726 rows of 10 m by 10 m size cells (Figure 11). This corresponds to a total of 3,552,108 computational cells. The 30 m and 10 m CCS simulations did not consider built infrastructure, whereas the transportation and building infrastructure features were included in 5 m and 3 m CCS simulations.

Figure 11. NCCHE's 10-m (CCS) resample of Sardis (1:75,000 map scale)

Figure 12 shows the observation profile, cross-section observation lines and observation points on downstream Little Tallahatchie River CL. More detailed information can be found in Durmus et al. [53]. The Sardis Site features I-55, US-51, two minor highways, a rail line, a small airport, churches, and low-density residential and commercial areas. The CCHE2D-FLOOD simulation module provided 2D raster maps of flood propagation for the entire 48 hours and data

files of flood arrival times, flood depths, flood discharges and floodwater velocities. The results of the flood simulations were generated for:

- 1 observation profile (along the river CL)
- 29 cross-section observation lines (perpendicular to the river CL)
- 12 observation points on cross-section observation lines (at selected infrastructure)

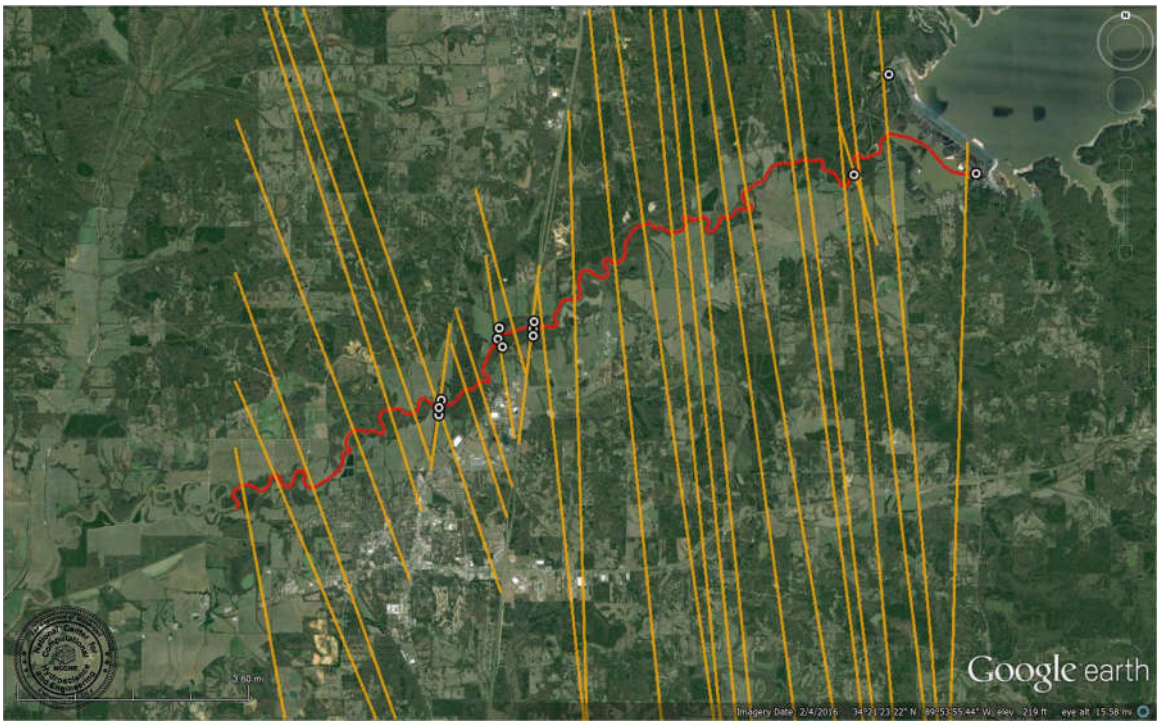

Figure 12. Observation profile (red), observation lines (orange) and observation points

The flood simulation used site planimetrics, river CL and cross-sections, which were created from 2 ft (61 cm) high-resolution aerial imagery. The discharge hydrograph (Figure 13) used in the flood simulations was "associated with a full spillway discharge" [57]. The hydrograph reaches a maximum discharge of 16,450 m^3/s at t = 1.97 hr. Typical duration of flood simulation from the starting point to the west end of the simulation domain was 48 hours.

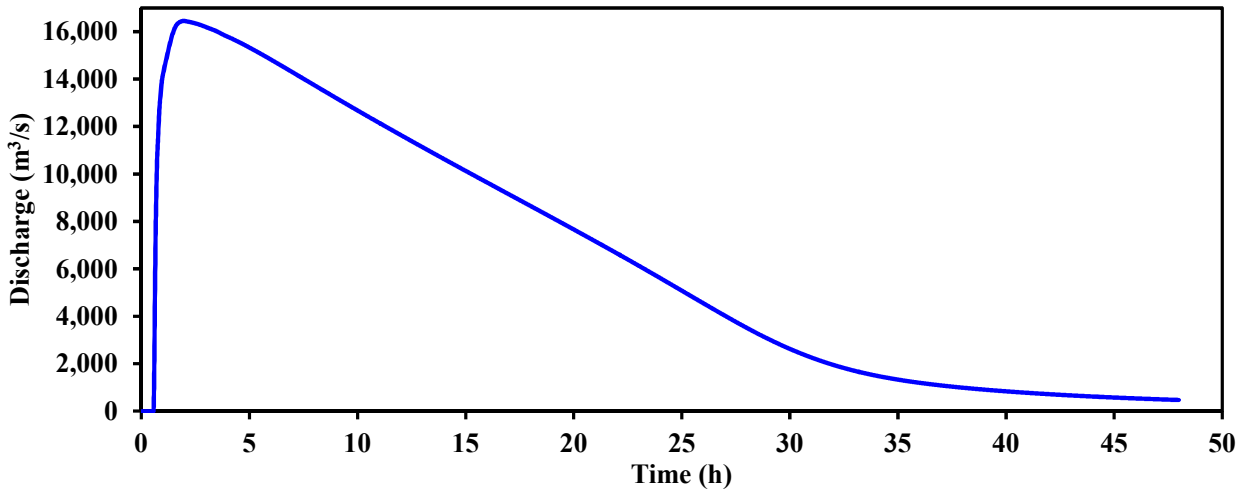

Figure 13. Discharge hydrograph of Sardis Site flood simulation

Flood scenarios were simulated based on resampled CCS. The discharge hydrograph for 30 m CCS was computed during the simulation by imposing a trapezoidal spillway formed in 0.44 hours. Discharge hydrographs for smaller cell sizes were obtained during the simulation with 30 m CCS and were directly imposed as a source downstream of the simulation start. Extreme flood simulation scenarios for different CCS are presented in Table 1.

Table 1. Extreme flood simulation scenarios

Computational Domain	30-m Resample	10-m Resample	5-m Resample	3-m Resample
Cell size (m × m)	30 × 30	10 × 10	5 × 5	3 × 3
Number of Columns	3,085	2,058	4,116	6,860
Number of Rows	2,589	1,726	3,452	5,753
Number of Cells	7,987,065	3,552,108	14,208,432	39,465,580
East-West Extent (km)	92.55	20.58	20.58	20.58
North-South Extent (km)	77.67	17.26	17.26	17.26
Spatial Reference	NAD_1983_UTM_Zone_16N			
Datum	D_North American_1983			
Min Elevation (m)	37.964	53.41	53.147	53.147
Max Elevation (m)	189.784	136.07	139.868	139.9
Structures Burned into the DEM?	No	No	Yes	Yes
Bridge Openings	Cleared	Cleared	Cleared	Cleared
Manning's Roughness	Overall Manning's Roughness of 0.035 $m^{-1/3}s$			

2.3 Simulated Flood Inundation Impacts on Transportation Infrastructure in Sardis

2.3.1 Results of the CCHE2D-FLOOD Flood Simulation

Visualization of the flood simulation is presented in Figure 14. It shows the transportation and building infrastructure feature locations and maximum floodwater depths in the floodplain.

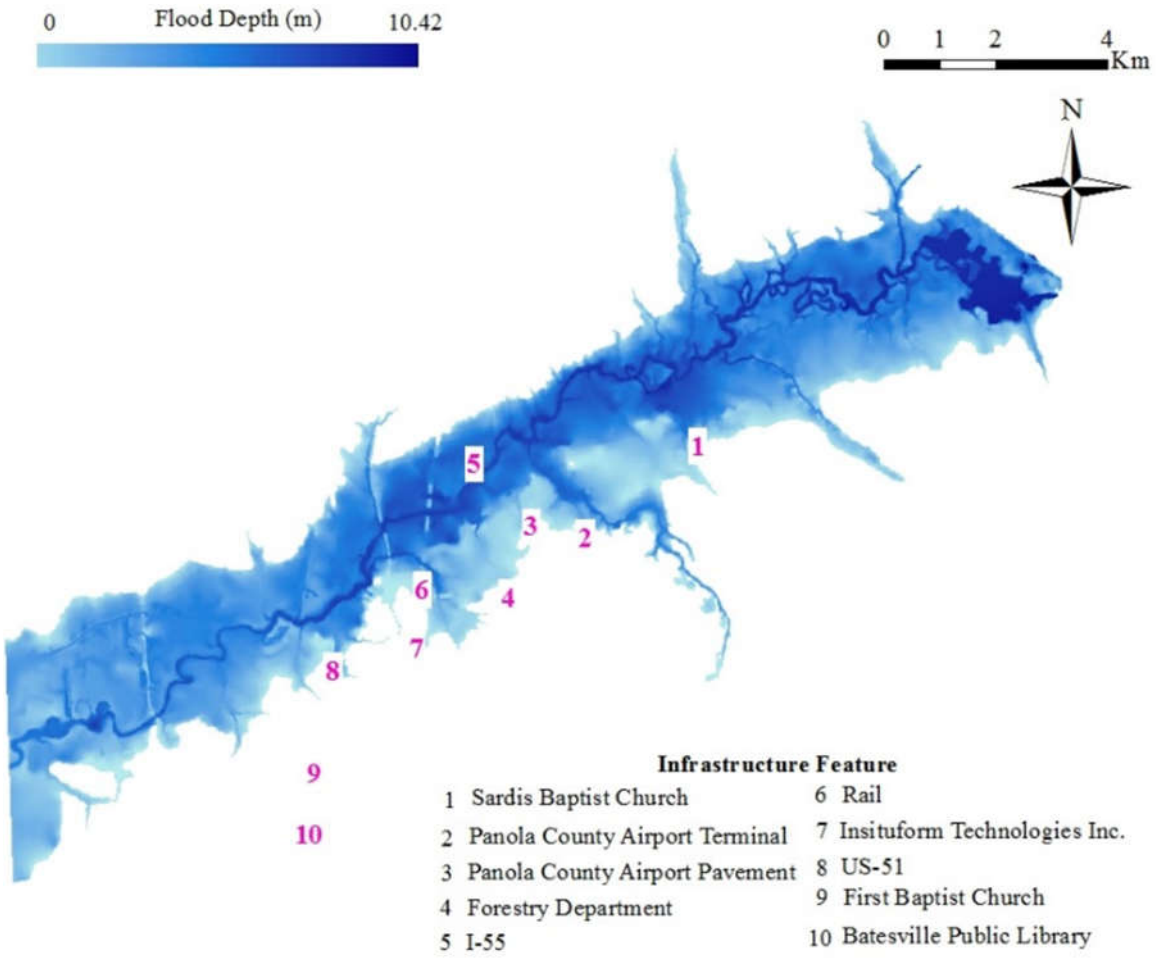

Figure 14. Visualization of NCCHE 10-m CCS flood simulation

Visualization of the flood simulation with infrastructure assets impacted by the inundation is presented in Figure 15. It shows the locations of transportation and building

features, and maximum flood depths. Geospatial analysis shows that total flood inundation covers an area of 22.46 mi^2 (58.16 km^2), where the floodwater depth reaches up to 34.19 ft (10.42 m) within the flood inundation area. The nearest building to the simulation start point is Sardis Lake Baptist Church at a linear distance of 4.4 miles (7.03 km). Batesville Public Library is located 10.3 miles (16.51 km) away from the simulation start point.

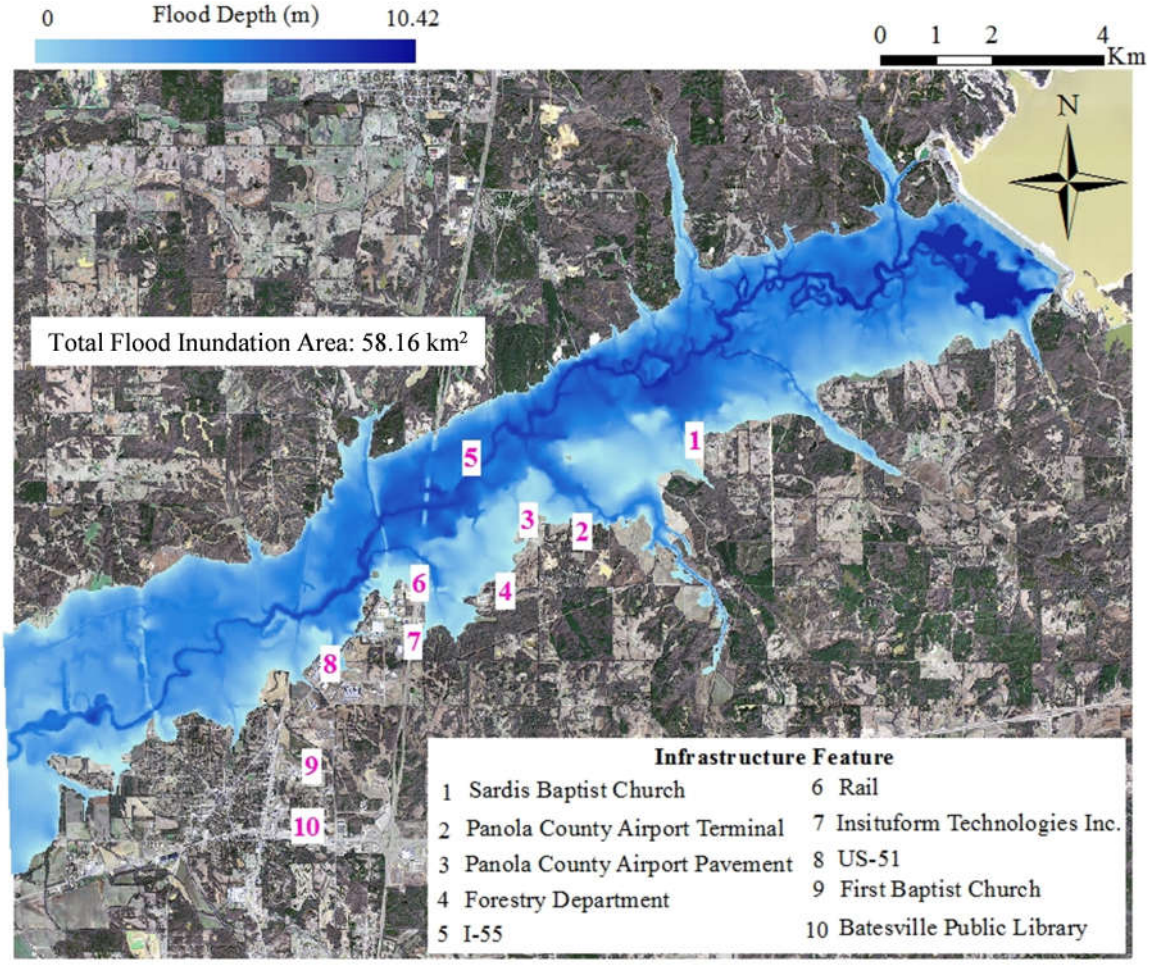

Figure 15. Visualization of NCCHE 10-m CCS flood simulation over the DEM of Sardis

A summary of the results for the transportation infrastructure in the study area is given in Table 2. In the 10 m CCS simulation, the flood arrives in less than 2.88 hours to I-55 Highway

and Rail Line bridges and in less than 3.36 hours to US-51 Highway bridge. The maximum floodwater depths are 7.94 m, 8.04 m and 7.53 m for I-55, Rail and US-51 bridges, respectively. The maximum floodwater velocity reaches 1.77 m/s (5.5 ft/s or 3.96 mph), 3.47 m/s (11.4 ft/s or 7.76 mph) and 2.63 m/s (8.6 ft/s or 5.88 mph) at I-55, Rail and US-51 bridges, respectively. These velocity values are the magnitudes of the floodwater velocity, and angle of attack is not taken into account.

Table 2. Flood simulation results at the transportation infrastructure

Infrastructure Feature	Linear Distance from Simulation Start	CCS	Type of Terrain	Flood Arrival Time	Floodwater H_{max}	Floodwater H_{final}	Floodwater v @ H_{max}	Floodwater v_{max}	
-	(km)	(m × m)	-	(hr)	(m)	(m)	(m/s)	(m/s)	(mph)
I-55 Bridge	11.9	30	N*	< 1.92	8.01	3.10	1.72	2.35	5.26
		10	N*	< 2.88	7.94	3.05	1.63	1.77	3.96
		5	NB**	< 2.88	9.78	5.00	1.56	3.14	7.02
		3	NB**	< 2.88	9.79	4.94	1.53	3.08	6.89
Rail Bridge	12.6	30	N*	< 2.40	8.05	3.48	2.63	3.73	8.34
		10	N*	< 2.88	8.04	3.46	2.54	3.47	7.76
		5	NB**	< 2.88	9.28	4.59	2.40	3.10	6.93
		3	NB**	< 2.88	9.32	4.58	2.47	3.07	6.87
US-51 Bridge	14.4	30	N*	< 2.40	7.62	3.97	2.42	2.42	5.41
		10	N*	< 3.36	7.53	3.94	2.63	2.63	5.88
		5	NB**	< 3.36	9.19	5.50	2.95	3.05	6.82
		3	NB**	< 3.36	9.18	5.48	3.02	3.14	7.02

* natural terrain only
** natural terrain with built infrastructure

Impacts of flood inundation on transportation infrastructure assets are presented in Table 3. The affected lengths of transportation infrastructure features are:

- 0.94 mi (1.52 km) of airport pavement
- 1.55 mi (2.50 km) of I-55 Highway
- 2.22 mi (3.58 km) of rail line
- 1.93 mi (3.10 km) of US-51 Highway

Maximum floodwater depths are:

- 9.68 ft (2.95 m) at airport pavement
- 26.1 ft (7.96 m) at I-55 Highway bridge
- 26.4 ft (8.04 m) at rail line bridge
- 24.7 ft (7.53 m) at US-51 Highway bridge

Maximum floodwater depths above transportation infrastructure features are:

- 6.4 ft (1.95 m) over airport pavement
- 0 ft (0 m) over I-55 Highway bridge
- 3.4 ft (1.04 m) over rail line bridge
- 1.7 ft (0.53 m) over US-51 Highway bridge

Table 3. Impacts of simulated flood on transportation infrastructure assets

Feature	Feature No.	Distance From Start (km)	Feature Height From Ground (m)	Maximum Floodwater Depth Above Ground (m)	Floodwater Depth Above Feature (m)	Affected Length of Feature (km)
Airport Pavement	3	9.97	1.00	2.95	1.95	1.52
I-55 Highway Bridge	5	11.90	8.00	7.96	0.00	2.50
Rail Line Bridge	6	12.61	7.00	8.04	1.04	3.58
US-51 Highway Bridge	8	14.36	7.00	7.53	0.53	3.10

Note: Feature height from ground is the height from river normal water surface for the bridges.

Table 4 presents the impacts of flood inundation on selected buildings in the flood simulation area. The Forestry Department and Batesville Public Library buildings are not affected by the simulated flood inundation given the fact that they are outside the floodplain.

Table 4. Impacts of simulated flood on building infrastructure assets

Feature	Feature No.	Distance From Start (km)	Feature Height From Ground (m)	Maximum Floodwater Depth Above Ground (m)	Floodwater Depth Above Feature (m)	Footprint Area (m^2)
Sardis Lake Baptist Church	1	7.03	5.00	1.84	0.00	2,059
Airport Terminal	2	9.95	6.00	0.15	0.00	95,106
Forestry Department	4	11.43	4.50	0.00	0.00	3,225
Insituform Technologies Inc.	7	12.74	6.50	0.00	0.00	3,218
First Baptist Church	9	15.46	5.00	0.00	0.00	1,368
Batesville Public Library	10	16.51	3.50	0.00	0.00	1,754

The 2D simulation results are summarized for transportation and building infrastructure features in Figure 16. Panola County Airport Pavement and US-51 Highway are completely inundated while Forestry Department, Insituform Technologies Inc., First Baptist Church and Batesville Public Library are not affected by simulated floodwater due to the fact they remain outside the floodplain. Detailed information can be found in Durmus et al. [53].

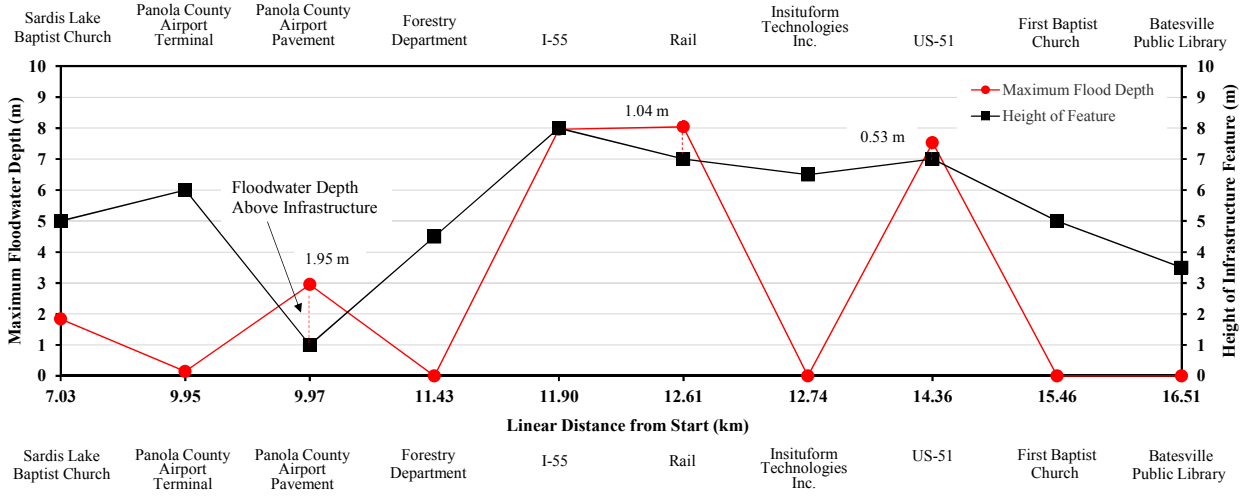

Figure 16. Floodwater depth at infrastructure features (10 m CCS simulation)

Key output of NCITEC Flood Disaster Resilient Transportation Infrastructure Project is presented in Appendix A.

2.3.2 Comparison of HEC-RAS and CCHE2D-FLOOD

Sardis Site flood simulation was performed in 1D HEC-RAS to assess the output differences between these flood simulation software. The same DEM of the area was used as the DEM input. The HEC-RAS software requires upstream and downstream boundary conditions whereas CCHE2D-FLOOD uses open boundary conditions. Table 5 represents the types of input and input parameters of the two flood simulations. Both of the software accepts any-resolution DEM.

Table 5. Input comparison between HEC-RAS and CCHE2D-FLOOD

Input Type	Input	HEC-RAS	CCHE2D-FLOOD
Geometry	River CL (km)	30.48	30.48
	Cross-section (km)	3 to 19	3 to 19
DEM	DEM	high-resolution ground DEM	
	Computational Domain	20,580 m W-E × 17,260 m N-S	
	CCS	varies	10 m × 10 m
Flow Data	Manning's n ($m^{-1/3}s$)	0.035	0.035
	Maximum Discharge (m^3/s)	16,450	16,450
	Domain Area (km^2)	355.21	355.21
	Simulation Time (hr)	24*	48
	Discharge Scenario	full spillway discharge	

* allowed maximum

Table 6 shows the comparison of output between 1D HEC-RAS and CCHE2D-FLOOD. According to Table 6, simulations results agree well with each other, where the maximum percent differences between calculated maximum flood depths and floodplain areas are less than

5%. The computational time of the simulation in 1D HEC-RAS is much smaller in comparison with CCHE2D-FLOOD. Details of the comparison can be found in Nguyen and Uddin [57].

Table 6. Output comparison between HEC-RAS and CCHE2D-FLOOD

Output	HEC-RAS	CCHE2D-FLOOD	% Difference
Maximum Channel Depth (m) @ 5 Cross-sections	9.71	9.32	4.22
	7.74	7.94	-2.52
	7.94	8.04	-1.24
	7.73	7.53	2.66
	6.05	5.81	4.13
Floodplain Area (km^2)	57.80	58.17	-0.64

Simulations are especially essential when the study is concerned with high priority protection areas [58]. Future prediction of riverine discharges is not possible by 2D flood simulations. An alternative to predict future riverine discharges is the Autoregressive Integrated Moving Average (ARIMA) method [59]. However, ARIMA modeling would require historical river gauge height and/or discharge data [59].

2.4 Field Evidence of Bridge Disasters Due to Floodwater Forces

FHWA lists 23 types of bridges in the United States [60]. In 2014, 40.7%, 248,284 out of 610,729, of total bridges in the U.S. were the "Stringer/Multi-Beam or Girder" type [60]. Furthermore, 29.2% (178,079) of the total bridges was reported as concrete (not including continuous concrete), whereas an additional 20.7% (126,169) was reported as prestressed concrete – not including prestressed concrete continuous [61]. Between 1980 and 2012, the number of bridge failures in the U.S. was reported as 1,062 [62]. Furthermore, 58% of those

bridge failures were girder bridges. Additionally, 28.3% of these failures were reported as due to floods.

Figures 17 and 18 show an aerial view of Biloxi Bay, Mississippi, and collapsed bridges between Harrison and Jackson counties, respectively in the aftermath of 2005 Hurricane Katrina. Mississippi was not the only state that was affected by the devastating forces of storm surge and floodwater. The Interstate 10 Highway bridge crossing Lake Pontchartrain in Orleans Parish of Louisiana was one of the bridges that was collapsed (Figure 19).

Figure 17. Aerial view of Biloxi Bay, MS after Hurricane Katrina
(Photo Credit: MCEER [63])

Figure 18. Bridge collapse on old route North of US-90, Biloxi Bay, MS, 2005
(Photo Credit: MCEER [63])

Figure 19. Collapsed I-10 Bridge over Lake Pontchartrain, Orleans Parrish, LA, 2005
(Photo Credit: MCEER [63])

2011 Hurricane Irene was another devastating event in U.S. history. Figure 20 shows a view of collapsed Forge Hill Road Bridge in New Windsor, New York. 2012 Hurricane Sandy was another weather-related disaster which caused huge economic losses in the United States. Mantoloking County in New Jersey was devastated by the disaster (Figure 21).

Figure 20. Washed-out Forge Hill Road Bridge after Hurricane Irene, New Windsor, NY (Photo Credit: Wikimedia.org)

Flash floods caused another bridge to collapse in Lafayette, Colorado in 2013. The collapsed bridge can be seen in Figure 22.

Figure 21. Aftermath of Hurricane Sandy in Mantoloking, NJ
(Photo Credit: Slate.com)

Figure 22. A collapsed bridge in Lafayette, CO, 2013
(Photo Credit: NOAA.gov)

In the summer of 2015, the Tex Wash Bridge on I-10 between Los Angeles, California and Phoenix, Arizona collapsed due to floods [64]. Views of the bridge are seen in Figures 23 and 24.

Figure 23. Collapsed Tex Wash Bridge on I-10 between CA and AZ, 2015
(Photo Credit: Gannett-cdn.com)

Figure 24. A close-up view of the Tex Wash Bridge superstructure after the collapse (Photo Credit: Gannett-cdn.com)

Vulnerability assessment of transportation infrastructure assets is an essential component of flood risk modeling. Protection of critical transportation infrastructure assets from extreme weather events such as floods would require the use of simulation results and an evaluation of their structural integrity, which will be described in Chapter III.

III. FLOOD DISASTER IMPACTS ON 3D-FE MODEL OF A BRIDGE STRUCTURE

3.1 Literature Review of Flood Disaster Impacts on Bridge Structures

3.1.1 Flood Impact Assessment of Bridge Structures

In 1973, the American Association of State Highway Officials (AASHO) [65] had put forward that "all piers and other portions" of bridge structures had to be designed to resist the maximum stresses generated by flowing water forces. It was recommended that the pressure on piers be calculated using the formula given in Equation 3.1 [65]. The AASHO formula did not consider a lateral hydrodynamic force (i.e. drag) coefficient.

$$P = KV^2 \tag{3.1}$$

where,

P = Pressure in pounds per square foot
V = Velocity of water in feet per second
K = A constant (1⅜ for square ends, ½ for angle ends where the angle is 30° or less and ⅔ for circular piers)

In 1984, based on an extensive literature review, USACE [66] presented a suggested formula by Morison et al. (Equation 3.2) for horizontal force per unit length of a vertical cylindrical pile. Experimental data were made available "primarily for the interaction of nonbreaking waves and vertical cylindrical piles" of coastal structures.

$$f = C_M \rho \frac{\pi D^2}{4} \frac{du}{dt} + C_D \frac{1}{2} \rho D u |u| \tag{3.2}$$

where,

f = Horizontal force per unit length of pile
C_M = Hydrodynamic force coefficient, the "inertia" or "mass" coefficient
ρ = Density of fluid (1,025 kg/m^3 for sea water)
D = Diameter of pile
u = Horizontal water particle velocity at the axis of the pile (calculated as if the pile were not there)
$\frac{du}{dt}$ = Total horizontal water particle acceleration at the axis of the pile (calculated as if the pile were not there)
C_D = Hydrodynamic force coefficient, the "drag" coefficient

The formula given in Equation 3.2 was based on the assumption that the flow was unidirectional (therefore u|u| instead of u^2) and justifiable only if it led to "sufficiently accurate predictions of wave force."

In 1986, Apelt [27] presented a thorough literature review for flood forces on bridges, which essentially pointed out the lack of studies on the subject. Experiments were carried out on two models of a 5-girder bridge with the scales of 1:100 and 1:25. Results of those experiments agreed with previous works, and average drag coefficients of 1.94 and 1.99 were measured when the water surface levels were at the bottom of the girders and on top of the bridge models, respectively.

In 1990, Wellwood and Fenwick [67] proposed a drag coefficient of 2.2 as a measure for a safer design of multi-girder bridge structures. Furthermore, a floodwater velocity higher than 2 m/s (6.56 ft/s) was considered "medium to high." The authors recommended further research for confirmation of the drag coefficient.

Jempson and Apelt [68] continued their research with experiments using a 1:25 bridge superstructure model consisting of five Type IV girder, a deck and edge curbs. They recommended a drag coefficient of 2.0 for Type III and Type IV girder bridges and deck unit bridges. Equation 3.3 presents the formula that was used to evaluate the drag coefficient:

$$C_d = \frac{F_d}{0.5\rho V^2 A} \tag{3.3}$$

where,

C_d = Drag coefficient
F_d = Drag force in the direction of flow
ρ = Fluid density
V = Fluid velocity
A = Projected superstructure area normal to the flow

In 1995, FHWA [69] recommended the use of Equation 3.4 for the calculation of lateral hydrodynamic drag forces for fully or partially submerged bridge superstructures. Recommended drag coefficient values were between 2.0 and 2.2.

$$F_d = C_d \rho H \frac{V^2}{2} \tag{3.4}$$

where,

F_d = Drag force per unit of length of bridge, N/m
C_d = Coefficient of drag
ρ = Density of water, 1,000 kg/m^3
H = Depth of submergence, m
V = Velocity of flow, m/s

In 2000, Jempson [28] did further experiments with six different scaled bridge superstructure models. This yielded design recommendations for loadings on bridge superstructures with improved charts for drag and moment coefficients. The formula expressed in Equation 3.5 was recommended for calculation of moment acting on bridge superstructures, allowing for eccentricity of drag and lift forces. The maximum velocity condition for bridge superstructures was 1.201 m/s.

$$M_{PF} = M_{GS} + F_D \times L_F \tag{3.5}$$

where,

M_{PF} = Moment generated at the point of fixity, kNm
M_{GS} = Moment generated at the girder soffit, kNm
F_D = Usual drag force, kN
L_F = Length of the lever arm from the point of fixity to the girder soffit, m

Plate experiments were done by NCHRP [70] in 2000. A rational model for calculation of forces for complete range of blockage ratios was presented. Using "average contracted flow as reference velocity," Equation 3.6 was recommended for the calculation of drag force. In this approach, the drag force was the difference between "hydrostatic force" and "water pressure force."

$$F_D = F_x - F_{hx} \tag{3.6}$$

where,

F_D = Drag force, N
F_x = Water pressure force on the plate in the streamwise direction that is due to

stream flow, N

F_{hx} = Hydrostatic force attributed to average streamwise pressure gradients, N

In 2003, Malawasi and Guadagnini [31] performed laboratory experiments to quantify hydrodynamic loads on a bridge deck with a rectangular cross-section. They argued that a drag coefficient of 3.40 would be the upper bound limit for bridges where the bridge length (l) to bridge thickness (s) ratio was greater than three. The l/s ratio certainly represented a "minimum" for real scale cases. However, they also concluded that FHWA's recommended formula (Equation 3.4) generally overestimated the drag forces.

In 2009, FHWA [32] developed "fitting equations" and design charts for different types of bridges, which were outcomes of physical experimentation and CFD simulation models. The drag coefficient (C_D) fitting equation for three and six-girder bridges, lift coefficient (C_L) fitting equation for three and six-girder bridges and moment coefficient (C_M) fitting equation for all bridge types are provided in Equations 3.7, 3.8 and 3.9:

$$C_D = Ae^{-2(h^*)^2} - Be^{-0.75(h^*)^2} + a \quad (3.7)$$

$$C_L = b(e^{-3.5(h^*)^2} - e^{-c(h^*)^{1.7}}) \quad (3.8)$$

$$C_M = d(h^*)^{\alpha} e^{-f(h^*)^2} + g \quad (3.9)$$

Coefficients A, B, a, b, c, d, f, g and α for 6-girder and 3-girder bridges were provided as well as the corresponding h^*_{crit} for each C_D, C_L and C_M value. The report also included the same variables for streamlined bridges "designed to reduce the force load during inundation." Results

of 6-girder bridge deck analysis showed that a major drop in the drag coefficient for an inundation ratio (h^*) of 0.5-0.8 was observed. However, as the bridge became more inundated ($h^* > 1.5$), the drag coefficient values were leveled off to around 2. It was also observed that the lift coefficients were all negative, which meant a pull-down force, and they rapidly became more negative as h^* roughly equaled 0.65. The peak moment coefficient was observed when the bridge was roughly halfway inundated. Results of the 3-girder bridge deck analysis were somehow similar to the 6-girder bridge deck analysis results. However, the approach velocities ranged from 0.25 m/s to 0.50 m/s. Critical drag coefficients 2.15, 1.95 and ~1.1 were recommended for 6-girder, 3-girder and streamlined bridges, respectively [32]. The 6-girder bridge model developed in this study was used by Azadbakht and Yim [33], which will be discussed later in this section.

Chen et al. [30] made a hydrodynamic investigation of a bridge collapse during Hurricane Katrina by two numerical models for US-90 Highway bridge across Biloxi Bay, Mississippi. It was concluded that "the bridge failure was caused by the wind waves accompanied by the storm surge generated by Hurricane Katrina." It was also found that bridge decks with lower low-chord elevation (i.e. bottom of girder elevation) than the critical elevation were subjected to "fatal wave impact." This study demonstrated the importance of the height of a bridge with respect to acting hydrodynamic effects during a weather related event.

In 2010, Guo et al. [35] investigated hydraulic forces on bridge decks. A well-written literature review was also a part of their report and significance of hydrodynamic loading generated by floodwater flow was emphasized, mentioning that it might cause overturning of the bridge deck and a possible failure of the superstructure. Their study was concerned with CFD and reduced scale experiments. The minimum drag coefficient (found to be 0.5-0.8) was found to

occur “perhaps” as the water reached the top of girders which was a transition to overtopping of the bridge deck.

In 2011, FEMA [29] recommended the use of Equation 3.10 for the calculation of lateral hydrodynamic drag forces for all flow velocities:

$$F_{dyn} = \frac{1}{2} C_d \rho V^2 A \tag{3.10}$$

where,

F_{dyn} = Horizontal drag force (lb) acting at the stillwater mid-depth (half way between the stillwater elevation and the eroded ground surface)
C_d = Drag coefficient
ρ = Mass density of fluid
V = Velocity of water (ft/sec)
A = Surface area of obstruction normal to flow (ft^2)

For Equation 3.10, mass density was assumed 1.94 slugs/ft^3 for fresh water and 1.99 slugs/ft^3 for saltwater. Recommended values for drag coefficient were 2.0 for square/rectangular piles and 1.2 for round piles. For other types of piles or “obstructions,” FEMA recommended a range of drag coefficients [29].

In 2014, Lwin et al. [34] demonstrated how the performance of observed bridges was affected due to storm surge, wind, and debris and barges. The study looked into wave forces on bridge decks, followed by a recommendation for estimation method and countermeasures to restore the functionality of transportation systems. They recommended estimated wave-induced vertical and horizontal load components, as given in Equations 3.11 through 3.14:

$$F_v = c_{v\text{-}va} F_v^* \tag{3.11}$$

$$F_h = [1 + c_r(N-1)] c_{h\text{-}va} F_h^* \tag{3.12}$$

$$F_v^* = \gamma(\Delta Z_v) A_v \tag{3.13}$$

$$F_h^* = \gamma(\Delta Z_h) A_h \tag{3.14}$$

where,

F_v = Estimated vertical wave-induced load component (uplift)
$c_{v\text{-}va}$ = Empirical coefficient for the vertical varying load
F_v^* = Reference vertical load
F_h = Estimated horizontal wave-induced load component (lateral)
c_r = Reduction coefficient for horizontal load from the blockage by the leading external girders
N = Number of girders supporting the bridge span deck
$c_{h\text{-}va}$ = Empirical coefficient for the horizontal varying load
F_h^* = Reference horizontal load
γ = Unit weight of water (10,078 N/m^3 for saltwater)
ΔZ_v = Difference between the elevation of the crest of the maximum wave and the elevation of the underside of the bridge deck
A_v = Area the bridge contributing to vertical uplift, i.e., the projection of the bridge deck onto the horizontal plane
ΔZ_h = Difference between the elevation of the crest of the maximum wave and the elevation of the centroid of A_h
A_h = Area of the projection of the bridge deck onto the vertical plane

Based on their study, Lwin et al. recommended a c_r value of 0.4. Despite the fact that their study is conservative and simple to apply, their approach was recommended for the estimation of wave loads on elevated bridges decks as "interim guidance."

Yim et al. [36] pointed out that even though many bridges survived the 2011 Great East Japan Earthquake, many of them were completely destroyed by the tsunami. According to Yim

et al., this was purely an indicator of the fact that seismic design codes do not necessarily embrace the loads generated by tsunami waves. They further concluded that even though it is normally not applicable to tsunamis due to their "much longer time and length scales," they were still able to compare their study results (i.e. horizontal drag force) with the American Association of State Highway and Transportation Officials (AASHTO) 2008 [71] formula (Equation 3.15), since their tsunami model was relatively steady:

$$F_{HC} = C_d A(\frac{\rho_w}{2})\frac{U_c^2}{1{,}000} \tag{3.15}$$

where,

F_{HC} = Horizontal drag force
C_d = Drag coefficient (taken as 2.5)
A = Projected area of superstructure per unit length
U_c = Current speed

Azadbakht and Yim [33] thoroughly reviewed the literature and estimated tsunami loads on bridges. They conducted experimental and numerical techniques for five bridges in two different scenarios: (i) initial impact and overtopping, and (ii) full inundation. They used a 6-girder bridge model to assess wave impacts. They developed formulas for maximum horizontal force, downward maximum force and maximum uplift force, as given in Equations 3.16, 3.17 and 3.18:

$$\begin{aligned} F_{H_{max}} &= F_{h\_hs} + F_d \\ &= 0.5\rho g(2h_0 - L_h)L_h + 0.5C_d\rho v^2 L_h \end{aligned} \tag{3.16}$$

$$F_{DV_{max}} = C_{DV}(F_{v\_hs} + F_{v\_s})$$

$$= C_{DV}[\rho g(h_0 - L_g - T_d)L_v + 0.5C_{v_s}\rho v^2 L_{sb}] \quad (3.17)$$

$$F_{UP_{max}} = C_{UP}(F_b + F_l)$$

$$= C_{UP}(\rho gV + 0.5C_l\rho v^2 L_v) \quad (3.18)$$

where,

$F_{H_{max}}$ = Maximum horizontal force
F_{h_hs} = Hydrostatic horizontal force
F_d = Drag force
ρ = Density of water
g = Acceleration of gravity
h_0 = Difference between the tsunami water free-surface elevation and low chord of the bridge
L_h = Height of the bridge superstructure
C_d = Drag coefficient
v = Tsunami flow velocity
$F_{DV_{max}}$ = Downward vertical force
C_{DV} = Empirical downward vertical force coefficient
F_{v_hs} = Hydrostatic downward vertical force
F_{v_s} = Slamming vertical force
L_g = Height of the bridge girder
T_d = Thickness of the bridge deck
L_v = Width of the bridge superstructure
C_{v_s} = Slamming coefficient in the vertical direction
L_{sb} = Effective length of the bridge deck for a vertical slamming force; $4 \cdot L_b$
$F_{UP_{max}}$ = Maximum uplift force
C_{UP} = Empirical uplift force coefficient
F_b = Buoyancy force

F_l = Lift force
V = Volume of the bridge per unit length
C_l = Lift coefficient

3.1.2 Finite Element Methodologies for Flood Impacts on Bridge Structures

In 2008, Witzany et al. [72] presented a numerical analysis of the response of a historic bridge (Charles Bridge, Czech Republic) exposed to a flood wave. The bridge, constructed in the 14th century, withstood "the great inundation of 2002," which was a 500-year flood. Their purpose was to come up with an optimum design and concept of repair. Being exposed to "permanently present and cyclic stress states caused by changes in temperature and moisture content," the longevity of the bridge was under a constant threat. It was concluded after the analysis of first response of the bridge vaults (to the effect of forced deformation) that sufficient securing was needed for the bridge piers' footings.

In 2010, Xiao et al. [73] investigated the time history of wave forces exerted on the Biloxi Bay Bridge (Mississippi, USA) during Hurricane Katrina. A wave-loading model was used that combined storm surge and wave propagation models for better understanding of hydrodynamic conditions during the incident. Results showed that uplift force on the submerged bridge superstructure exceeded the bridge's own weight and that the maximum uplift wave force occurred when the storm surge water level reached the top of the superstructure.

In 2014, another finite element model was conducted for wave forces generated by tsunamis [36]. The objective of the study was to obtain the pressures and forces; therefore, the superstructure was modeled as rigid. The bridge model was linear elastic, and the purpose was to analyze the displacements and whether the bridge superstructure elements would reach their section capacity. Their simulation was conducted "for 60 seconds of the hydrograph around the

peak flow when the tsunami overtops the superstructure." It was noted that the vertical forces were reasonable in comparison with the buoyancy force. The model had approximately 74,000 nodes and 36,000 elements. Results showed that the horizontal drag force from the model was more than 200% of the estimated horizontal drag force (Equation 3.15). It was observed that maximum tsunami loads, given as force per unit length of the bridge, were not as high as the resisting capacity of the bridge. Ratio of the bridge resisting capacity to horizontal tsunami loads was 3.31, whereas the ratio of the bridge resisting capacity to vertical loads was 1.01. It was also reported that there were no suitable formulas to predict vertical force on the superstructure.

Azadbakht and Yim [33] modeled and analyzed a strip section of a bridge superstructure subjected to tsunami wave forces. Using a time history of 200 to 400 seconds, they used two different finite element models where the smallest mesh sizes were 5.08 cm (2 in) and 2.5 mm (0.1 in). The computational time step was 5×10^{-5} seconds. The number of elements was between 30,000 and 100,000. Drag, lift and moment coefficient results were in agreement with those indicated by FHWA [32].

3.1.3 Summary of Literature Review of Flood Disaster Impacts on Bridge Structures

This literature review shows that empirically derived drag coefficients have been used to calculate lateral drag/hydrodynamic forces. Additionally, no 2D numerical simulation of floodwater (for flow propagation, velocity, floodwater depth, discharge and flood arrival time) has been performed. Reference points on the bridge cross-sections for overturning moments are not correctly positioned (they are positioned at the center of mass), or otherwise has it been assumed that the bridge superstructure is fixed to the substructure, which is often not the case. Furthermore, no recommendation has been provided for estimating flood velocities. No

assessment of structural integrity has been reported, which would consider overturning moment generated by lateral floodwater forces and resisting moment of the bridge superstructure. It is also understood that lateral floodwater forces have been calculated by empirical equations. However, more importantly, bridge bearings have not been considered as part of the finite element analyses. Finally, more often, bridge structures are partially modeled.

3.2 Disaster Vulnerability Assessment of Highways Subjected to Floodwater

3.2.1 Highway Embankments and Levees/Dikes

Slope stability analyses for US-51 Highway embankment were performed using GeoSlope Software (Student License) [74] to assess the structural integrity of the embankment. Three different inundation scenarios were considered for the analyses: (i) 3 m, (ii) 7 m and (iii) 11 m. Analyses were performed using Janbu's Method and Ordinary Method for factor of safety (FS) against sliding. A schematic of the embankment is presented in Figure 25. Height of the embankment from the ground level is 7 m. Total width of the embankment is 63 m with 21 m top width. The slopes are 1:3 on both sides of the embankment.

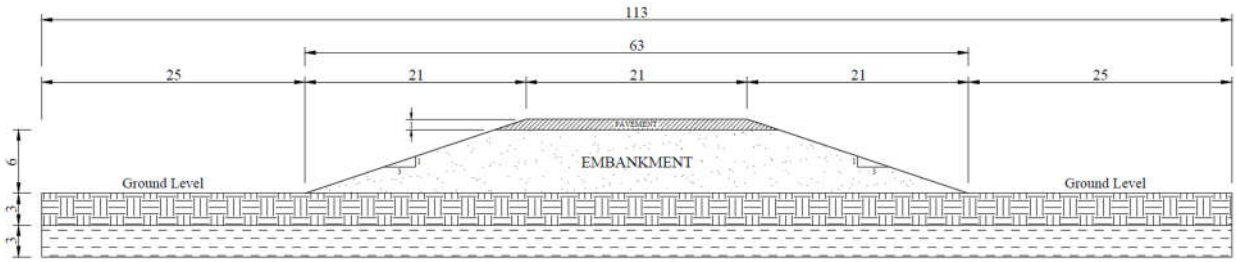

Figure 25. Schematic of US-51 Highway embankment

The embankment and subsoil are assumed to have properties between SM and SC [75] soil types of Unified Soil Classification System (USCS). For 3 m inundation depth, embankment is assumed moist with a unit weight of 20.6 kN/m^3 and cohesion of 23.9 kPa. For 7 m inundation depth, embankment is assumed to have a unit weight of 20.9 kN/m^3 and cohesion of 18 kPa. Finally, for 11 m inundation depth, embankment is assumed saturated with a unit weight of 21.2 kN/m^3 and cohesion of 12 kPa. The internal friction angle is assumed 25° for all cases. Unit weight, cohesion and internal friction angle of the pavement are assumed 22.8 kN/m^3, 0 kPa and 40°, respectively. Locations of the centers of critical toe/slope circles are represented with red dots. Soil properties used in different analysis scenarios are presented in Table 7.

Table 7. Slope stability analyses soil properties

Inundation Depth (m)	3.0		7.0		11.0		Internal Friction Angle
	Moist Unit Weight	Cohesion	Unit Weight	Cohesion	Saturated Unit Weight	Cohesion	
	(kN/m^3)	(kPa)	(kN/m^3)	(kPa)	(kN/m^3)	(kPa)	(°)
$\gamma_{pavement}$	22.78	0	22.78	0	22.78	0	40
$\gamma_{embankment}$	20.56	23.94	20.90	17.96	21.24	11.97	25
$\gamma_{subsoil}$	20.56	23.94	20.90	17.96	21.24	11.97	25

(i) Floodwater Inundation of 3 m: Slope stability analyses for 3 m floodwater inundation yielded a 3.12 FS against sliding. FS for the opposite side slope was lower (2.88). When the embankment was inundated on both sides, slope stability analysis yielded a FS of 2.68. Screen views of the software are presented in Figures 26, 27 and 28, respectively.

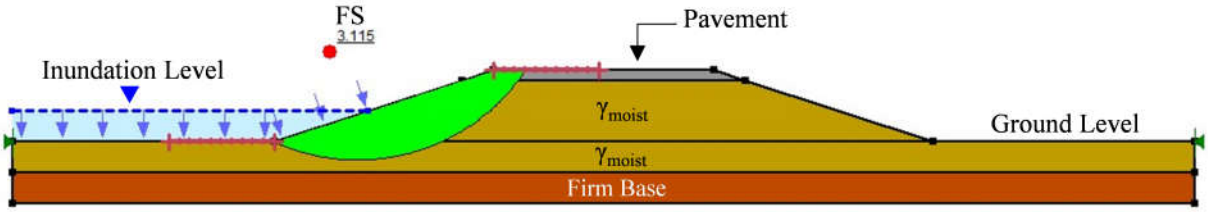

Figure 26. US-51 embankment at 3 m inundation

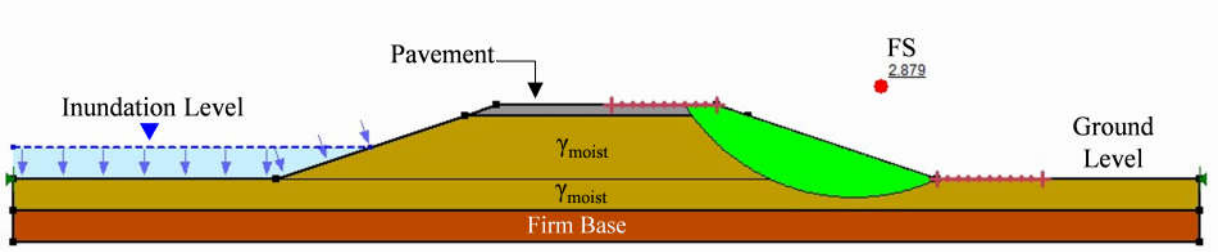

Figure 27. US-51 embankment at 3 m inundation – opposite side slope

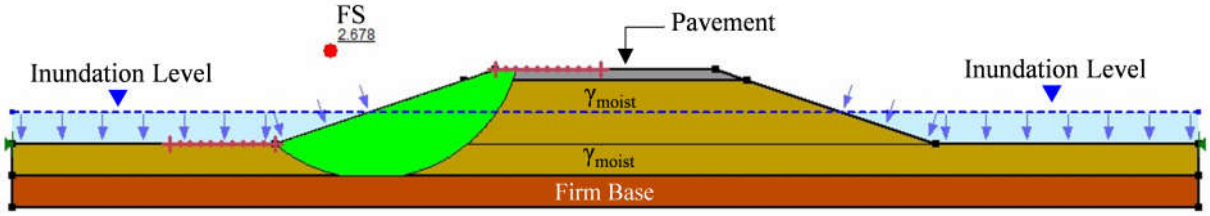

Figure 28. US-51 embankment at 3 m inundation on both sides

(ii) Floodwater Inundation of 7 m: Slope stability analyses for 7 m floodwater inundation yielded a 3.41 FS against sliding. FS for the opposite side slope was lower (2.56). Screen views of the software are presented in Figures 29 and 30, respectively.

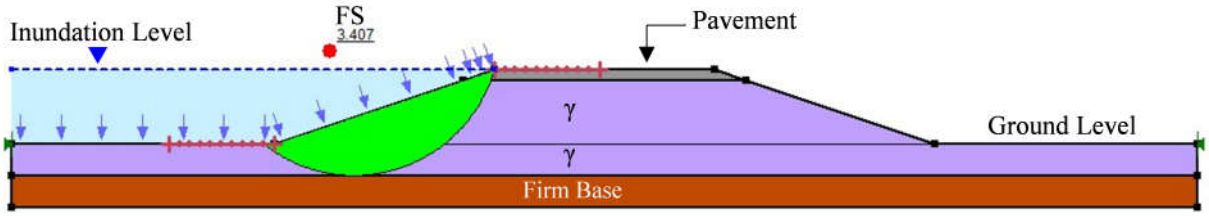

Figure 29. US-51 embankment at 7 m inundation

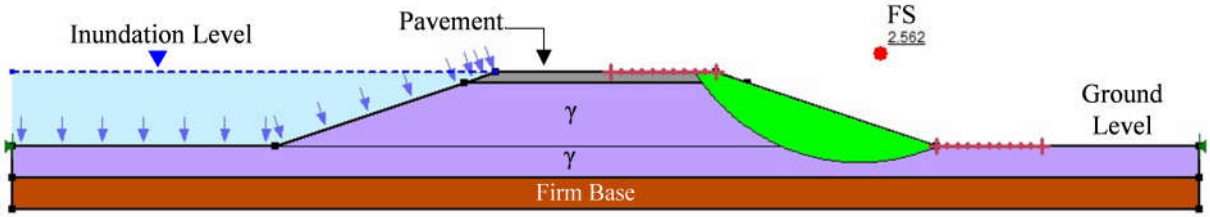

Figure 30. US-51 embankment at 7 m inundation – opposite side slope

(iii) Floodwater Inundation of 11 m: At 11 m floodwater inundation, FS against sliding was 2.75 as shown in Figure 31.

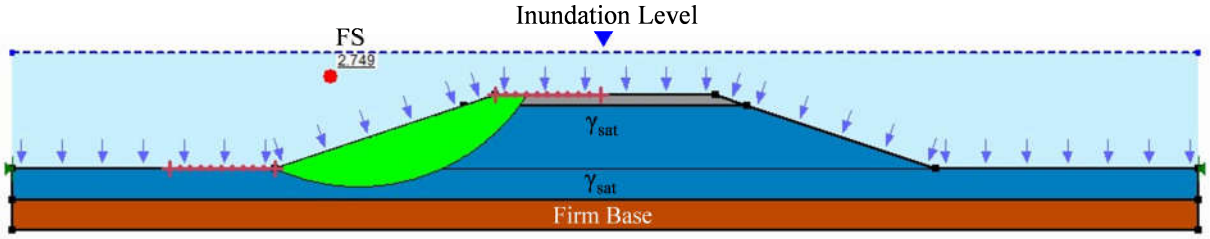

Figure 31. US-51 embankment at 11 m inundation

It is seen from the FS results that the opposite side slope at 7 m inundation is the most critical case. Janbu's Method and Ordinary Method were preferred due to the fact that these

methods yielded the lowest FS values. However, it is recommended that Morgenstern-Price or Spencer methods be employed for slope stability analysis, as they satisfy both force and moment equilibriums [76]. Therefore, in determination of FS for different slope angles, analyses are performed once again with the Spencer's Method. Given the lowest FS values from Janbu's Method and Ordinary Method, slope stability is performed for 7 m inundation only. Results are provided in Figure 32.

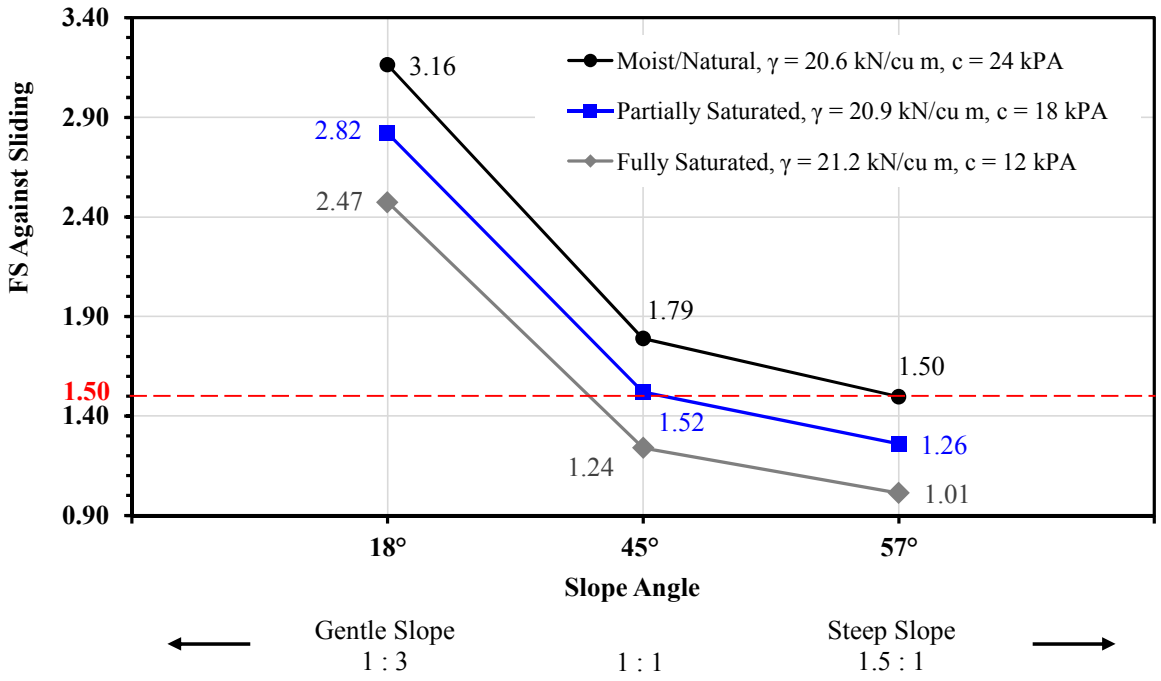

Figure 32. FS against sliding at 7 m flood inundation (Spencer's Method)

It is seen that FS against sliding decreases with increasing slope and also with increasing unit weight and/or decreasing cohesion of the embankment. Given the fact that the side slopes of US-51 Highway embankment are 1:3, it can be concluded that the embankment is safe against a slope failure.

3.2.2 Scouring at Bridge Foundations

Scouring occurs when the floodwater flow velocity exceeds the force required to move the riverbed material [77]. Current scouring calculations are empirical and do not take into consideration the embankment stability, flood debris accumulation (which results in additional scour), upstream catchment conditions, or deposition of sediment during a flooding event [77].

For all three bridges (I-55, Rail and US-51) in the Sardis Site, depth-averaged local velocity of the floodwater at the central observation point (at river CL) can be as high as 3 m/s (9.84 ft/s), approximately. This is a relatively high flow velocity that will be capable of eroding and transporting sediment particles up to a diameter of 0.10 m [55]. Pier scour under both live-bed and clear-water conditions is computed by the Equation 3.19 [78]. Velocity results of the 3 m CCS simulation are used in scouring calculations.

$$y_s = 2.0K_1K_2K_3\left(\frac{a}{y_p}\right)^{0.65}\left(F_p\right)^{0.61}y_p \tag{3.19}$$

where,

y_s = Scour depth (ft)
K_1 = Coefficient for pier-nose shape
K_2 = Coefficient for flow attack angle (depends also on pier length to width ratio)
K_3 = Coefficient for bed form condition
a = Pier width (ft)
y_p = Flow depth at the upstream of the pier (ft)
F_p = Froude number of the flow upstream of the pier

I-55 Highway bridge: The local scour around the 10 ft-diameter I-55 bridge piers in the main channel (Figure 33) is estimated as 5.27 m (17.29 ft). Unless the pier foundations are

sufficiently deep and/or appropriate local scour prevention measures are taken, the bridge may be at risk due to excessive scour [79].

Rail Bridge: The flow overtops the rail bridge with a depth more than 1 m. Based on the estimated size of piers, the local scour around the slender piers in the main channel is estimated as 5.36 m (17.59 ft). This is a quite substantial scour depth. Unless the pier foundations are sufficiently deep and/or appropriate local scour prevention measures are taken, the integrity of the bridge may be in danger due to excessive scour.

Figure 33. A view of the I-55 Highway bridge over Little Tallahatchie River
(Photo Credit: MDOT Bridge Division)

US-51 Highway bridge: The local scour around the rectangular pier (0.58 m by 0.26 m) in the main channel of US-51 Highway bridge is estimated as 2.00 m (6.56 ft). This is a reasonable scour depth. The piers are penetrated deep into the ground. Thus, there is no significant danger to the structure. A view of the US-51 Highway bridge over Little Tallahatchie River is seen in Figure 34.

Figure 34. A view of the US-51 Highway bridge over Little Tallahatchie River
(Photo Credit: MDOT Bridge Division)

The assessment of scour potential shows that there is no significant danger to the US-51 Highway bridge. However, further evaluation of scour potential is recommended per guidelines and countermeasures of the FHWA [69, 80, 81].

3.2.3 Structural Integrity of Bridge Superstructure

Structural integrity assessment of US-51 Highway bridge is presented in this section using floodwater inundation results generated with 10 m CCS. The structural integrity assessment is performed for lateral (i) lateral pseudo-static and (ii) lateral hydrodynamic cases. The following assumptions are made after studying the design drawings of the US-51 Highway bridge (courtesy of MDOT Bridge Division):

- Girder type: AASHTO I-Beam Type IV [82]
- Girder height: 4.5 ft
- Girder cross-section bottom width: 1.83 ft [83]
- Girder cross-section area: 4.16 ft^2 [83]
- Girder spacing: 6 ft
- Bridge deck/slab width: 30 ft (typical 2-lane highway bridge)
- Bridge slab thickness: 1 ft
- Number of girders: 6
- Span width: 30 ft (i.e. girder and slab lengths)
    a. Slab lateral area, A_{rs}: 30 ft^2
    b. Girder lateral area, A_{rg}: 135 ft^2
- Unit weight of slab and girders: 150 pcf
- Unit weight of floodwater: 62.4 pcf

The bridge superstructure rests on pile caps (Figure 35). It is assumed that bridge pile caps, as well as piers and foundations, are capable of withstanding the generated lateral flowing floodwater forces. An examination of photos from several bridge failure cases during the 2005 Hurricane Katrina and the 2011 Hurricane Irene shows that most bridge superstructures washed away when the floodwater reached the height of the girders. Therefore, overturning moments are calculated in this research with respect to the interface (edge) of girders and pile caps.

Figure 35. A view of the US-51 Highway Bridge
(Photo Credit: MDOT Bridge Division)

A general schematic of the highway bridge is represented in Figure 36 based on the MDOT drawings of the US-51 Highway bridge. For analysis purposes, a 30-ft section of bridge superstructure that extends 15 ft on each side of a pile cap is considered. This is based on the assumption of a typical superstructure-pile interface for the entire bridge. Bridge railings etc. are not considered in the calculations. The gap between two girders is ignored (Figure 36).

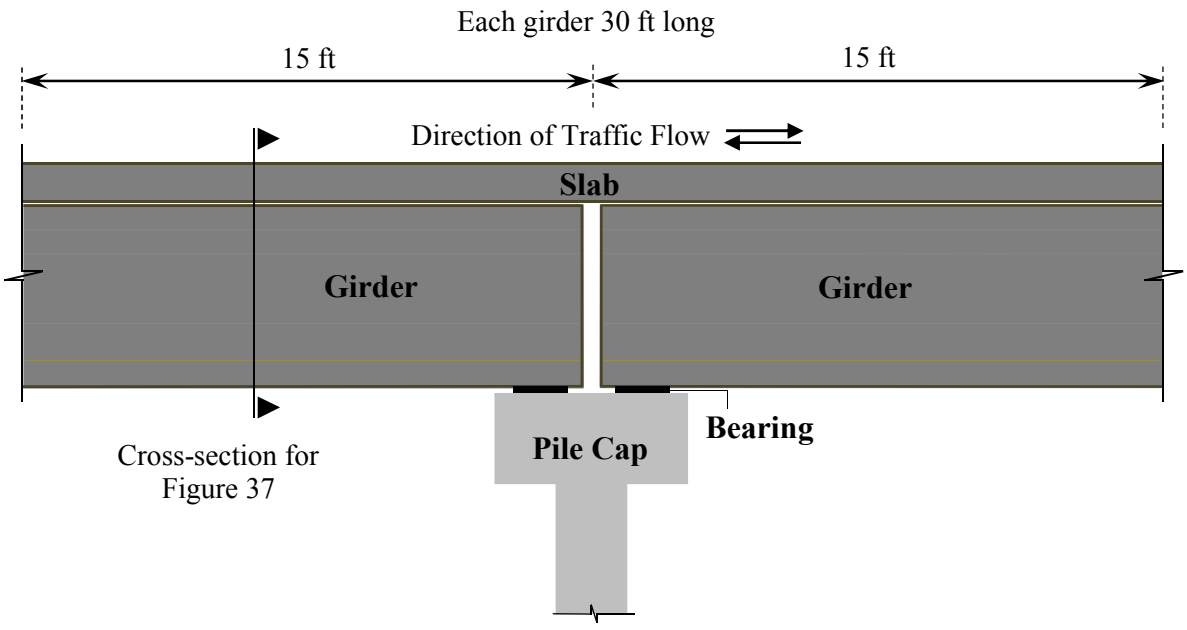

Figure 36. Schematic of a 30-ft section of the bridge superstructure

A schematic of the bridge superstructure cross-sections is presented in Figure 37. Three scenarios of floodwater inundation are considered for the analyses:

- Scenario 1: Floodwater is at the bottom of the bridge slab.
- Scenario 2: Floodwater is level with the top of the bridge superstructure.
- Scenario 3: The bridge superstructure is under 0.53 m of floodwater.

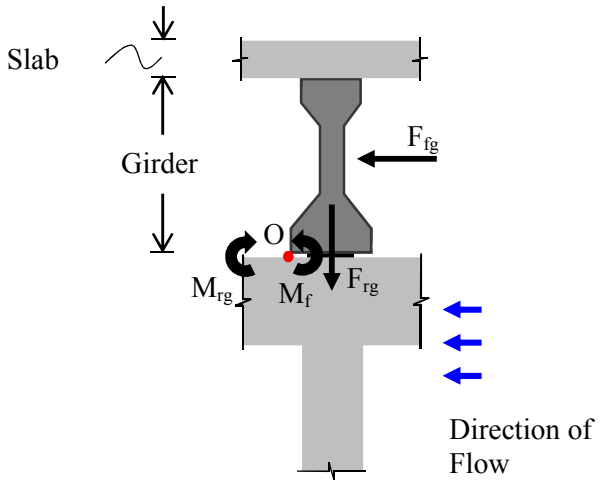

(a)

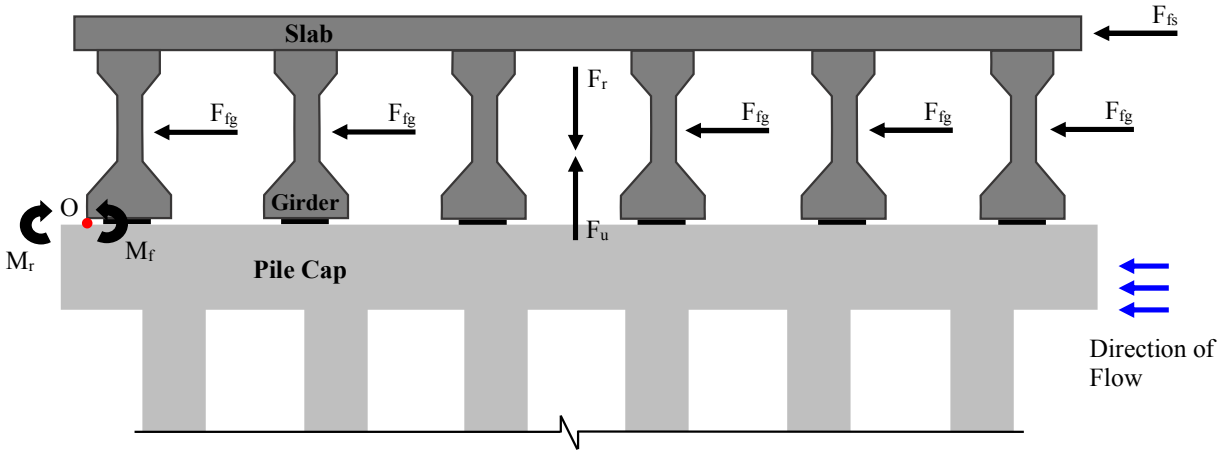

(b)

Figure 37. Bridge superstructure cross-section (a) single girder (b) entire girders

3.2.3.1 Pseudo-static Analysis

The structural integrity analysis presented in this section is for floodwater inundation assuming that the floodwater flow exerts pseudo-static force, i.e. not stagnant, and is enough to

generate the lateral forces on the bridge structure. One foot of floodwater in the flow direction is assumed to act on the sides of girders and/or slab. Bearings are ignored in the calculations.

Bridge Structural Integrity Assessment: Single Girder Case (Scenario 1): This scenario is about a hypothetical single girder subjected to floodwater force. Dead load of the deck and uplift affects are ignored in this scenario.

Calculation of Resisting Moment

Resisting force (girder), F_{rg} = Effective girder length × Girder cross-section area × Unit weight of girder
= (15+15) ft × 4.16 ft^2 × 150 pcf
= 18,720 lb

Resisting lever arm (girder), L_{rg} = (Girder cross-section bottom width) ÷ 2
= 1.83 ft ÷ 2
= 0.915 ft

Resisting moment (girder), M_{rg} = $F_{rg} \times L_{rg}$
= 18,720 lb × 0.915 ft
= 17,129 lb·ft

Calculation of Floodwater (Overturning) Moment

Lateral floodwater force (girder), F_{fg} = Girder height x Effective girder length x Unit weight of floodwater
= 4.5 ft × (15+15) ft × 62.4 pcf × 1 ft
= 8,424 lb

Floodwater force lever arm (girder), L_{fg} = Girder height ÷ 2
= 4.5 ft ÷ 2
= 2.25 ft

Floodwater moment (girder), M_{fg} = $F_{fg} \times L_{fg}$

= 8,424 lb × 2.25 ft
= 18,954 lb·ft

FS against overturning (girder) = $M_{rg} \div M_f$
= 17,129 lb·ft ÷ 18,954 lb·ft
= 0.90

Bridge Structural Integrity Assessment: Entire Superstructure (Scenario 1): This scenario considers the entire superstructure. Floodwater level is at the top of the girders. Dead load of the superstructure and uplift affects are also taken into account.

Calculation of Resisting Moment

Resisting force (girders), F_{rg} = Weight of a single girder × Number of girders
= 18,720 lb × 6
= 112,320 lb

Resisting lever arm (girders), L_{rg} = (Number of girders 1) × Girder spacing ÷ 2
= (6 1) × 6 ft ÷ 2
= 15 ft

Resisting moment (girders), M_{rg} = $F_{rg} \times L_{rg}$
= 112,320 lb × 15 ft
= 1,684,800 lb·ft

Resisting force (slab), F_{rs} = Volume of slab x Unit weight of slab
= 30 ft × 30 ft × 1 ft × 150 pcf
= 135,000 lb

Resisting lever arm (slab), L_{rs} = (Slab width) ÷ 2
= 30 ft ÷ 2
= 15 ft

Resisting moment (slab), M_{rs} $= F_{rs} \times L_{rs}$
$= 135{,}000 \text{ lb} \times 15 \text{ ft}$
$= 2{,}025{,}000 \text{ lb·ft}$

Total resisting moment, M_r $= M_{rg} + M_{rs}$

$= 1{,}684{,}800 \text{ lb·ft} + 2{,}025{,}000 \text{ lb·ft}$
$= 3{,}709{,}800 \text{ lb·ft}$

Calculation of Floodwater (Overturning) Moment

Floodwater force (girders), F_{fg} = Girder height × Effective girder length × Number of girders × Unit weight of floodwater
$= 4.5 \text{ ft} \times (15+15) \text{ ft} \times 6 \times 62.4 \text{ pcf} \times 1 \text{ ft}$
$= 50{,}544 \text{ lb}$

Floodwater lever arm (girders), L_g = (Girder height) ÷ 2
$= 4.5 \text{ ft} \div 2 = 2.25 \text{ ft}$

Floodwater moment (girders), M_{fg} $= F_{fg} \times L_{fg}$
$= 50{,}544 \text{ lb} \times 2.25 \text{ ft}$
$= 113{,}724 \text{ lbs·ft}$

Calculation of Uplift Moment

Uplift force (girders), F_{ug} = Total volume of girders × Unit weight of floodwater
$= 6 \times 30 \text{ ft} \times 4.16 \text{ ft}^2 \times 62.4 \text{ pcf}$
$= 46{,}725 \text{ lb}$

Floodwater lever arm (girders), L_{ug} = (Slab width) ÷ 2
$= 30 \text{ ft} \div 2$
$= 15 \text{ ft}$

Uplift moment (girders), M_{ug} $= F_{ug} \times L_{ug}$
$= 46{,}725 \text{ lb} \times 15 \text{ ft}$
$= 700{,}875 \text{ lb·ft}$

Total overturning moment, M_f = $M_{fg} + M_{ug}$
= 113,724 lb·ft + 700,875 lb·ft
= 814,599 lb·ft

FS against overturning = $M_r \div M_f$
= 3,709,800 lb·ft ÷ 814,599 lb·ft
= 4.55

Bridge Structural Integrity Assessment: Entire Superstructure (Scenario 2): This scenario considers the entire superstructure. Floodwater level is at the top of the slab/deck. Dead load of the superstructure and uplift affects are also taken into account.

Total resisting moment, M_r = $M_{rg} + M_{rs}$
= 1,684,800 lb·ft + 2,025,000 lb·ft
= 3,709,800 lb·ft

Calculation of Floodwater (Overturning) Moment

Floodwater moment on girders, M_{fg} = $F_{fg} \times L_{fg}$
= 50,544 lb × 2.25 ft
= 113,724 lbs·ft

Floodwater force (slab), F_s = Slab height × Effective slab length × Unit weight of floodwater
= 1.0 ft × (15+15) ft × 62.4 pcf × 1 ft
= 1,872 lb

Floodwater lever arm (slab), L_{fs} = [(Slab height) ÷ 2] + Girder height
= (1.0 ft ÷ 2) + 4.5 ft
= 5 ft

Floodwater moment (slab), M_{fs} = $F_{fg} \times L_{fs}$
= 1,872 lb × 5 ft

= 9,360 lb·ft

Total floodwater moment, M_f = $M_{fg} + M_{fs}$
= 113,724 lb·ft + 9,360 lb·ft
= 123,084 lb·ft

Calculation of Uplift Moment

Uplift moment (girders), M_{ug} = $F_{ug} \times L_{ug}$
= 46,725 lb × 15 ft
= 700,875 lb·ft

Uplift force (slab), F_{us} = Total volume of slab × Unit weight of floodwater
= 30 ft × 30 ft^2 × 62.4 pcf
= 56,160 lb

Uplift moment (slab), M_{us} = $F_{us} \times L_{us}$
= 56,160 lb × 15 ft
= 842,400 lb·ft

Total uplift moment, M_{ft} = $M_{ug} + M_{us}$
= 700,875 lb·ft + 842,400 lb·ft
= 1,543,275 lb·ft

Total overturning moment, M_{ft} = $M_f + M_{ft}$
= 123,084 lb·ft + 1,543,275 lb·ft
= 1,666,359 lb·ft

FS against overturning = $M_r \div M_{ft}$
= 3,709,800 lb·ft ÷ 1,666,359 lb·ft
= 2.23

Acting moments in the pseudo-static analysis are summarized in Table 8. Calculated moments are for 1 ft of lateral floodwater. FS against overturning is 0.90 for the hypothetical single girder case. Furthermore, FS for superstructure ranges between 2.23 and 4.55, depending on the inundation level at the bridge superstructure.

Table 8. Pseudo-static analysis acting moments (1 ft of lateral floodwater)

Scenario	Inundation Level	Resisting Moment*		Uplift Moment*		Lateral Moment*		Total Overturning Moment*	FS against Overturning
		Girder	Slab	Girder	Slab	Girder	Slab		
Single Girder	**	17,129	-	-	-	18,954	-	18,954	0.90
Superstructure	Top of Girder	1,684,800	2,025,000	700,875	-	113,724	-	814,599	4.55
Superstructure	Top of Slab	1,684,800	2,025,000	700,875	842,400	113,724	9,360	1,666,359	2.23

* moments are in lb·ft.
** inundation/uplift effect is not considered.

Table 9 presents calculated FS values for given lateral extents of the floodwater flow. It is shown that 1 ft of floodwater is enough to overturn a single girder. When the lateral extent of floodwater is 20 ft, the FS of the entire superstructure is 1.39, which is less than the commonly used FS criterion of 1.50. The critical lateral extent of floodwater flow for each case is summarized at the bottom of Table 9.

Table 9. Calculated FS for different floodwater lateral extents

Lateral Extent of Floodwater in Flow Direction (ft)	Scenario 1 (No uplift) Single Girder	Scenario 1 (Inundation at top of girders) Entire Superstructure	Scenario 2 (Inundation at top of deck) Entire Superstructure
1	0.90	4.55	2.23
5	0.18	2.92	1.72
10*	0.09	2.54	1.55
20*	< 0.05	2.25	1.39
30*	0.03	2.02	1.25
50*	< 0.02	1.67	1.05
100*	< 0.01	1.17	0.75
Critical Lateral Extent	1 ft	100 ft	20 ft

* Lateral extent is for slab and floodwater flow-facing girder only.
Lateral extent for remaining girders remains 6 ft (i.e. girder spacing).

3.2.3.2 Lateral Hydrodynamic Analysis

The structural integrity analysis presented in this section is for floodwater inundation assuming that the floodwater flow exerts lateral hydrodynamic force on the bridge structure. The FEMA equation is used (Equation 3.20) for the calculation of hydrodynamic drag forces [29]. Further assumptions are as follows:

- Floodwater flow velocity, V = 9 ft/s
- Coefficient of drag, $C_D = 2.0$

$$F_{dyn} = 0.5 C_d \rho V^2 A \tag{3.20}$$

Bridge Structural Integrity Assessment: Single Girder Case (Scenario 1): Lateral hydrodynamic floodwater force (F_{hg}) acts on the mid-height of the girder as a concentrated force. Floodwater force generates the floodwater moment (M_{hg}), which acts to overturn the girder. On the other hand, the resisting moment by girders (M_{rg}) is generated by the weight of the girders (F_{rg}) and acts against M_{hg}. Moments are calculated with reference to point O as shown in Figure 37. Bearings are ignored in the calculations. Note that this analysis does not consider the dead load of the deck.

Calculation of Resisting Moment

The resisting moment (girder) remains the same as in pseudo-static analysis:

Resisting moment (girder), M_{rg} = 17,129 lb·ft

Calculation of Floodwater (Overturning) Moment

Hydrodynamic floodwater force, F_{hg} $= 2.0 \times 62.4$ pcf $\times 135$ ft$^2 \times (9$ ft/s$)^2 \div 2$
$= 682{,}344$ lb.ft/s^2
$= 21{,}208$ lb

Floodwater force lever arm, L_{hg} = (Girder height) $\div 2$
$= 4.5$ ft $\div 2$
$= 2.25$ ft

Floodwater moment, M_{hg} $= F_{hg} \times L_{hg}$
$= 21{,}208$ lb $\times 2.25$ ft
$= 47{,}718$ lb·ft

FS against overturning $= M_{rg} \div M_{hg}$
$= 17{,}129$ lb·ft $\div 47{,}718$ lb·ft
$= 0.36$

It can be seen from the results that a single girder is vulnerable to overturning even with 1 ft of floodwater force. Once the girder is displaced, it will possibly hit a neighbor girder, and this may cause catastrophic failure of the bridge superstructure. A girder height of 4.5 ft is considered in the calculation of lateral hydrodynamic forces. However, the actual lateral area of the girder is greater than 30 ft^2 due to the cross-section of the girder (I-beam rather than rectangular).

The case presented so far has analyzed the effect of floodwater flow exerting lateral hydrodynamic force to the girder. This hydrodynamic force acting on the bridge superstructure is 2.53 times higher than the pseudo-static force generated by flowing floodwater [84]. Uplift force

is not included in the preceding single girder analysis, which will further reduce the FS. That will be investigated next.

Bridge Structural Integrity Assessment: Entire Superstructure (Scenario 1): Lateral hydrodynamic floodwater force on the slab (F_{hs}) and girders (F_{hg}) and floodwater uplift force (F_u), also contribute to the overturning moment (M_h). The resisting moment (M_r) is generated by the weight of the superstructure (F_r). Bearings are ignored in the calculations.

Calculation of Resisting Moment

The resisting moment of the bridge superstructure remains unchanged.

Total resisting moment, M_r = 3,709,800 lb·ft

Calculation of Floodwater (Overturning) Moment

Lateral hydrodynamic force (girders), F_{hg} = $6 \times [2.0 \times 62.4 \text{ pcf} \times 135 \text{ ft}^2 \times (9 \text{ ft/s})^2 \div 2]$
= 4,094,064 lb.ft/s^2
= 127,247 lb

Floodwater force lever arm (girders), L_{hg} = (Girder height) ÷ 2
= 4.5 ft ÷ 2
= 2.25 ft

Floodwater moment (girders), M_{hg} = $F_{hg} \times L_{hg}$
= 127,247 lb × 2.25 ft
= 286,306 lb·ft

Calculation of Uplift Moment

Uplift force (girders), F_{ug} = Total volume of girders × Unit weight of floodwater
= 6 × 30 ft × 4.16 ft^2 × 62.4 pcf
= 46,725 lb

Floodwater lever arm (girders), L_{ug} = (Slab width) ÷ 2
= 30 ft ÷ 2
= 15 ft

Uplift moment (girders), M_{ug} = $F_{ug} \times L_{ug}$
= 46,725 lb × 15 ft
= 700,875 lb·ft

Total overturning moment, M_h = $M_{hg} + M_{fss}$
= 286,306 lb·ft + 700,875 lb·ft
= 987,181 lb·ft

FS against overturning = $M_r \div M_h$
= 3,709,800 lb·ft ÷ 987,181 lb·ft
= 3.76

Bridge Structural Integrity Assessment: Entire Superstructure (Scenario 2): This scenario is also a lateral hydrodynamic loading case and, uplift force caused by floodwater is included. Bearings are ignored in the calculations.

Calculation of Resisting Moment

The resisting moment of the bridge superstructure remains the same as in Scenario 1.

Total resisting moment, M_r = $M_{rg} + M_{rs}$
= 1,684,800 lb·ft + 2,025,000 lb·ft
= 3,709,800 lb·ft

Calculation of Floodwater (Overturning) Moment

Floodwater moment (girders), M_{hg} = $F_{hg} \times L_{hg}$

= 127,247 lb × 2.25 ft

= 286,306 lb·ft

Floodwater force (slab), F_{fs} = 2.0 × 62.4 pcf × 30 ft^2 × (9 ft/s)^2 ÷ 2

= 151,632 lb.ft/s^2

= 4,713 lb

Floodwater lever arm (slab), L_{hs} = (Slab thickness) ÷ 2 + Girder height

= ½ ft + 4.5 ft

= 5 ft

Floodwater moment (slab), M_{hs} = F_{hs} × L_{hs}

= 4,713 lb × 5 ft

= 23,565 lb·ft

Total floodwater moment, M_h = M_{hg} + M_{hs}

= 286,306 lb·ft + 23,565 lb·ft

= 309,871 lb·ft

Calculation of Uplift Moment

Floodwater uplift force (girders), F_{ug} = Total volume of girders x Unit weight of floodwater

= 6 × 30 ft × 4.16 ft^2 × 62.4 pcf

= 46,725 lb

Floodwater uplift force (slab), F_{us} = Volume of slab × Unit weight of floodwater

= 1 ft × 30 ft × 30 ft × 62.4 pcf

= 56,160 lb

Total floodwater uplift force, F_u = F_{ug} + F_{us}

= 46,725 lb + 56,160 lb

= 102,885 lb

Floodwater lever arm (superstructure), L_{fss} = (Slab width) ÷ 2
= 30 ft ÷ 2
= 15 ft

Uplift moment (superstructure), M_{fss} = $F_u \times L_{fss}$
= 102,885 lb × 15 ft
= 1,543,275 lb·ft

Total overturning moment, M_h = $M_h + M_{fss}$
= 309,871 lb·ft + 1,543,275 lb·ft
= 1,853,146 lb·ft

FS against overturning = $M_r \div M_h$
= 3,709,800 lb·ft ÷ 1,853,146 lb·ft
= 2.00

Acting moments in the hydrodynamic analysis are summarized in Table 10. FS against overturning is 0.36 for the hypothetical single girder case. FS for superstructure ranges between 2.00 and 3.76, depending on the inundation level at the bridge superstructure.

Table 10. Acting moments due to lateral hydrodynamic forces

Scenario	Inundation Level	Resisting Moment*		Uplift Moment*		Lateral Moment*		Total Overturning Moment*	FS against Overturning
		Girder	Slab	Girder	Slab	Girder	Slab		
Single Girder	**	17,129	-	-	-	47,718	-	47,718	0.36
Superstructure	Top of Girder	1,684,800	2,025,000	700,875	-	286,306	-	987,181	3.76
Superstructure	Top of Slab	1,684,800	2,025,000	700,875	842,400	286,306	23,565	1,853,146	2.00

* moments are in lb·ft.
** inundation effect is not considered.

Bridge Structural Integrity Assessment: Entire Superstructure (Scenario 3): Scenario 3 is where the floodwater overflows 0.53 m above the bridge superstructure. This scenario combines

lateral, uplift and dead load of flowing floodwater. Full 0.53 m floodwater overflowing the bridge superstructure introduces the weight of the floodwater acting against the overturning risk of the superstructure, which will result in a higher FS. Therefore, this analysis is not pursued further. A comparison of the pseudo-static and hydrodynamic loading cases is presented in Table 11.

Table 11. Comparison of FS for pseudo-static and hydrodynamic loading cases

(a) FS in pseudo-static loading

Lateral Extent of Floodwater in Flow Direction (ft)	Scenario 1 (No uplift) Single Girder	Scenario 1 (Inundation at top of girders) Entire Superstructure	Scenario 2 (Inundation at top of deck) Entire Superstructure
1	0.90	4.55	2.23
5	0.18	2.92	1.72
10*	0.09	2.54	1.55
20*	< 0.05	2.25	1.39
30*	0.03	2.02	1.25
50*	< 0.02	1.67	1.05
100*	< 0.01	1.17	0.75
Critical Lateral Extent	1 ft	100 ft	20 ft

* Lateral extent is for slab and floodwater flow-facing girder only.
Lateral extent for remaining girders remains 6 ft (i.e. girder spacing).

(b) FS in hydrodynamic loading

Lateral Extent of Floodwater in Flow Direction (ft)	Scenario 1 (No uplift) Single Girder	Scenario 1 (Inundation at top of girders) Entire Superstructure	Scenario 2 (Inundation at top of deck) Entire Superstructure
Not Applicable (N/A)	0.36	3.76	2.00

3.3 Floodwater Impact Simulation on 3D-FE Model of US-51 Highway Bridge

Floodwater impact simulation on 3D-FE model of US-51 Highway bridge on Little Tallahatchie River is performed using LS-PrePost 4.1 of LS-DYNA R8 [85].

3.3.1 Units and Material Properties

LS-DYNA accepts any set of consistent units [86]. Table 12 shows the units used in the proceeding 3D-FE analyses of the US-51 Highway bridge.

Table 12. 3D-FE analyses units

Measurement	Units Used
Length	meter (m)
Time	second (s)
Mass	kilogram (kg)
Force	Newton (N)
Gravitational Acceleration	9.81

3.3.2 Geometry of the Bridge Model

Drawings of the US-51 Highway bridge were acquired as a courtesy of MDOT. Based on the bridge drawings, a schematic of the bridge was created, as shown in Figure 38. According to the schematic, the bridge consists of 17 spans ranging between 12.82 m and 30 m. The bridge runs north-south bound over piles penetrating into the natural ground with a 50-year design stage elevation of 60.41 m. The 100-year scour line can also be seen in the schematic.

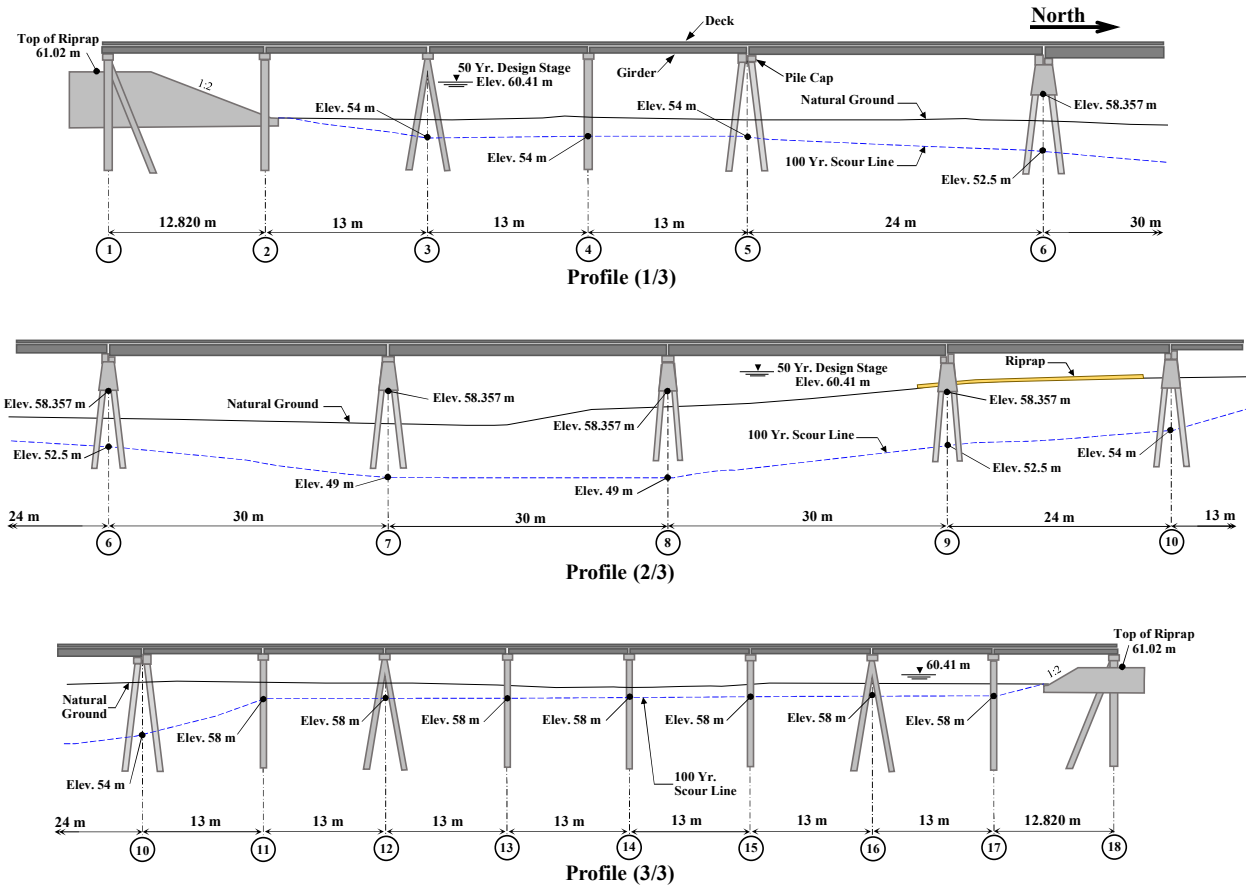

Figure 38. Schematic of the US-51 Highway bridge

Table 13 presents the girder types and span lengths of the US-51 Highway bridge over Little Tallahatchie River in Sardis. Of the bridge girders, 72 of them are AASHTO Type I, 10 of them are Type III and 15 girders are Type IV [87]. Total length of the girders along the bridge centerline is 273.6 m.

Table 13. Bridge girder types and span lengths

Gridline	Span Length (m)	AASHTO Girder Type	Number of Girders	Girder Spacing* (m)	Remarks
1-2	12.8	I	6	2.2	South Abutment
2-3	13	I	6	2.2	
3-4	13	I	6	2.2	
4-5	13	I	6	2.2	
5-6	24	III	5	2.74	
6-7	30	IV	5	2.74	
7-8	30	IV	5	2.74	
8-9	30	IV	5	2.74	
9-10	24	III	5	2.74	Middle Span
10-11	13	I	6	2.2	
11-12	13	I	6	2.2	
12-13	13	I	6	2.2	
13-14	13	I	6	2.2	
14-15	13	I	6	2.2	
15-16	13	I	6	2.2	
16-17	13	I	6	2.2	
17-18	12.8	I	6	2.2	North Abutment

* center-to-center

The cross-section of an I-beam and corresponding dimensions of the girders are represented in Figure 39. Dimensions of I-beam Type I, Type II and Type III are retrieved from MDOT drawings of US-51, which are in metric units. After studying the MDOT drawings, dimensions of Type I and Type II girders are assumed to be the same.

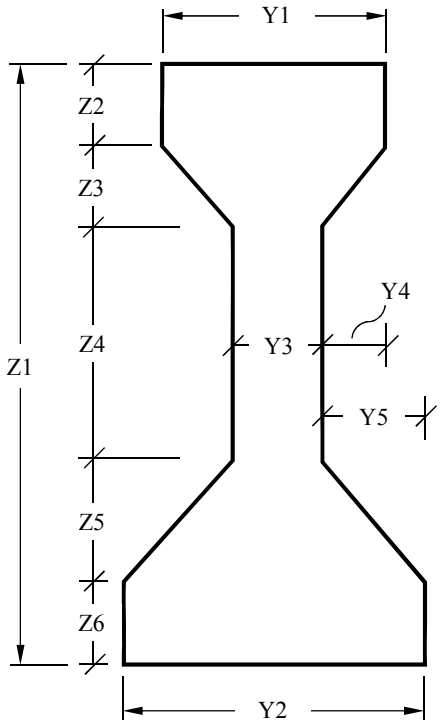

Type	Y1	Y2	Y3	Y4	Y5	Z1	Z2	Z3	Z4	Z5	Z6
I, II	0.350	0.460	0.200	0.075	0.130	0.710	0.100	0.075	0.275	0.130	0.130
III	0.410	0.560	0.180	0.115	0.190	1.145	0.180	0.115	0.480	0.190	0.180
IV	0.510	0.660	0.200	0.155	0.230	1.370	0.200	0.155	0.580	0.230	0.205

Figure 39. Cross-section of an I-beam

The entire structure is modeled due to the fact that no symmetry is applicable. A side view of the bridge model is shown in Figure 40. Figure 41 presents isometric views of the bridge at north and south abutments.

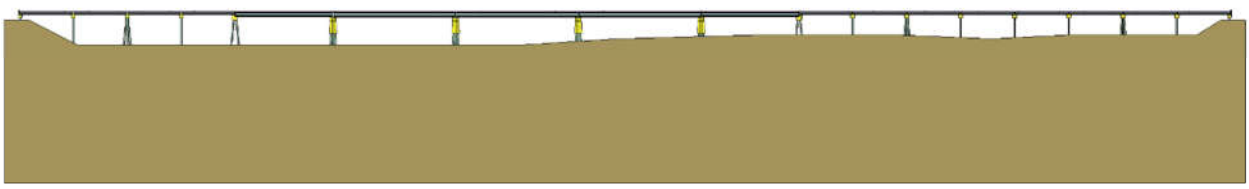

Figure 40. LS-DYNA side view of the bridge

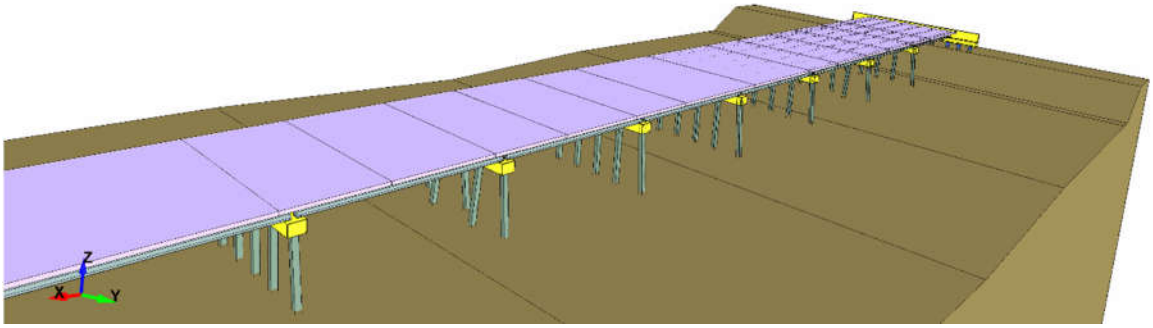

(a)

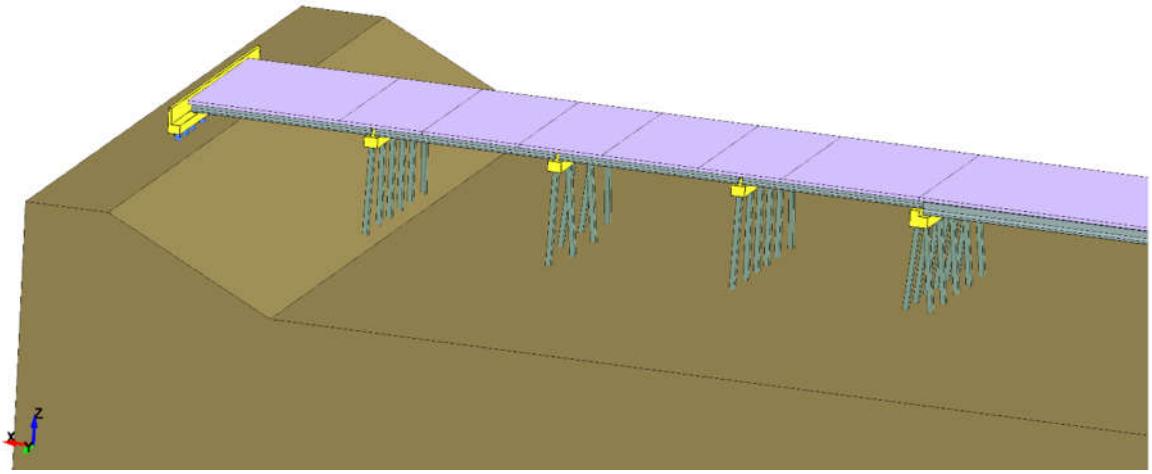

(b)

Figure 41. LS-DYNA isometric views of (a) north abutment (b) south abutment

A close-up view of a pile cap can be seen in Figure 42. Pile caps are where bridge elements interact with each other. From 3D-FE simulation point of view for flood impact analysis, pile caps (where girders rest over neoprene bearings) are the structural connection of concern.

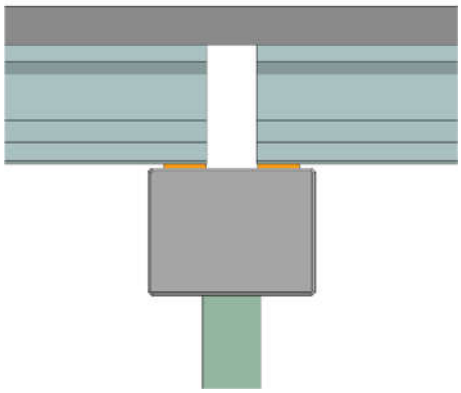

(a)

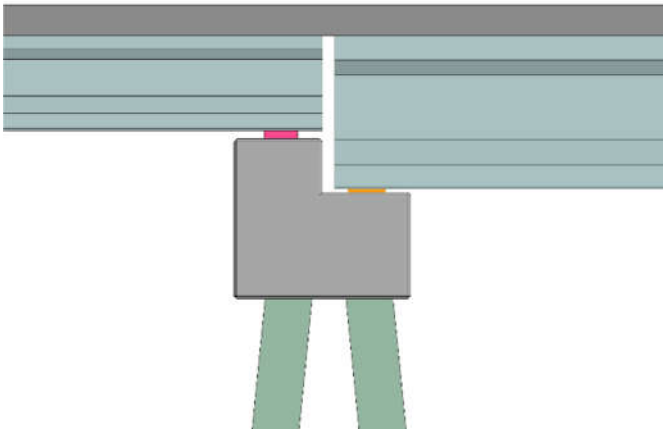

(b)

Figure 42. LS-DYNA close-up views of pile caps: (a) same girders (b) different girders

Material, section and element formulation of the bridge model components are provided in Table 14. Slabs, girders, pile caps and piles are modeled as reinforced concrete. Bearings are neoprene type material and foundation is soil. All of the bridge components are modeled as elastic solid except the foundation, which is elastic shell [88]. Assumed material properties of the bridge model components are provided in Table 15.

Table 14. Material, section and element formulation of bridge model components

Structural Component	Material	Section	Material (MAT)	Element Formulation (ELFORM)
Slab	Reinforced concrete	Solid	001 (MAT_ELASTIC)	2
Girder	Reinforced concrete	Solid	001 (MAT_ELASTIC)	-2
Bearing	Neoprene	Solid	001 (MAT_ELASTIC)	1
Pile Cap	Reinforced concrete	Solid	001 (MAT_ELASTIC)	1
Pile	Reinforced concrete	Solid	001 (MAT_ELASTIC)	2
Foundation	Soil	Shell	001 (MAT_ELASTIC)	2

Table 15. Material properties of bridge model components

Structural Component	Density (kg/m^3)	Density (pcf)	Young's Modulus (Pa)	Young's Modulus (psi)	Poisson's Ratio -
Slab	2,307	144	2.458E+10	3.565E+06	0.150
Girder	2,403	150	3.840E+10	5.570E+06	0.150
Bearing	1,300	81	3.800E+06	5.512E+02	0.499
Pile Cap	2,483	155	3.044E+10	4.415E+06	0.150
Pile	2,681	167	4.257E+10	6.174E+06	0.206
Foundation	2,166	135	4.875E+06	7.071E+02	0.250

3.3.3 Meshing of the Bridge Model

US-51 Highway bridge model has 97 girders (95,495 elements with 180,716 nodes) sitting on a total of 194 neoprene bearings (4,120 elements with 12,222 nodes). A total of 28 slab sections (24,628 elements with 52,642 nodes) in the 3D-FE model forms the bridge deck. The bridge superstructure rests on 18 pile caps (19,542 elements with 28,791 nodes), which are supported by a total of 146 piles (11,664 elements with 26,553 nodes). The entire bridge model, sitting on the foundation soil (18,271 elements with 18,640 nodes), consists of 484 parts, 173,720 elements made up of 319,564 nodes (Table 16).

Table 16. Number of parts, elements and nodes in the 3D-FE model

Structural Component	Number of Parts	Number of Elements	Number of Nodes
Slab	28	24,628	52,642
Girder	97	95,495	180,716
Bearing	194	4,120	12,222
Pile Cap	18	19,542	28,791
Pile	146	11,664	26,553
Foundation	1	18,271	18,640
Total	484	173,720	319,564

3.3.4 Boundary Conditions

Nodes of girder-end bottom-edges are restrained against translation in x and z directions. Nodes of piles at the foundation interface (bottom surfaces of the piles) and all nodes of the foundation are restrained against translation in all directions. Every node of the 3D-FE bridge model is restrained against rotations about x, y and z directions. Tables 17 and 18 represent prescribed boundary conditions and corresponding degree of freedom (DOF) in the 3D-FE model of US-51 Highway bridge.

Total number of DOF is calculated using Equation 3.21:

$$\text{Total DOF} = (3 \times \text{Total Number of Nodes}) - \text{Prescribed DOF} \quad (3.21)$$

$$= (3 \times 319{,}564) - [3 \times (52{,}642 + 180{,}054 + 12{,}222 + 28{,}791 + 24{,}931) + 662]$$

$$\text{Total DOF} = 62{,}110$$

Table 17. Prescribed boundary conditions

	Boundary Condition					
Structural Component	T_X	T_Y	T_Z	R_X	R_Y	R_Z
Slab						
Girder						
End Sections						
Remaining Nodes						
Bearing						
Pile Cap						
Pile						
Bottom Nodes						
Remaining Nodes						
Foundation						

Note: " " denotes fixed translation/rotation (T/R).

Table 18. Prescribed and total number of DOF

	Prescribed DOF					
Structural Component	T_X	T_Y	T_Z	R_X	R_Y	R_Z
Slab	52,642	52,642	52,642	-	-	-
Girder						
End Sections	-	662	-	-	-	-
Remaining Nodes	180,054	180,054	180,054	-	-	-
Bearing	12,222	12,222	12,222	-	-	-
Pile Cap	28,791	28,791	28,791	-	-	-
Pile						
Bottom Nodes	-	-	-	-	-	-
Remaining Nodes	24,931	24,931	24,931	-	-	-
Foundation	-	-	-	-	-	-

Information screen displaying the 3D-FE model information is given in Figure 43. All elements are modeled as deformable – no rigid elements are present in the model.

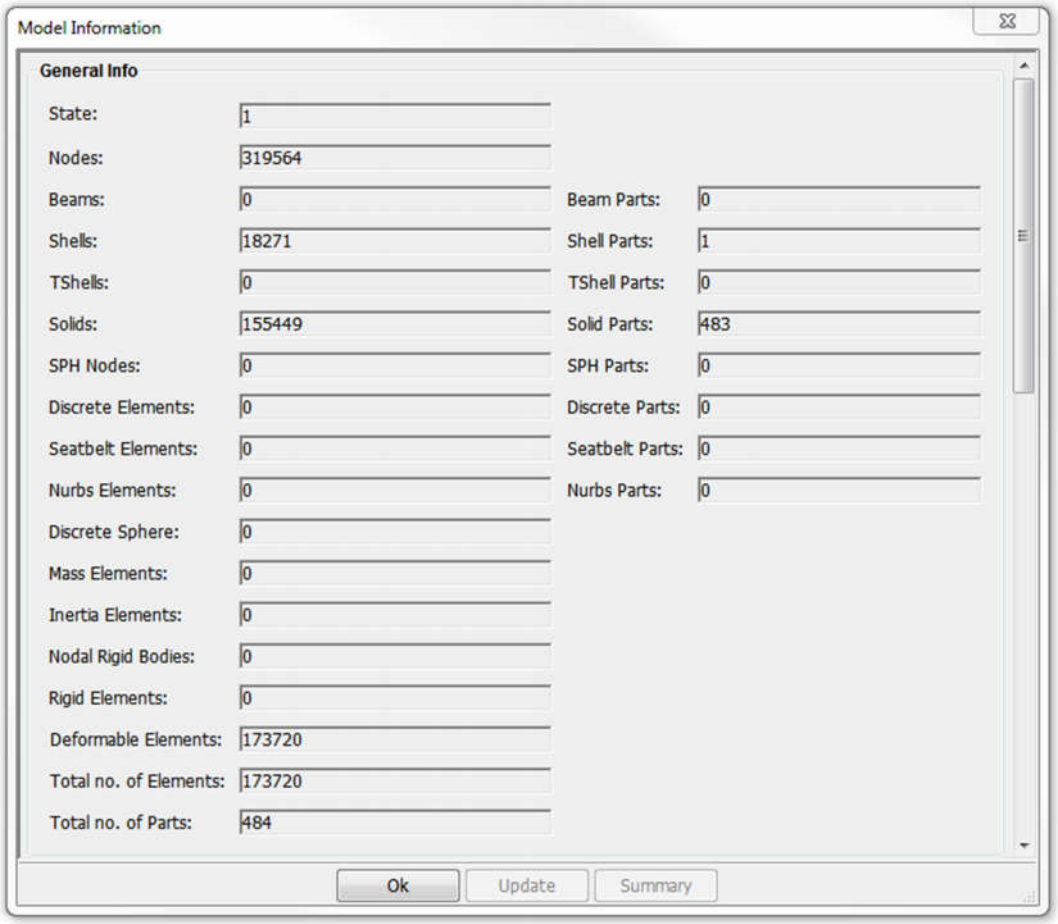

Figure 43. LS-DYNA Model Information

3.3.5 LS-DYNA Contact Definitions

Two types of contact are defined, both of which are segmental. However, surfaces of slab-girder and pile cap-pile contacts are constrained to each other. Table 19 shows the segment based contact definitions in the 3D-FE bridge model. Constrained contact surfaces (girder-slab and pile cap-pile) have static and dynamic friction coefficients of 1.0 and 0.9, respectively. Other

contact surfaces (girder-bearing and bearing-pile cap) have static and dynamic friction coefficients of 0.3 and 0.2, respectively [89].

Table 19. 3D-FE segment based contact definitions

Contact Definition	Master	Slave	Coefficient of Friction (Static)	Coefficient of Friction (Dynamic)
Constraint_Surface_to_Surface	Girder	Slab	1.0	0.9
Constraint_Surface_to_Surface	Pile	Pile Cap	1.0	0.9
Surface_to_Surface	Girder	Bearing	0.3	0.2
Surface_to_Surface	Pile Cap	Bearing	0.3	0.2

3.3.6 Load/Pressure Curve

According to the flood simulation output (Figure 44), floodwater depth at t = 0 is 5.7 m (18.7 ft), which is higher than the bottom elevation of Type IV girders, which is 5.4 m (17.7 ft). Depth of floodwater at next output time step (t = 1,728 sec) is 6.7 m (22.0 ft), which is enough to cover the entire girders and the bridge slab. Maximum floodwater depth is observed at t = 12,096 sec as 7.53 m (24.7 ft).

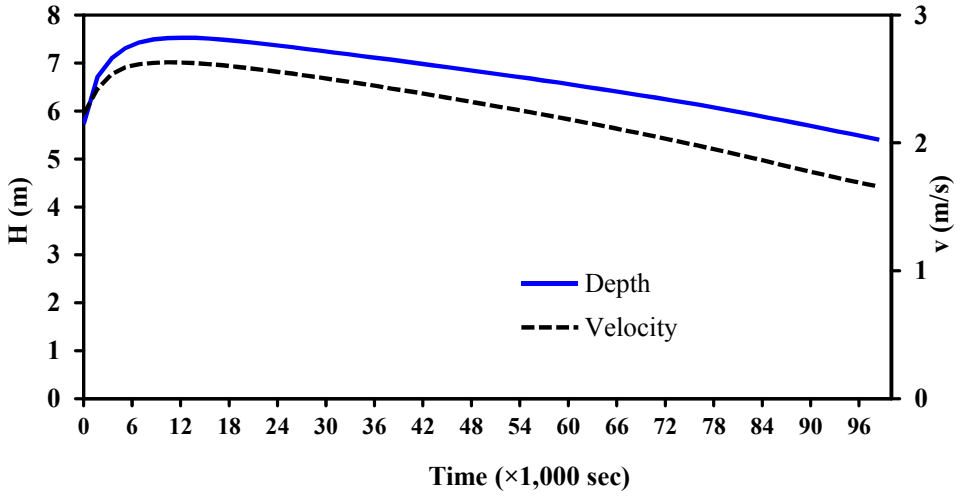

Figure 44. Floodwater depth and velocity at US-51 Highway bridge

Furthermore, depth of floodwater starts falling below the bottom elevation of the girders after 98,496 seconds. It is also observed that maximum velocity is observed at t = 10,368 sec at a magnitude of 2.63 m/s (8.63 ft/s). Therefore, the rest of the time steps are not considered as they are obsolete in terms of floodwater elevation and floodwater velocity magnitude. Initial floodwater velocity is 2.23 m/s (7.32 ft/s). These data constitute the background for the hydrodynamic force curves that will be used in the proceeding 3D-FE simulations (Table 20).

Table 20. Flood simulation output velocities

Time (sec)	Velocity (m/s)	v^2 (m^2/s^2)	Remarks
0	2.23	4.95	Initial
1,728	2.42	5.87	
3,456	2.54	6.45	
5,184	2.59	6.73	
6,912	2.62	6.85	
8,640	2.63	6.91	
10,368	2.63	6.93	Maximum
129,600	1.54	2.38	Final

In order to represent the floodwater velocities as realistically as possible, the initial, maximum and minimum velocities are extracted from the floodwater depth and velocity curve for the center of channel at US-51 (Figure 44). Resulting velocity plots are given in Figure 45. These velocity plots are the basis of loading in the undertaken LS-DYNA simulations.

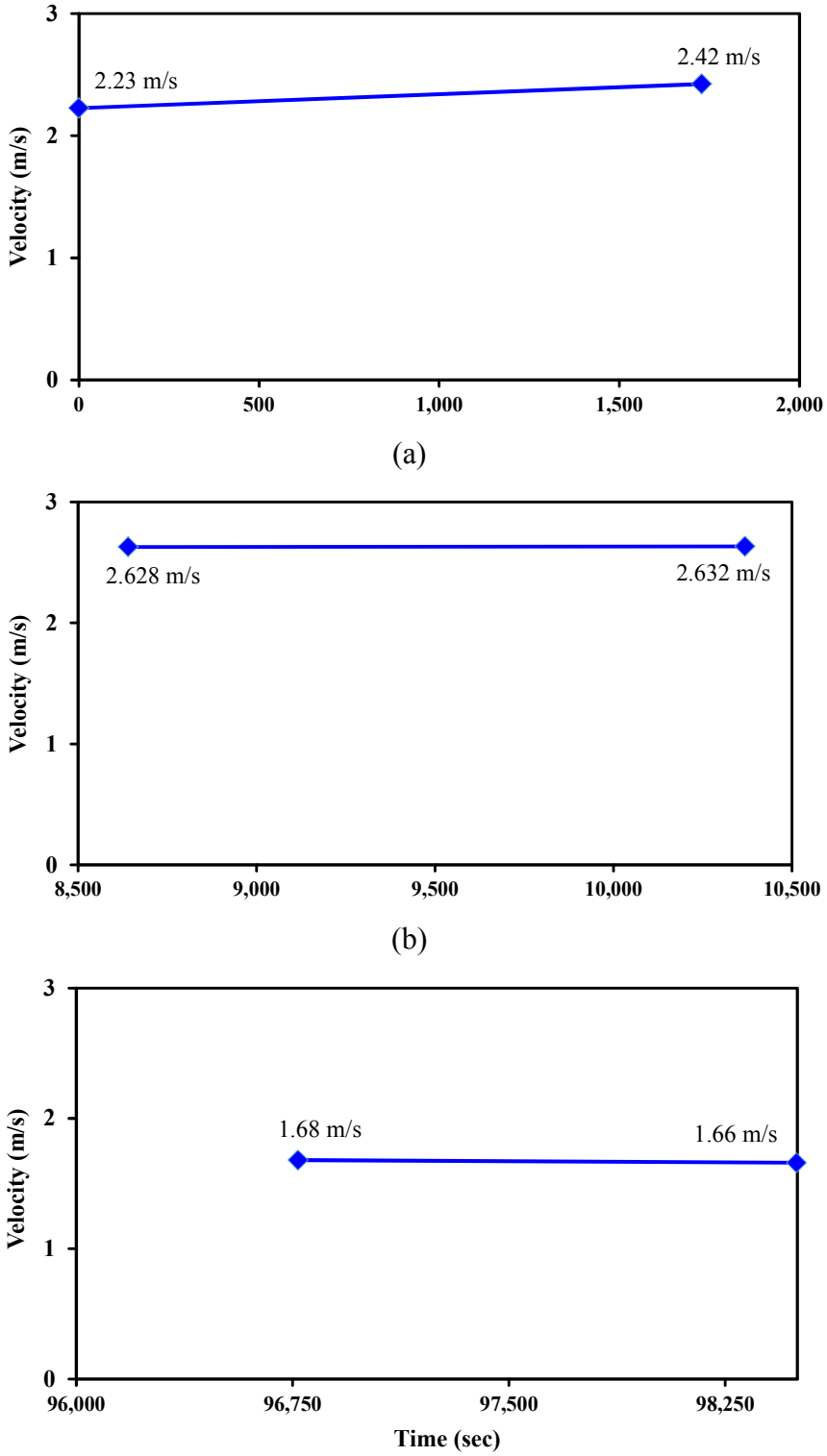

Figure 45. Floodwater velocity plots (a) initial (b) maximum and (c) minimum

It is recommended to check the model in LS-DYNA entirely before running an analysis (Figure 46). Model checking lets the user check the model in terms of element quality as well as keywords and contact. All errors in a keyword check must be avoided for a successful initialization of an analysis, whereas warnings are less strict for an analysis to be performed.

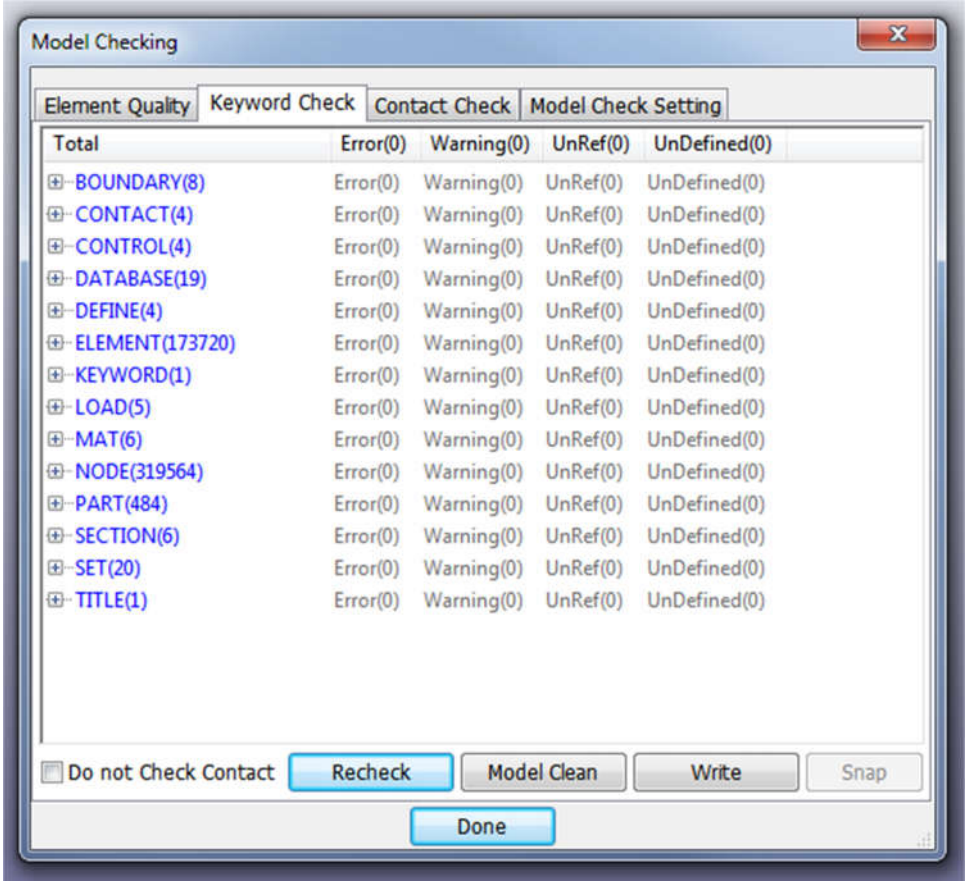

Figure 46. LS-DYNA Model Checking results

3.3.7 LS-DYNA Keywords

The LS-DYNA keywords used are *BOUNDARY, *CONTACT, *CONTROL, *DATABASE, *DEFINE, *ELEMENT, *KEYWORD, *LOAD, *MAT, *NODE, *PART, *SECTION, *SET and *TITLE (Figure 47). Table 21 shows the list of the keywords (after [86]).

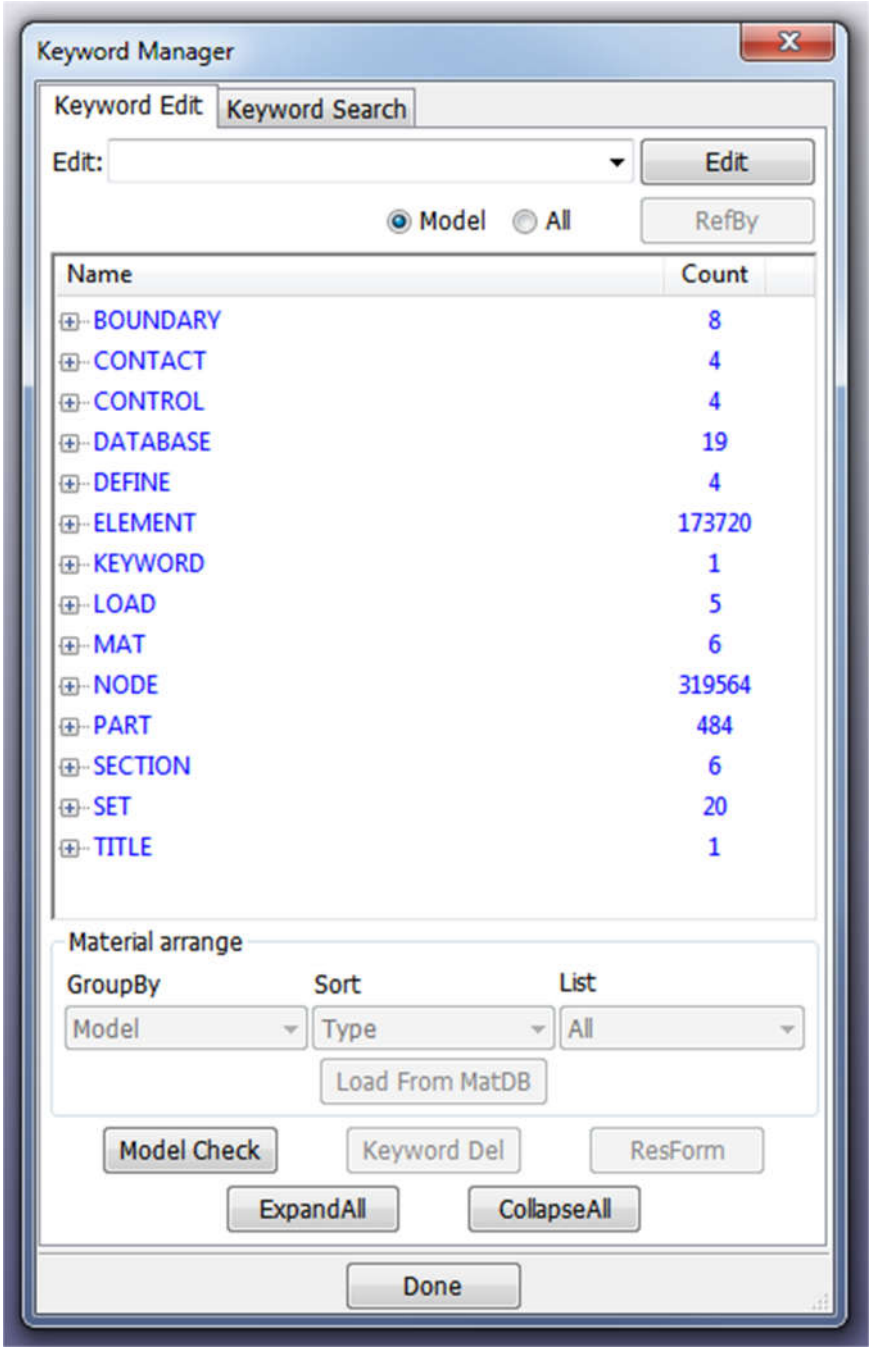

Figure 47. LS-DYNA Keyword Manager showing the model keywords

Table 21. 3D-FE model keywords

Topic	Component	Keywords Used
Boundary Conditions	Restraints	*BOUNDARY_SPC_SET
Contacts	Default for contacts	*CONTROL_CONTACT
	Definition of contacts	*CONTACT_CONSTRAINT_SURFACE_TO_SURFACE
		*CONTACT_SURFACE_TO_SURFACE
Coordinate System	Coordinate System	*DEFINE_COORDINATE _SYSTEM
Geometry	Element	*ELEMENT_SHELL
		*ELEMENT_SOLID
	Node	*NODE
		*SET_NODE_LIST
	Segment	*SET_SEGMENT
Keyword	Keyword	*KEYWORD
Loading	Gravity (body) load	*CONTROL_DYNAMIC_RELAXATION
		*LOAD_BODY_Z
	Load curve	*DEFINE_CURVE
	Pressure load	*LOAD_SEGMENT_SET
Materials	Hourglass	*CONTROL_HOURGLASS
	Material	*MAT_ELASTIC
	Part	*PART
	Section	*SECTION_SHELL
		*SECTION_SOLID
Output Control	ASCII time history files	*DATABASE_ASCII_OPTION
	Binary plot/time history	*DATABASE_BINARY_D3PLOT
	Extent	*DATABASE_EXTENT_BINARY
		*DATABASE_EXTENT_MOVIE
		*DATABASE_EXTENT_MPGS
Termination	Termination time/cycle	*CONTROL_TERMINATION
Title	Title	*TITLE

3.3.8 Other Assumptions

- Bridge railings are ignored.
- Transverse slopes on bridge slab surface are ignored.
- Concrete joint beams between girders are ignored.
- Concrete diaphragm walls at internal supports (i.e. pile caps) are ignored.
- Chamfers are ignored – except along the bottom length of girders.

- All piles are assumed concrete-encased steel H pile.
- All bearings are assumed neoprene type.
- Foundation soil is assumed to be one layer.
- Debris forces are not considered.

3.3.9 LS-DYNA Simulation Type and Computational Effort

The default LS-DYNA analysis is employed in the 3D-FE simulations (i.e. nonlinear, dynamic and explicit). The governing differential equation of motion is given in Equation 3.22 [90]:

$$[M]\ddot{X} + [C]\dot{X} + [K]X = F(t) \tag{3.22}$$

where,

[M] = Mass matrix
[C] = Damping factor
[K] = Stiffness matrix
$\ddot{X}$ = Vector of acceleration
$\dot{X}$ = Vector of velocity
X = Vector of displacement

Equation 3.22 is integrated in order to come up with displacements at the nodes for any given time t. Stresses and strains are calculated using kinematic and constitutive differential equations. Damping is not considered in this study.

The 3D-FE simulations are performed on 64-bit Windows 7 Professional operating system with Intel® Core™ i7-3770K CPU@3.50 GHz and 16GB of RAM. Workstations were

also equipped with NVIDIA Quadro K5000 video cards (4GB GDDR5 memory). Table 22 presents the computational effort for the 3D-FE simulations performed.

Table 22. Computational effort for the 3D-FE simulations

	3D-FE Simulation No.								
Computational Effort	1	2	3	4	5	6	7	8	9
Problem Time (sec)	1.00	1.00	1.00	1.00	1.00	1.00	1.00	1.00	1.00
Number of CPU	6	6	7	7	7	7	7	7	7
Problem Cycle	289,734	289,733	289,734	289,733	289,734	289,734	289,734	289,734	289,734
Elapsed Time (hh:mm:ss)	12:16:31	12:17:05	12:39:25	12:48:34	14:11:44	12:55:00	12:06:14	14:02:09	13:59:10

3.3.10 Final Results of the Floodwater Impact Simulation

Under given lateral hydrodynamic floodwater forces, the pressure acting on the bridge superstructure has values between 1,243 Pa (0.18 psi) for Simulation 1 and 6,917 Pa (1.00 psi) for Simulations 6 through 9 (Table 23).

Table 23. Floodwater velocity, coefficient of friction, pressure and maximum displacement

	3D-FE Simulation No.								
Input	1	2	3	4	5	6	7	8	9
Floodwater velocity (m/s)	1.12	2.23	2.23	2.23	1.66	2.63	2.63	2.63	2.63
Floodwater velocity (ft/s)	3.66	7.32	7.32	7.32	5.45	8.63	8.63	8.63	8.63
Static coefficient of friction*	0.3	0.3	0.3	0.3	0.3	0.3	0.7	0.3	0.3
Dynamic coefficient of friction*	0.2	0.2	0.2	0.2	0.2	0.2	0.6	0.2	0.2
Output									
Pressure (Pa)	1,243.2	4,972.9	4,972.9	4,972.9	2,755.6	6,916.9	6,916.9	6,916.9	6,916.9
Pressure (psi)	0.18	0.72	0.72	0.72	0.40	1.00	1.00	1.00	1.00
Maximum displacement in floodwater direction (m)	0.123	0.899	1.402	1.448	0.809	2.359	2.388	2.083	2.422
Maximum displacement in floodwater direction (ft)	0.40	2.95	4.60	4.75	2.65	7.74	7.83	6.83	7.95

* girder-bearing-pile cap interface

Loaded bridge components and corresponding maximum displacements in the floodwater direction (y direction) are presented in Table 24. Only front girders are loaded in Simulations 1

and 2. All of the girders are loaded in the rest of simulations. Simulations 4 through 8 additionally have the slab (laterally) loaded, and uplift to the slab is considered. Simulation 9 has the piles and pile caps loaded. The maximum displacement range is between 0.098 m (Simulation 1) and 2.422 m (Simulation 9).

Table 24. Maximum displacements in floodwater direction

	3D-FE Simulation No.								
Loading	1	2	3	4	5	6	7	8*	9*
Front Girders**									
All Girders									
Slab									
Uplift***									
Piles									
Pile Caps									
Simulation Time (s)	Maximum Displacement in Floodwater Flow Direction (m)								
0.00	0.000	0.000	0.000	0.000	0.000	0.000	0.000	0.000	0.000
0.05	0.002	0.009	0.009	0.009	0.005	0.013	0.013	0.013	0.013
0.10	0.011	0.023	0.027	0.028	0.019	0.037	0.037	0.037	0.037
0.15	0.018	0.030	0.047	0.047	0.034	0.061	0.061	0.061	0.061
0.20	0.020	0.047	0.074	0.075	0.050	0.096	0.099	0.096	0.096
0.25	0.022	0.055	0.101	0.103	0.064	0.148	0.148	0.148	0.148
0.30	0.027	0.077	0.142	0.146	0.082	0.213	0.214	0.213	0.213
0.35	0.040	0.092	0.187	0.193	0.107	0.279	0.280	0.279	0.278
0.40	0.056	0.118	0.246	0.253	0.141	0.364	0.364	0.363	0.362
0.45	0.073	0.146	0.303	0.312	0.173	0.454	0.455	0.453	0.453
0.50	0.085	0.181	0.372	0.382	0.211	0.561	0.561	0.557	0.555
0.55	0.091	0.223	0.449	0.462	0.255	0.679	0.680	0.673	0.670
0.60	0.103	0.255	0.532	0.548	0.304	0.800	0.801	0.793	0.790
0.65	0.114	0.281	0.616	0.635	0.354	0.922	0.924	0.916	0.912
0.70	**0.123**	0.321	0.706	0.728	0.406	1.053	1.054	1.046	1.057
0.75	0.123	0.397	0.807	0.832	0.464	1.222	1.233	1.195	1.240
0.80	0.119	0.479	0.910	0.940	0.526	1.416	1.428	1.353	1.436
0.85	0.119	0.565	1.025	1.059	0.591	1.631	1.647	1.526	1.661
0.90	0.117	0.679	1.148	1.186	0.662	1.871	1.892	1.708	1.906
0.95	0.111	0.772	1.275	1.316	0.734	2.104	2.123	1.895	2.148
0.99	0.098	0.899	1.402	1.448	0.809	2.358	2.388	2.083	2.422
1.00	0.098	**0.899**	**1.402**	**1.448**	**0.809**	**2.359**	**2.388**	**2.083**	**2.422**

* with channel bed/foundation soil
** girders facing floodwater
*** slab only

The response of US-51 Highway bridge model to lateral hydrodynamic forces (i.e. displacement in floodwater direction) is seen in LS-DYNA screen captures as shown in Figures 48 through 51.

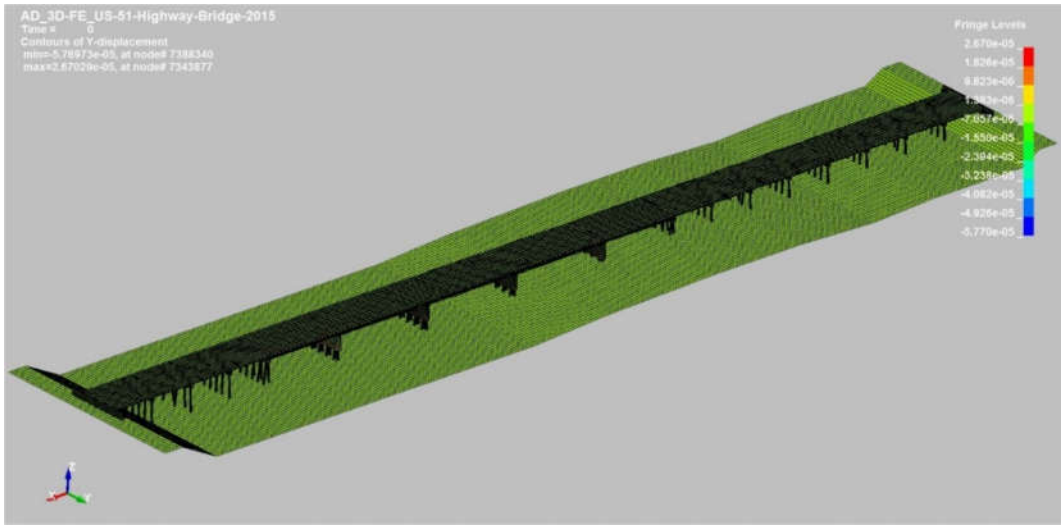

(a)

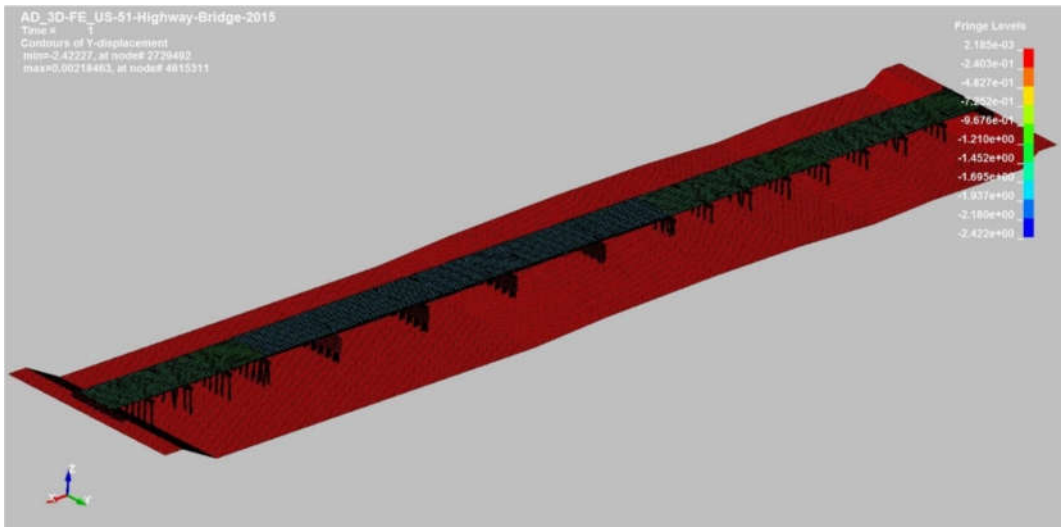

(b)

Figure 48. Entire bridge at (a) t = 0 and (b) t = 1 sec

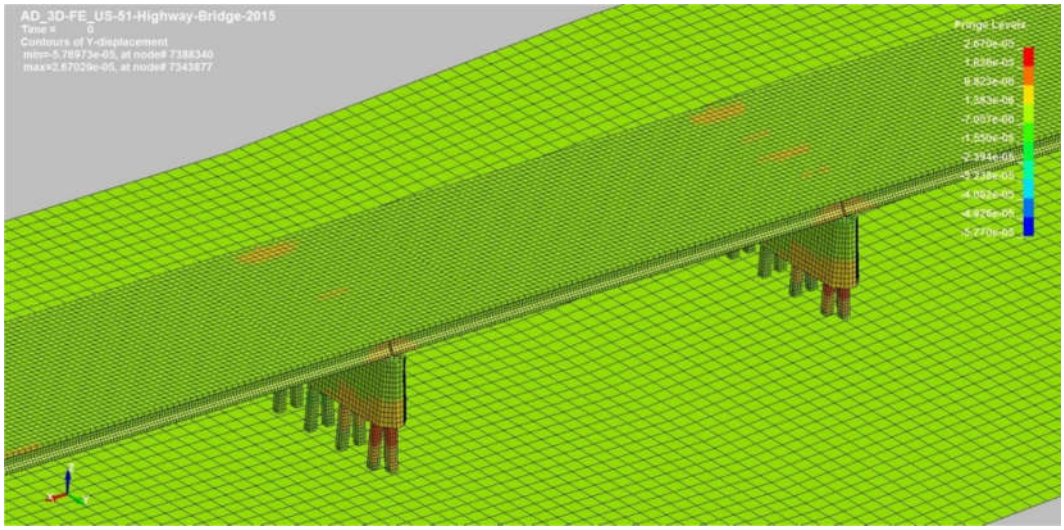

(a)

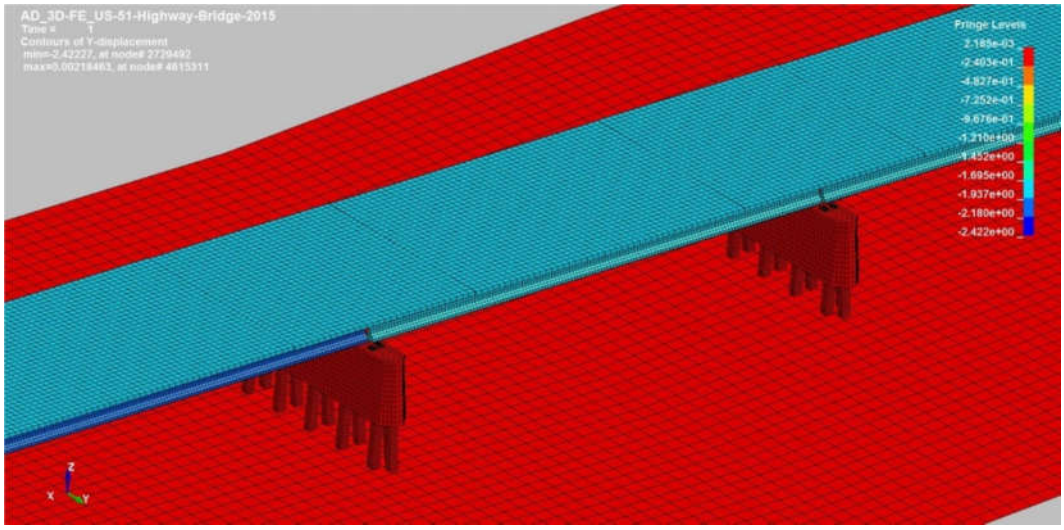

(b)

Figure 49. An internal span (a) t = 0 and (b) t = 1 sec

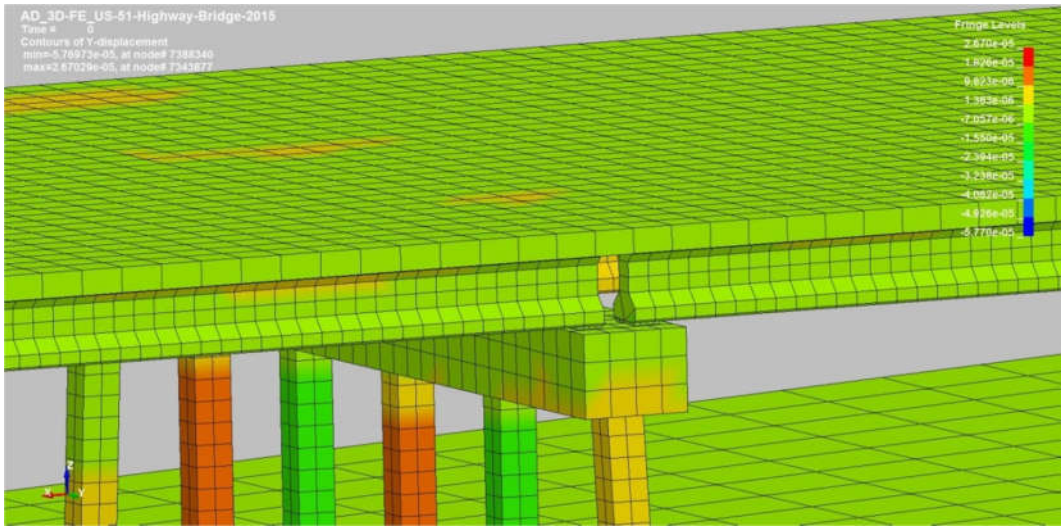

(a)

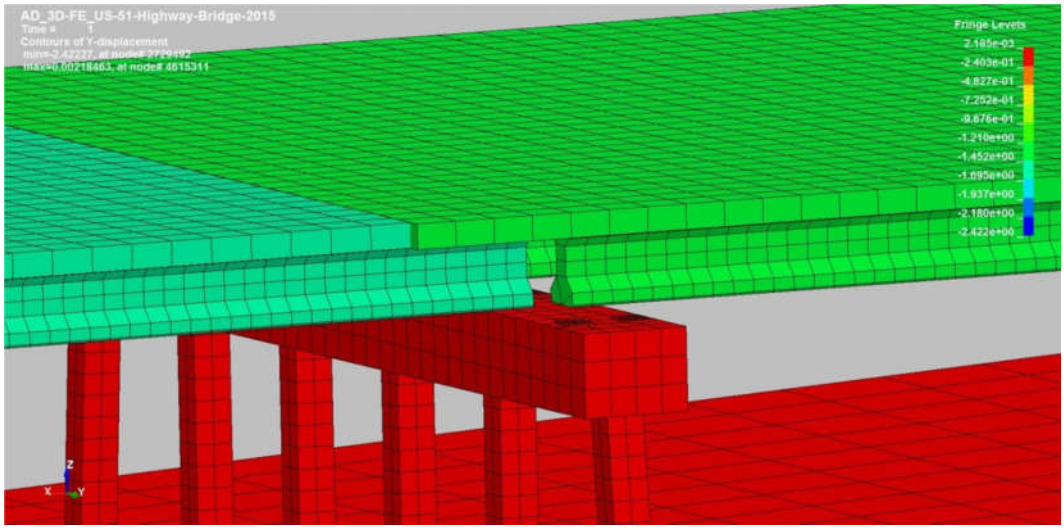

(b)

Figure 50. A pile cap at (a) t = 0 and (b) t = 1 sec

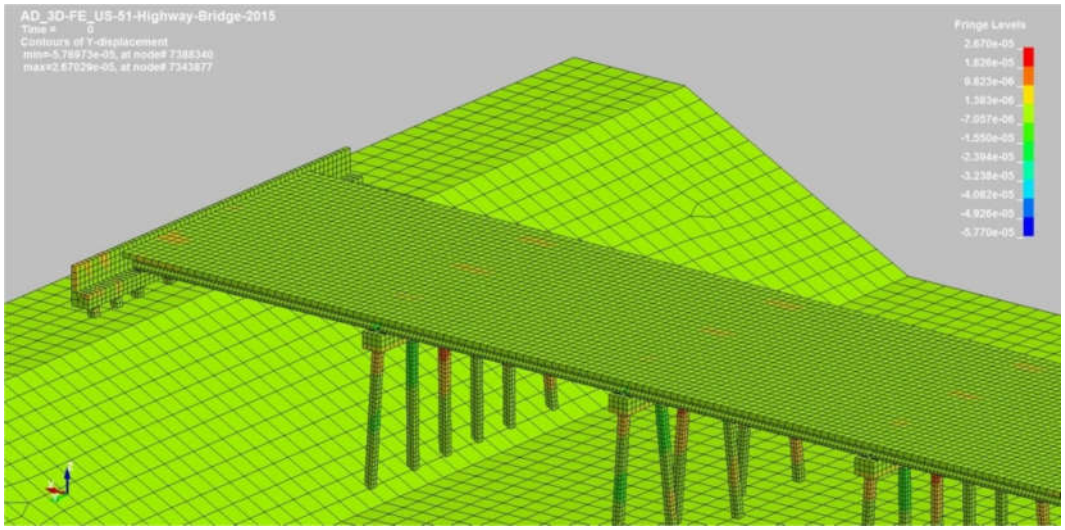

(a)

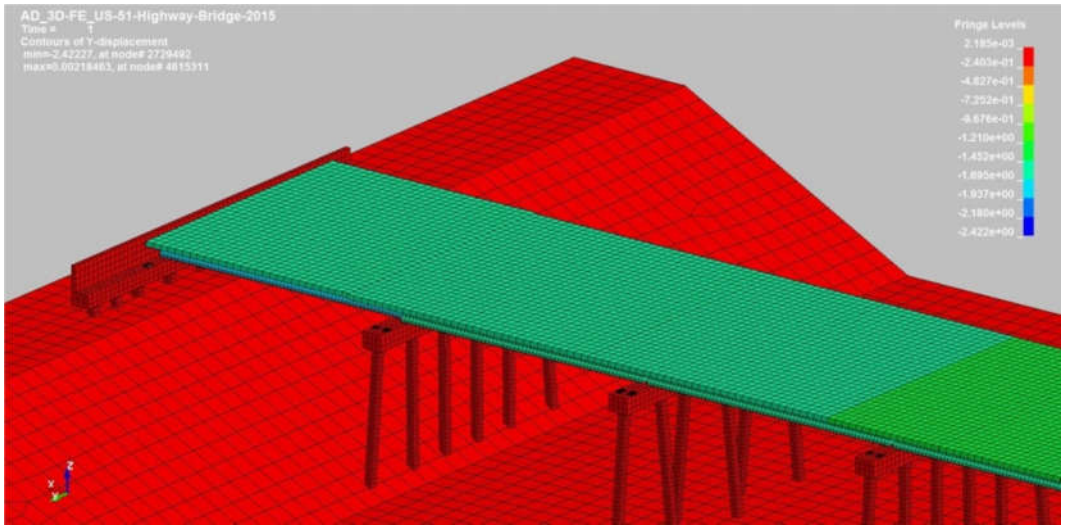

(b)

Figure 51. South abutment at (a) t = 0 and (b) t = 1 sec

Figure 52 displays the vertical contact force between girders and bearings over the simulation time. Maximum vertical contact force is 620,000 N.

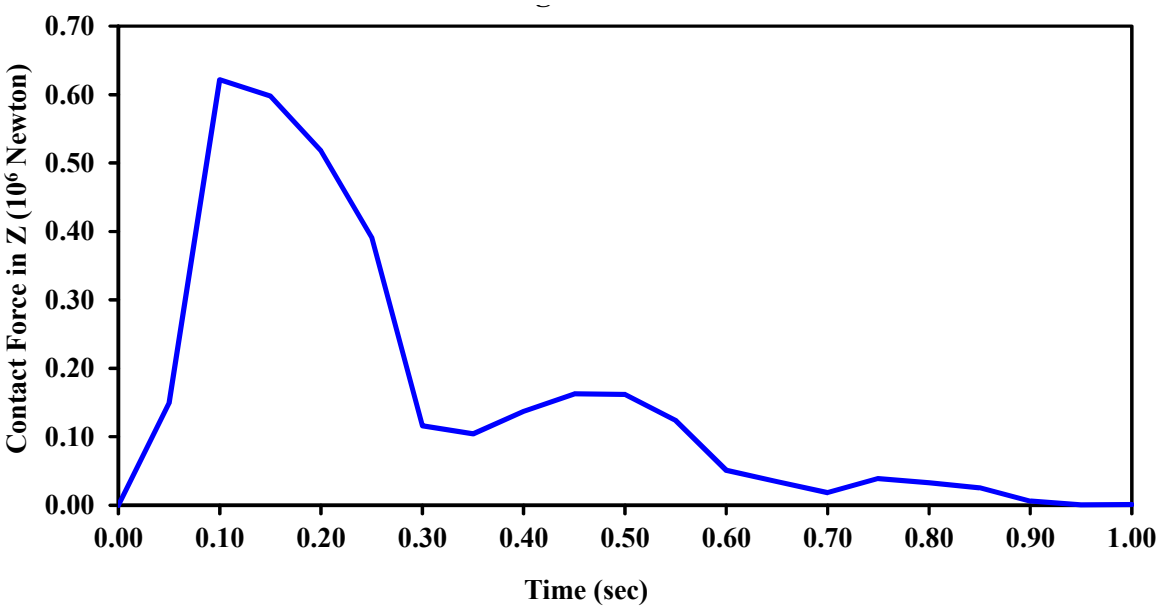

Figure 52. US-51 Highway bridge girder-bearing vertical contact force

3.4 Lessons Learned from the Results of US-51 Highway Bridge 3D-FE Simulation

Next sections in this chapter discuss the lessons learned from the results of the US-51 Highway bridge 3D-FE simulation.

3.4.1 Failure of Bridge Superstructure due to Sliding of Girders

Lateral displacement ranging between 0.098 m (Simulation 1) and 2.422 m (Simulation 9) indicates that superstructure of US-51 Highway bridge will most likely collapse under indicated hydrodynamic floodwater forces.

Figure 53 displays the maximum displacements of three 3D-FE simulations plotted versus floodwater velocities. Displacement of the superstructure increases with increasing floodwater velocity.

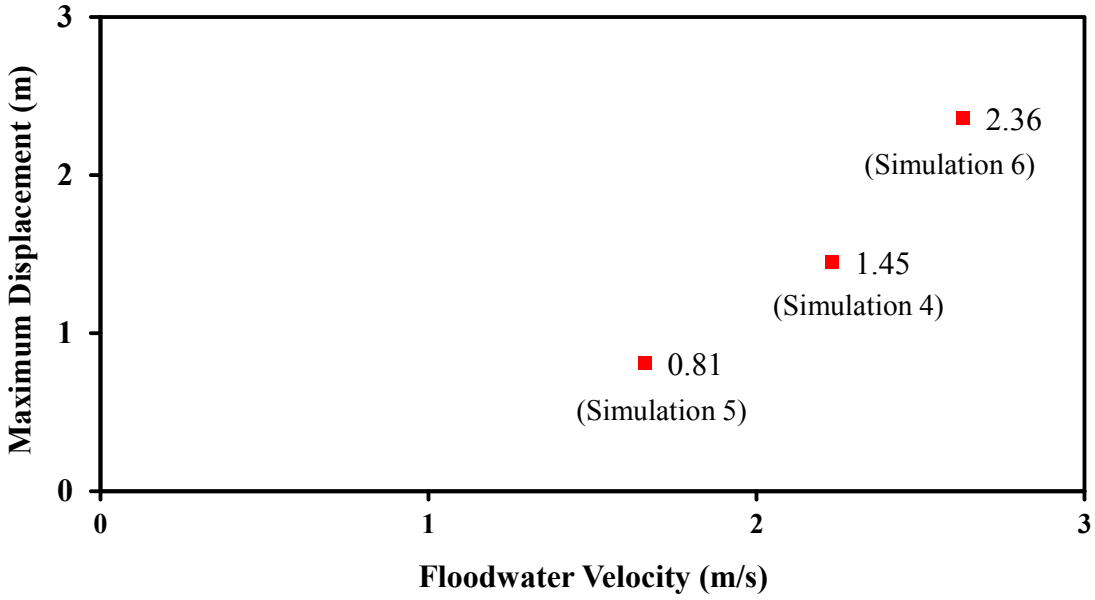

Figure 53. Maximum displacement vs. floodwater velocity

There is no indicator in NBI [23] whether bridge superstructure type is an integral type etc. Integral abutment bridges are "where the superstructure and substructure move together to accommodate the required translation and rotation" [91]. Fully integrated abutment bridges (FIAB) are those where bridge superstructure is directly connected/fixed to substructure [91]. Semi-integrated abutment bridges (SIAB) are those where "backwall portion of the substructure is directly connected with the superstructure" [91]. In the case of SIAB, girders rest on bearings, and bearings rest on pile caps. Therefore, the US-51 Highway bridge can be regarded as an example of SIAB.

Approximate calculations of the total weight and lateral area of US-51 Highway bridge are presented in Tables 25 and 26. Lateral force required to initiate superstructure movement and lateral hydrodynamic force acting on the bridge are calculated as 10,804 kN and 12,585 kN, respectively.

Table 25. Weight of US-51 Highway bridge superstructure

	No.	Cross-section (m^2)	Length (m)	Density (kg/m^3)	Weight (kgf)
Slab	28	3.858	273.6	2,307	2,434,718
Girder					
Type I	72	0.213	13	2,403	478,946
Type III	10	0.365	24	2,403	210,417
Type IV	15	0.507	30	2,403	548,094
				Superstructure Total Weight (kgf)	3,672,175
				Superstructure Total Weight (kN)	36,012
				Static Coefficient of Friction (referring to Table 19)	0.3
				Lateral Force Required to Initiate Superstructure Movement (kN)	10,804

Table 26. Lateral area of US-51 Highway bridge superstructure

	No.	Lateral Area (m^2/m)	Length (m)	Lateral Area (m^2)
Slab	28	0.30	273.6	82.1
Girder				
Type I	72	0.79	13	744.0
Type III	10	1.27	24	305.1
Type IV	15	1.53	30	688.3
			Superstructure Total Lateral Area (m^2)	1,819.5
			Pressure on Unit Lateral Area (referring to Table 23) (Pa)	6,916.9
			Lateral Hydrodynamic Force on Superstructure (kN)	12,585

FS against sliding = 10,804 ÷ 12,585

= 0.86

White [91] reports the number of FIAB and SIAB in the United States as more than 9,000 and more than 4,000, respectively. With a deliberate overestimation of the number of FIAB, and a deliberate underestimation of the total number of bridges in the United States, 10,000 FIAB out of total 600,000 would correspond to less than 2% of the U.S. total bridge inventory.

The results of the 3D-FE simulation and FS of the bridge superstructure against sliding agree with field evidence (Figure 54). Even though the right hand side girders of the superstructure seem to have not displaced as much, this issue needs immediate attention.

Figure 54. US-90 to I-10 Ramp Bridge over Mobile Bay, AL after Hurricane Katrina (Photo Credit: MCEER [63])

3.4.2 Failure of Dowel Bars

It was observed that the bearings used in the US-51 Highway bridge are of neoprene/elastomeric type [92]. The thickness of the bearings is generally less than 2” which was ignored in the calculations and 3D-FE simulations (Figure 55). A dowel type steel rod is used to maintain the alignment of the girder during temperature-related movements of the girder. The dowel is inserted through the hole in the bearing such that the top end of the dowel is inside the bottom part of the girder and the bottom end of the dowel is secured inside the top part of the pile cap.

Figure 55. A typical neoprene bridge bearing
(Photo Credit: MDOT Bridge Division)

The sole purpose of the bearing-dowel assembly for the girder is to facilitate the girder movement during thermal expansion and contraction. Neoprene bearings between girders and pile caps are provided to accommodate movement of girders due to daily and seasonal temperature changes. As explained earlier, they are held in a desired location by a small steel rod

embedded in girders and pile caps. Their purpose is to ensure that the neoprene bearings stay in place. Any movement of the girder (above the pile cap) will destabilize and potentially rupture the bearings. Consequently, they will fail to function properly and allow for temperature-related movement. Depending on the contact pressure and type of neoprene bearing, it would be reasonable to assume that concrete-to-concrete friction coefficient will be higher than concrete-to-bearing friction coefficient [93, 94]. When bearings fail, the stress in girders will also increase, and the temperature-related girder movement will be restrained due to bearing failure.

Referring to Figure 52, lateral force required to displace a Type IV girder – with a 0.3 static coefficient of friction is 620,000 N × 0.3 = 186,000 N.

It is necessary to evaluate the dowel bar stability in terms of shear stress that the dowel will be subjected to during relative displacement of girders and pile caps. The following assumptions are made for the dowel bar stability analysis:

- Minimum yield strength of steel, F_y = 50 ksi [95]
- Dowel bar diameter = 3 cm

Noting that 50 ksi = 344.7 MPa, allowable shear stress in dowel bars is calculated using Equation 3.23 [95]:

$$F_v = 0.33 \times F_y \tag{3.23}$$

$$F_v = 0.33 \times 344.7 \text{ MPa}$$
$$= 113.75 \text{ MPa}$$

Cross-section area of a dowel bar = 0.0007 m^2

Total cross-section area of two dowel bars = 0.0014 m^2

Shear stress in dowel bars is calculated with Equation 3.24:

$$\tau = \frac{F}{A} \tag{3.24}$$

τ = 186,000 N ÷ 0.0014 m^2
= 132,857,143 Pa
= 132.9 MPa

FS against shear = 113.75 MPa ÷ 132.9 MPa
= 0.86

It is concluded that the dowel bars are vulnerable and highly likely to fail under the lateral forces generated in girder-bearing surfaces. Possible debris forces on the bridge, which should be evaluated for any type of a flooding scenario [70], are outside the scope of this research.

3.4.3 Parametric Study

A parametric study was done (3D-FE Simulation No. 10) to help understand the effects of girder density, girder Young's Modulus etc. on lateral maximum displacement. Results of this preliminary parametric study are given in Table 27.

Table 27. Parametric study results

	3D-FE Simulation No.	
Independent Variables	9 (concrete girder)	10 (steel girder)
Floodwater velocity (m/s)	2.63	2.63
Girder density (kg/m^3)	2,403	7,210
Girder Poisson's ratio	0.15	0.27
Girder Young's Modulus (MPa)	3.840E+04	2.068E+05
Coefficient of friction (static)	0.3	0.3
Coefficient of friction (dynamic)	0.2	0.2
Dependent Variables		
Pressure on girders (Pa)	6,917	6,917
Weight of 13-m Span (kgf)	174,482	292,077
Maximum displacement in floodwater direction (m)	2.422	1.015

It is seen that the mass of a typical 13-m span is 174,482 kg in original analysis, whereas 292,077 kg in steel girder case (67.4% increase). The displacement of girder-deck assembly is 58.1% less in the steel girder case (1.015 m vs. 2.422 m) due to higher Young's Modulus of steel and higher mass of the superstructure.

The response of modified US-51 Highway bridge (3D-FE Simulation 10) to lateral hydrodynamic forces (i.e. displacement in floodwater direction) is seen in LS-DYNA screen capture as shown in Figure 56.

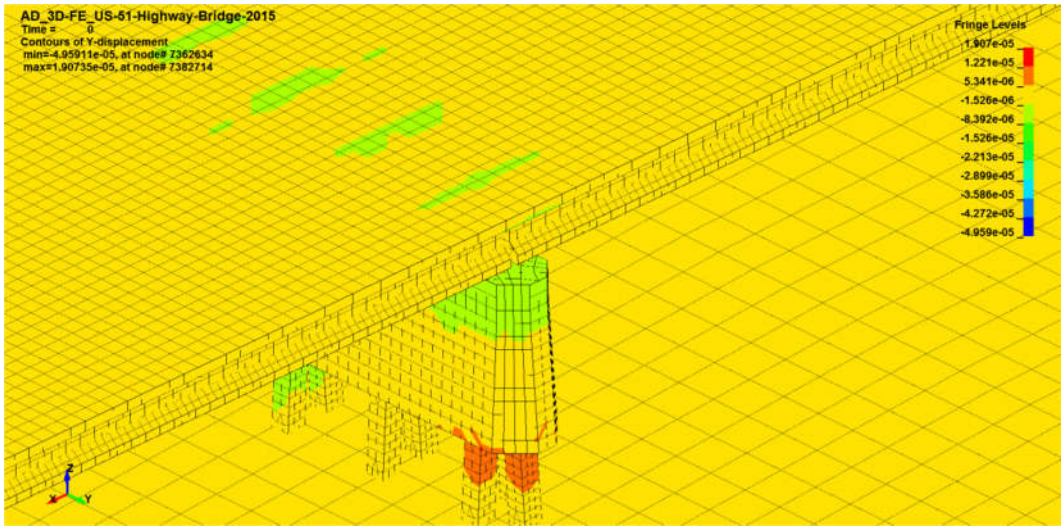

(a)

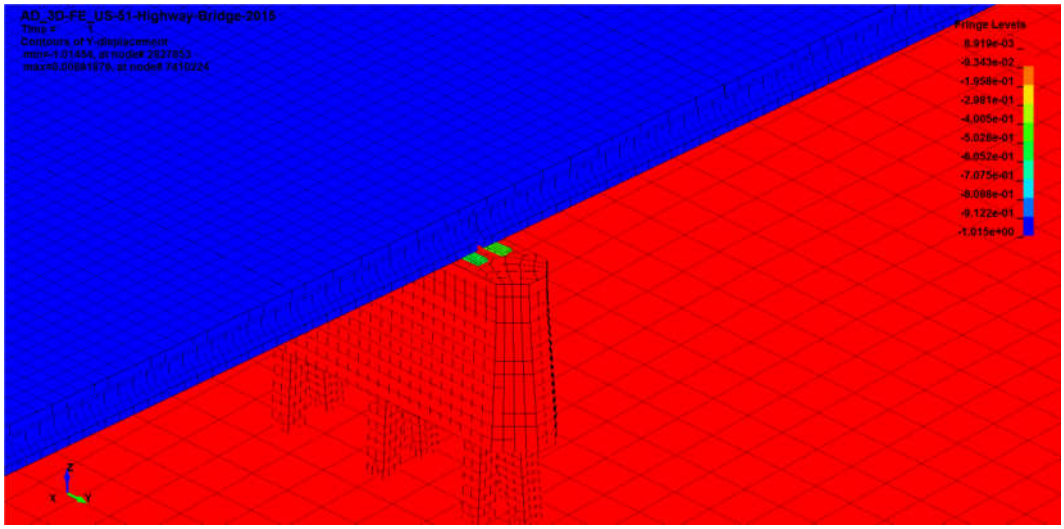

(b)

Figure 56. Parametric study: A pile cap at (a) t = 0 and (b) t = 1 sec

It is recommended to advance the parametric study for better understanding of structural properties of bridge components – especially of the superstructure – on lateral displacement under given hydrodynamic forces.

IV. FLOOD DISASTER RESILIENT BRIDGE STRUCTURES AND HARDENING

4.1 Framework for Structural Integrity Assessment of Bridges Subjected to Floods

A framework for structural integrity assessment of bridges subjected to floods is presented in Figure 57. The framework aims to help understand the hardening needs of a bridge superstructure and its foundation by structural integrity assessment and evaluation of scour potential, respectively. The framework yields four decisions:

- Harden Entire Bridge.
- Harden Superstructure.
- Harden Foundation.
- Bridge Safe – no immediate need for hardening.

Proximity of a bridge to a river, levee, dam, etc. is considered as a firm criterion in the framework. However, evaluating every bridge in an inventory is recommended for a successful flood disaster resilience assessment. Depending on the superstructure's FS against overturning/sliding and dowel shear stability, a bridge Flood Resilience Index (FRI) is proposed on a scale of 1 to 4 (Table 28).

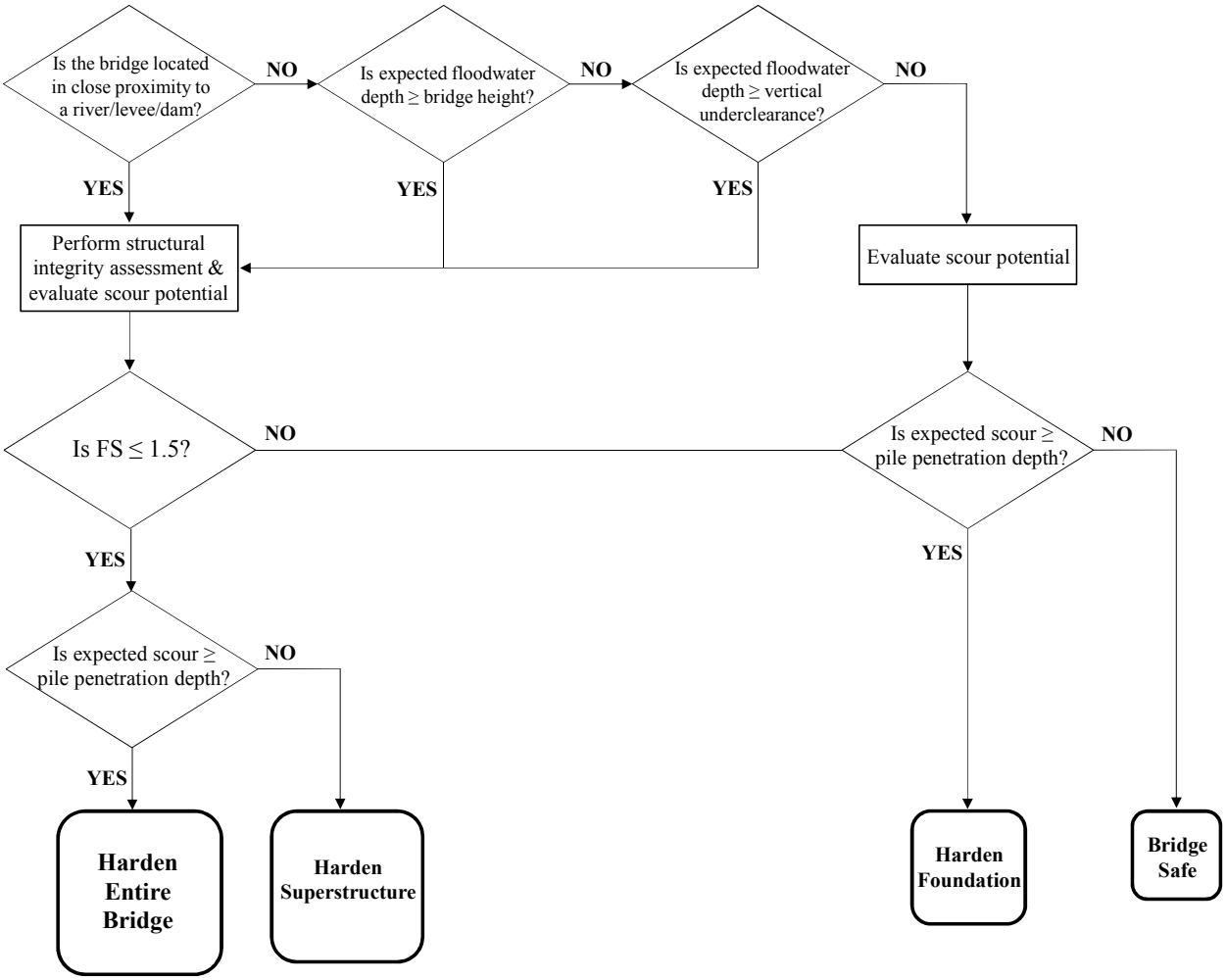

Figure 57. Structural integrity assessment framework

Table 28. Flood Resilience Index (FRI)

FRI	Rating	FS
1	Imminent Failure	< 1.0
2	High Risk	1.0-1.5
3	Moderate Risk	1.5-2.0
4	Low Risk	> 2.0

4.2 Enhanced Design and Hardening for Flood Disaster Resilient Bridges

4.2.1 Enhanced Design Considerations

It has been shown that vulnerability of a highway bridge to floodwater forces depends on bridge height from adjacent ground. This is coupled with floodwater flow velocity and geometrical properties of the bridge elements that affect the hydrodynamic drag coefficient. Vertical dimensions of bridge elements such as girder height and slab thickness present the surface area on which floodwater forces would generate pseudo-static and lateral hydrodynamic pressure acting against the structural integrity of the bridge. The number of girders and girder spacing play important roles on how much force will be exerted on the bridge superstructure. The following recommendations will help design flood disaster resilient bridges:

- Implementation of floodwater forces to bridge design codes is critical for new bridges.
- It is shown that total width of the bridge superstructure (i.e. dimension that is perpendicular to the traffic flow direction) acts in favor of the structural integrity of the bridge structure by providing resisting moment. This would mean a more stable bridge structure as the total width of the bridge increases.
- Girders should be anchored to the substructure.
- A possible strategy for new design is using extra rebar/reinforcement along the web of the girders. Note that these moments are outside the scope of this research.
- The preliminary/concept design stage of a bridge structure is critical, as changing the bridge elevation, bridge structure type etc. pose too many challenges at a later design stage [77]. Resilience of not only the bridge structure, but also the waterway and bridge approach network should be considered at the preliminary design stage.

- Outputs of flood modeling and numerical simulations need to be processed and interpreted prior to application/implementation in bridge design works [77]. There is currently no comprehensive approach that describes how debris effects are assessed at bridge structures during flooding events. It is recommended to use historical records for this purpose. Measures for reducing the likelihood of debris accumulation should also be considered [77]. This can be achieved by sufficient widths of openings against possible accumulation of debris [96].
- Serviceability of the road and bridge networks after a flooding event remains crucial, as a potential overtopping will render the bridge structures impassable [77]. The importance of the bridge and roads need to be clearly defined, especially for those crossing channels and rivers.
- Another problem is present when the floodplain is wider than the main channel of the river. When the bridge deck level is close to the average water level, this makes the bridge more vulnerable to the impacts of flooding. On the other hand, a higher bridge crossing, while improving the resilience of the bridge structure, would require a higher embankment and/or approach and therefore result in significant afflux and an increased blockage of flow area [77]. This would additionally result in significantly longer and more expensive bridge structures. “A means of assessing the economic requirements offset against the required network resilience” would help in an optimum bridge design length, elevation and position [77].

4.2.2 Enhanced Hardening Considerations

Damages during flooding include stripping of approach pavement, undermining of abutments, scouring of approach embankments, build-up of debris on the bridge and deposition on approaches as well as sedimentation in river channels [77]. Volume of debris from a minor flooding event can easily reach 2,000 m^3 [77]. Consequences of inadequate infrastructure resilience include not only economic but also humanitarian and social costs (Figure 58).

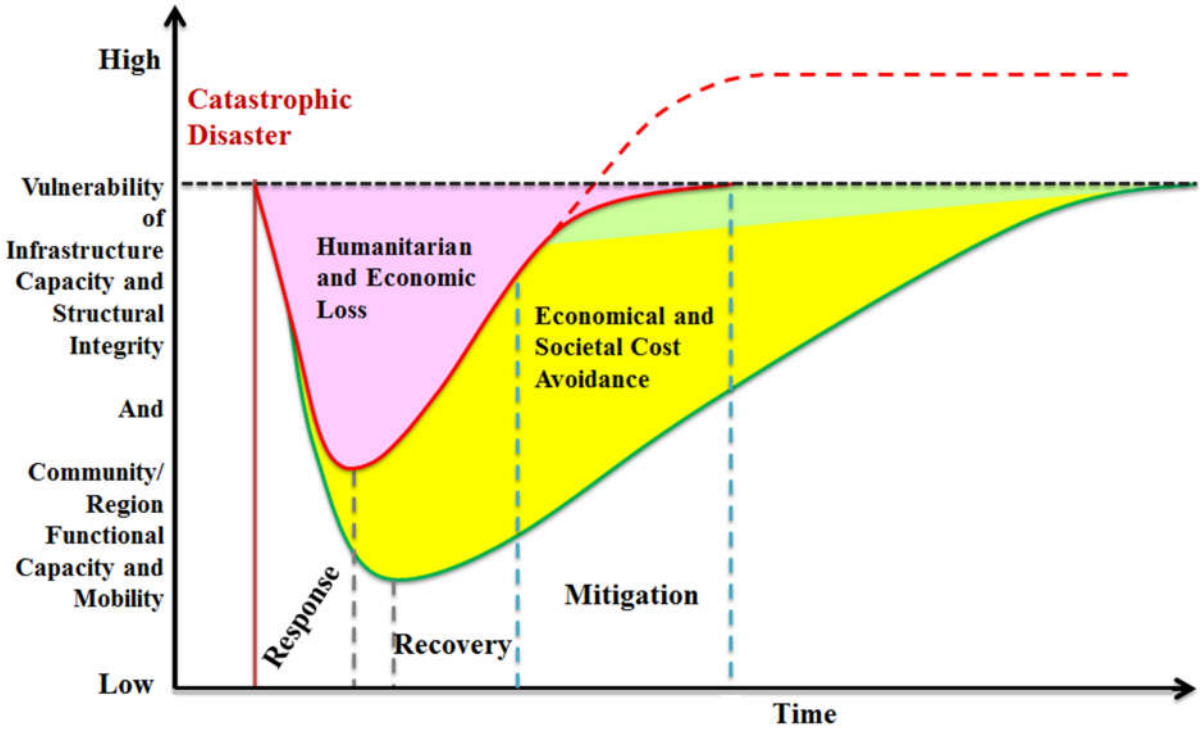

Figure 58. Consequences of inadequate infrastructure resilience
(after Hynes and Ross in CRSI [97])

Superstructures of bridges that experienced horizontal foundation movements of 1-2" were distressed [98]. It was also shown that bridges were inherently more vulnerable to horizontal movements than vertical movements (i.e. settlements). Abutment damages and

horizontal movement appeared to be more frequent for horizontal foundation movements of 2" and greater [98]. Bearings were also affected [98]. Exposed piles need attention as after flood scour may cause a tilt/rotation by a few inches at the pile top, which would contribute to failure [96].

The following recommendations will help to safeguard vulnerable bridges by hardening:

- Original bridge designs should be checked for structural and hydraulic deficiency against the relatively new criteria introduced by FHWA [69, 80, 81].
- Shear blocks are being used, but not always. Figure 59 shows a survived bridge during 2005 Hurricane Katrina in Biloxi Bay, Mississippi. It is recommended to provide shear blocks on every pile cap and to both sides of each girder. Required shear section will be determined by the type of material, i.e. concrete, FRP etc. This should be evaluated with value engineering (VE) analysis of life cycle cost (LCC).
- A possible strategy for hardening is using steel plates to be fixed along the web(s) of girders. This would help resist horizontal moments (along z direction) due to lateral floodwater forces. Note that these moments are outside the scope of this research.
- Inspection and flood watch reports [96] are essential for any type of bridge.
- It can be assumed with confidence that uplift forces will not be able to lift up the bridge structure, and this is based on the fact that unit weight of bridge materials are higher than that of floodwater. However, uplift forces act against the gravity, therefore against the dead weight of the bridge. Therefore, given the fact that the superstructures are – most of the time – not connected/fixed to the substructure, restraint against uplift forces is recommended.

- Modes of past bridge failures should also be investigated, e.g. is bridge failure due to local failure of girders or exposed piles [96].
- For every scour-critical bridge, tracing of the history of past floods and effective countermeasures is recommended [96].

Figure 59. Shear blocks at a concrete girder bridge in Biloxi Bay, MS
(Photo credit: MCEER [63])

- Bridges should be checked if diaphragms, joint beams between girders and cross frames adequately brace the girders [96]. If not, providing a girder restraining system is recommended towards the goal of flood disaster resilient bridges. This will ensure

uniform movement of girders to accommodate temperature changes, which will also protect the bearings in their place as intended. For example, 1 ft wide U-shaped steel plates can be mounted below all the girders at two locations on every span. The steel plate would function as a "stirrup" to hold the girders together and prevent misalignment of girders. The length of each stirrup will be determined by the distance between girders.

- An alternative material is thick fiber-reinforced plastic (FRP) plates to be glued by epoxy on the bottom of girders at a minimum of two locations on every span.

As mentioned earlier, climate impacts of SLR, hurricanes and ocean storm surges present other threats to the coastal infrastructure [13].

4.3 Resilience Management in View of Ocean Wave Surges due to SLR and Tsunamis

Research shows that flood hazard due to heavy rainfall and tsunami on coastal areas are more disastrous than the SLR, which is expected gradual [99] over many decades. The methodology described in Chapter III as well as design and hardening considerations can be applied to coastal infrastructure for ocean wave surge from SLR and abrupt tsunamis [99].

Coastal cities should be reevaluated against the possible risk of land submerge associated with tsunami wave surge inundation and abrupt SLR. One option would be constructing seawalls using innovative materials such as FRP [12]. For the case of gradual SLR, populations of coastal areas can be moved – gradually – away from the coast. Floodgates could be given consideration for the case of deltas and river openings. A magnitude of 100-year flood has a 1 percent chance

of happening in any year [100]. It can be argued that a 100-year event can happen two times in five consecutive years. Therefore, the need for flood disaster resilient bridges is imminent.

4.4 Implementation of Flood Disaster Resilience for Bridge Management

A framework showing transportation infrastructure disaster resilience improvement is shown in Figure 60. As mentioned earlier, critical transportation infrastructure assets include highways, rail lines, bridges, ports, terminals, airports, underground utilities and pipelines.

Disaster resilience and climate adaptation requires identifying, assessing, communicating and mitigating risk, which requires continuous renewal and improvement.

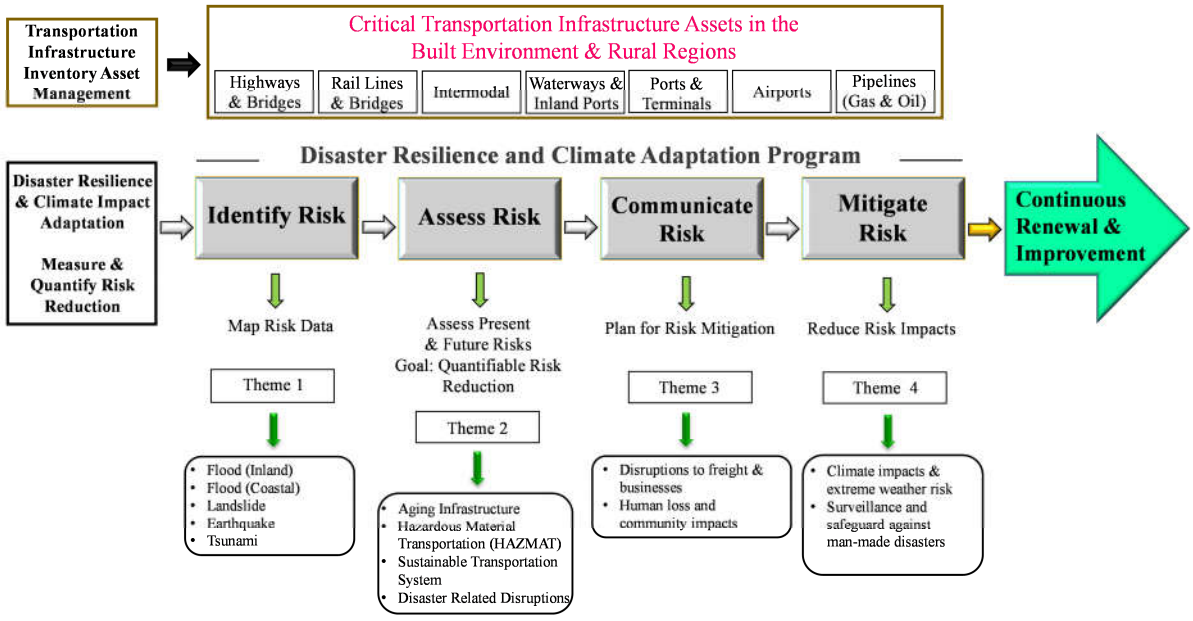

Figure 60. Framework for transportation infrastructure disaster resilience improvement

Implementation of flood disaster resilience for bridge management can be achieved by optimization based prioritization for BMS, which will be described in Chapter V.

V. GEOSPATIAL DECISION SUPPORT SYSTEM FOR SUSTAINABLE BRIDGE MANAGEMENT SYSTEMS

5.1 Review of BMS Practice

BMS gained significance after the collapse of the Silver Bridge on Ohio River, WV, in 1967. The following year, the U.S. Congress introduced provisions to Federal Aid Highway Act for National Bridge Inspection Standard (NBIS) [101]. The standard for the first bridge inspection program was issued in 1971. Pioneering research on BMS framework, NCHRP Report 300, was released in 1987 [37]. Later, FHWA supported Pontis BMS [102] optimization in 1993, and NCHRP completed the development of BRIDGIT software in 1994 [103, 104].

Bridge monitoring is an essential component of BMS practice. The NCHRP reported in Synthesis 300 that in the last 10 to 15 years, the topic of performance measures gained "substantial notoriety" [105]. The need for developing improved data was put forward in Synthesis 397 of the NCHRP as "more powerful and flexible optimization procedures and economic analysis tools" [106].

The AASHTOWare™ Bridge Management Software (BrM), formerly known as Pontis, is being used widely by many states in the U.S. and abroad as the primary network-level bridge management software [107]. It was reported by Gutkowski and Arenella [108] that eventually the current inspection procedures based on the NBIS will be expanded with more details.

BMS is practiced in Alberta, Manitoba, Nova Scotia, Ontario, Quebec and Prince Edward Island territories of Canada. Research is ongoing for the initiative for Canadian National Bridge

Inventory [109]. Switzerland has an ongoing research for a BMS called KUBA-MS which is based on the underlying principles of Pontis [110]. Differences are due to bridge maintenance practices in the U.S. and Switzerland.

Despite the continuing improvements in BMS methodologies, current bridge management systems do not include an indicator of flood disaster impacts as a part of optimization formulation [37, 39, 40, 102, 104, 111].

5.2 Optimization Based Prioritization for BMS

Geospatial analysis is used in identifying bridges over rivers/channels as shown in the geospatial maps in Figures 61, 62 and 63. More geospatial maps are presented in Appendix B.

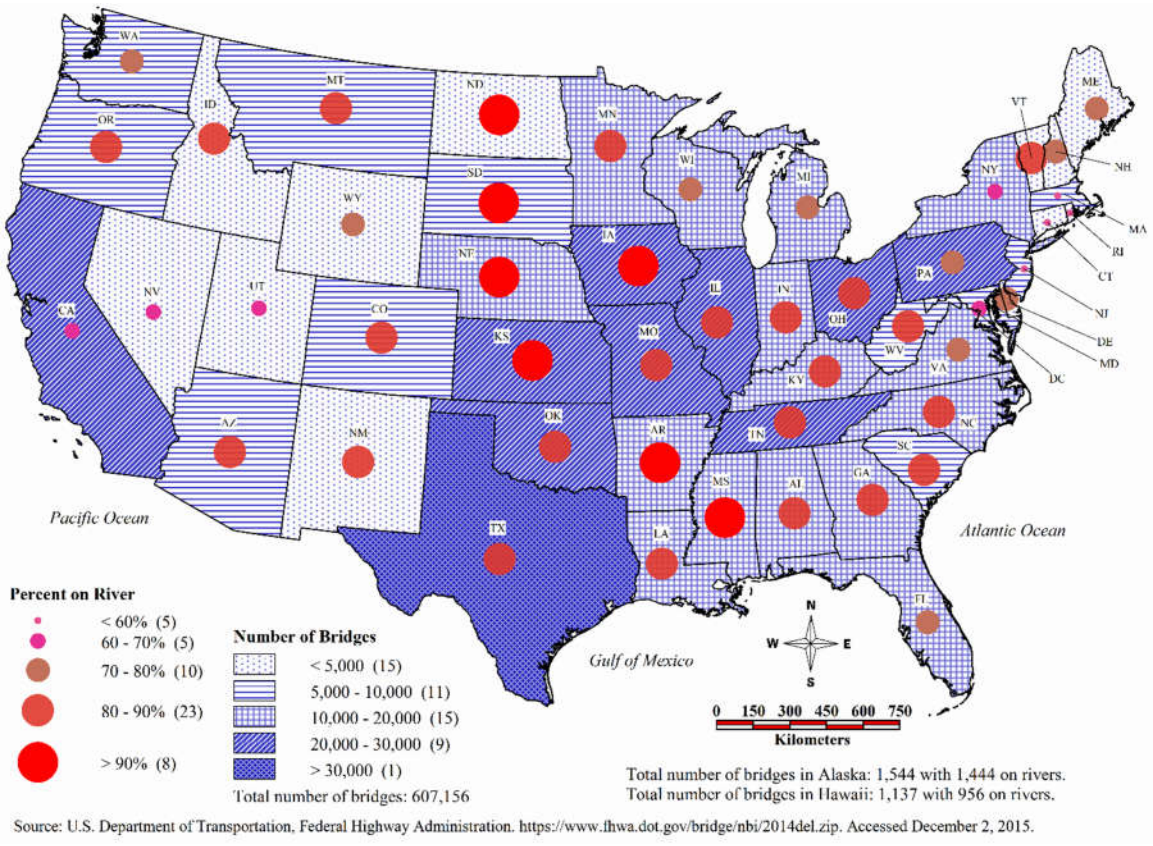

Figure 61. Number of bridges and percentage of bridges on rivers by state, 2014

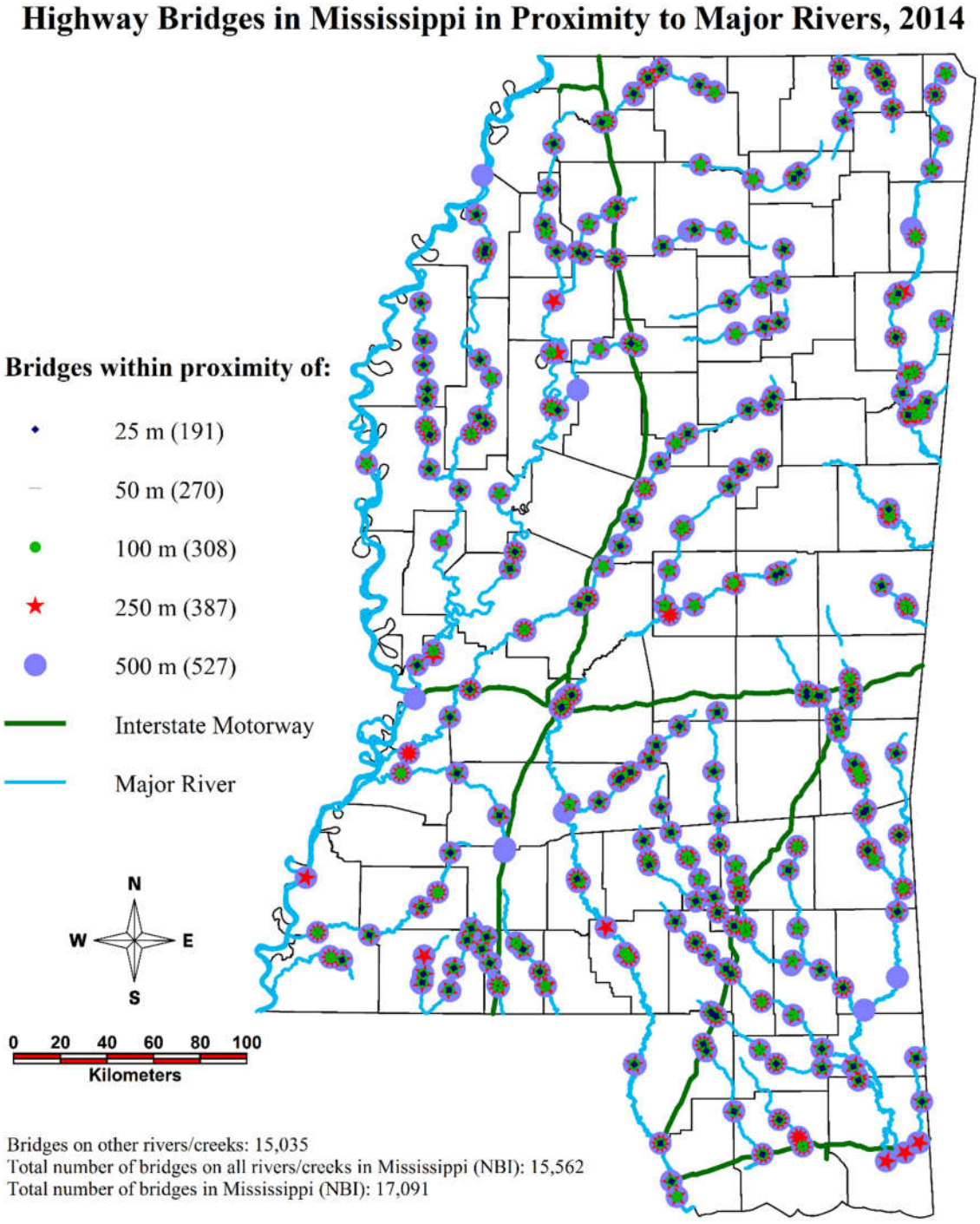

Figure 62. Highway bridges in Mississippi in proximity to major rivers, 2014

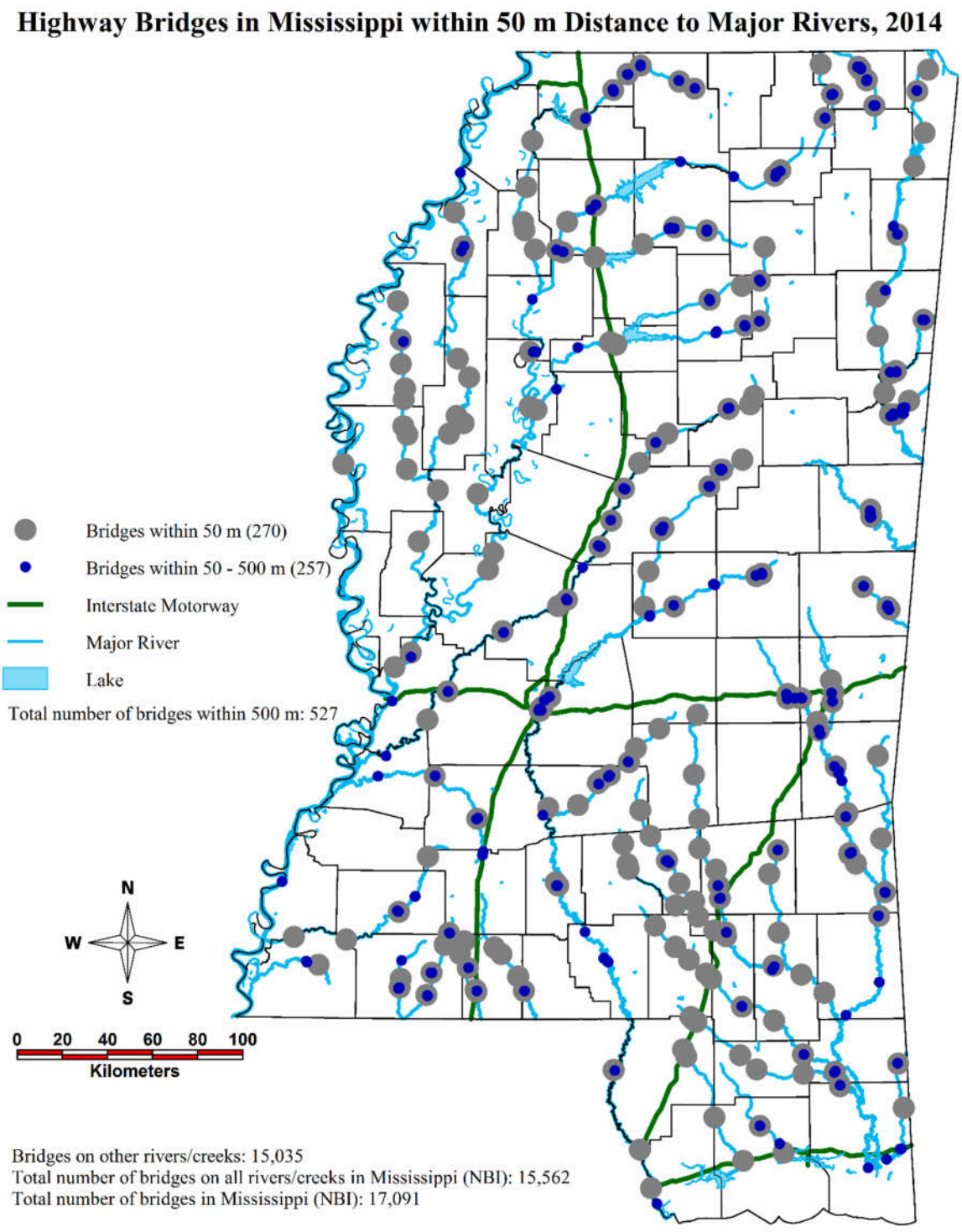

Figure 63. Highway bridges in Mississippi in 50 m proximity to major rivers, 2014

A bridge Flood Vulnerability Rating (FVR) is proposed as presented in Table 29.

Table 29. Bridge FVR for extreme flood events

FVR	Rating	Vertical Underclearance*	Comments	Annual Exceedance Probability [45]
1	Catastrophic Risk	< 2 m	10 to 50 year flood	0.1 - 0.02
2	Very High Risk	2-4 m	50 to 100 year flood	0.02 - 0.01
3	High Risk	4-6 m	50 to 100 year flood	0.02 - 0.01
4	Moderate Risk	6-8 m	100 to 500 year flood	0.01 - 0.002
5	Low Risk	8-10 m	500 to 1,000 year flood	0.002 - 0.001**
6	Very Low Risk	> 10 m	1,000 year flood	0.001**

* height between river water surface and bottom of superstructure
** estimated

Bridge inspectors need to be asked by agencies to record the vertical clearance of bridges over rivers/channels. Peak discharge and water elevation historical data are available by USGS [112]. If vertical clearance of a bridge is less than the peak crest height/water surface elevation, immediate reconstruction/hardening action is required. Vertical underclearance is the height from the river water level to the bottom of the superstructure. According to the FVR, US-51 Highway, I-55 Highway and rail bridges fall into categories 3, 4 and 4, respectively.

Figure 64 displays the number of bridges in Mississippi which are in 25-500 m proximity to major rivers. It is recommended to use 50 m proximity to identify bridges for reconstruction/hardening strategies.

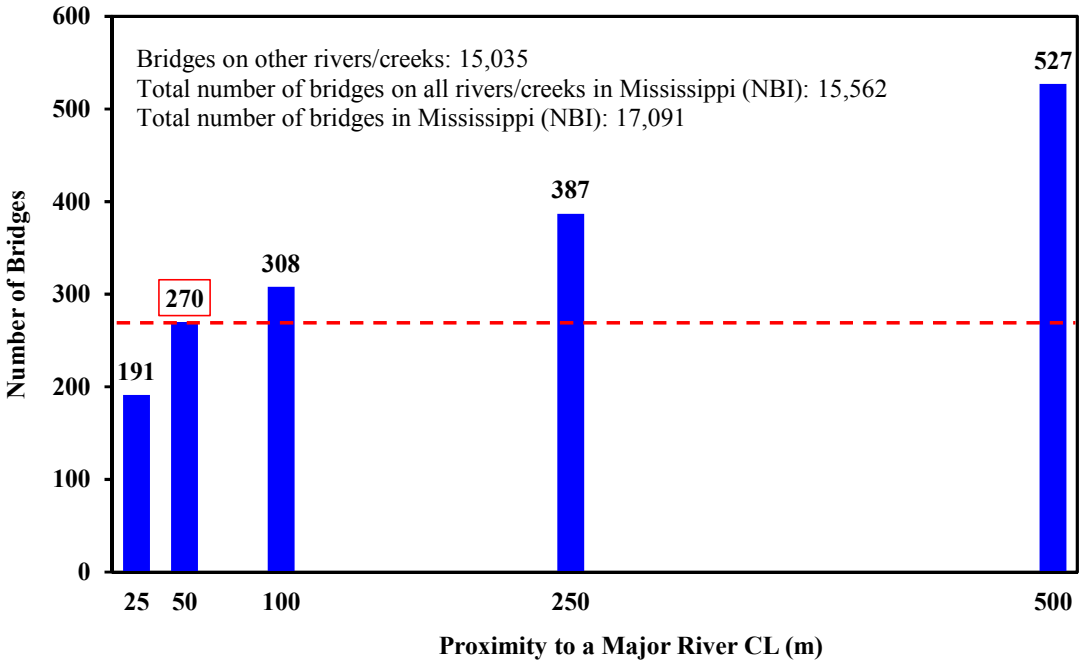

Figure 64. Number of bridges in Mississippi in proximity to major rivers, 2014

For the purpose of optimization based prioritization, the following objective function is used, as given in Equation 5.1:

$$\text{Maximize} \sum_{n=1}^{N} B_n$$

$$\sum_{n=1}^{N} B_n = p_1 \sum_{i=1}^{I} (c_a - c_r)_i + p_2 \sum_{j=1}^{J} (c_a - c_r)_j + p_3 \sum_{k=1}^{K} (c_a - c_h)_k +$$

$$+ p_4 \sum_{l=1}^{L} (c_a - c_h)_l + p_5 \sum_{m=1}^{M} (c_a - c_h)_m + p_6 \sum_{r=1}^{R} (c_a - c_h)_r \qquad (5.1)$$

where,

B = Benefit for each bridge, $c_a - c_r$, $c_a - c_h$

N = Total number of identified bridges across FVR categories 1 to 6

c_a = Cost avoidance (disruption and economic loss) for each bridge

c_r = Reconstruction cost for FVR categories 1 and 2

c_h = Hardening cost for FVR categories 3 to 6

p_1 through p_6 = Flood probability for FVR categories 1 to 6

I, J, K, L, M, R= Optimized number of bridges in each FVR category

Subject to the following constraints:

(All variables) ≥ 0
$N \geq (I+J+K+L+M+R)$
Maximum number of identified bridges in FVR category 1 $\geq I$
Maximum number of identified bridges in FVR category 2 $\geq J$
Maximum number of identified bridges in FVR category 3 $\geq K$
Maximum number of identified bridges in FVR category 4 $\geq L$
Maximum number of identified bridges in FVR category 5 $\geq M$
Maximum number of identified bridges in FVR category 6 $\geq R$
Budget $\geq$ Total cost of reconstruction/hardening, C

$$C = p_1 \sum_{i=1}^{I} (c_r)_i + p_2 \sum_{j=1}^{J} (c_r)_j + p_3 \sum_{k=1}^{K} (c_h)_k + p_4 \sum_{l=1}^{L} (c_h)_l + p_5 \sum_{m=1}^{M} (c_h)_m + p_6 \sum_{r=1}^{R} (c_h)_r$$

Table 30. Data used in budget optimization problem related to reconstruction/hardening

FVR Group	Estimated Number of Spans	Identified Number of Bridges	Flood Probability	Unit Cost of Reconstruction ($)	Unit Cost of Hardening ($)	Unit Cost Avoidance ($)	Unit Net Benefit ($)	Net Benefit ($)
Catastrophic Risk	1 - 2	27	0.1	5,000,000	-	15,000,000	10,000,000	27,000,000
Very High Risk	2 - 5	54	0.02	10,000,000	-	15,000,000	5,000,000	5,400,000
High Risk	5 - 10	81	0.02	-	5,000,000	15,000,000	10,000,000	16,200,000
Moderate Risk	5 - 15	54	0.01	-	1,000,000	4,000,000	3,000,000	1,620,000
Low Risk	5 - 20	27	0.002	-	1,000,000	4,000,000	3,000,000	162,000
Very Low Risk	> 10	27	0.001	-	1,000,000	4,000,000	3,000,000	81,000
		Total: 270				Total Net Benefit ($)		50,463,000

Table 30 displays the data used in budget optimization problem related to reconstruction or hardening. It is assumed that total 270 bridges identified in 50 m proximity to a river/channel are already prioritized in FVR groups. Total net benefit in Table 30 (for all identified number of bridges in each FVR group) is based on the assumption that budget is not constrained. If a budget

constraint of $15 million is considered, linear programming (LP) optimization Solver selects 15 bridges from FVR category 1 for reconstruction/hardening.

It is recommended to enhance the objective function by including additional decision variables such as highway functional class, age, traffic level as well as considering prioritization across the FVR groups.

It is recommended to include vertical clearance of bridges and flood probability for a sustainable BMS. Therefore, an enhanced BMS framework is proposed in Figure 65. Bridges crossing rivers/channels should be given priority. However, information on vertical underclearance should exist for every bridge in an inventory. It is recommended that the NBI has its "Item 54 - Minimum Vertical Underclearance" populated by requiring inspectors to measure and record these data for all bridges in the floodplain. Overall safety rating of bridges in NBI should be reevaluated by incorporating the FVR to the NBI. The following NBI attributes can be considered for enhanced prioritization:

- Item 6 - Features Intersected
- Item 26 - Functional Classification of Inventory Route
- Item 27 - Year Built
- Item 29 - Average Daily Traffic
- Item 30 - Year of Average Daily Traffic
- Item 37 - Historical Significance
- Item 42 - Type of Service
- Item 43 - Structure Type, Main
- Item 44 - Structure Type, Approach Spans
- Item 45 - Number of Spans in Main Unit
- Item 48 - Length of Maximum Span
- Item 49 - Structure Length
- Item 61 - Channel and Channel Protection
- Item 107 - Deck Structure Type
- Item 109 - Average Daily Truck Traffic
- Item 113 - Scour Critical Bridges
- Item 114 - Future Average Daily Traffic

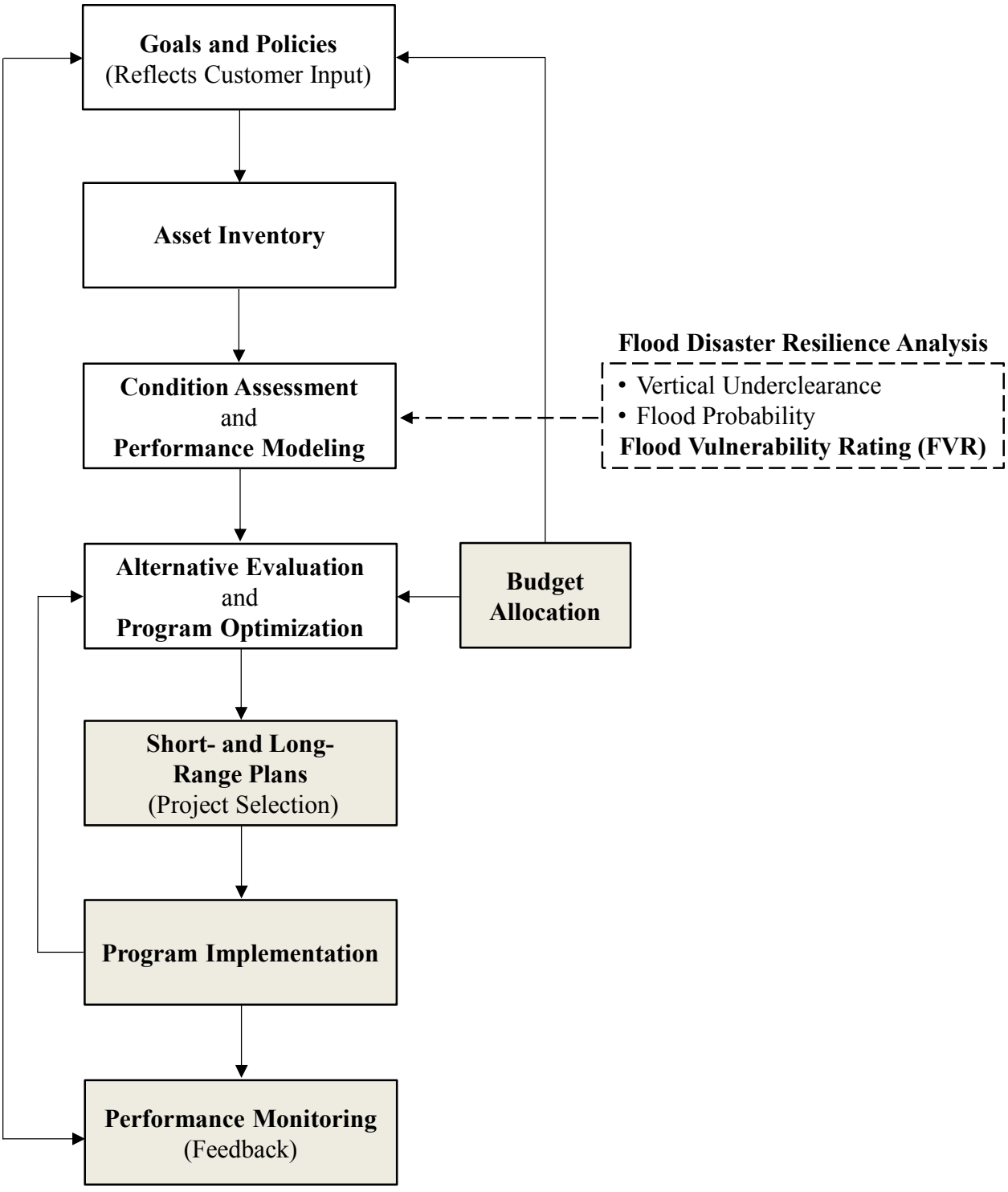

Figure 65. An enhanced BMS framework
(after Uddin et al. [21])

5.3 LCA for Reconstruction/Hardening of Bridges

Life cycle economic analysis is a critical component of infrastructure asset management [21]. It has no relationship with financing of a project [21]. Economic analyses should include LCA of every cost item available in the project life cycle [21]. Applications of VE also require the practice of LCA of costs and benefits over the analysis period. Total LCC of a project is expressed as present-worth LCC. According to FHWA report [113], majority of states in the U.S. do not consider life cycle cost in "making long term economical decisions in the bridge management processes" [113]. Basic concept of LCC, shown in Figure 66, indicates that in-service maintenance of infrastructure has the largest influence on the total LCC. It does not consider bridge failure due to natural disasters.

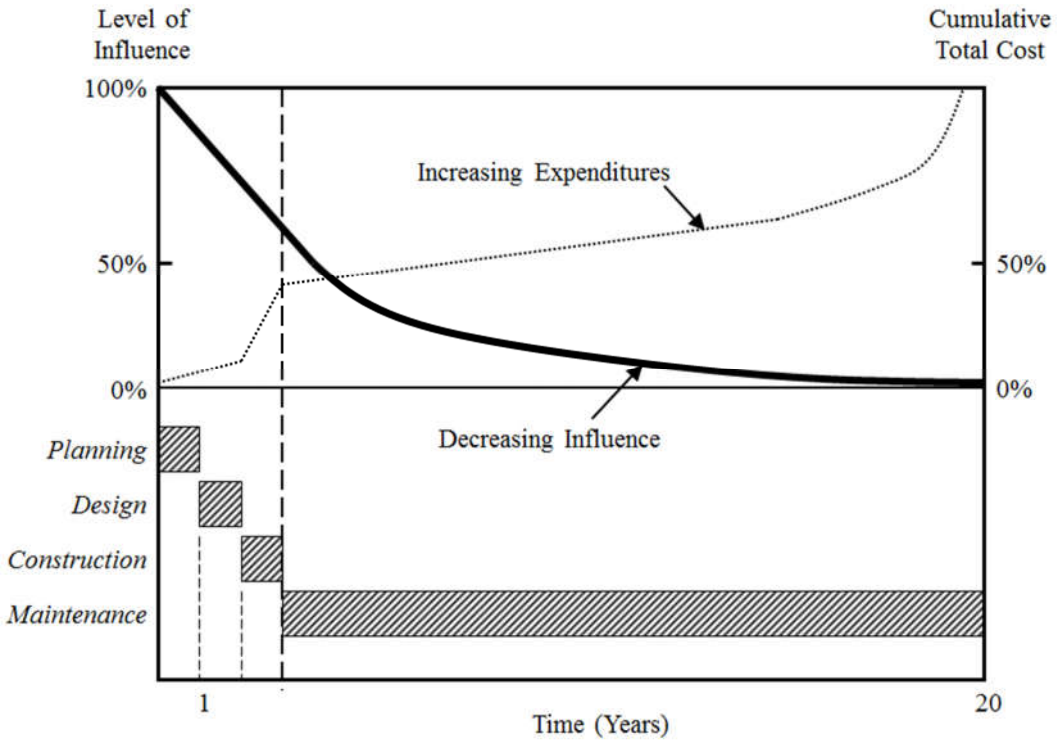

Figure 66. Basic concept of LCC
(Used with permission [21])

Infrastructure performance curves considering maintenance intervention and catastrophic disasters are shown in Figure 67. Traditional asset management systems do not consider failure and disruptions of service arising from catastrophic disasters. Next, traditional LCC equation and an example LCA is presented for the comparison of LCC of a bridge with and without a pre-planned hardening strategy.

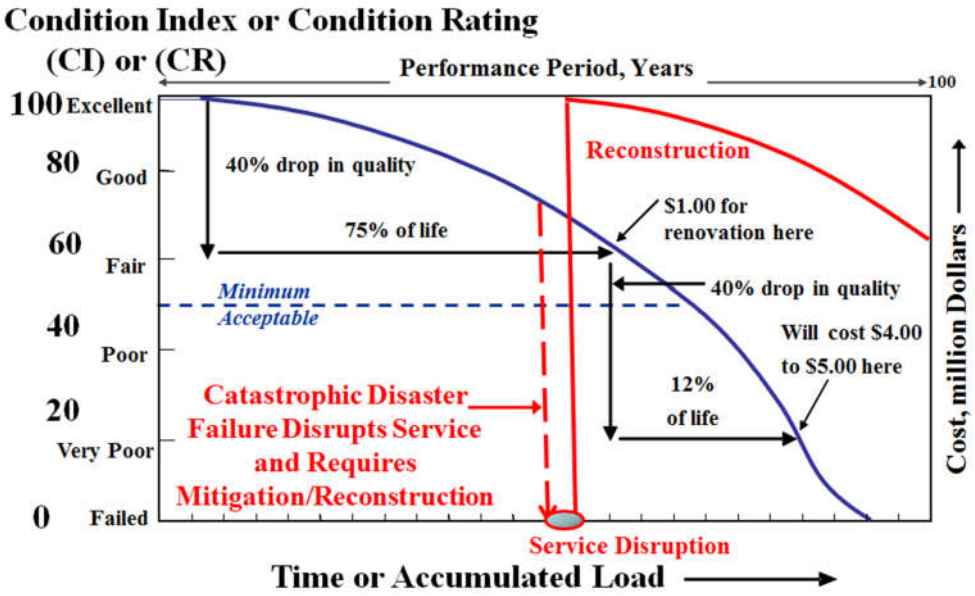

Figure 67. Infrastructure performance curves for LCA considering catastrophic disasters (Used with permission [114])

Traditionally, total present-worth of costs is calculated using Equation 5.2 without considering failure due to catastrophic disasters (after Uddin et al. [21] and Hudson et. Al 115]):

$$TPWC_{x1,n} = (ICC)_{x1} +$$

$$+\sum_{t=0}^{n}\left\{\text{pwf}_{i,t}\left[(\text{CC})_{x1,t}+(\text{MO})_{x1,t}+(\text{UC})_{x1,t}\right]+\text{uspwf}_{i,n}(\text{MO})_{x1,n}\right\}-$$

$$-\text{pwf}_{i,n}(\text{SV})_{x1,n} \tag{5.2}$$

where,

$\text{TPWC}_{x1,n}$ = Total present-worth of costs for alternative x1 for analysis period of n years

$(\text{ICC})_{x1}$ = Initial capital costs of construction, etc. for alternative x1

$\text{pwf}_{i,t}$ = Present-worth factor for discount rate, i for t years, $\frac{1}{(1+i)^t}$

$\text{uspwf}_{i,n}$ = Uniform series present-worth factor for discount rate, i for n years, $\frac{(1+i)^n-1}{i(1+i)^n}$

$(\text{CC})_{x1,t}$ = Capital costs of construction, etc. for alternative x1 in year t where $t < n$

$(\text{MO})_{x1,t}$ = Maintenance plus operation costs for alternative x1 in year t

$(\text{MO})_{x1,n}$ = Maintenance costs for alternative x1 for analysis period of n years

$(\text{UC})_{x1,t}$ = User costs, if applicable, for alternative x1 in year t

$(\text{SV})_{x1,n}$ = Salvage value, if any, for alternative x1 at the end of the analysis period

i = Annual discount rate or cost of capital

n = Number of years to when the sum will be saved (i.e. analysis period)

In the following example, LCC analysis is presented for a highway concrete bridge with and without considering hardening for flood disaster resilience. An existing (initial capital costs of construction are zero) 300 m long and 10 m wide concrete girder highway bridge is considered for the LCA. Base scenario is the traditional M,R&R practice. However, for the LCA considering flood resilience, two other scenarios are evaluated.

In a modified base scenario (scenario 1), the agency has not planned for hardening the bridge with respect to flood disasters. Assume that an extreme flood disaster due to a 500-year flood event occurs after 10 years, and the bridge superstructure is washed away. The bridge remains closed to traffic for the next one year. Salvage value is neglected. Analysis period (i.e. life cycle), n is 100 years and annual cost of capital, i is 0.05. After a review of bridge M,R&R costs in the United States [116, 117, 118], the following cost assumptions are made:

- Agency annual maintenance cost = $20,000 per year
- User costs (direct and indirect) due to abrupt failure of the bridge in year 10:
  - Cost due to disruption to services in year 10 = $4 million
  - Economic loss over one year in year 10 = $96 million

  Total user cost over one year in year 10 = $100 million
- Agency costs due to abrupt failure of the bridge and reconstruction over one year in year 10:
  - Cost of demolition and cleaning of river channel in year 10 = $1 million
  - Cost of flood resilient bridge design and construction considering increased vertical underclearance in year 10 = $9 million

  Total agency cost over one year in year 10 = $10 million
  - Major repair cost of superstructure in year 40 = $2 million
  - Major repair cost of superstructure in year 70 = $2 million

Present-worth of agency annual maintenance cost for 100 years:

$$(\mathrm{MO})_{1,100} = \$20{,}000 \times \frac{(1+0.05)^{100}-1}{0.05(1+0.05)^{100}} = \$396{,}958$$

Present-worth of user costs in year 10:

$$(UC)_{1,10} = \$100 \text{ million} \times \frac{1}{(1+0.05)^{10}} = \$61,391,325$$

Present-worth of agency reconstruction cost in year 10:

$$(CC)_{1,10} = \$10 \text{ million} \times \frac{1}{(1+0.05)^{10}} = \$\ 6,139,133$$

Present-worth of agency cost for major repair of superstructure in year 40:

$$(MO)_{1,40} = \$2 \text{ million} \times \frac{1}{(1+0.05)^{40}} = \$284,091$$

Present-worth of agency cost for major repair of superstructure in year 70:

$$(MO)_{1,70} = \$2 \text{ million} \times \frac{1}{(1+0.05)^{70}} = \$65,732$$

Total present-worth of costs for scenario 1 (the modified base scenario) for analysis period of 100 years:

$$TPWC_{1,100} = \$68,277,239$$

An alternative scenario (scenario 2) involves pre-planning of bridge hardening for flood resilience. The agency plans for flood disaster resilience by hardening the bridge after five years. The bridge remains closed to traffic for three months in year 5. Salvage value is neglected. Analysis period (i.e. life cycle), n is 100 years and annual cost of capital, i is 0.05. After a review of bridge M,R&R costs in the United States [116, 117, 118], the following cost assumptions are made:

- Agency annual maintenance cost = $20,000 per year
- User costs (direct and indirect) due to service disruption during hardening in year 5:
  - Cost due to disruption to services for 3 months in year 5 = $1 million
  - Economic loss over 3 months in year 5= $24 million

  Total user cost over three months in year 5 = $25 million
- Agency costs due to planned hardening of the bridge in year 5:
  - Cost of demolition and cleaning of river channel = $0.5 million
  - Flood resilient bridge design and construction considering increased vertical underclearance = $9 million

  Total agency cost over three months in year 5= $9.5 million
  - Major repair cost of superstructure in year 40 = $2 million
  - Major repair cost of superstructure in year 70 = $2 million

Present-worth of agency annual maintenance cost for 100 years:

$$(\text{MO})_{2,100} = \$20{,}000 \times \frac{(1+0.05)^{100}-1}{0.05(1+0.05)^{100}} = \$396{,}958$$

Present-worth of user costs in year 5:

$$(\text{UC})_{2,5} = \$25 \text{ million} \times \frac{1}{(1+0.05)^{5}} = \$19{,}588{,}154$$

Present-worth of agency reconstruction cost in year 5:

$$(\text{CO})_{2,5} = \$9.5 \text{ million} \times \frac{1}{(1+0.05)^{5}} = \$7{,}443{,}499$$

Present-worth of agency cost for major repair of superstructure in year 40:

$$(\text{MO})_{2,40} = \$2 \text{ million} \times \frac{1}{(1+0.05)^{40}} = \$284{,}091$$

Present-worth of major repair cost of superstructure in year 70:

$$(\text{MO})_{2,70} = \$2 \text{ million} \times \frac{1}{(1+0.05)^{70}} = \$65{,}732$$

Total present-worth of costs for scenario 2 considering bridge hardening for analysis period of 100 years:

$$\text{TPWC}_{2,100} = \$27{,}778{,}434$$

The results of the present-worth LCA are based on that if planned for flood resilience, the disruption and user costs will occur for about three months, compared to one year in unplanned scenario (i.e. abrupt failure of the bridge). The results show that there is a 59.3% decrease in the present-worth LCC ($68,277,239 vs. $27,778,434) for the pre-planned bridge hardening for flood resilience compared to the abrupt bridge failure.

5.4 Research Significance

Research significance is summarized as follows:

- A framework with Flood Resilience Index is proposed for structural integrity assessment of bridge structures subject to floodwater forces.
- Enhanced design and hardening considerations for flood disaster resilient bridge structures are recommended.

- Optimization based prioritization is recommended for BMS, which considers vertical underclearance criteria and flood disaster risk probability.
- Flood Vulnerability Rating on a scale of 1 (catastrophic risk) to 6 (very low risk) is proposed.
- An enhanced geospatial DSS is recommended, which considers Flood Vulnerability Rating.

VI. SUMMARY, CONCLUSIONS AND RECOMMENDATIONS

6.1 Summary

Floods are the most common and damaging natural disaster. More than 4,400 occurrences of flood disasters have been reported globally between 1900 and 2016. Climate impacts are expected to intensify weather related flooding events, and sea level rise expected worldwide will increase the risk of coastal disasters. Transportation infrastructure, vital to the economy and society of every country, is especially prone to the inland and coastal floods. Bridge superstructures are under the constant threat of these natural disasters. Superstructures can be washed away due to lateral forces generated by floodwater. Floodwater can also accelerate scouring around bridge piers, which contributes to bridge failure.

Objectives of this research were to implement flood inundation model for selected multimodal surface transportation corridor sites, use a 3D-FE model of a reinforced concrete highway bridge over a river for analyzing flood impacts, assess structural integrity of the highway bridge structure subjected to lateral floodwater forces and recommend a geospatial DSS framework for sustainable bridge maintenance management considering flood risk vulnerability. This research scope was limited to Sardis, Panola County, Mississippi and US-51 Highway bridge on downstream Little Tallahatchie River in the floodplain site.

This research reviewed computational flood modeling, finite element and structural assessment methodologies for flood impacts on bridge structures. The research also reviewed BMS practice in the United States. The research used the results of Project 2012 – 25: “Disaster

Protection of Transport Infrastructure and Mobility Using Flood Risk Modeling and Geospatial Visualization," which was conducted by the CAIT. The project was pursued with the expertise in geospatial visualization of built infrastructure of CAIT and flood modeling and simulation expertise of NCCHE.

A 2D flood inundation model was implemented for Sardis. Results of NCCHE's 10-m CCS flood simulation were analyzed in terms of floodwater velocity, height, arrival and discharge. Impacts of floodwater inundation were evaluated at transportation and building infrastructure assets. The results of the flood 10-m CCS flood simulation were used in disaster vulnerability assessment of highways subjected to floodwater. Embankment stability analysis for US-51 Highway and structural integrity assessment of US-51 Highway bridge superstructure subjected to lateral floodwater forces were performed. A 3D-FE model of the US-51 Highway bridge was developed in LS-DYNA R8 based on the drawings of MDOT. Floodwater impacts on the 3D-FE model of the bridge were simulated. A framework structural integrity assessment of bridges subjected to floods was presented. Enhanced design and hardening considerations were discussed.

6.2 Conclusions

Major conclusions of the research follow:

- Flood hazard assessment using computational flood modeling
    - Geospatial analysis showed that total flood inundation covered an area of 22.46 mi2 (58.16 km2), where the maximum floodwater reached up to 34.19 ft (10.42 m) within the flood inundation area.

- Simulated flood arrived in less than 2.88 hours to I-55 and Rail bridges, and in less than 3.36 hours to US-51 Highway bridge.
- Maximum floodwater was 7.94 m, 8.04 m and 7.53 m at I-55 Highway, rail and US-51 Highway bridges, respectively.
- Maximum floodwater velocity reached 1.77 m/s (5.5 ft/s), 3.47 m/s (11.4 ft/s) and 2.63 m/s (8.6 ft/s) at I-55 Highway, rail and US-51 Highway bridges, respectively.
- Maximum floodwater over I-55 Highway, rail and US-51 Highway bridges were 0 ft (0 m), 3.4 ft (1.04 m) and 1.7 ft (0.53 m), respectively.
- NCCHE's scour analyses estimated local scour around the bridge piers as were 5.27 m (17.29 ft), 5.36 m (17.59 ft) and 2.00 m (6.56 ft) for I-55 Highway, rail and US-51 Highway bridges, respectively.

- Flood disaster impacts on bridge structures
  - It was seen in slope stability analysis of US-51 Highway embankment that FS against sliding decreased with increasing slope and also with increasing unit weight and/or decreasing cohesion of the embankment. It was concluded that US-51 Highway embankment was safe against a slope failure.
  - In pseudo-static analysis, FS against overturning was 0.90 for the hypothetical single girder case. FS for superstructure ranges between 2.23 and 4.55, depending on the inundation level at the bridge superstructure.
  - In lateral hydrodynamic analysis, FS against overturning was 0.36 for the hypothetical single girder case. FS for superstructure ranged between 2.00 and 3.76, depending on the inundation level at the bridge superstructure.

- Lateral displacements of US-51 Highway bridge superstructure in 3D-FE simulations ranged between 0.098 and 2.422 m indicating that superstructure will most likely collapse under lateral hydrodynamic floodwater forces.
- It was concluded after dowel bar stability analysis that the dowel bars were vulnerable and highly likely to fail under the lateral forces generated in girder-bearing surfaces.
- A Flood Vulnerability Rating on a scale of 1 (catastrophic risk) to 6 (very low risk) was used for a case study of 270 bridges on major rivers, which were analyzed using an objective function of maximum benefit considering reconstruction and hardening costs, and indirect cost avoidance from traffic disruption related to bridge failure.
- An enhanced BMS framework must consider bridge hardening for flood resilience, based on Flood Vulnerability Rating.

6.2.1 Innovation and Contribution to Sustainable BMS Practice

The following list describes the innovation and contribution of this research to sustainable BMS practice:

- A structural integrity assessment framework with Flood Resilience Index for bridge structures subject to floodwater forces.
- Enhanced design and hardening considerations for flood disaster resilient bridge structures.
- Optimization based prioritization for BMS, which considers vertical underclearance criteria and flood disaster risk probability.

- FVR on a scale of 1 (catastrophic risk) to 6 (very low risk).
- An enhanced geospatial DSS, which considers FVR.

6.2.2 Overall Benefit to Transportation Infrastructure and Society

This dissertation advances flood risk assessment and resilience management methodologies for transportation infrastructure in the United States and across the globe. The proposed geospatial DSS can be used by transportation, highway and bridge management agencies to prioritize highway and rail bridges for reconstruction and hardening strategies against flood disasters.

6.3 Recommendations for Future Research

The following recommendations are offered for future research in disaster vulnerability assessment of highways subjected to floodwater, structural integrity of bridge superstructures, flood impacts on bridge structures and further 3D-FE analysis:

- Disaster vulnerability assessment of highways subjected to floodwater
    - Toe/circle failure were assumed. Base failure should also be considered.
    - Lowest factor of safety values do not necessarily imply the best practical path. The most critical slope failure surface should be investigated.
    - The slope stability analyses presented did not consider the effects of moving water, floating debris and sediments etc.
    - The MDOT drawings of US-51 Highway bridge include properties of soil layers.
- Structural integrity of bridge superstructures
    - Density of floodwater is expected to be greater than freshwater.

- As the CCS gets smaller, precision increases. Flood simulations with 3 m and 5 m computational cells yield higher floodwater depths and velocity. This would mean that the FS calculations and 3D-FE simulations were conservative.
- Stability analysis of highway embankments and levees/dikes is recommended considering shear strength of the embankment soil.

- Flood impacts on bridge structures and 3D-FE methodology
  - Stones, wood, debris etc., depending on their masses/dimensions, will have additional impact forces that will act as a concentrated/distributed load on bridge elements.
  - Appropriate boundary conditions/restraints can be prescribed to see the effects in terms of stresses and strains.
  - Additional 3D-FE simulations should be considered by varying static/dynamic coefficients of friction for contact mechanics problems.
  - It is recommended to advance the 3D-FE study for steel girder bridges using appropriate structural shapes and properties.
  - Refined mesh is recommended for steel girder bridges. Accordingly, coefficients of friction need to be studied in detail.
  - The floodwater impact analysis methodology presented in this research can be applied to coastal bridges for hurricanes and tsunamis, where expected wave surge velocities will be higher.

REFERENCES

LIST OF REFERENCES

[1] Guha-Sapir, D., R. Below and P. Hoyois. EM-DAT: International Disaster Database. Université Catholique de Louvain, Brussels, Belgium. http://www.emdat.be. Accessed May 30, 2012 and December 15, 2015.

[2] Jha, A. K., R. Bloch and J. Lamond. Cities and Flooding: A Guide to Integrated Urban Flood Risk Management for the 21st Century. The World Bank, Washington, D.C., 2012. http://www.gfdrr.org/gfdrr/sites/gfdrr.org/files/urbanfloods/pdf/Cities%20and%20Flooding%20Guidebook.pdf. Accessed May 19, 2014.

[3] Yonetani, M. Global Estimates 2014, People Displaced by Disasters. Internal Displacement Monitoring Centre, Norwegian Refugee Council, September 2014. http://reliefweb.int/sites/reliefweb.int/files/resources/201409-global-estimates.pdf. Accessed September 19, 2014.

[4] Historic Winter Flood Along Mississippi River Sets Record in Cape Girardeau, January 6, 2016. https://weather.com/news/news/mississippi-river-flooding-december-2015. Accessed June 25, 2016.

[5] West Virginia floods: At least 20 dead in 'once-in-1,000-year' event. http://www.upi.com/Top_News/US/2016/06/24/West-Virginia-floods-At-least-20-dead-in-once-in-1000-year-event/7281466771562/. Accessed June 29, 2016.

[6] National Preparedness Report. U.S. Department of Homeland Security, March 30, 2014. https://s3-us-gov-west-1.amazonaws.com/dam-production/uploads/140734679623491bc4

8efa09591e927c5c2e19fea3550/2014%20NPR_FINAL_508.pdf. Accessed August 19, 2014.

[7] Fact Sheet 2007-3009, Natural Hazards – A National Threat. USGS, U.S. Department of the Interior, February 2007. http://pubs.usgs.gov/fs/2007/3009/2007-3009.pdf. Accessed April 28, 2016.

[8] Fact Sheet 2006-3026, Flood Hazards – A National Threat. USGS, U.S. Department of the Interior, January 2006. http://pubs.usgs.gov/fs/2006/3026/2006-3026.pdf. Accessed March 14, 2014.

[9] Significant Flood Events, As of February 29, 2016. http://www.fema.gov/significant-flood-events. Accessed April 28, 2016.

[10] Billion Dollar U.S. Weather Disasters. National Oceanic and Atmospheric Administration (NOAA) Satellite and Information Service, 2010. http://www.ncdc.noaa.gov/oa/reports/billionz.html. Accessed June 10, 2012.

[11] Weiss, D. J. and S. Manning. Extreme Weather, Extreme Damage. Center for American Progress, 2013. http://www.americanprogress.org/issues/green/news/2014/03/27/86532/2013-extreme-weather-extreme-damage. Accessed May 10, 2014.

[12] Durmus, A. Geospatial Assessment of Sustainable Built Infrastructure Assets and Flood Disaster Protection. *M.S. Thesis*, University of Mississippi, August 2012.

[13] Melillo, J. M., T. C. Richmond and G. W. Yohe, Eds., Climate Change Impacts in the United States: The Third National Climate Assessment, U.S. Global Change Research Program, 2014. http://s3.amazonaws.com/nca2014/low/NCA3_Climate_Change_Impacts_in_the_United%20States_LowRes.pdf?download=1. Accessed May 23, 2014.

[14] National Climate Assessment: The Big Picture. The Climate Reality Project. http://forms.climaterealityproject.org/page/-/National%20Climate%20Assessment/NCA_Overview.pdf. Accessed May 23, 2014.

[15] Samenow, J. Weather Service: BWI witnessed "between a 500 year and 1,000 year rainfall." http://www.washingtonpost.com/blogs/capital-weather-gang/wp/2014/08/14/weather-service-bwi-witnessed-between-a-500-year-and-1000-year-rainfall/. Accessed August 15, 2014.

[16] Reeves, J. and J. Linderman. South Carolina floods leave a shared sense of memories lost, October 10, 2015. http://bigstory.ap.org/article/c62e76c777fb446c9776405cc64ad59c/south-carolina-floods-leave-shared-sense-memories-lost. Accessed November 3, 2015.

[17] Fernandez, M. and R. Pérez-Peña. Rain Spreads Destruction in Houston, Killing Four, May 26, 2015. http://www.nytimes.com/2015/05/27/us/texas-rains-bring-flooding-to-houston-area.html. Accessed August 10, 2015.

[18] Fact Sheet: The President's Climate Data Initiative: Empowering America's Communities to Prepare for the Effects of Climate Change, 2014, http://www.whitehouse.gov/the-press-office/2014/03/19/fact-sheet-president-s-climate-data-initiative-empowering-america-s-comm. Accessed March 28, 2014.

[19] The President's Climate Action Plan, Executive Office of the President, The White House, June 2013. http://www.whitehouse.gov/sites/default/files/image/president27sclimateactionplan.pdf. Accessed March 28, 2014.

[20] Risk Mapping, Assessment, and Planning (Risk MAP) Multi-Year Plan: Fiscal Years 2010-2014. Fiscal Year 2009 Report to Congress, March 16, 2009. Federal Emergency

Management Agency. http://www.fema.gov/media-library-data/20130726-1650-20490-4732/fema_risk_map_plan.pdf. Accessed March 14, 2014.

[21] Uddin, W., W. R. Hudson and R. Haas. *Public Infrastructure Asset Management*. 2nd Edition, McGraw-Hill, New York, 2013.

[22] Bridges by State and County. U.S. Department of Transportation, FHWA, 2013. http://www.fhwa.dot.gov/bridge/nbi/no10/county13.xlsx. Accessed May 22, 2014.

[23] National Bridge Inventory. U.S. Department of Transportation, FHWA. http://www.fhwa.dot.gov/bridge/nbi.cfm. Accessed April 27, 2015.

[24] 2013 Report Card for America's Infrastructure, American Society of Civil Engineers (ASCE), March 2013. http://www.infrastructurereportcard.org/a/documents/2013-Report-Card.pdf. Accessed March 9, 2014.

[25] HEC-RAS. http://www.hec.usace.army.mil/software/hec-ras/. Accessed April 1, 2015.

[26] Cook, A. C. Comparison of One-Dimensional HEC-RAS with Two-Dimensional FESWMS Model in Flood Inundation Mapping. *M.S. Thesis*, Purdue University, May 2008. http://web.ics.purdue.edu/~vmerwade/reports/2008_02.pdf. Accessed October 3, 2014.

[27] Apelt, C. J. Flood Forces on Bridges. *Proceedings, 13th Australian Road Research Board (ARRB)/5th REAA Conference*, 1986, Vol. 13, Part 6, pp. 40-46. http://114.111.144.247/Presto/content/Detail.aspx?q=aHlkcm9keW5hbWlj&ctID=MjE1ZTI4YzctZjc1YS00MzQ4LTkyY2UtMDJmNTgxYjg2ZDA5&rID=MTMyMg==&qcf=&ph=VHJ1ZQ==&bckToL=VHJ1ZQ==&. Accessed April 17, 2015.

[28] Jempson, M. A. Flood and Debris Load on Bridges. *PhD Thesis*, University of Queensland, Australia, March 2000. https://espace.library.uq.edu.au/eserv/UQ:206022/

Flood_and_Debris_Loads_on_Bridges_PhD_Thesis_Mark_Jempson.pdf. Accessed April 25, 2014.

[29] Coastal Construction Manual: Principles and Practices of Planning, Siting, Designing, Constructing, and Maintaining Residential Buildings in Coastal Areas. 4th Edition. FEMA P-55, Volume II. Federal Emergency Management Agency (FEMA), August 2011. http://www.fema.gov/media-library-data/20130726-1510-20490-1986/fema55_volii_combined_rev.pdf. Accessed March 2, 2015.

[30] Chen, Q., L. Wang and H. Zhao. Hydrodynamic Investigation of Coastal Bridge Collapse during Hurricane Katrina. *ASCE Journal of Hydraulic Engineering*, Vol. 135, No. 3, March 2009, pp. 175-186. http://ascelibrary.org/doi/pdf/10.1061/%28ASCE%290733-9429%282009%29135%3A3%28175%29. Accessed August 21, 2014.

[31] Malawasi, S. and A. Guadagnini. Hydrodynamic Loading on River Bridges. *ASCE Journal of Hydraulic Engineering*, Vol. 129, No. 11, November 2003, pp. 854-861. http://ascelibrary.org/doi/pdf/10.1061/%28ASCE%290733-9429%282003%29129%3A11%28854%29. Accessed August 21, 2014.

[32] Kerenyi, K., T. Sofu and J. Guo. Hydrodynamic Forces on Inundated Bridge Decks, Report No. FHWA-HRT-09-028. U.S. Department of Transportation, FHWA, 2009. http://www.fhwa.dot.gov/publications/research/infrastructure/hydraulics/09028/09028.pdf. Accessed April 25, 2014.

[33] Azadbakht, M. and S. C. Yim. Simulation and Estimation of Tsunami Loads on Bridge Superstructures. *ASCE Journal of Waterway, Port, Coastal, and Ocean Engineering*, Vol. 141, Issue 2, June 5, 2014, 10.1061/(ASCE)WW.1943-5460.0000262, 04014031.

http://ascelibrary.org/doi/pdf/10.1061/%28ASCE%29WW.1943-5460.0000262. Accessed March 13, 2015.

[34] Lwin, M. M., W. P. Yen and J. J. Shen. Effects of Hurricane Katrina on the Performance of U.S. Highway Bridges. *ASCE Journal of Performance of Constructed Facilities*, Vol. 28, No. 1, February 1, 2014, pp. 40-48. http://0-eds.b.ebscohost.com.umiss.lib.olemiss.edu/eds/Citations/FullTextLinkClick?sid=9ab90fb8-2d5f-46be-a7ae-f8c40ca8a656@sessionmgr110&vid=4&id=pdfFullText. Accessed March 11, 2015.

[35] Guo, J., D. M. Admiraal and T. C. Zhang. Computational Design Tool for Bridge Hydrodynamic Loading in Inundated Flows of Midwest Rivers, 2010. http://matc.unl.edu/assets/documents/matcfinal/Guo_ComputationalDesignToolforBridgeHydrodynamicLoadinginInundatedFlowsofMidwestRivers.pdf. Accessed February 22, 2015.

[36] Yim, S. C., Y. Wei, M. Azadbakht, S. Nimmala and T. Potisuk. Case Study for Tsunami Design of Coastal Infrastructure: Spencer Creek Bridge, Oregon. *ASCE Journal of Bridge Engineering*, May 13, 2014, 10.1061/(ASCE)BE.1943-5592.0000631, 05014008. http://ascelibrary.org/doi/pdf/10.1061/%28ASCE%29BE.1943-5592.0000631. Accessed March 13, 2015.

[37] Hudson, S. W., R. F. Carmichael III, L.O. Moser, W. R. Hudson and W. J. Wilkes. Report 300: Bridge Management Systems. National Academy of Sciences, Transportation Research Board (TRB), National Cooperative Highway Research Program (NCHRP), Washington, D.C., 1987.

[38] Lee, J. Method for Construction of Reliable Bridge Condition Rating Models Based on Limited Inspection Records. *PhD Thesis*, Griffith University, Australia, July 2007.

[39] Patidar, V., S. Labi, K. C. Sinha and P. Thompson. Report 590: Multi-Objective Optimization for Bridge Management Systems. National Academy of Sciences, Transportation Research Board (TRB), NCHRP, 2007. http://onlinepubs.trb.org/onlinepubs/nchrp/nchrp_rpt_590.pdf. Accessed April 1, 2015.

[40] Robert, W. E., D. I. Gurenich and R. E. Thompson. Multi-Period Bridge Investment Optimization Utilizing Pontis Results and Budget Constraints by Work Type. Transportation Research Board (TRB), Annual Meeting, Washington, D.C., 2009. http://docs.trb.org/prp/09-2853.pdf. Accessed April 2, 2015.

[41] What Happened? http://fukushimaontheglobe.com/the-earthquake-and-the-nuclear-accident/whats-happened. Accessed June 18, 2016.

[42] Center for Advanced Infrastructure Technology, University of Mississippi. http://www.olemiss.edu/projects/cait/ncitec/. Accessed June 18, 2016.

[43] National Center for Intermodal Transportation for Economic Competitiveness (NCITEC) Project 2012 – 25. Center for Advanced Infrastructure Technology, University of Mississippi. http://www.olemiss.edu/projects/cait/ncitec/NCITE_2012_25_UM_Uddin_Altinakar.pdf. Accessed June 18, 2016.

[44] Glover, T. J. *Pocket Ref*. Ergon Technical Development, 2nd Edition, August 1995, Sequoia Publishing, Inc., Littleton, Colorado.

[45] Engineering Principles and Practices of Retrofitting Flood-Prone Residential Structures FEMA 259. 2nd Edition, June 2001. Federal Emergency Management Agency (FEMA), MD.

[46] FEMA Flood Map Service Center : Welcome! https://msc.fema.gov/portal. Accessed June 21, 2016.

[47] FEMA Flood Map Service Center : FAQs. https://msc.fema.gov/portal/resources/faq. Accessed June 21, 2016.

[48] Flood Zones. http://www.fema.gov/flood-zones. Accessed June 21, 2016.

[49] HEC-RAS River Analysis System, Hydraulic Reference Manual Version 4.1. U.S. Army Corps of Engineers. http://www.hec.usace.army.mil/software/hec-ras/documentation/HEC-RAS_4.1_Reference_Manual.pdf. Accessed June 15, 2016.

[50] CCHE2D. National Center for Computational Hydroscience and Engineering. https://www.ncche.olemiss.edu/cche2d. Accessed June 15, 2016.

[51] Altinakar, M. S., E. E. Matheu and M. McGrath. New Generation Modeling and Decision Support Tools for Studying Impacts of Dam Failures. *Proceedings, ASDSO Dam Safety 2009 Annual Conference*, September 27-October 1, 2009, Hollywood, FL.

[52] Altinakar, M. S., M. Z. McGrath and V. P. Ramalingam. An Enhanced Two-Dimensional Numerical Model for Simulating Floods Due to Dam and Levee Break/Breaching. *Proceedings, International Conference on Hydroscience and Engineering (ICHE-2010)*, Chennai, India, August 2-5, 2010.

[53] Durmus, A., Q. Nguyen, M. Z. McGrath, M. S. Altinakar and W. Uddin. Numerical Modeling and Simulation of Extreme Flood Inundation to Assess Vulnerability of Transportation Infrastructure Assets. *TRB 94th Annual Meeting*, *Online Proceedings*, Washington, D.C., January 10-14, 2015.

[54] Altinakar, M. S., M. McGrath, V. P. Ramalingam and W. Uddin. Two-Dimensional Flood Modeling for the Assessment of Impacts on Critical Infrastructures. *University Transportation Center (UTC) Conference for the Southeastern Region*, University of Alabama at Birmingham. Birmingham, Alabama, March 26-27, 2015.

[55] National Center for Intermodal Transportation for Economic Competitiveness (NCITEC) Project 2012 ─ 25: Disaster Protection of Transport Infrastructure and Mobility Using Flood Risk Modeling and Geospatial Visualization, Final Report. Center for Advanced Infrastructure Technology (CAIT), May 2015.

[56] Accuracy Assessment of the U.S. Geological Survey National Elevation Dataset, and Comparison with Other Large-Area Elevation Datasets – SRTM and ASTER, U.S. Department of Interior, U.S. Geological Survey, Open-File Report 2014-1008, 2014.

[57] Nguyen, Q. and W. Uddin. Applications of Shuttle Radar DEM Data and Landsat-8 Satellite Imagery for HEC-RAS Floodplain Modeling. The National Hydrologic Warning Council (NHWC) Transmission, January 2016, pp. 2-4. https://s3.amazonaws.com/ClubExpressClubFiles/617218/documents/The_NHWC_Transmission--January_2016_1768766209.pdf?AWSAccessKeyId=AKIAIB6I23VLJX7E4J7Q&Expires=1466798395&response-content-disposition=inline%3B%20filename%3DThe_NHWC_Transmission—January_2016.pdf&Signature=Yy4VEi28Ho17q83oJu91zVAzez8%3D. Accessed June 24, 2016.

[58] Alcaraz, C. and S. Zeadally. Critical Infrastructure Protection: Requirements and Challenges for the 21st Century. *International Journal of Critical Infrastructure Protection*, Vol. 8, January 2015, pp. 53-66. http://ac.els-cdn.com/S1874548214000791/1-s2.0-S1874548214000791-main.pdf?_tid=587cea94-db0d-11e4-a939-00000aacb35d&acdnat=1428181289_24a424b09edaa4177ba9599bd0b995cb. Accessed April 4, 2015.

[59] McCleary, R. and R. A. Hay, Jr. *Applied Time Series Analysis for the Social Sciences*. Sage Publications, 1980, California.

[60] Structure Types, 2014 (Counts). U.S. Department of Transportation, FHWA. http://www.fhwa.dot.gov/bridge/nbi/no10/strtyp14.xlsx. Accessed April 27, 2015.

[61] Material Types, 12/2014 (Counts). U.S. Department of Transportation, FHWA. http://www.fhwa.dot.gov/bridge/nbi/no10/mat14.xlsx. Accessed April 27, 2015.

[62] Lee, G. C., S. B. Mohan, C. Huang and B. N. Fard. A Study of U.S. Bridge Failures (1980-2012). Technical Report MCEER-13-0008. University at Buffalo, State University of New York, June 15, 2013. http://mceer.buffalo.edu/pdf/report/13-0008.pdf. Accessed June 7, 2016.

[63] Preliminary Damage Reports on Bridges, MCEER Earthquake Engineering to Extreme Events. http://mceer.buffalo.edu/research/Reconnaissance/Katrina8-28-05/damage_reports_bridges.asp. Accessed June 8, 2016.

[64] California I-10 Bridge Linking Los Angeles to Phoenix Collapses, July 21, 2015. http://www.npr.org/2015/07/21/425054375/california-i-10-bridge-linking-los-angeles-to-phoenix-collapses. Accessed August 10, 2015.

[65] American Association of State Highway Officials (AASHO). Standard Specifications for Highway Bridges, 11th Edition, Washington, D.C., 1973. https://law.resource.org/pub/us/cfr/ibr/001/aashto.bridges.1973.pdf. Accessed August 19, 2014.

[66] Coastal Engineering Research Center, Department of the Army, Waterways Experiment Station, Corps of Engineers. Shore Protection Manual Vol. II, 4th Edition, Washington, D.C., 1984. https://archive.org/download/shoreprotectionm02unit/shoreprotectionm02unit.pdf. Accessed April 20, 2015.

[67] Wellwood, N. and J. A. Fenwick. Flood Loading Methodology for Bridges. *Proceedings, 15th Australian Road Research Board (ARRB) Conference*, 1990, Part 3, pp. 315-341.

http://114.111.144.247/Presto/content/Detail.aspx?q=aHlkcm9keW5hbWlj&ctID=MjE1ZTI4YzctZjc1YS00MzQ4LTkyY2UtMDJmNTgxYjg2ZDA5&rID=MTA4MA==&qcf=&ph=VHJ1ZQ==&bckToL=VHJ1ZQ==&. Accessed April 17, 2015.

[68] Jempson, M. A. and C. J. Apelt. Hydrodynamic Forces on Partially and Fully Submerged Bridge Superstructures. *Proceedings, 16th Australian Road Research Board (ARRB) Conference*, 1992, Part 3, pp. 67-79. http://114.111.144.247/Presto/content/Detail.aspx?q=aHlkcm9keW5hbWlj&ctID=MjE1ZTI4YzctZjc1YS00MzQ4LTkyY2UtMDJmNTgxYjg2ZDA5&rID=MzE4&qcf=&ph=VHJ1ZQ==&bckToL=VHJ1ZQ==&. Accessed April 17, 2015.

[69] Stream Stability at Highway Structures. 2nd Edition, Hydraulic Engineering Circular (HEC) No. 20. U.S. Department of Transportation, FHWA, November 1995. http://www.fhwa.dot.gov/engineering/hydraulics/pubs/hec/hec20si.pdf. Accessed April 17, 2015.

[70] Parola, A. C., C. J. Apelt and M. A. Jempson. Report 445: Debris Forces on Highway Bridges. National Academy of Sciences, Transportation Research Board (TRB), NCHRP, 2000. http://onlinepubs.trb.org/onlinepubs/nchrp/nchrp_rpt_445.pdf. Accessed May 22, 2014.

[71] American Association of State Highway and Transportation Officials (AASHTO). Guide Specifications for Bridges Vulnerable to Coastal Storms, Washington, D.C., 2008.

[72] Witzany, J., T. Cejka and R. Zigler. Failure Resistance of Historic Stone Bridge Structure of Charles Bridge. II: Susceptibility to Floods. *ASCE Journal of Performance of Constructed Facilities*, Vol. 22, No. 2, April 1, 2008, pp. 83-91. http://ascelibrary.org/

doi/pdf/10.1061/%28ASCE%290887-3828%282008%2922%3A2%2883%29. Accessed March 13, 2015.

[73] Xiao, H., W. Huang and Q. Chen. Effects of Submersion Depth on Wave Uplift Force Acting on Biloxi Bay Bridge Decks during Hurricane Katrina. *Computers & Fluids 39*, 2010, pp. 1390-1400. https://0-hermes.lib.olemiss.edu.umiss.lib.olemiss.edu/illiad/illiad.dll?Action=10&Form=75&Value=633936. Accessed March 16, 2015.

[74] SLOPE/W 2012 slope stability analysis. GEO-SLOPE International. http://www.geo-slope.com/products/slopew.aspx. Accessed June 17, 2016.

[75] Koloski, J. W., S. D. Schwarz and D. W. Tubss. Geological Properties of Geologic Materials. Engineering Geology in Washington, Vol. I. Washington Division of Geology and Earth Resources Bulletin 78, 1989, pp. 19-26. http://file.dnr.wa.gov/publications/ger_b78_engineering_geol_v1_pt1of5.pdf. Accessed June 24, 2016.

[76] Stability Modeling with SLOPE/W. An Engineering Methodology, GEO-SLOPE International Ltd., May 2014 Edition. http://downloads.geo-slope.com/geostudioresources/books/8/13/slope%20modeling.pdf. Accessed August 15, 2014.

[77] Leeson, D., C. Fulmer and K. Heron. Flood Resilient Bridge Design: Case Studies From Challenging Design Environments. *9th Austroads Bridge Conference*, Sydney, New South Wales, 2014. http://114.111.144.247/Presto/content/Detail.aspx?q=ZGVicmlz&ctID=MjE1ZTI4YzctZjc1YS00MzQ4LTkyY2UtMDJmNTgxYjg2ZDA5&rID=NTI0Mw==&qcf=&ph=VHJ1ZQ==&bckToL=VHJ1ZQ==&. Accessed April 17, 2015.

[78] NCITEC Workshop: Extreme Flood Inundation Mapping and Risk Modeling of Transportation Infrastructure Assets. National Center for Computational Hydroscience &

Engineering (NCCHE) and Center for Advanced Infrastructure Technology (CAIT). December 5, 2014, School of Engineering, University of Mississippi.

[79] Durmus, A., Q. Nguyen, M. Z. McGrath, M. S. Altinakar and W. Uddin. Numerical Modeling and Simulation of Extreme Flood Inundation To Assess Vulnerability of Transportation Infrastructure Assets, *University Transportation Center (UTC) Conference for the Southeastern Region*, University of Alabama at Birmingham. Birmingham, Alabama, March 26-27, 2015.

[80] Evaluating Scour at Bridges. 5th Edition, HEC No. 18. U.S. Department of Transportation, FHWA, April 2012. http://www.fhwa.dot.gov/engineering/hydraulics/pubs/hif12003.pdf. Accessed June 25, 2016.

[81] Bridge Scour and Stream Instability Countermeasures. HEC No. 23. U.S. Department of Transportation, FHWA, July 1997. http://www.fhwa.dot.gov/engineering/hydraulics/pubs/hec/hec23.pdf. Accessed June 25, 2016.

[82] PCI, Precast Prestressed Concrete Bridge Design Manual, 2nd Edition. Precast/Prestressed Concrete Institute (PCI), Illinois, 2003.

[83] Xanthakos, P. P. *Theory and Design of Bridges*, John Wiley & Sons, Inc., New York, 1994.

[84] Durmus, A. and W. Uddin. Extreme Flood Simulation and Inundation Impacts on Structural Integrity of Bridges. National Hydrologic Warning Council (NHWC) Transmission, September 2015, pp. 1-2. https://s3.amazonaws.com/ClubExpressClubFiles/617218/documents/The_NHWC_Transmission--September_2015_616435355.pdf?AWSAccessKeyId=AKIAIB6I23VLJX7E4J7Q&Expires=1466178359&response-content-disposition=inline%3B%20filename%3DThe_NHWC_Transmission--

September_2015.pdf&Signature=1URvMU5DKzUD7dmMfQNbeXxMYpA%3D. Accessed June 17, 2016.

[85] LS-DYNA, Livermore Software Technology Corporation. http://www.lstc.com/products/ls-dyna. Assessed June 14, 2016.

[86] LS-DYNA Keyword User's Manual Volume I, LS-DYNA R8, 03/23/15 (r:6319), Livermore Software Technology Corporation (LSTC).

[87] Mississippi Standard Specifications For Road and Bridge Construction, Mississippi Department of Transportation, Jackson, 1996.

[88] LS-DYNA Keyword User's Manual Volume II Material Models, LS-DYNA R8, 03/18/15 (r:6307), Livermore Software Technology Corporation (LSTC).

[89] Bridge Bearings. Caltrans Memo to Designers 7-1, June 1994. http://www.dot.ca.gov/hq/esc/techpubs/manual/bridgemanuals/bridge-memo-to-designer/page/Section%207/7-1.pdf. Accessed November 26, 2014.

[90] Uddin, W., R. M. Hackett, A. Joseph, Z. Pan and A. B. Crawley. Three-Dimensional Finite-Element Analysis of Jointed Concrete Pavement with Discontinuities. Transportation Research Board (TRB), Transportation Research Record (TRR) 1482, 1995, pp. 26-32.

[91] White, H. 2nd. Integral Abutment Bridges: Comparison of Current Practice Between European Countries and the United States of America. Special Report 152. New York Department of Transportation, Transportation Research and Development Bureau, July 2007. https://www.dot.ny.gov/divisions/engineering/technical-services/trans-r-and-d-repository/SR152.pdf?nd=nysdot. Accessed July 2, 2016.

[92] Uddin, W. Personal Communication with Justin Walker, Director of Structures-State Bridge Engineer, Bridge Division, Mississippi Department of Transportation, Jackson, Mississippi, October 16, 2014.

[93] LFRD Bridge Design Specifications, American Association of State Highway and Transportation Officials (AASHTO), Washington, D.C., 2012.

[94] ACI, Building Code Requirements for Structural Concrete (ACI 318-08) and Commentary, American Concrete Institute (ACI), Michigan, 2008.

[95] Merritt, F. S. Ed. *Standard Handbook for Civil Engineers*. Second Edition, McGraw-Hill Book Company, 1976.

[96] Uddin, W. Personal Communication with Mohiuddin A. Khan. Mississippi, July 2, 2015.

[97] Community Resilience System Initiative (CRSI) Steering Committee Final Report, Community Resilience System Initiative, August 2011. Community and Regional Resilience Institute, Washington, D.C. http://www.resilientus.org/wp-content/uploads/2015/04/CRSI-Final-Report-1.pdf. Accessed July 1, 2016.

[98] Moulton, L. K., H. V. S. GangaRao and G. T. Halvorsen. Tolerable Movement Criteria for Highway Bridges, Report No. FHWA/RD-85/107. U.S.Department of Transportation, FHWA, October 1985. http://isddc.dot.gov/OLPFiles/FHWA/011756.pdf. Accessed November 25, 2015.

[99] Nguyen, Q. Extreme Weather Disaster Resilient Port and Waterway Infrastructure for Sustainable Global Supply Chain. *PhD Dissertation*, University of Mississippi, 2016 (In Progress).

[100] Floods: Recurrence Intervals and 100-year floods. The USGS Water Science School. https://water.usgs.gov/edu/100yearflood.html. Accessed April 27, 2016.

[101] National Bridge Inspection Standards. U.S. Department of Transportation, FHWA. http://www.fhwa.dot.gov/bridge/nbis.cfm. Accessed April 27, 2015.

[102] Thompson, P. D. and F. D. Harrison. Pontis Version 2.0 User's Manual: A Network Optimization System for Bridge Improvements and Maintenance, Report No. FHWA-SA-93-083. U.S. Department of Transportation, FHWA, December 1993.

[103] NCHRP 12-28(02)A [Completed] Bridge Management Systems Software. http://apps.trb.org/cmsfeed/TRBNetProjectDisplay.asp?ProjectID=301. Accessed July 6, 2016.

[104] Hawk, H. BRIDGIT: User-Friendly Approach to Bridge Management. Transportation Research Board (TRB), Transportation Research Circular 498, June 2000. http://onlinepubs.trb.org/onlinepubs/circulars/circ498/v1_E07.pdf. Accessed April 1, 2016.

[105] Synthesis 300: Performance Measures for Research, Development, and Technology Programs. National Academy of Sciences, Transportation Research Board (TRB), NCHRP, 2001.http://onlinepubs.trb.org/onlinepubs/nchrp/nchrp_syn_300.pdf. Accessed April 1, 2015.

[106] Synthesis 397: Bridge Management Systems for Transportation Agency Decision Making. National Academy of Sciences, Transportation Research Board (TRB), NCHRP, 2009. http://onlinepubs.trb.org/onlinepubs/nchrp/nchrp_syn_397.pdf. Accessed April 1, 2015.

[107] AASHTOWare Bridge Management. http://aashtowarebridge.com/. Accessed April 1, 2015.

[108] Gutkowski, R. M. and N. D. Arenella. Investigation of Pontis – A Bridge Management Software, August 1998. http://www.mountain-plains.org/pubs/pdf/MPC98-95.pdf. Accessed April 1, 2015.

[109] Recent Development of Bridge Management Systems in Canada. Hammad, A., J. Yan, B. Mostofi. Paper prepared for presentation at the Bridges - Economic and Social Linkages (B) Session, 2007 Annual Conference of the Transportation Association of Canada, Saskatoon, Saskatchewan. http://conf.tac-atc.ca/english/resourcecentre/readingroom/conference/conf2007/docs/s7/hammad.pdf. Accessed April 1, 2016.

[110] Hajdin, R. BMS Development in Switzerland. ASCE Structures 2000. Advanced Technology in Structural Engineering. http://ascelibrary.org/doi/pdf/10.1061/40492%282000%2953. Accessed March 12, 2015.

[111] Hearn, G., P. D. Thompson, W. Mystkowski and W. Hyman. Report 668: Framework for a National Database System for Maintenance Actions on Highway Bridges. National Academy of Sciences, Transportation Research Board (TRB), NCHRP, 2010. http://onlinepubs.trb.org/onlinepubs/nchrp/nchrp_rpt_668.pdf. Accessed on April 2, 2015.

[112] USGS Surface-Water Data for the Nation. USGS. http://waterdata.usgs.gov/nwis/sw. Accessed July 3, 2016.

[113] Bridge Management Questionnaire Report. U.S. Department of Transportation, FHWA Office of Asset Management, December, 2010. http://www.fhwa.dot.gov/bridge/management/bms.pdf. Accessed on April 1, 2015.

[114] Uddin, W. *Disaster Resilience Management of Infrastructure Systems: Computational Modeling and Geospatial Technologies*. Taylor & Francis, 2016 (In Progress).

[115] Hudson, W. R., R. Haas and W. Uddin. *Infrastructure Management*. McGraw Hill, New York, 1997.

[116] Bridge Preservation Guide. FHWA-HIF-11042. U.S. Department of Transportation, FHWA, August 2011. http://www.fhwa.dot.gov/bridge/preservation/guide/guide.pdf. Accessed June 27, 2016.

[117] Bridge Replacement Unit Costs 2013. U.S. Department of Transportation, Federal Highway Administration (FHWA). http://www.fhwa.dot.gov/bridge/nbi/sd2013.cfm. Accessed July 6, 2016.

[118] Element Unit and Failure Costs and Functional Improvement Costs for Use in the MN/DOT Pontis Bridge Management System. MN/RC – 2004-05. http://www.lrrb.org/media/reports/200405.pdf. Accessed March 31, 2016.

APPENDIX

APPENDIX A

Key Output of NCCHE 2D Flood Simulations (CCHE2D-FLOOD)

A1. CCHE2D-FLOOD Floodwater Depth Along River Centerline for 10 m CCS Simulation

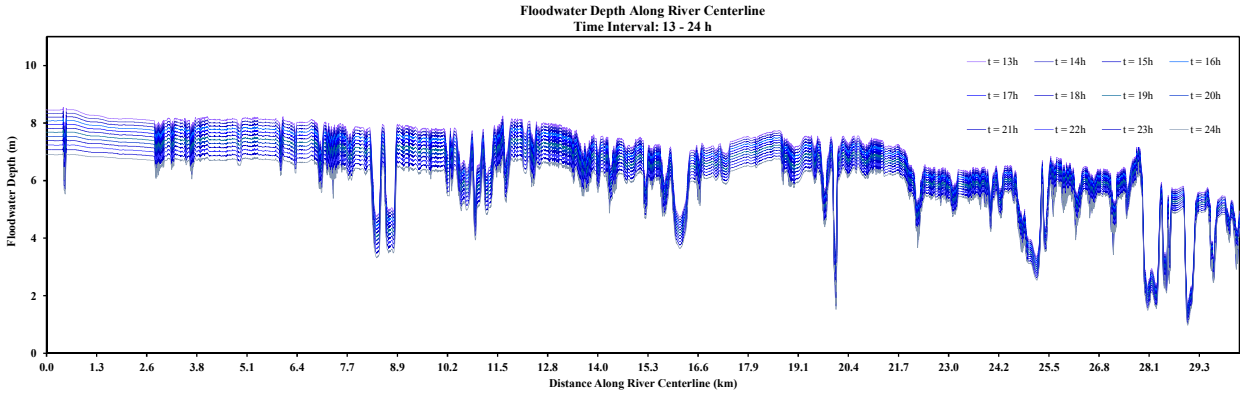

(a)

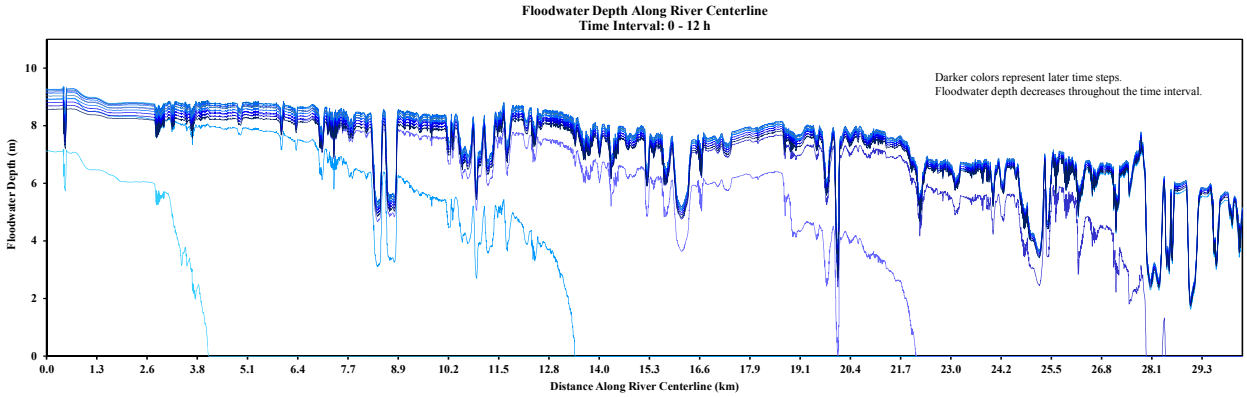

(b)

Figure A.1.1 CCHE2D-FLOOD floodwater depth along river centerline for 10 m CCS simulation (a) 0-12 h (b) 13-24 h

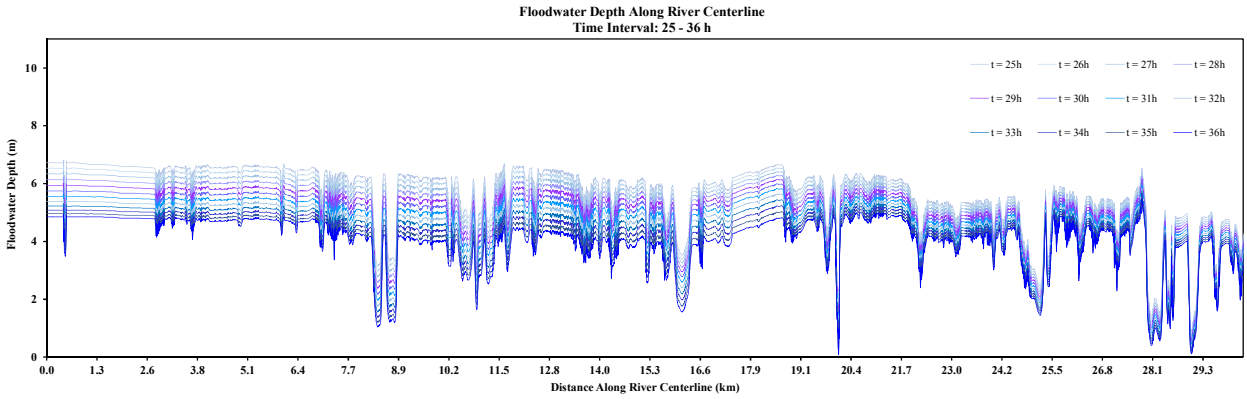

(a)

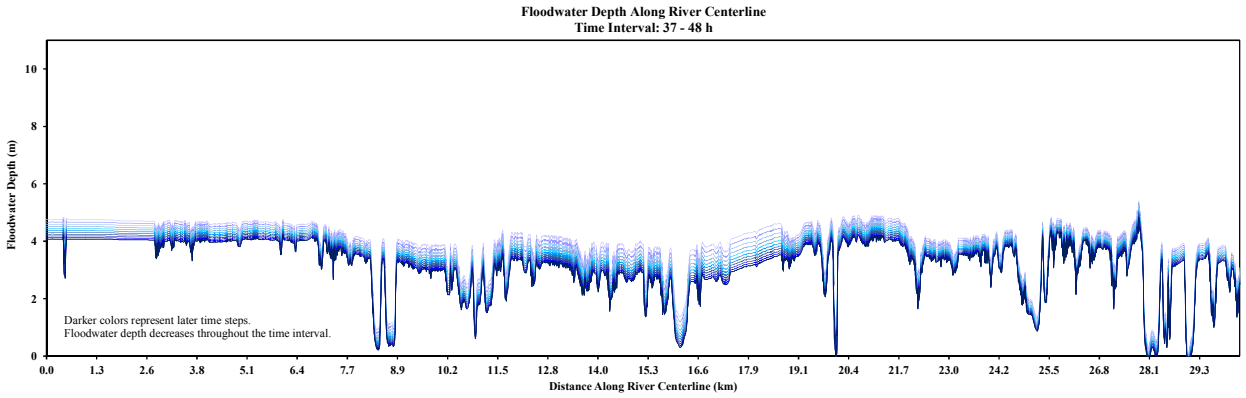

(b)

Figure A.1.2 CCHE2D-FLOOD floodwater depth along river centerline for 10 m CCS simulation (a) 25-36 h (b) 37-48 h

A2. CCHE2D-FLOOD Discharge Output at Observation Lines

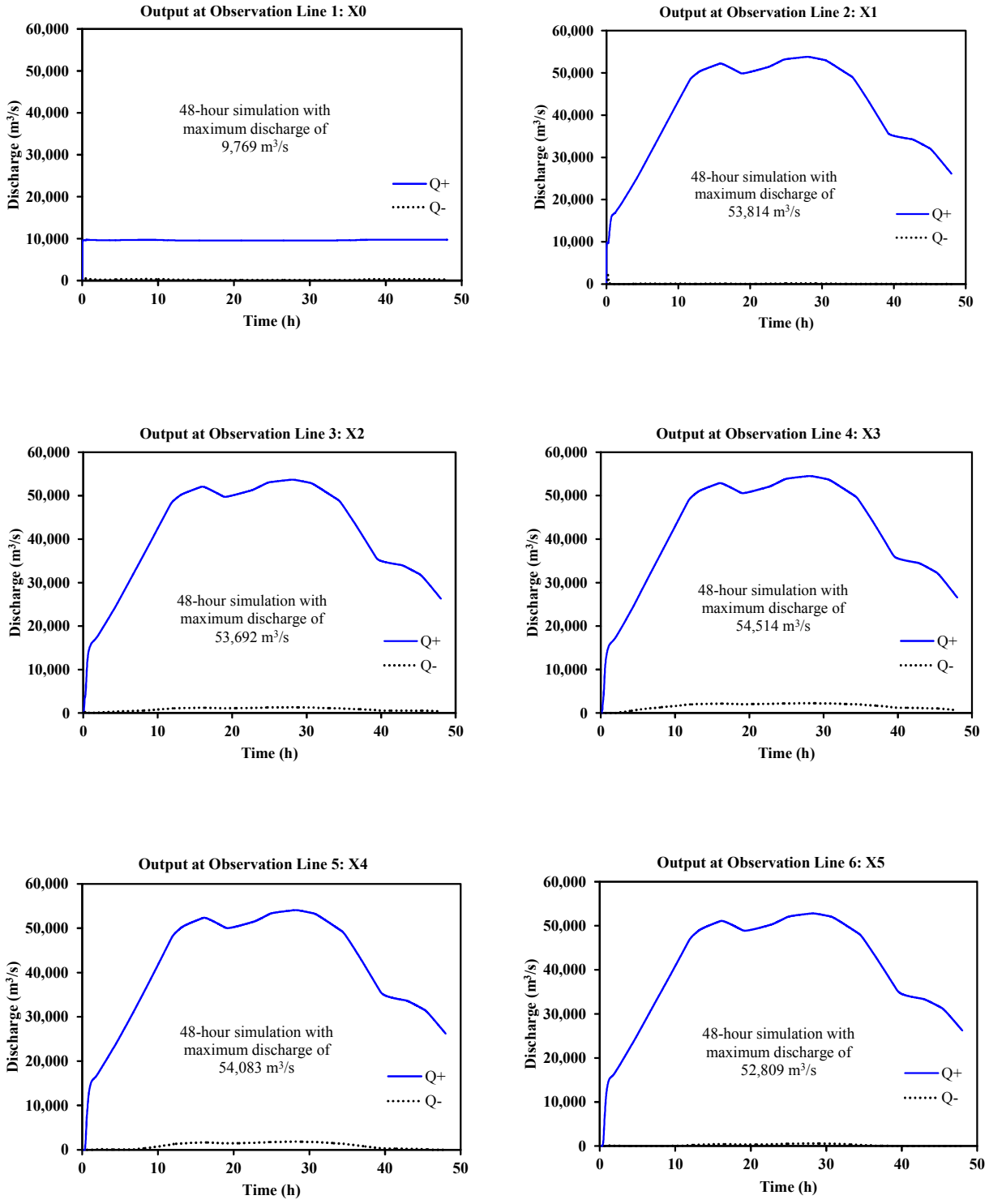

Figure A.2.1 CCHE2D-FLOOD discharge output at observation lines 1-6

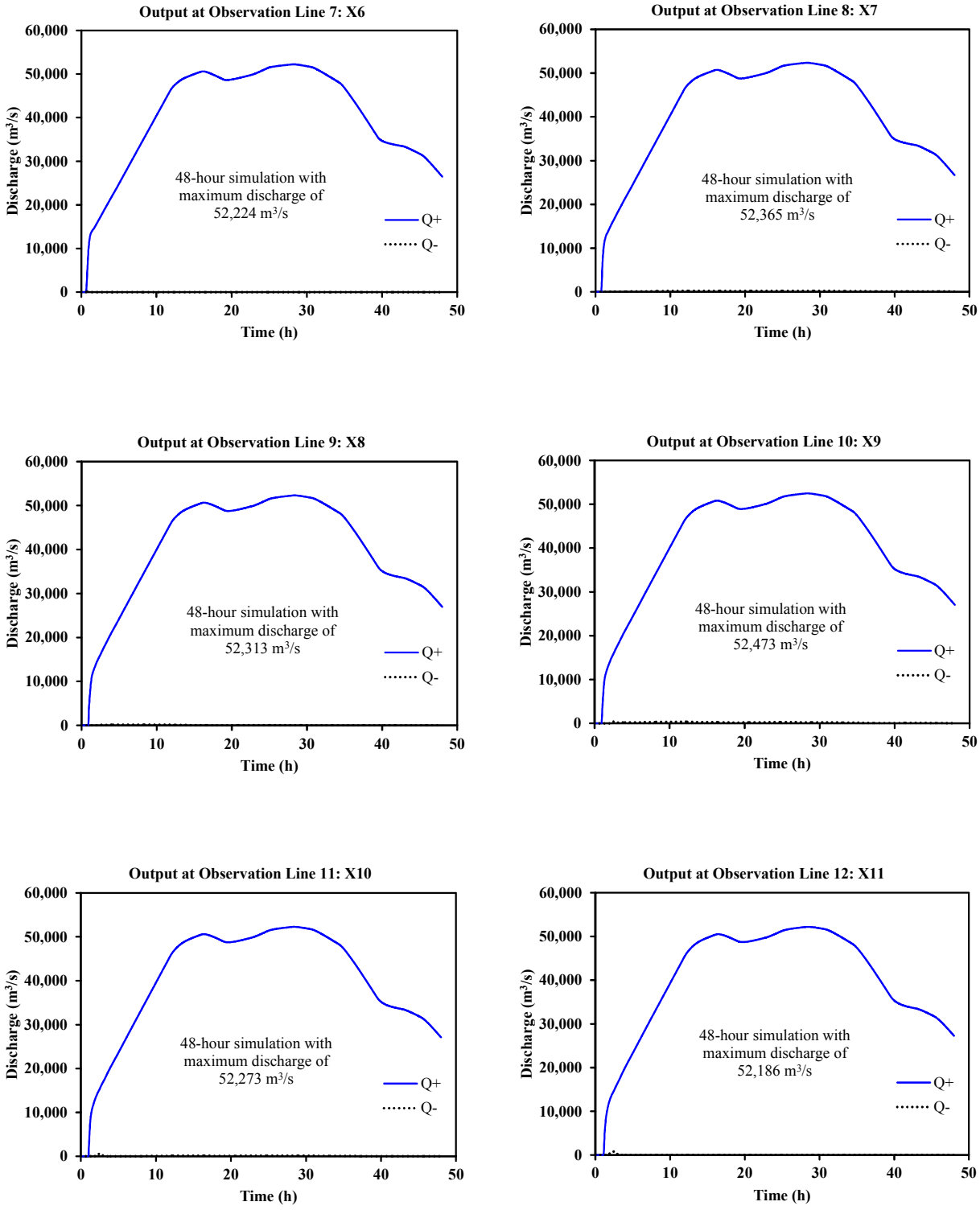

Figure A.2.2 CCHE2D-FLOOD discharge output at observation lines 7-12

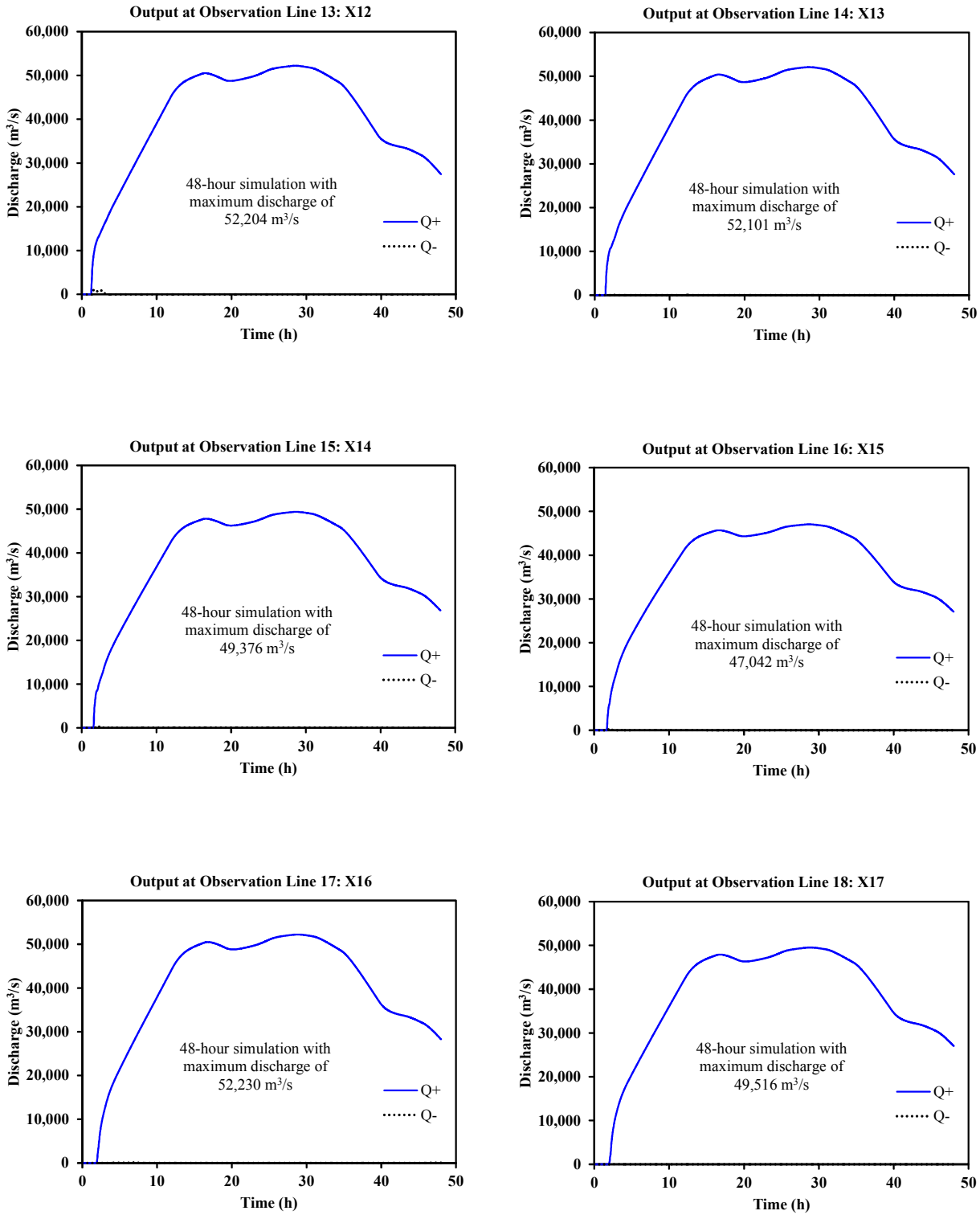

Figure A.2.3 CCHE2D-FLOOD discharge output at observation lines 13-18

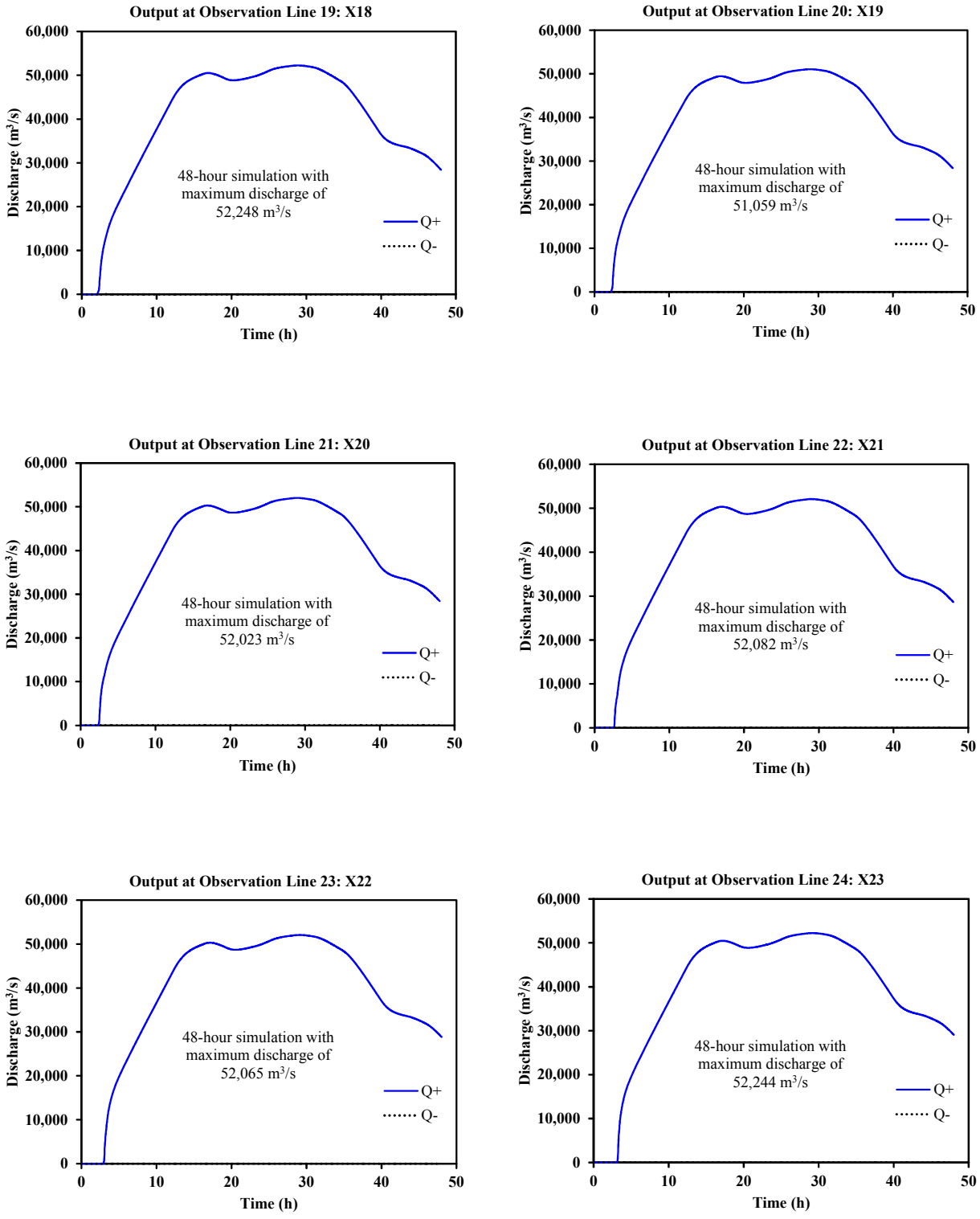

Figure A.2.4 CCHE2D-FLOOD discharge output at observation lines 19-24

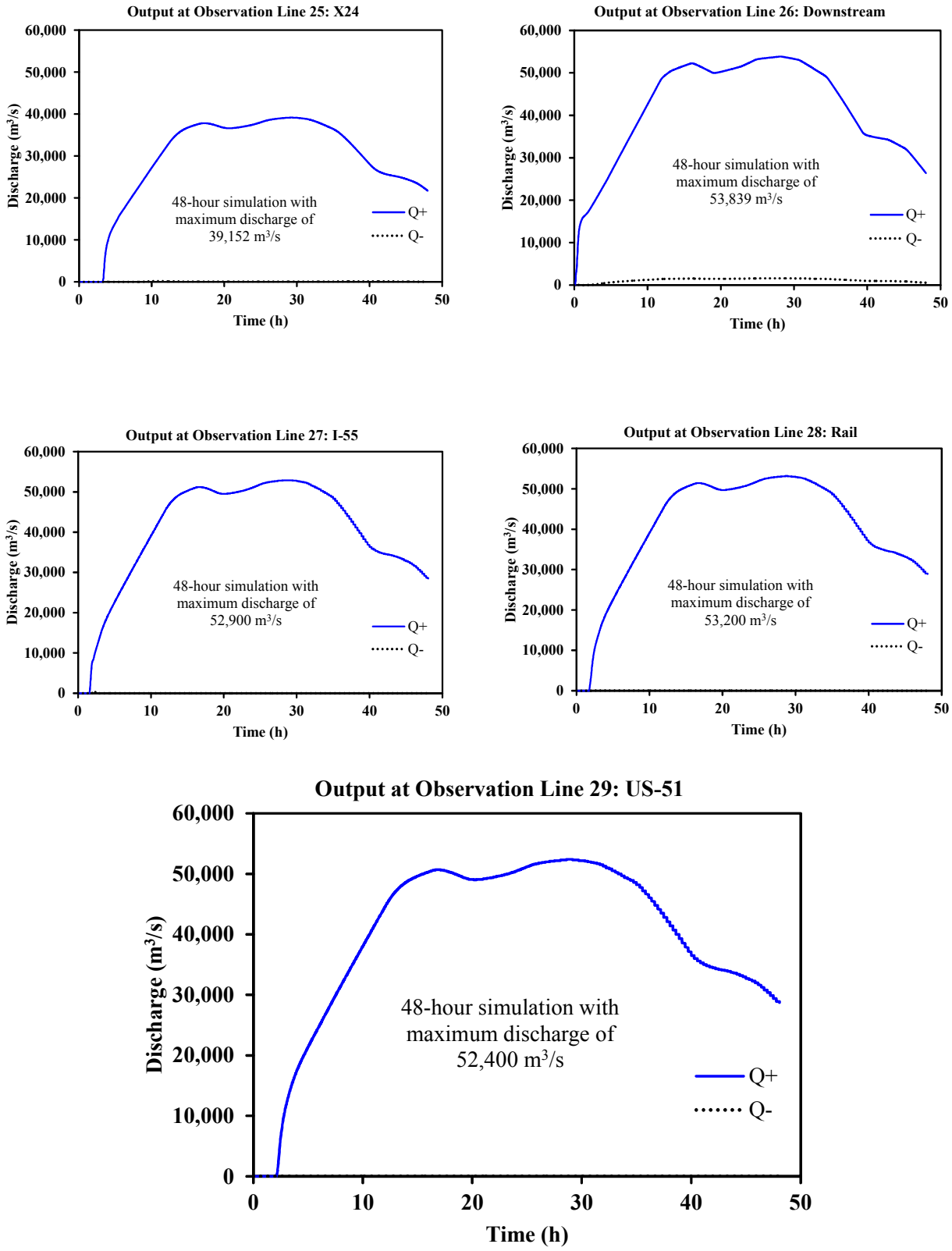

Figure A.2.5 CCHE2D-FLOOD discharge output at observation lines 25-29

A3. CCHE2D-FLOOD Floodwater Depth and Velocity Output: 3 m CCS Simulation

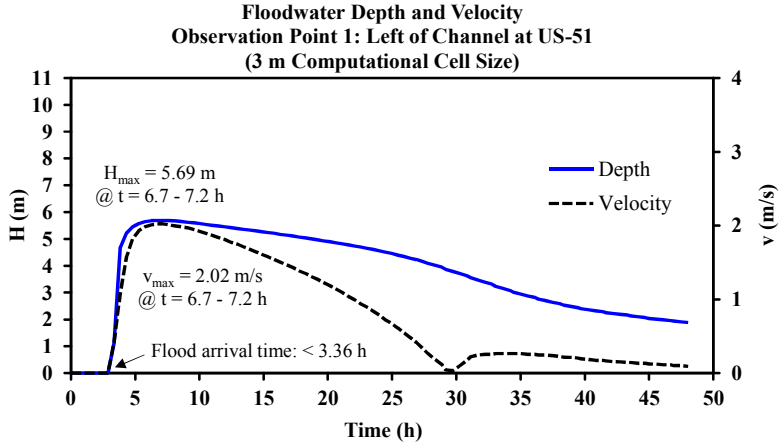

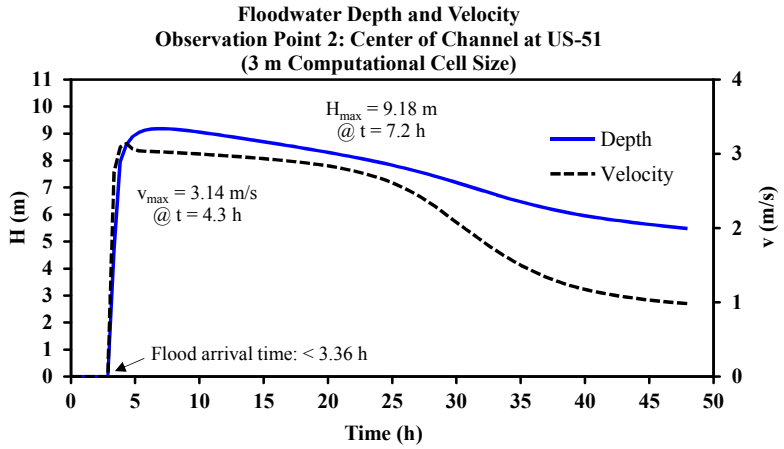

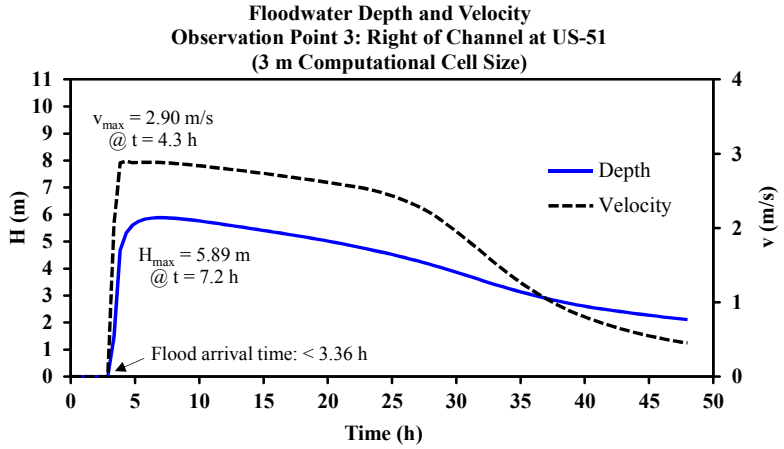

Figure A.3.1 CCHE2D-FLOOD floodwater depth and velocity output at observation points 1-3

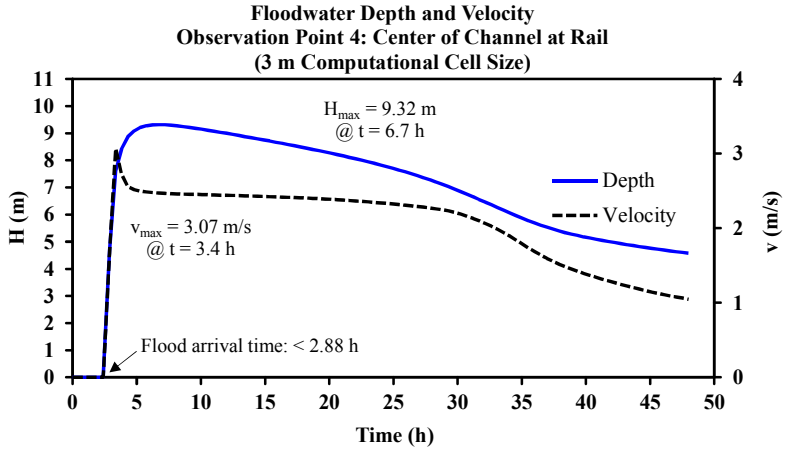

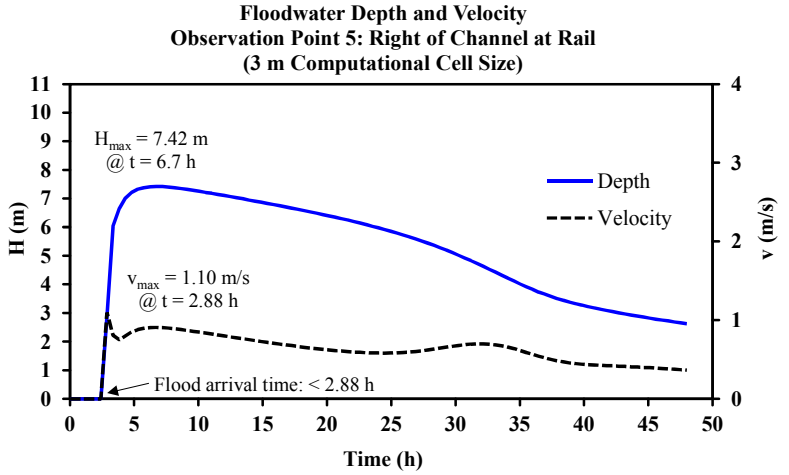

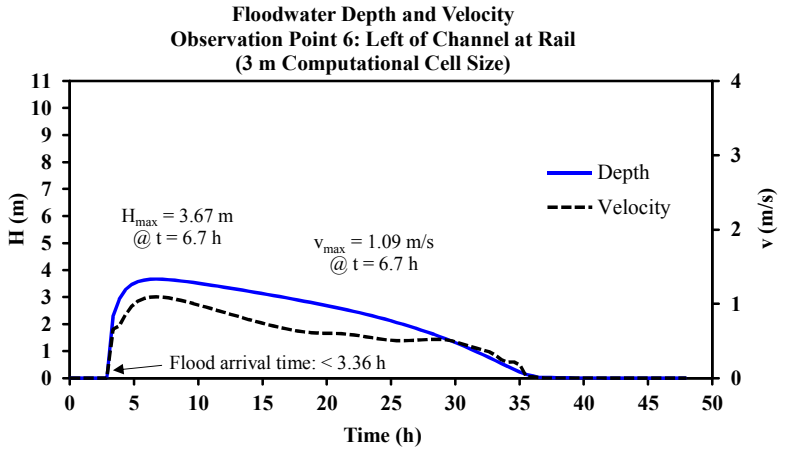

Figure A.3.2 CCHE2D-FLOOD floodwater depth and velocity output at observation points 4-6

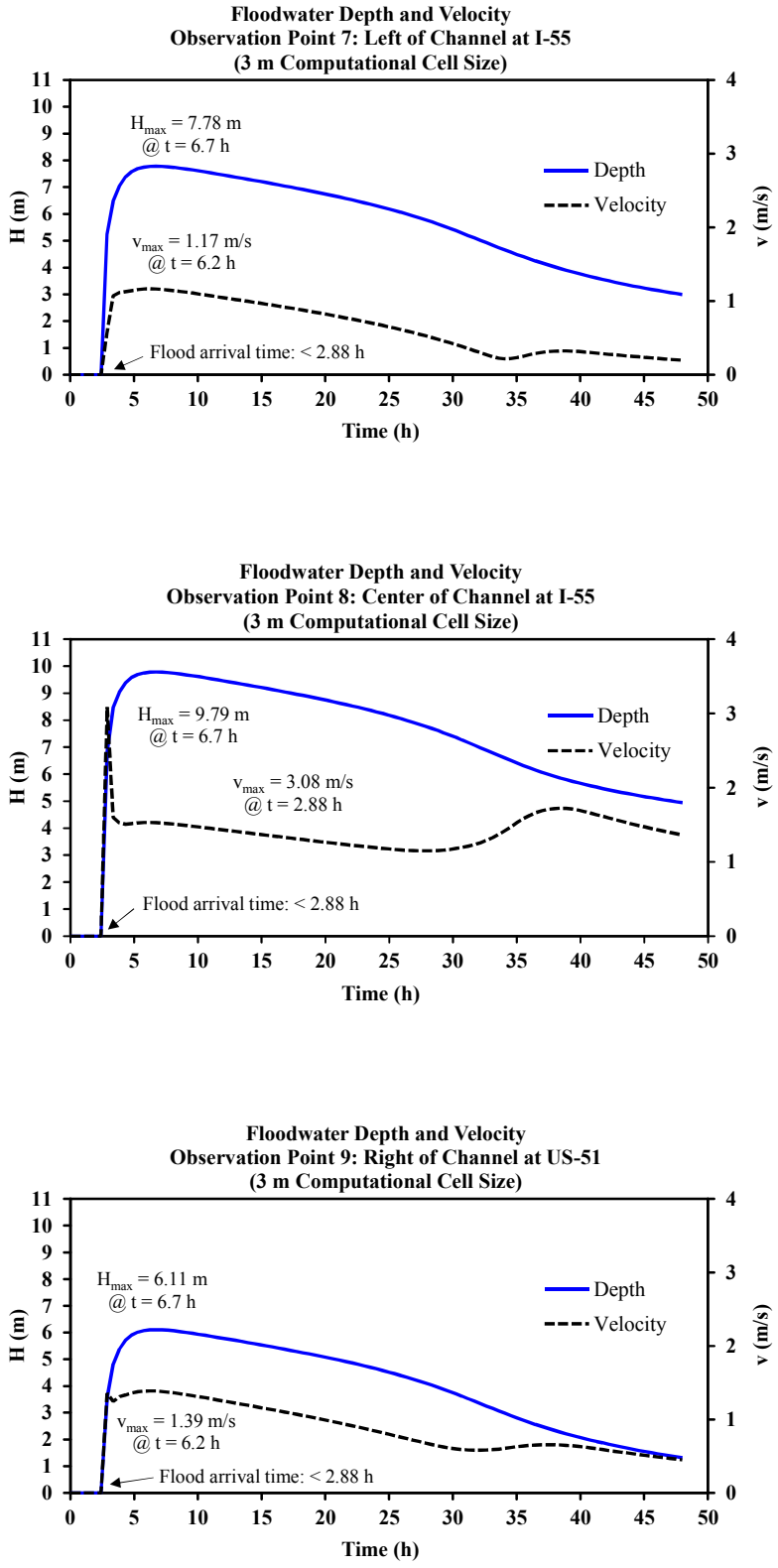

Figure A.3.3 CCHE2D-FLOOD floodwater depth and velocity output at observation points 7-9

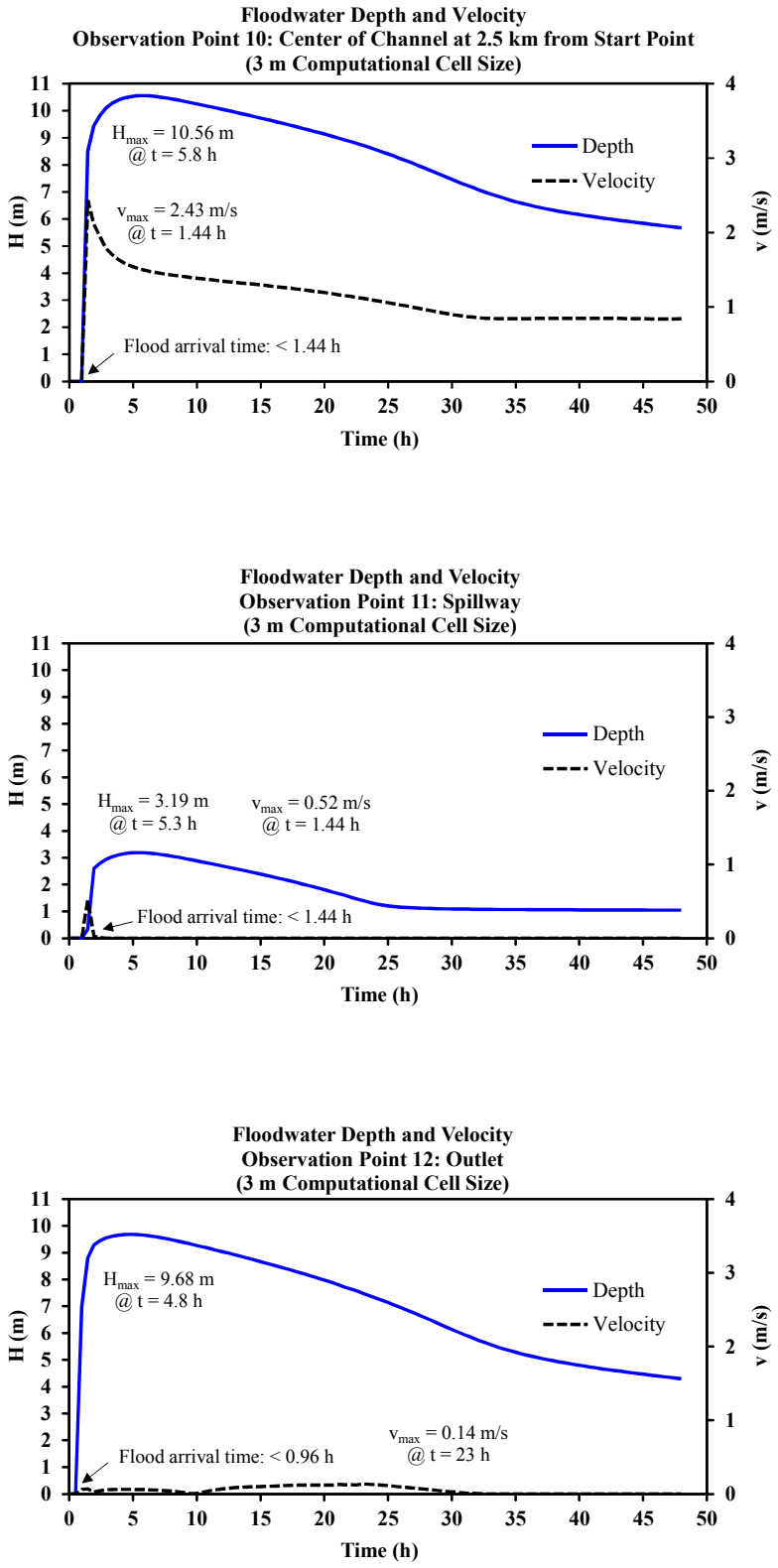

Figure A.3.4 CCHE2D-FLOOD floodwater depth and velocity output at observation points 10-12

A4. CCHE2D-FLOOD Floodwater Depth and Velocity Output: 5 m CCS Simulation

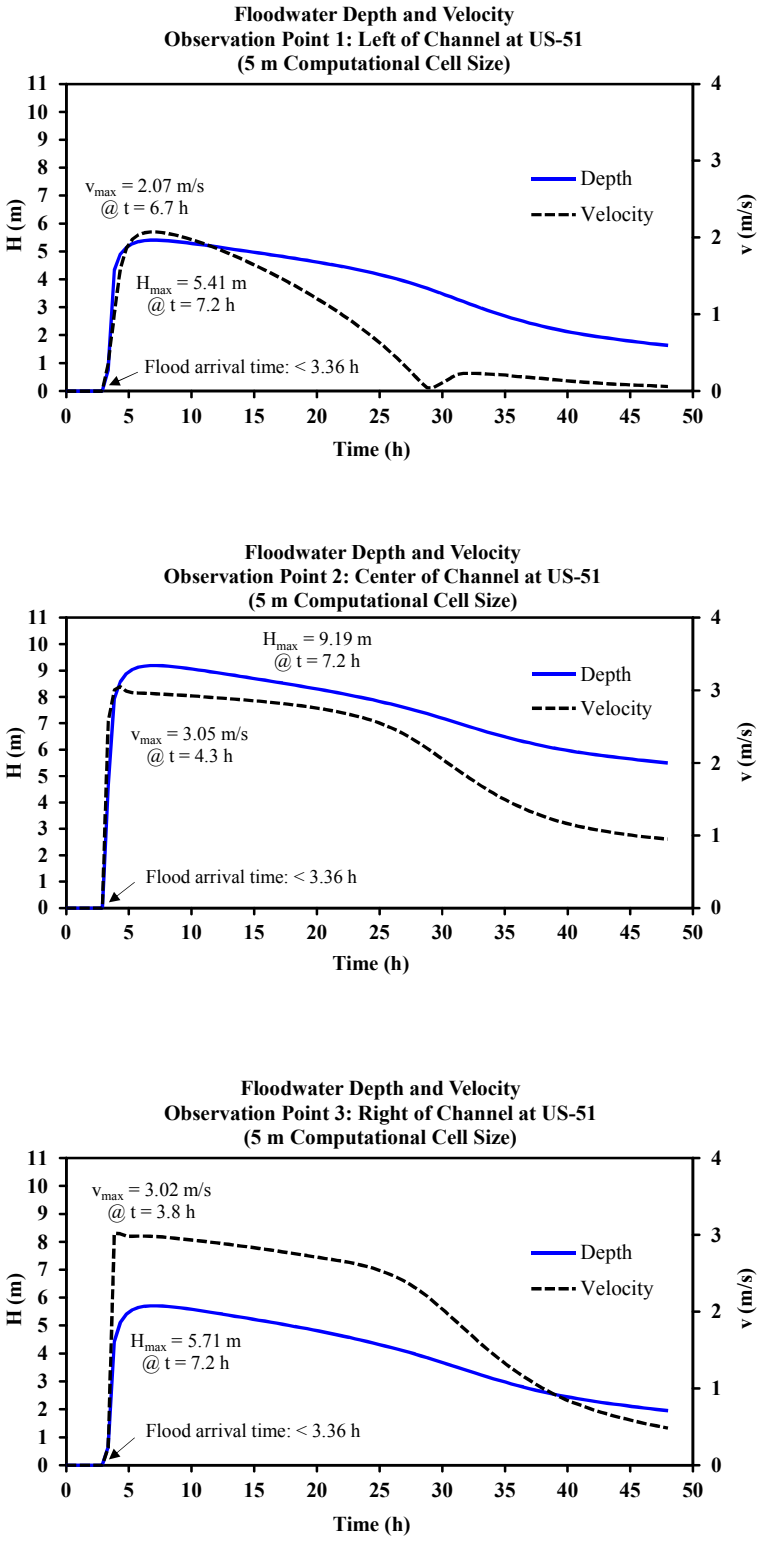

Figure A.4.1 CCHE2D-FLOOD floodwater depth and velocity output at observation points 1-3

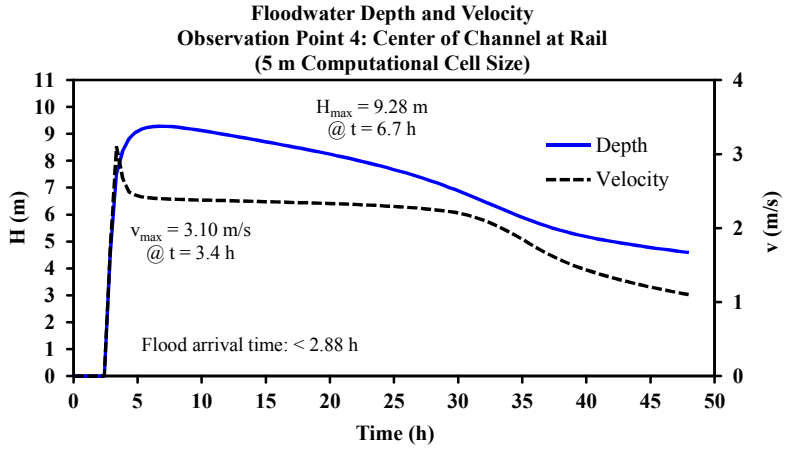

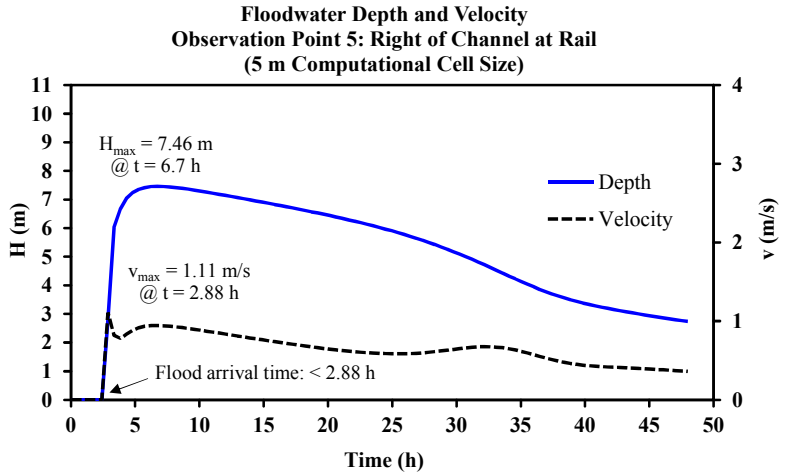

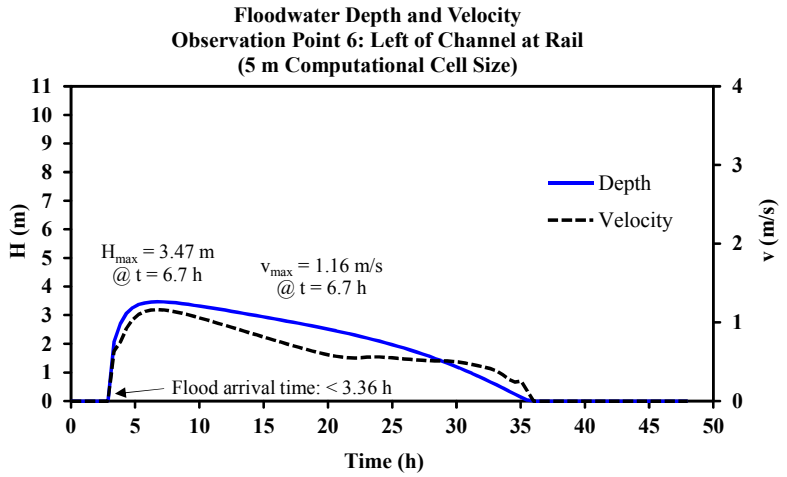

Figure A.4.2 CCHE2D-FLOOD floodwater depth and velocity output at observation points 4-6

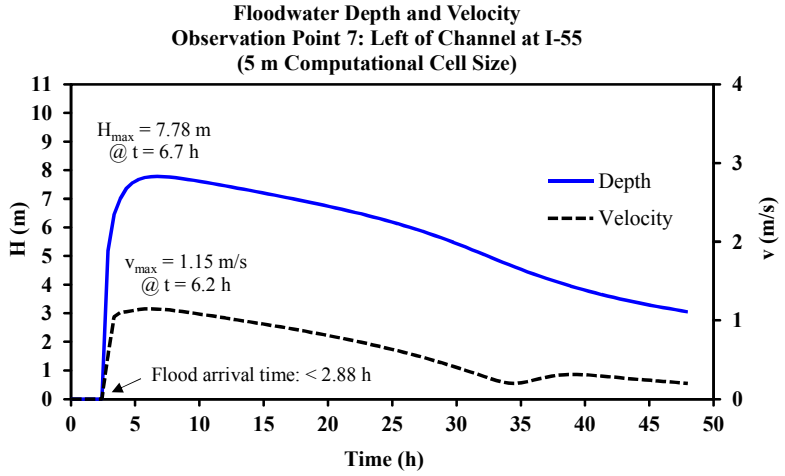

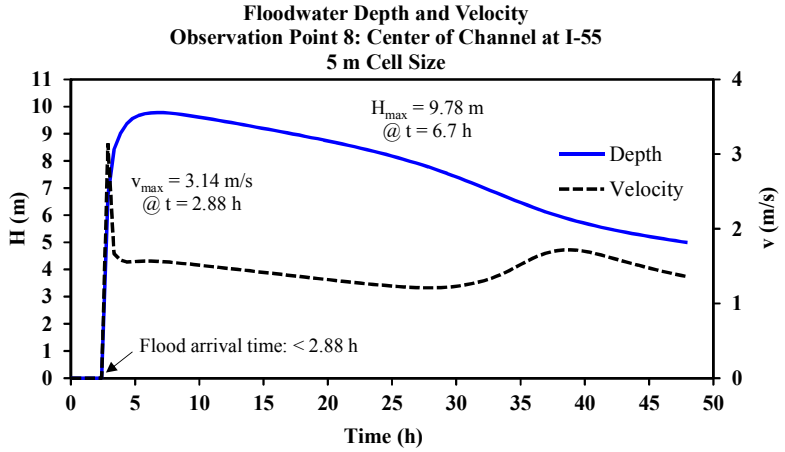

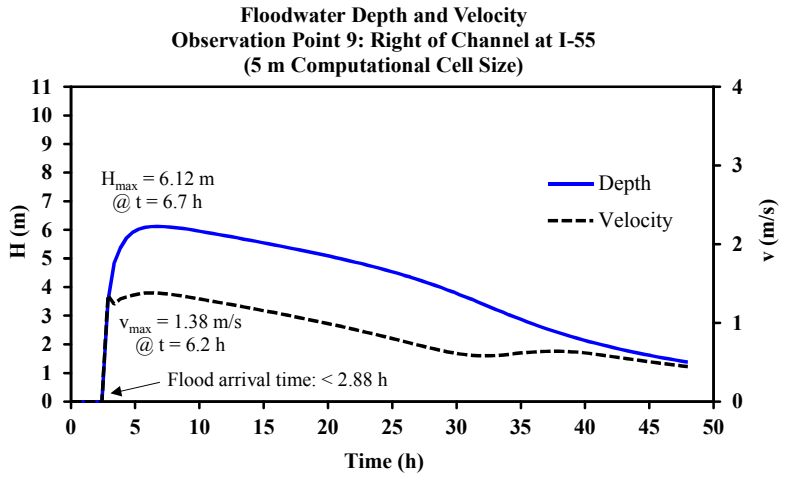

Figure A.4.3 CCHE2D-FLOOD floodwater depth and velocity output at observation points 7-9

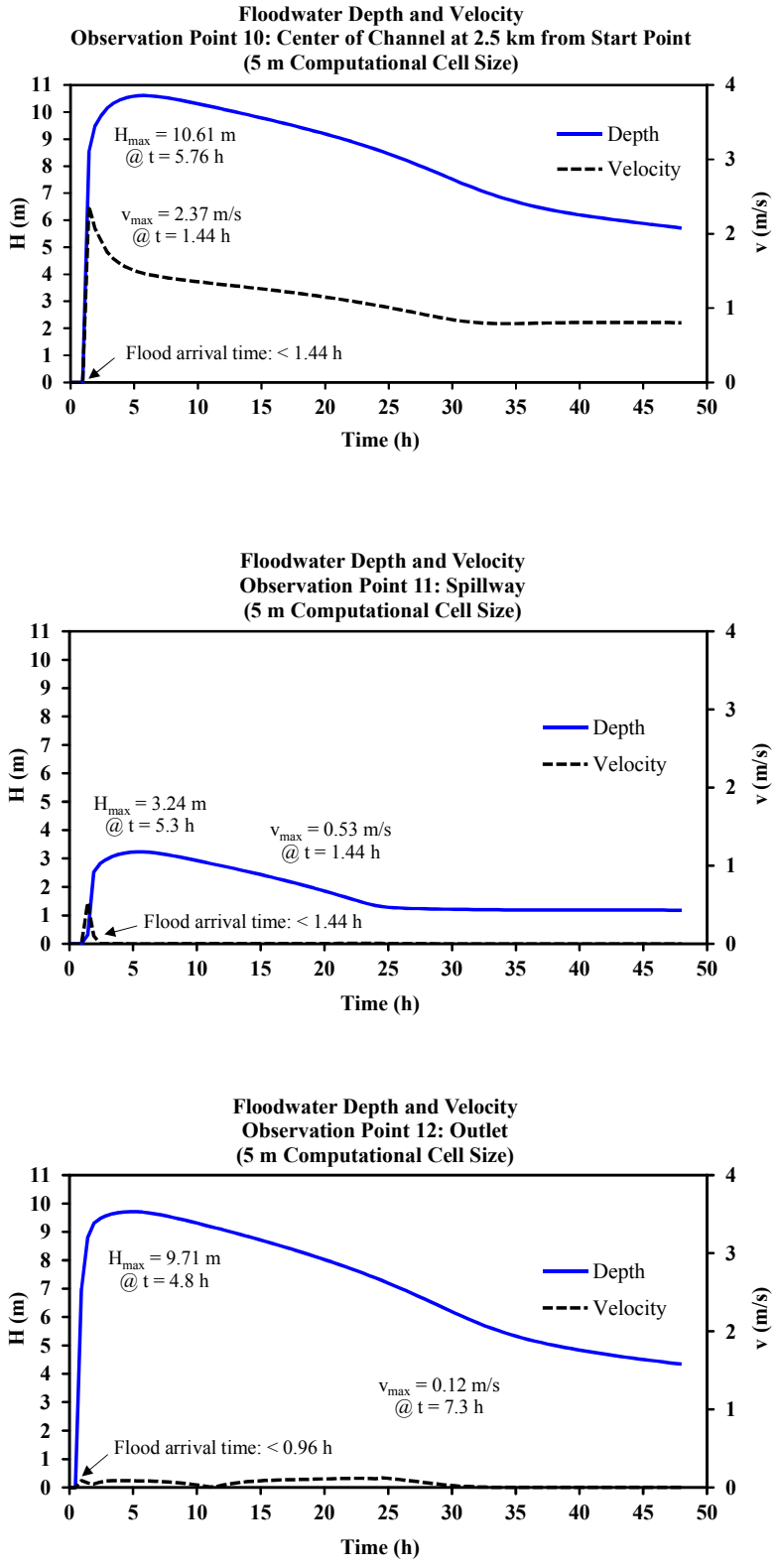

Figure A.4.4 CCHE2D-FLOOD floodwater depth and velocity output at observation points 10-12

A5. CCHE2D-FLOOD Floodwater Depth and Velocity Output: 10 m CCS Simulation

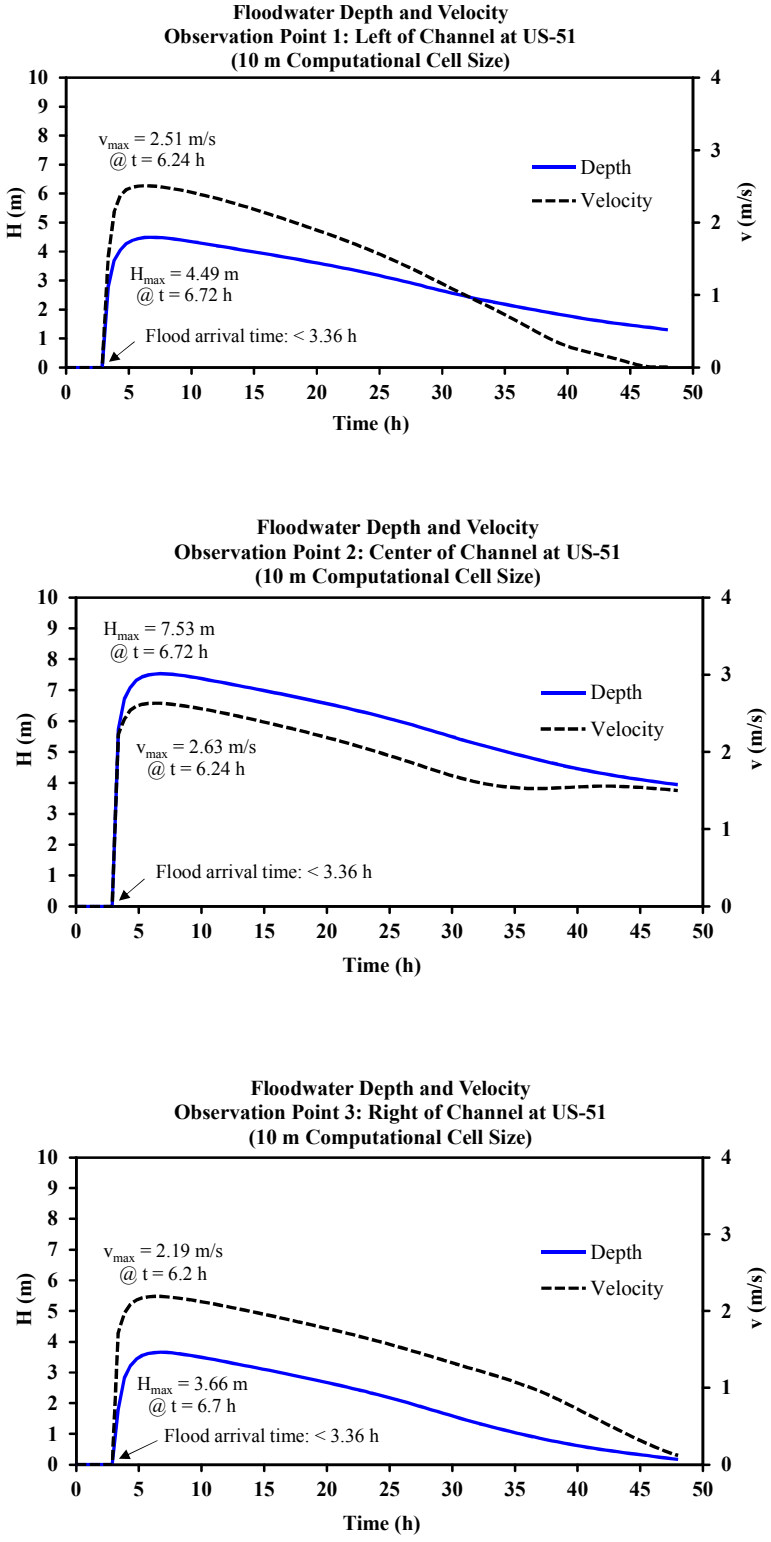

Figure A.5.1 CCHE2D-FLOOD floodwater depth and velocity output at observation points 1-3

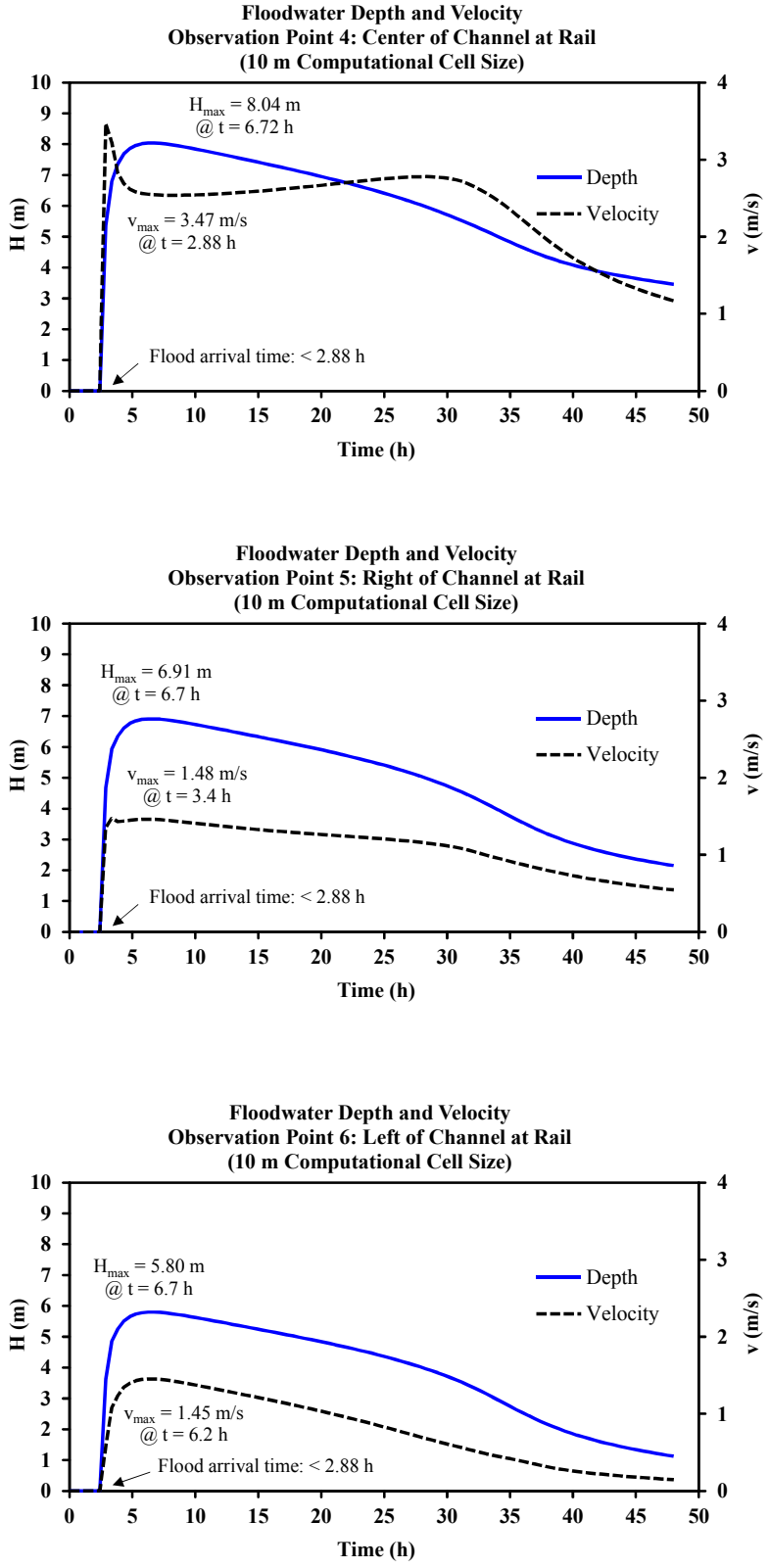

Figure A.5.2 CCHE2D-FLOOD floodwater depth and velocity output at observation points 4-6

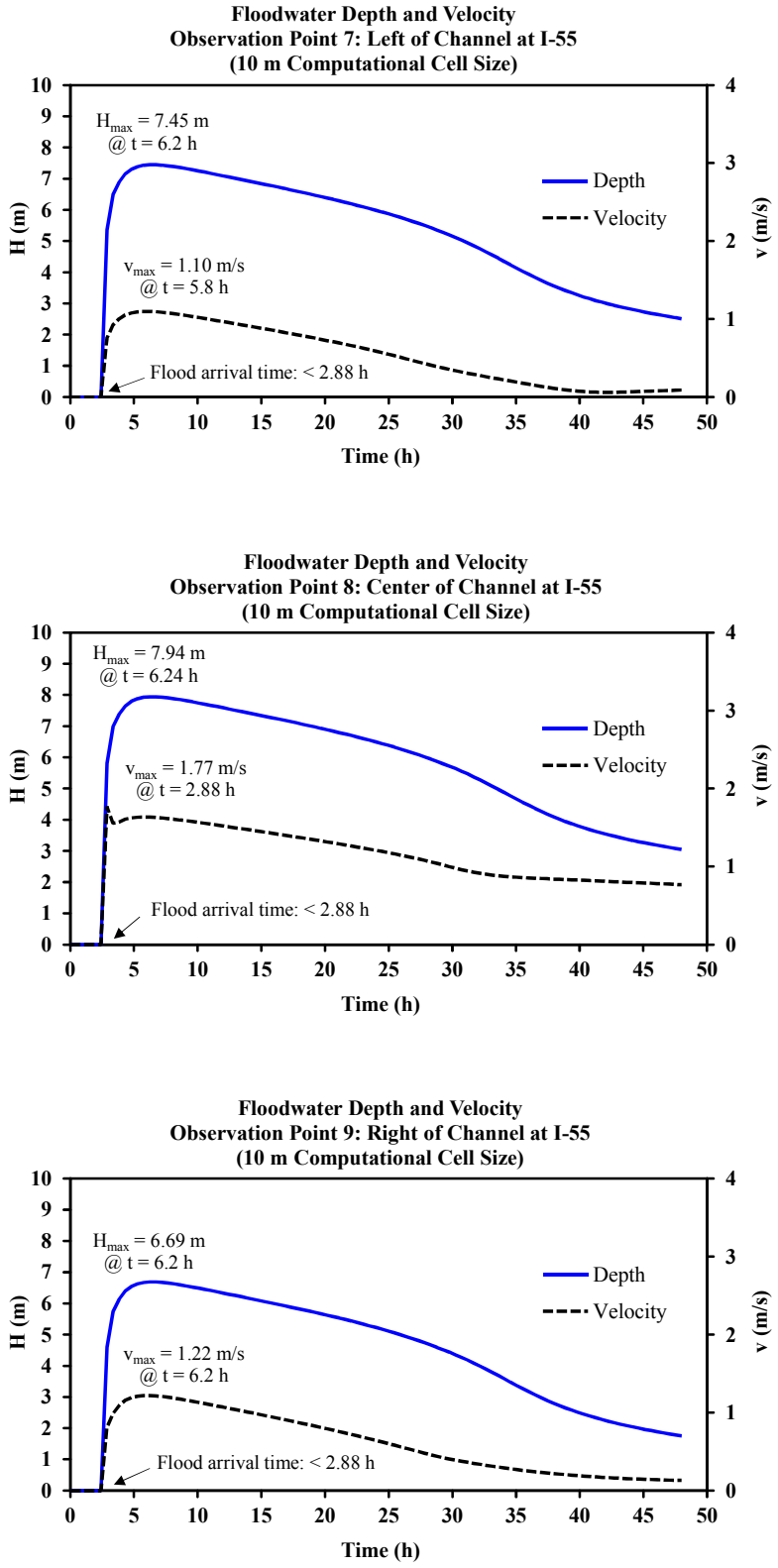

Figure A.5.3 CCHE2D-FLOOD floodwater depth and velocity output at observation points 7-9

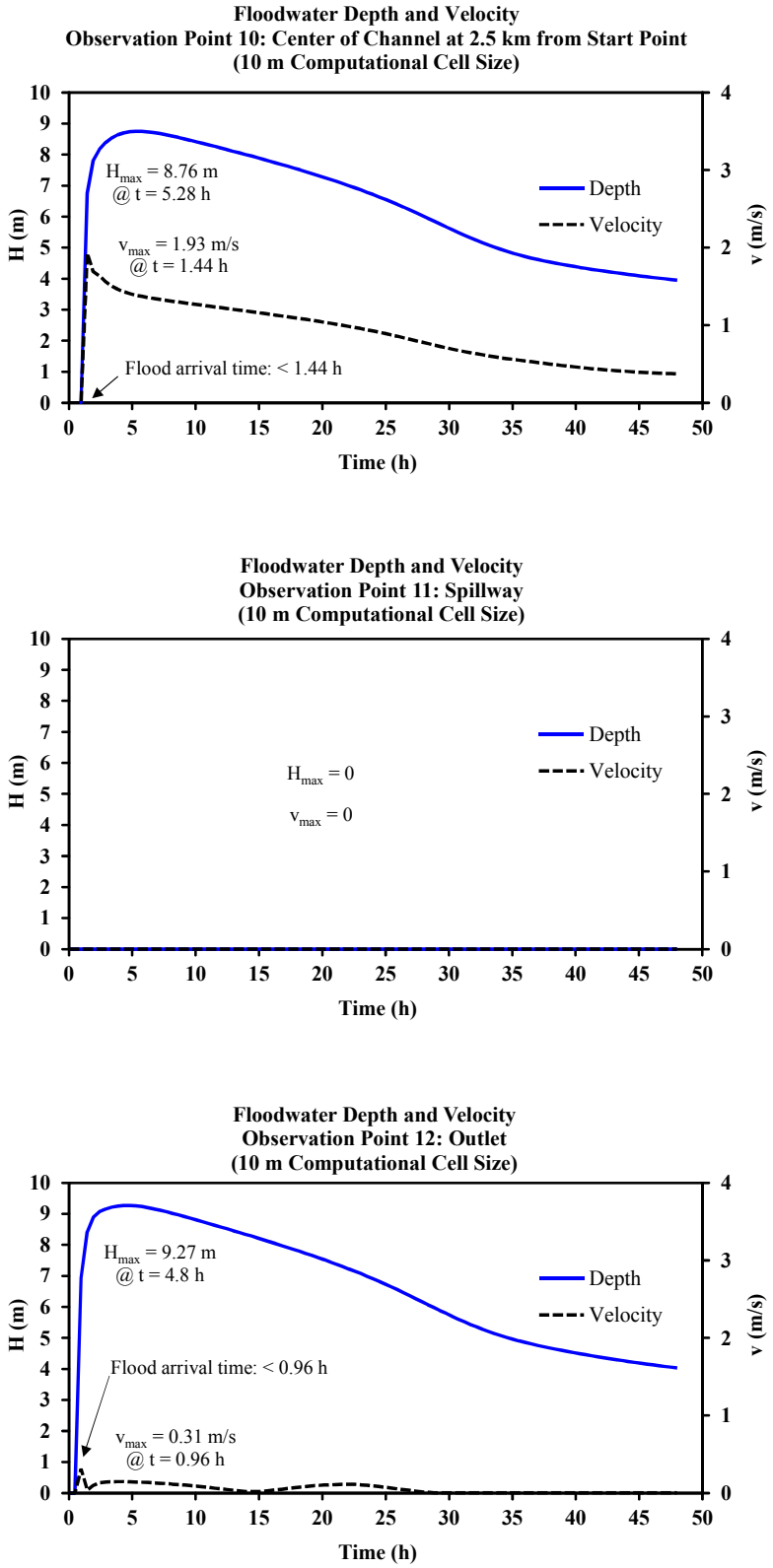

Figure A.5.4 CCHE2D-FLOOD floodwater depth and velocity output at observation points 10-12

A6. CCHE2D-FLOOD Floodwater Depth and Velocity Output: 30 m CCS Simulation

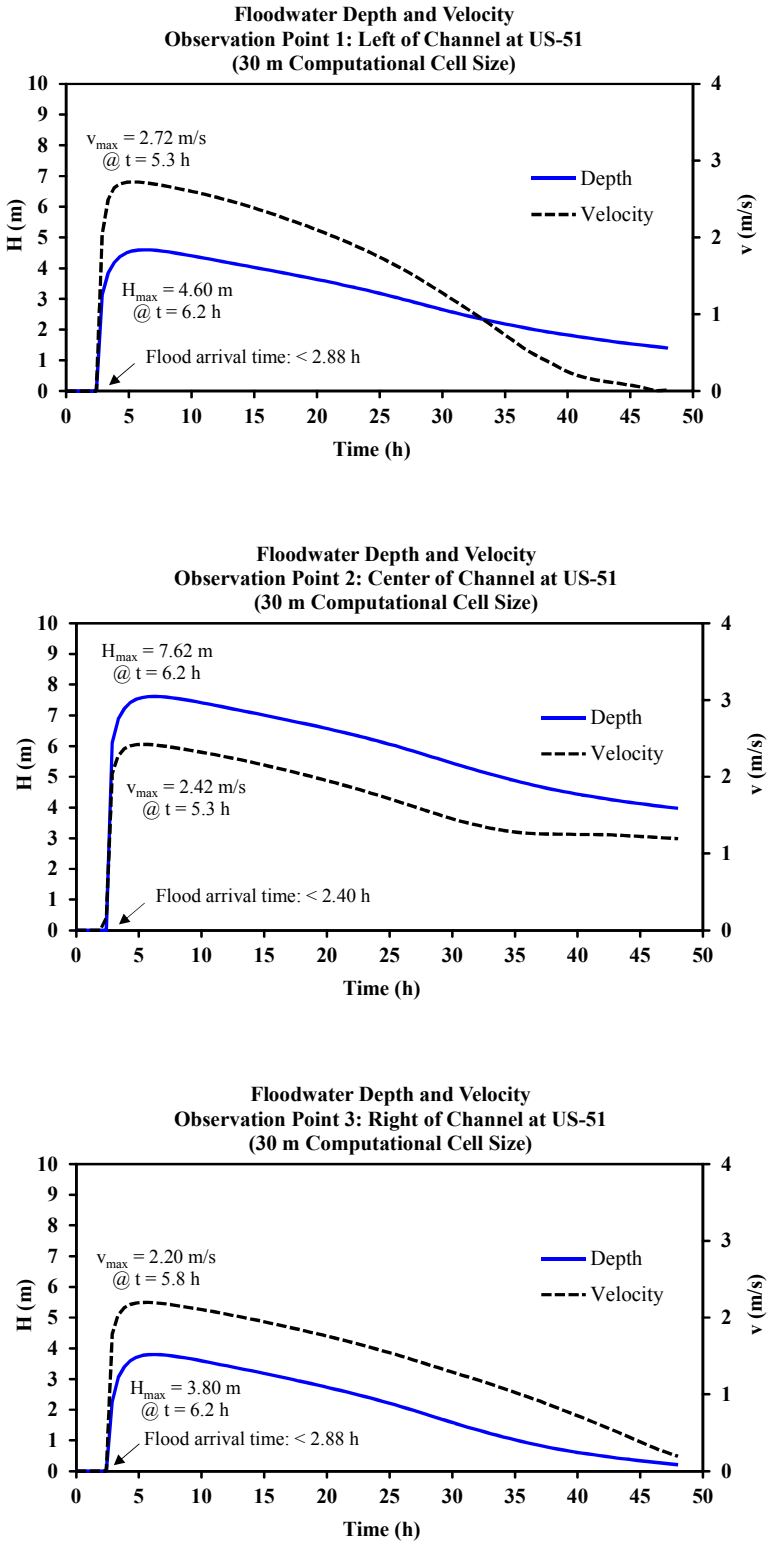

Figure A.6.1 CCHE2D-FLOOD floodwater depth and velocity output at observation points 1-3

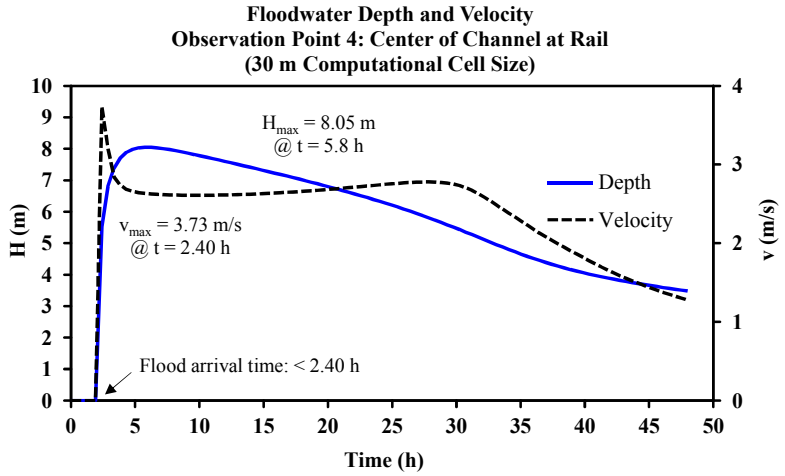

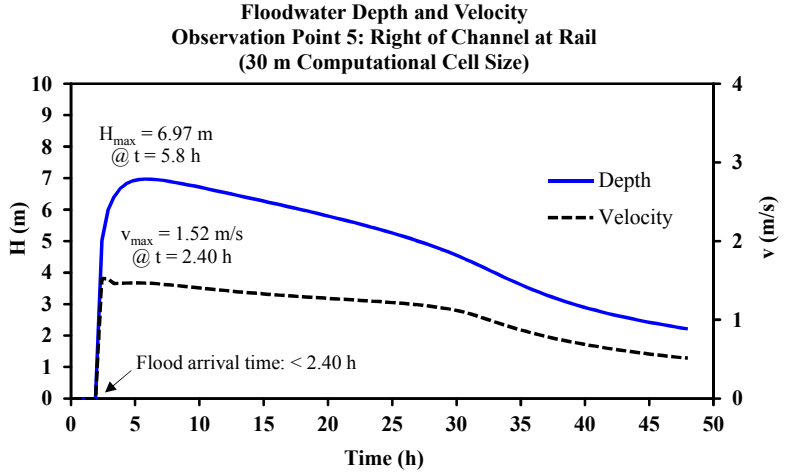

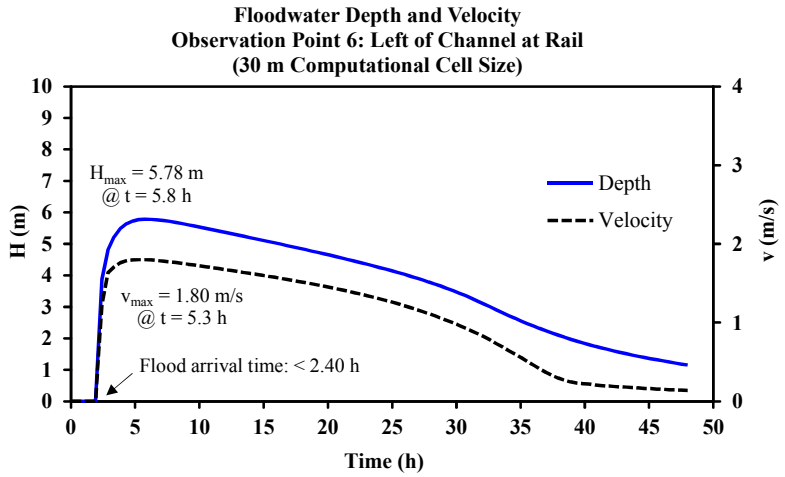

Figure A.6.2 CCHE2D-FLOOD floodwater depth and velocity output at observation points 4-6

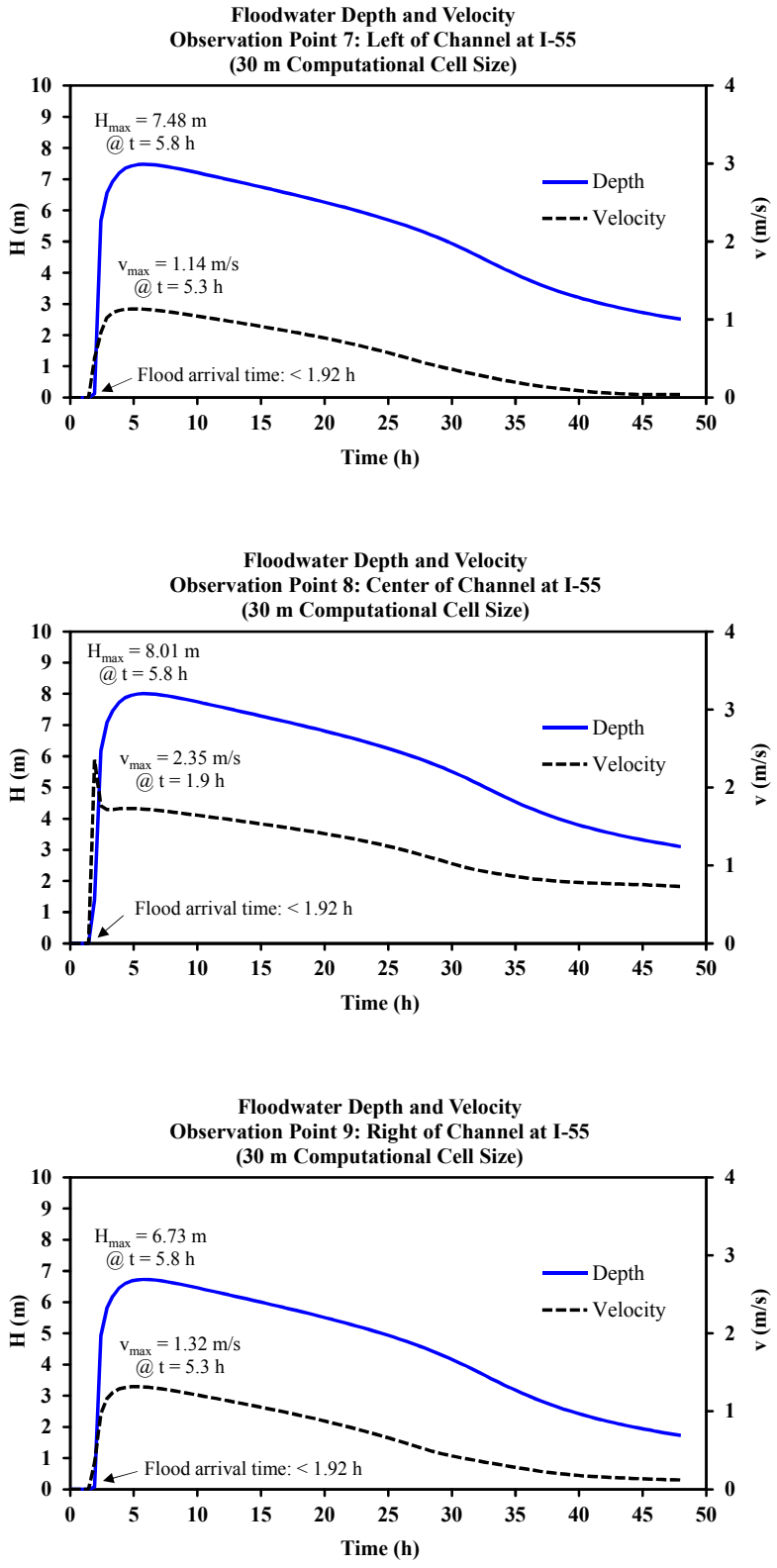

Figure A.6.3 CCHE2D-FLOOD floodwater depth and velocity output at observation points 7-9

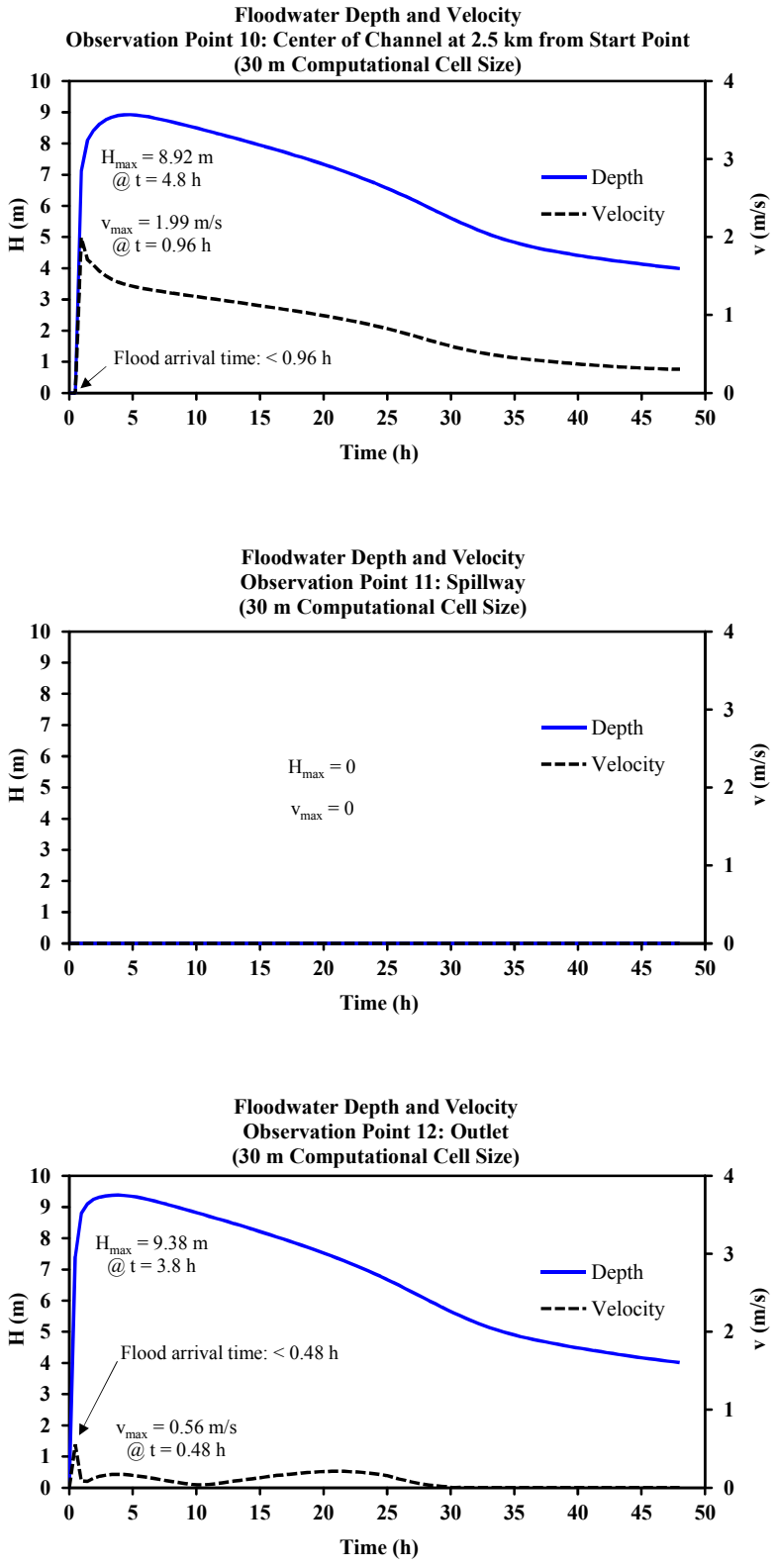

Figure A.6.4 CCHE2D-FLOOD floodwater depth and velocity output at observation points 10-12

APPENDIX B

Geospatial Maps of United States and Mississippi

B1. Geospatial Maps of United States

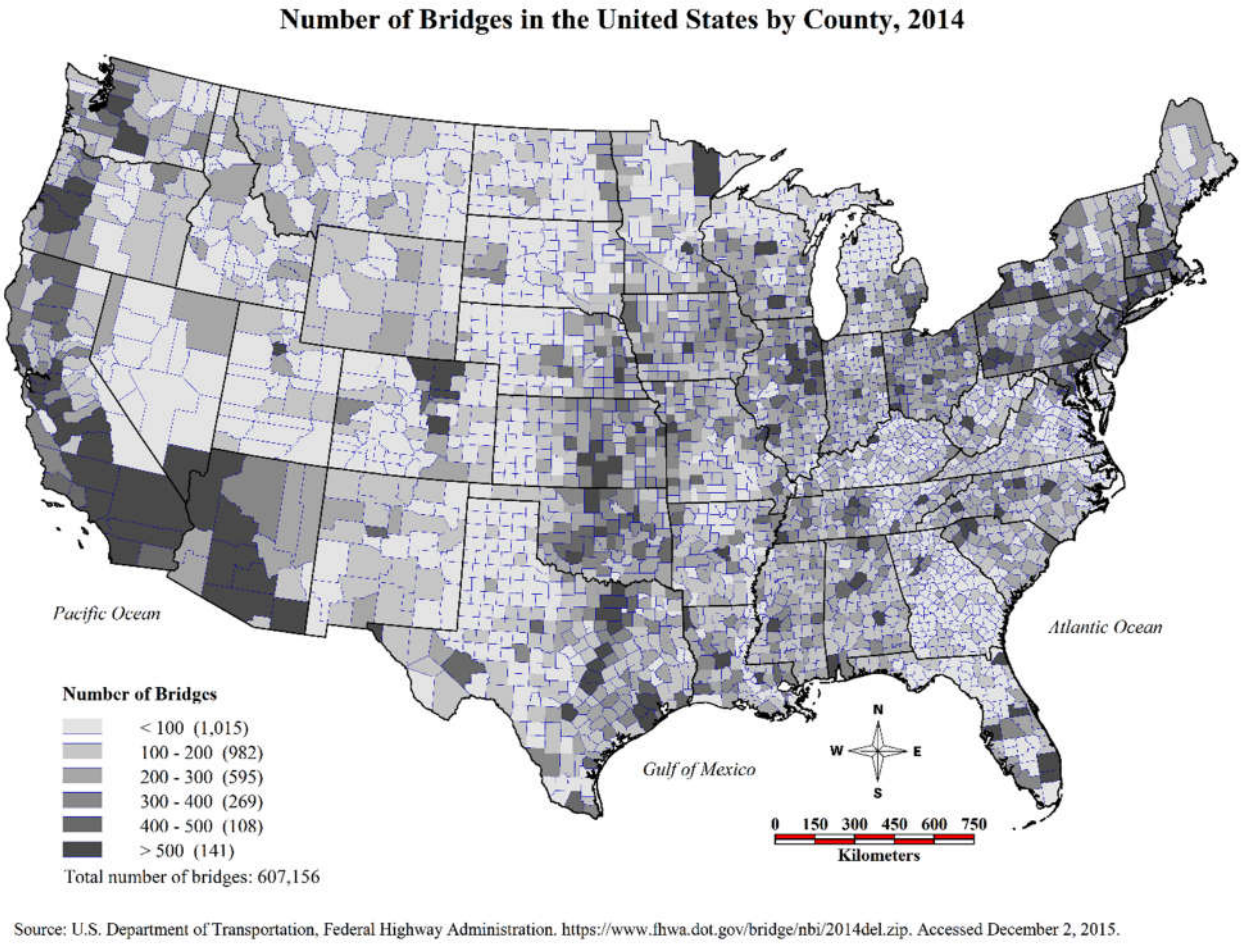

Source: U.S. Department of Transportation, Federal Highway Administration. https://www.fhwa.dot.gov/bridge/nbi/2014del.zip. Accessed December 2, 2015.

Figure B.1.1. Number of bridges in the United States by County, 2014

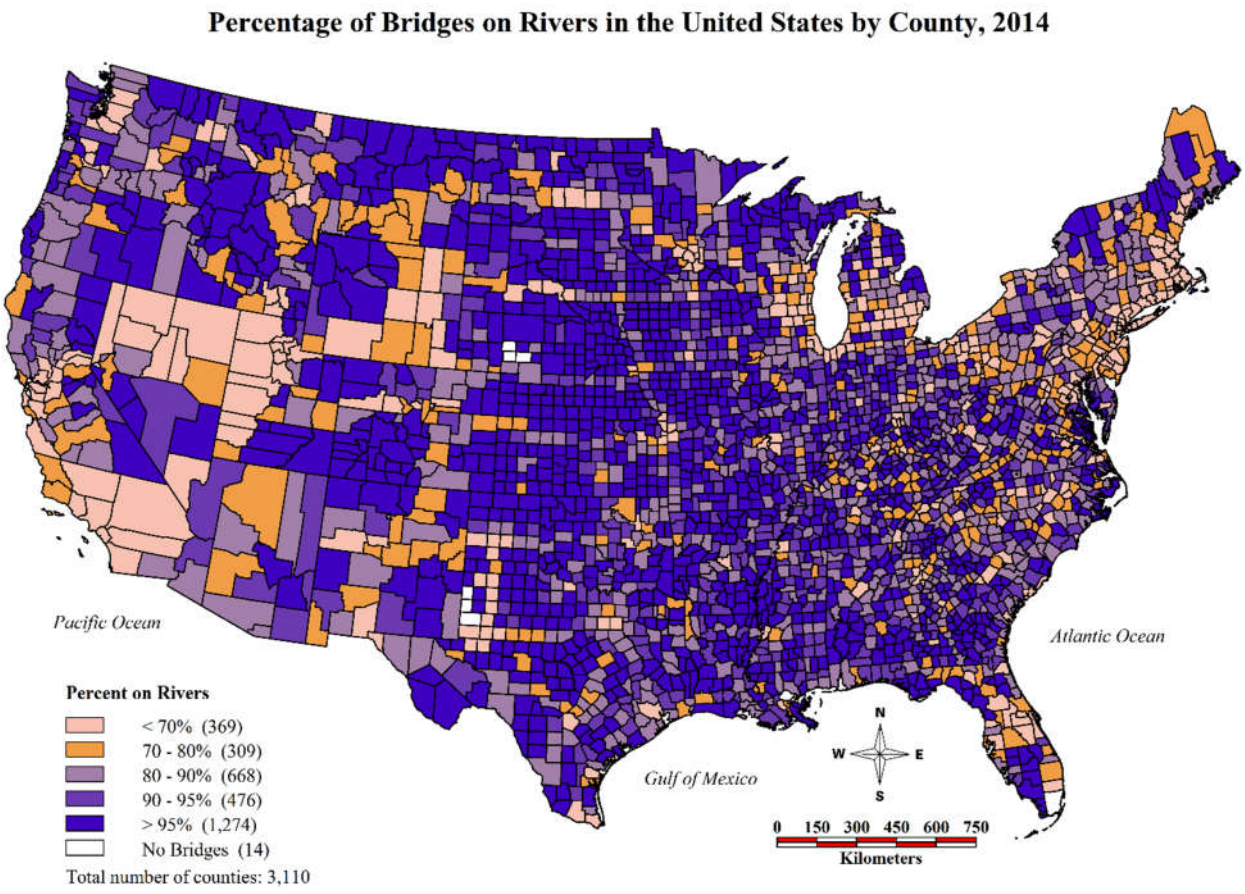

Source: U.S. Department of Transportation, Federal Highway Administration. https://www.fhwa.dot.gov/bridge/nbi/2014del.zip. Accessed December 2, 2015.

Figure B.1.2. Percentage of bridges on rivers in the United States by County, 2014

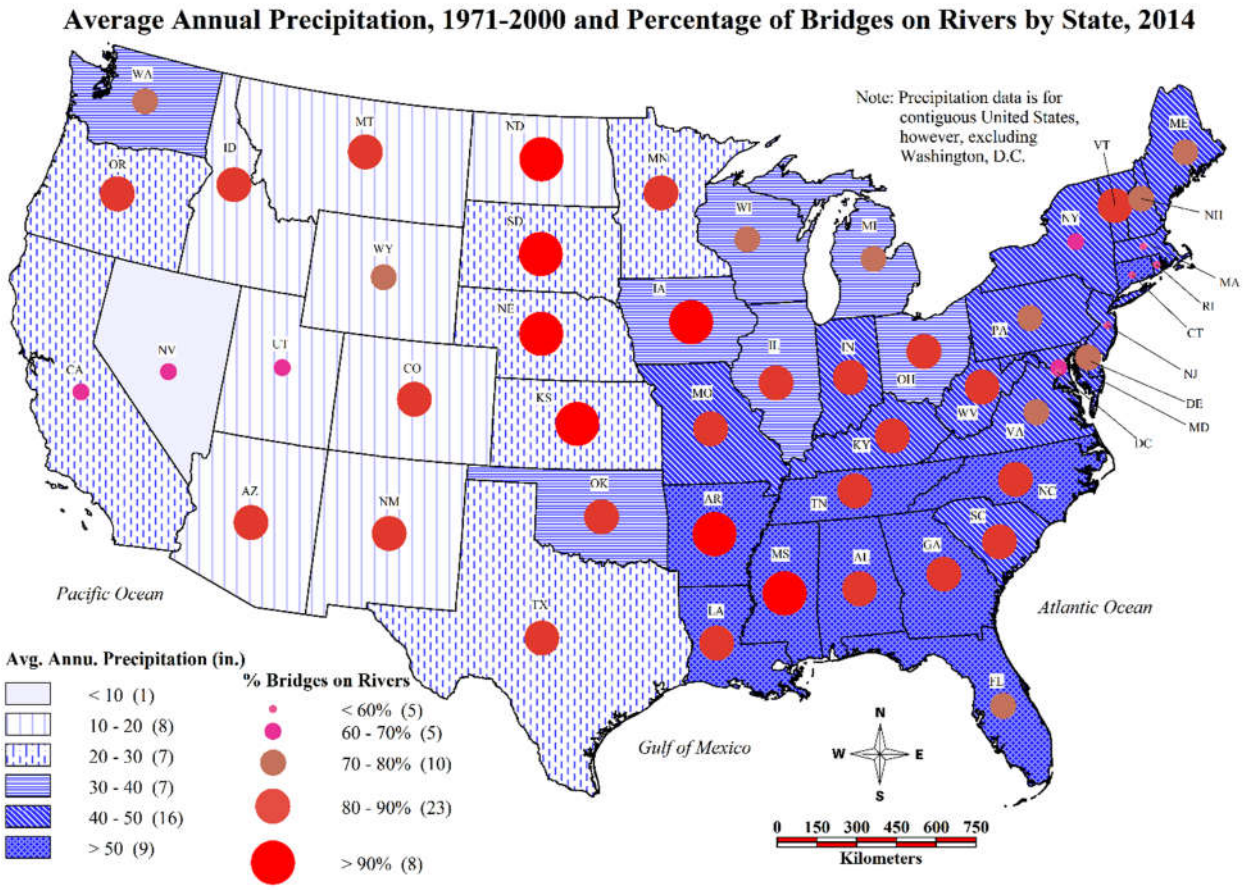

Figure B.1.3. Average annual precipitation, 1971-2000 and percentage of bridges on rivers by state, 2014

B2. Geospatial Maps of Mississippi

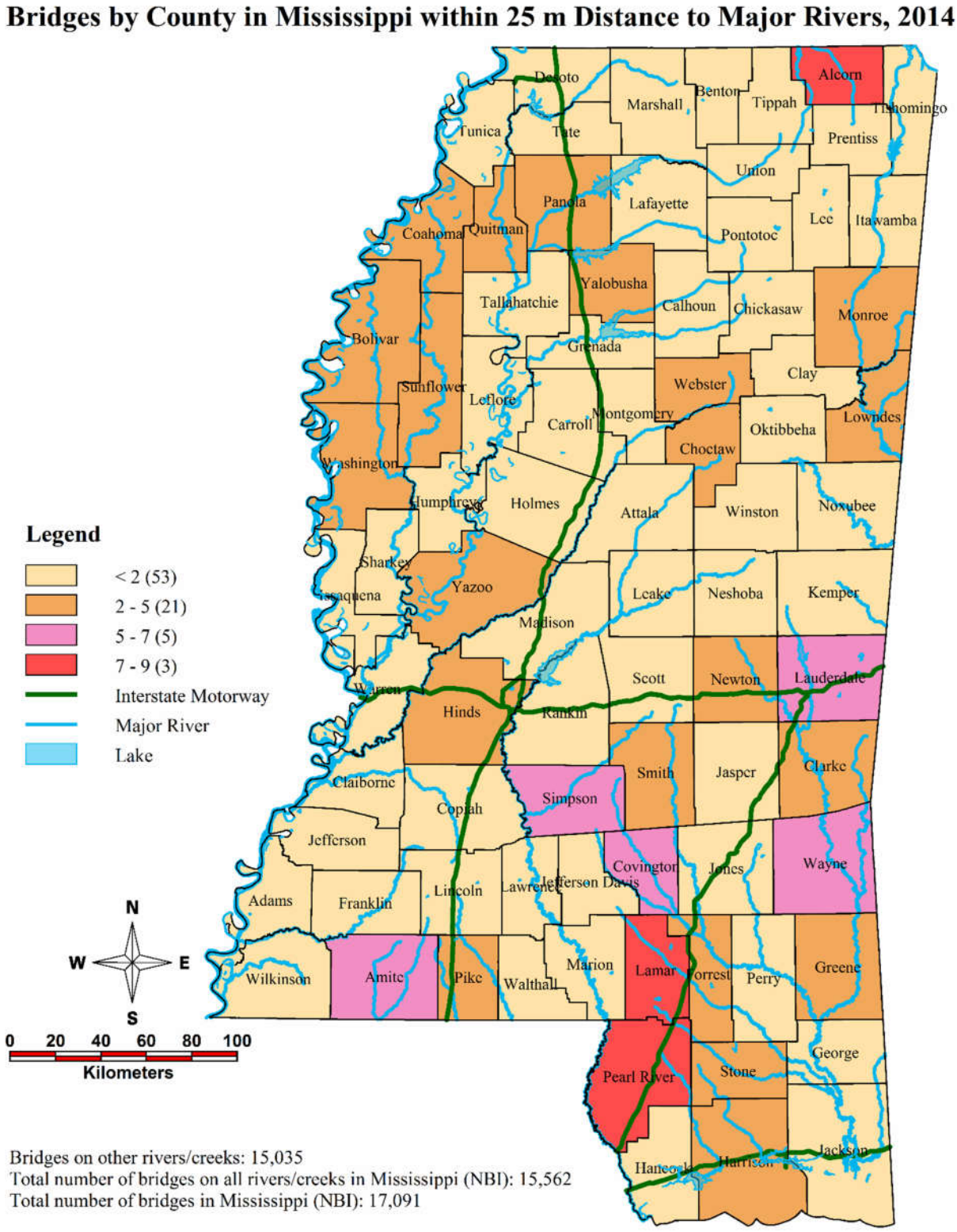

Figure B.2.1. Bridges by county in Mississippi in 25 m proximity to major rivers, 2014

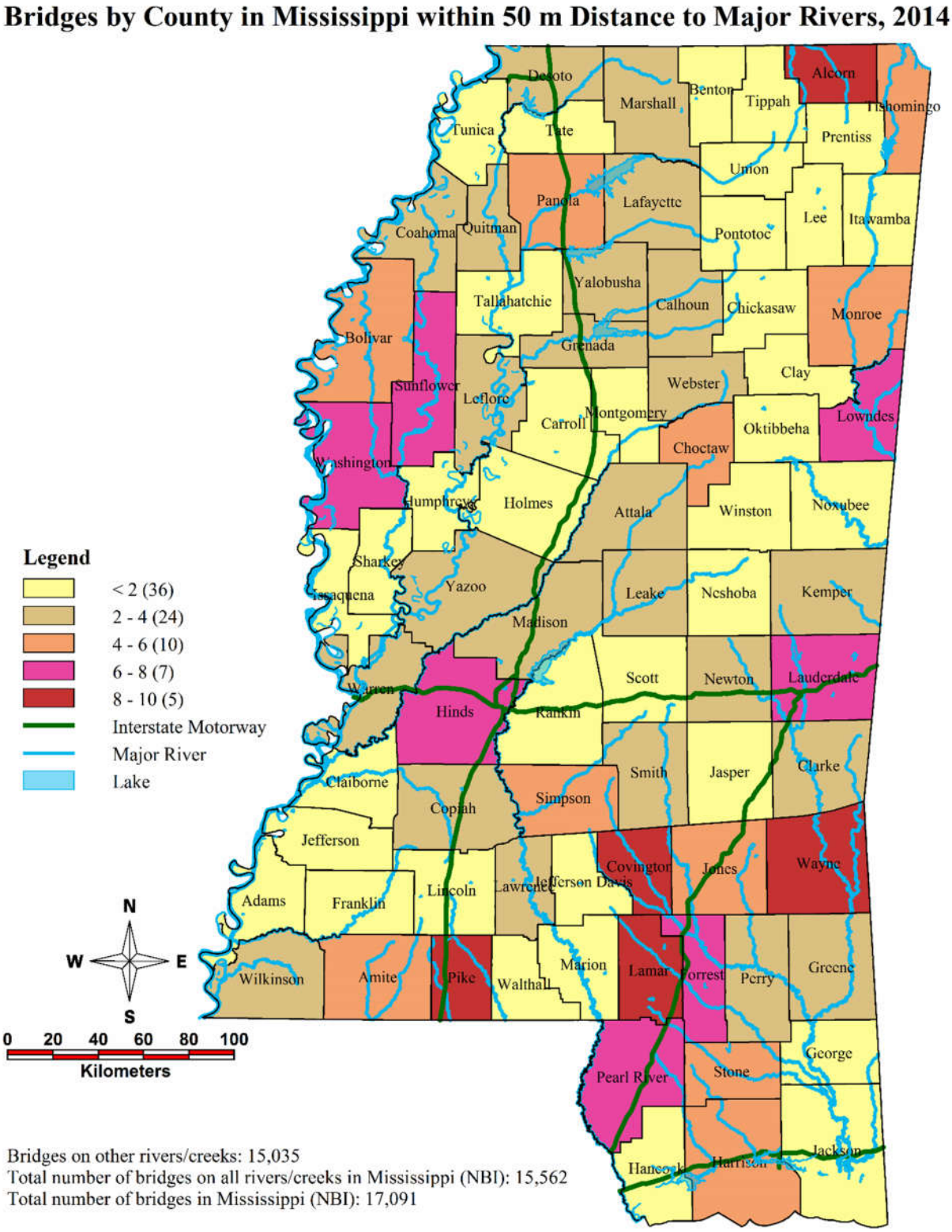

Figure B.2.2 Bridges by county in Mississippi in 50 m proximity to major rivers, 2014

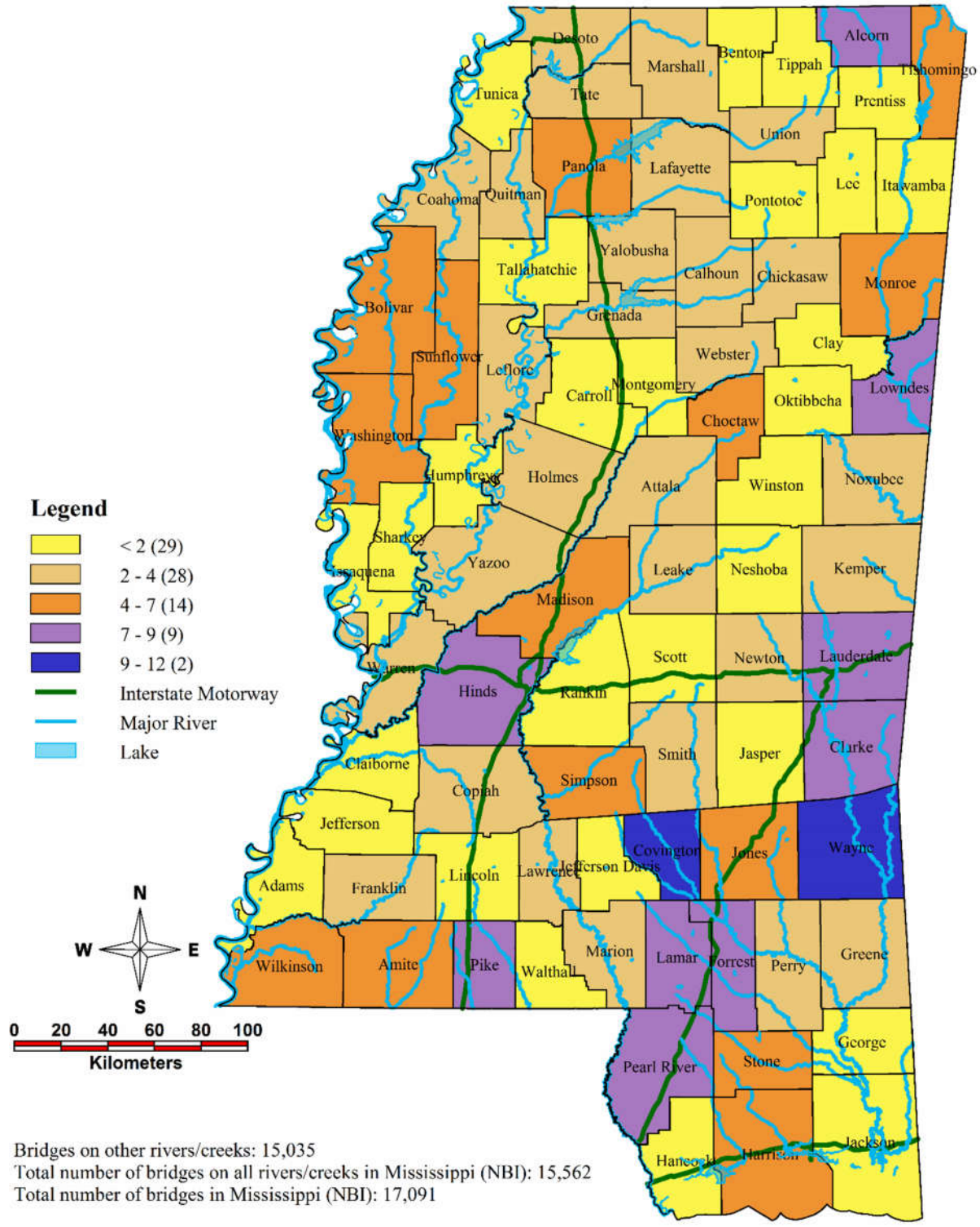

Figure B.2.3 Bridges by county in Mississippi in 100 m proximity to major rivers, 2014

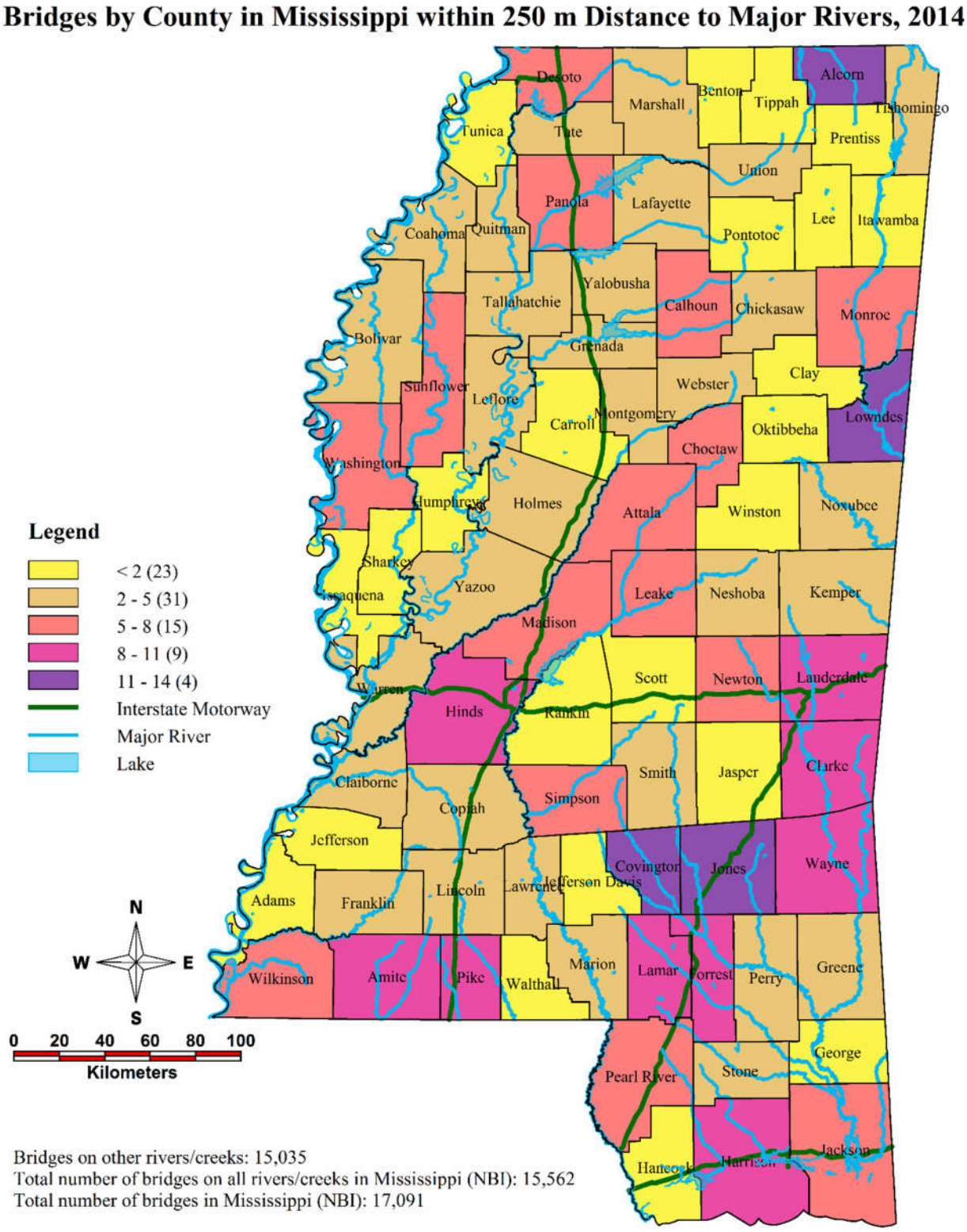

Figure B.2.4 Bridges by county in Mississippi in 250 m proximity to major rivers, 2014

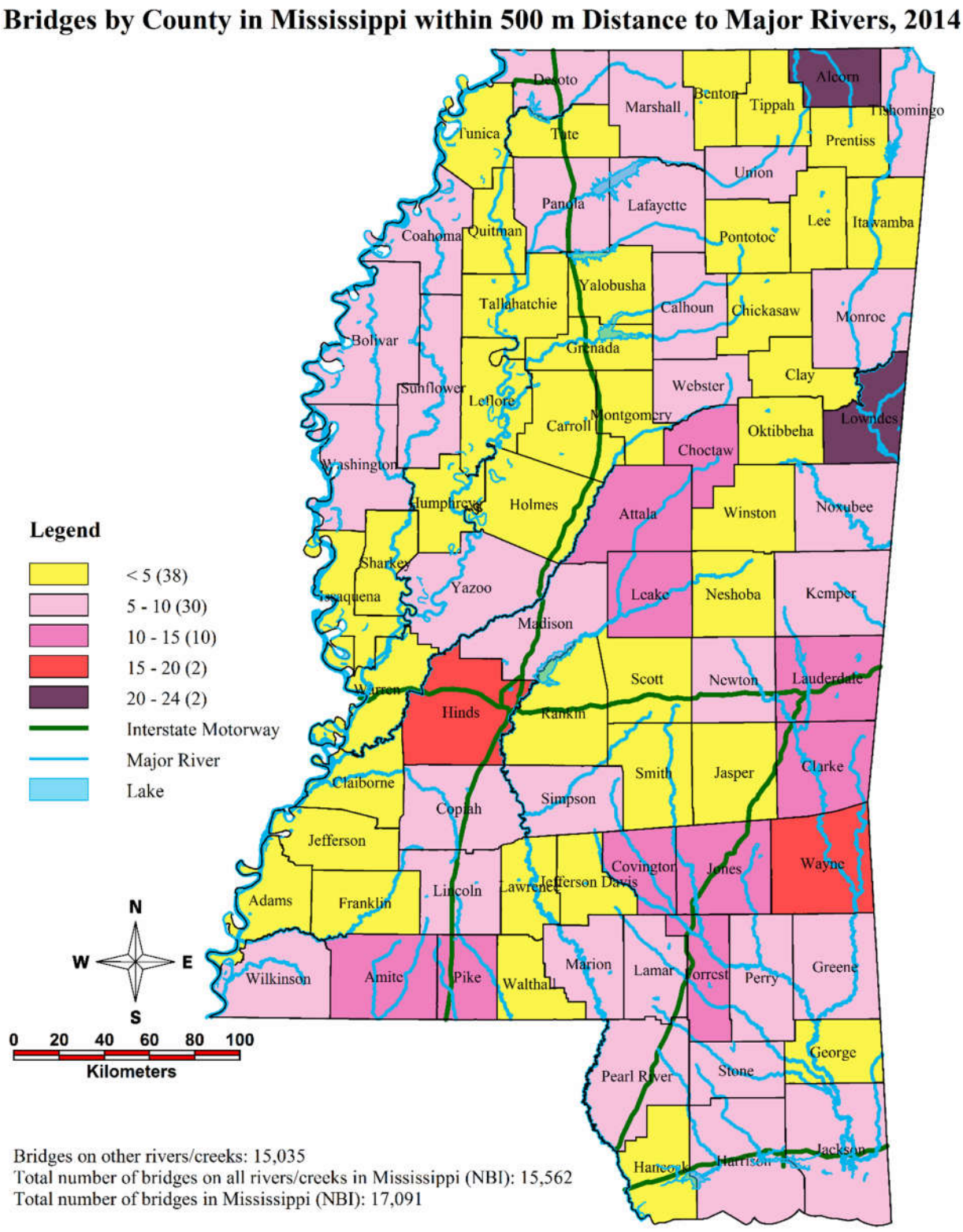

Figure B.2.5. Bridges by county in Mississippi in 500 m proximity to major rivers, 2014

VITA

Born on 8 July 1982, Alper Durmus grew up in Maksem, Bursa. He attended elementary, middle and high schools in the hometown. He received a bachelor's degree from Istanbul Technical University in 2004 and a master's degree from University of Mississippi in 2012, both in civil engineering. He worked as an engineer in North America, Middle East, Northern Europe and Asia Pacific. During his doctoral research at the University of Mississippi, he worked under the guidance of Dr. Waheed Uddin, professor and director of the Center for Advanced Infrastructure Technology.